Catalytic ring-opening polymerization of cyclic esters to biodegradable polyesters using *N,N'*- and *N,O*-ligand supported Cu(II), Mg(II) and Zn(II) complexes

by

WISDOM A. MUNZEIWA

Submitted in fulfilment of the academic requirements of Doctor of Philosophy in Chemistry School of Chemistry and Physics College of Agriculture, Engineering and Science, University of KwaZulu-Natal, Westville Campus, Durban, South Africa

DECLARATION 1: PLAGIARISM

I, Wisdom A. Munzeiwa declare that:

(i) The research reported in this dissertation, except where otherwise indicated or acknowledged, is my original work.

(ii) This dissertation has not been submitted in full or in part for any degree or examination to any other university;

(iii) this dissertation does not contain other persons' data, pictures, graphs or other information, unless specifically acknowledged as being sourced from other persons;

(iv) this dissertation does not contain other persons' writing, unless specifically acknowledged as being sourced from other researchers. Where other written sources have been quoted, then:

   (a) Their words have been re-written, but the general information attributed to them has been referenced;

   (b) where their exact words have been used, their writing has been placed inside quotation marks, and referenced;

(v) where I have used material for which publications followed, I have indicated in detail my role in the work;

(vi) this dissertation is primarily a collection of material, prepared by myself, published as journal articles or presented as a poster and oral presentations at conferences. In some cases, additional material has been included;

(vii) this dissertation does not contain text, graphics or tables copied and pasted from the Internet, unless specifically acknowledged, and the source being detailed in the dissertation and in the references sections.

Signed: __███████████████   Wisdom A. Munzeiwa

Date: 23rd August 2018

DECLARATION 2 – PUBLICATIONS

Details of contribution to publications that form part and/or include research presented in this thesis (include papers published and in preparation). My role in each paper is indicated. The (*) indicates corresponding author.

Paper 1

Wisdom A. Munzeiwa, Bernard Omondi* and Vincent O. Nyamori, Zn(II) and Cu(II) unsymmetrical formamidine complexes as effective initiators for ring-opening polymerization of cyclic esters, *Applied Organometallic Chemistry*. 2018; e4247.

My contribution: Performed all experimental work contributed significantly to the interpretation of the results and prepared the paper. This was achieved under the guidance of my supervisors.

Paper 2

Wisdom A. Munzeiwa, Bernard Omondi* and Vincent O. Nyamori, Synthesis and polymerization kinetics of ε-caprolactone and ʟ-lactide to low molecular weight polyesters catalysed by Zn(II) and Cu(II) *N*-hydroxy-*N,N′*-diarylformamidine complexes**, *Polyhedron* 2017, 138, 295.

My contribution: The research reported is based on the data I collected from the experimental ring-opening polymerization of ε-caprolactone and lactides and I drafted the article. This was achieved under the guidance of my supervisors.

Paper 3

Wisdom A. Munzeiwa, Bernard Omondi* and Vincent O. Nyamori, *N,O*-Amino-phenolate Mg(II) and Zn(II) Schiff base complexes: Synthesis and application in ring -opening polymerization of ε-caprolactone, ʟ-lactide and *rac*-lactide, Manuscript in preparation.

My contribution: I synthesized the complexes, carried out the characterization and catalysis testing. I prepared the manuscript under the guidance of my supervisors.

Paper 4

Wisdom A. Munzeiwa, Bernard Omondi* and Vincent O. Nyamori, Stereoselective ring-opening polymerization and homo- and co-polymerization of lactides and ε-caprolactone by chiral Zn(II) pyridyl complexes, Manuscript in preparation.

My contribution: Performed all experimental work contributed significantly to the interpretation of the results and prepared the paper. This was achieved under the guidance of my supervisors.
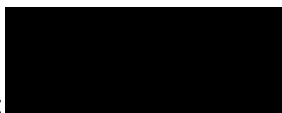
<div align="center">

CONFERENCES PARTCIPATION

</div>

Wisdom A. Munzeiwa, Bernard Omondi and Vincent O. Nyamori, Ring-opening polymerization of caprolactone using Cu(II) and Zn(II) unsymmetrical formamidine complexes, Poster presentation at the College of Agriculture, Engineering and Science research day, 22th September 2015, Pietermaritzburg campus, UKZN.

Wisdom A. Munzeiwa, Bernard Omondi and Vincent O. Nyamori, Synthesis, crystal structures of Cu(II) and Zn(II) formamidine complexes and their application in ring-opening polymerization, Poster presentation at the 42nd National Convention: South African Chemical Institute, Durban, South Africa, 29th November – 4th December 2015.

Wisdom A. Munzeiwa, Bernard Omondi and Vincent O. Nyamori, Zn(II) and Cu(II) hydroxyformamidine complexes: Synthesis, crystal structures and catalytic activity in ring - opening polymerization of ε-caprolactone and lactides, Poster presentation at the College of Agriculture, Engineering and Science research day, 29th November 2016, Howard campus, UKZN.

Signed:

Name: Wisdom A Munzeiwa Date:23rd Aug 2018………………………

ABSTRACT

Over the past decades, there has been a tremendous increase in market demand for polyesters and their co-polymers. Of interest, polycaprolactone (PCL) and polylactides (PLA) which are biodegradable have found widespread applications in the packaging and biomedical fields. Polyesters are produced *via* ring-opening polymerization (ROP) process using metal-based metal-catalyst/initiators, with industrial production relying on tin(II) compounds. Despite the intense research efforts devoted to this area, there are still considerable limitations. For example, in case of chiral lactides monomers very few catalytic systems are capable of stereoselective synthesis. In addition, there is also lack of control of the polymerization process to curb side reactions which results in low molecular weight polymers with broad molecular distributions. Furthermore, the toxicological effects associated with tin compounds pose a danger if polymers are applied in the biomedical field since it is difficult to completely remove remnant catalyst from the polymer matrices.

Thus, this thesis investigated the synthesis of less toxic metal complexes such as zinc, copper and magnesium supported by strategically designed ligands and their application in ROP. Four different class of ligands were explored as supports namely formamidine, *N*-hydroxy formamidine, Schiff base phenoxide and chiral amino pyridyl ligands and thirty complexes were synthesized and reported in this thesis. The steric and electronic properties of the ligands were fine-tuned to influence the catalytic activity and the polymer properties.

The effect of the nature of the metal—oxygen bond which is prerequisite for ring-opening polymerization was investigated. Complexes with acetate and alkoxide reactive ligands were synthesised where the oxygen was not part of the ligand system. *N*-hydroxy formamidine and Schiff base phenoxide ligands contain the oxygen heteroatom as part of the ligand backbone. All the complexes polymerized caprolactone and lactides with appreciable activity, however for hydroxy formamidine ligands the polymerization complexes were more active only in the presence of co-initiator. The effect of auxiliary ligands such as acetates, alkoxides was also investigated. The polymerization data showed that catalytic activity depended on the metal identity, steric crowding and auxiliary ligands. Generally, zinc acetate complexes were more active achieving complete monomer conversion within 68 h compared to 120 h for the copper analogues.

Magnesium-amino phenolate complexes showed greater activity, attaining 99% monomer conversion in less than 32 h as compared to 55 h for the zinc analogues. The zinc pyridyl alky and alkoxide complexes showed excellent activity, achieving 100% monomer conversion within 1 min at room temperature. Bulk substituents and electron withdrawing substituent resulted in reduced catalytic activity.

All catalytic systems produced low molecular weight polymers ranging from 1200 to 10 500 g mol^{-1} with relatively broad molecular weight distributions and PDIs that lie between 1.2 and 2 pointing to semi-living polymerization. Chiral ligand supported catalysts showed good stereoselectivity in polymerization of *rac*-lactide (*rac*-LA) with P_r values *ca* 0.70. The role of the solvent was studied, and it was observed that coordinating solvent such as THF retards the polymerization as they compete with the monomer for catalytic active sites. Detailed abstracts are given in each of chapters 3 to 6.

ACKNOWLEDGEMENTS

PREFACE

The experimental work described in this thesis was carried out in the School of Chemistry and Physics, University of KwaZulu-Natal, Westville Campus, Durban from March 2014 to December 2017, under the supervision of Dr Bernard Owaga and Professor Vincent O. Nyamori.

These studies represent original work by the author and have not otherwise been submitted in any form for any degree or diploma to any tertiary institution. Where use has been made of the work of others, it has been duly acknowledged in the text.

The chapters in this thesis are written as a set of discrete research papers, with an overall introduction, and final conclusion. Some of the chapters have been published or submitted for publication in internationally-recognised peer-reviewed journals.

LIST OF ABBREVIATIONS AND SYMBOLS

OAc	Acetate anion
AMM	Activated-monomer mechanism
Å	Ångstrom
br	Broad
CIM	Coordination-insertion mechanism
COSY	Correlation spectroscopy
calcd.	Calculated
EPR	Electron paramagnetic resonance
ε-CL	epsilon-Caprolactone
°C	Degrees Celsius
δ	Delta = Chemical shift in ppm
d	Doublet
D-LA	D-Lactide
D,L-LA	D,L-Lactide
DCM	Dichloromethane
DFT	Density function theory
DMF	Dimethylformamide
DOSY	Diffusion-ordered spectroscopy
ESI-MS	Electrospray ionization mass spectrometry
FT-IR	Fourier transform infrared spectroscopy
g	Gram(s)
g mol^{-1}	Gram per mole
GPC	Gel permeation chromatography
h	Hour(s)
Hz	Hertz
^{i}Pr	Isopropyl
i	Isotactic
J	Coupling constant

k_{app}	Apparent rate of propagation
LAs	Lactides
ʟ-LA	ʟ-lactide
m	Multiplet
Me	Methyl
min	Minute(s)
mL	Millilitres
mmol	Millimoles
mol	Moles
M_n	Number average molecular weight
M_w	Weight average molecular weight
NMR	Nuclear magnetic resonance
NOESY	Nuclear overhauser effect spectroscopy
PDI	Polydispersity index
PCL	Polycaprolactone
PLA(s)	Polylactide(s)
Pm	Probability of *meso* enchainment
ppm	Parts per million
Pr	Probability of racemic enchainment
ROP	Ring-opening polymerization
rac-LA	Racemic lactide
SEC	Size exclusion chromatography
s	Singlet
t	Triplet
THF	Tetrahydrofuran

TABLE OF CONTENTS

Contents	Page

Chapter 2 Literature review

A perspective into ring-opening polymerization of ε-caprolactone and lactides: Effects of, ligand, catalyst structure and system dynamics, on activity and polymer properties

Chapter 3

Zn(II) and Cu(II) unsymmetrical formamidine complexes as effective initiators for ring-opening polymerization of cyclic esters

Chapter 4

Synthesis and polymerization kinetics of ε-caprolactone and ʟ-lactide to low molecular weight polyesters catalysed by Zn(II) and Cu(II) *N*-hydroxy-*N,N′*-diarylformamidine complexes

Chapter 5

N,O-**Amino-phenolate Mg(II) and Zn(II) Schiff base complexes: Synthesis and application in ring-opening polymerization of ε-caprolactone and lactides**

Chapter 6

Stereoselective ring-opening polymerization, homo- and co-polymerization of lactides and ε-caprolactone catalysed by chiral Zn(II) pyridyl complexes

Chapter 7

General conclusions and future prospects

List of tables

List of figures

List of schemes

Chapter 1   Introduction

This thesis investigates the synthesis and characterization of organometallic complexes and their use in synthesis of polyesters by ring-opening polymerization (ROP) reactions of cyclic esters. In this introductory chapter, background of polyesters, their preparation, applications, polymerization reactions kinetics and mechanisms are presented.

1.1   Background

Polymers can be categorised into two major groups based on their sources, i.e. synthetic or natural. Natural polymers are found in nature and are derived from biomass and animal sources. Some examples include starch and cellulose which comprise of sugar-based units, proteins (consist of amino acid repeat units), deoxyribonucleic acid (DNA, made up of nucleotides) and natural rubber (isoprene repeat unit). Synthetic polymers are manufactured mainly from petroleum-based monomers and in particular, for example, polyethylene, polystyrene and poly(vinyl alcohol). Principally these synthetic polymers can be fine-tuned to meet specific qualities suited for certain applications. The main drawback in their application is that they are not biocompatible and biodegradable. In addition, the probable extinction of natural fossil, resources like coal, oil and natural gases, which are feedstocks for these synthetic polymers, have necessitated the need to exploit the use of bio-renewable resource. Increasing fears concerning environmental issue like global warming and polymer waste disposal challenges have also forced society to petition for sustainable and green products.[1]

The definition of "sustainable polymer" encompass multi-faceted approachs where the material must meet consumer requirements without negative effects on the environment, health, and economy. Among the sustainable polymers that may be considered, polyesters present a sizable percentage, and possess many attractive attributes. They can potentially replace petroleum-based polymers because they are biocompatible, biodegradable and can be bio-derived. Due to their inherent properties, they have been widely used in medical devices,[2,3] packaging,[4] construction[5] and electronic devices.[6] A summary of applications is presented in Figure 1.1.
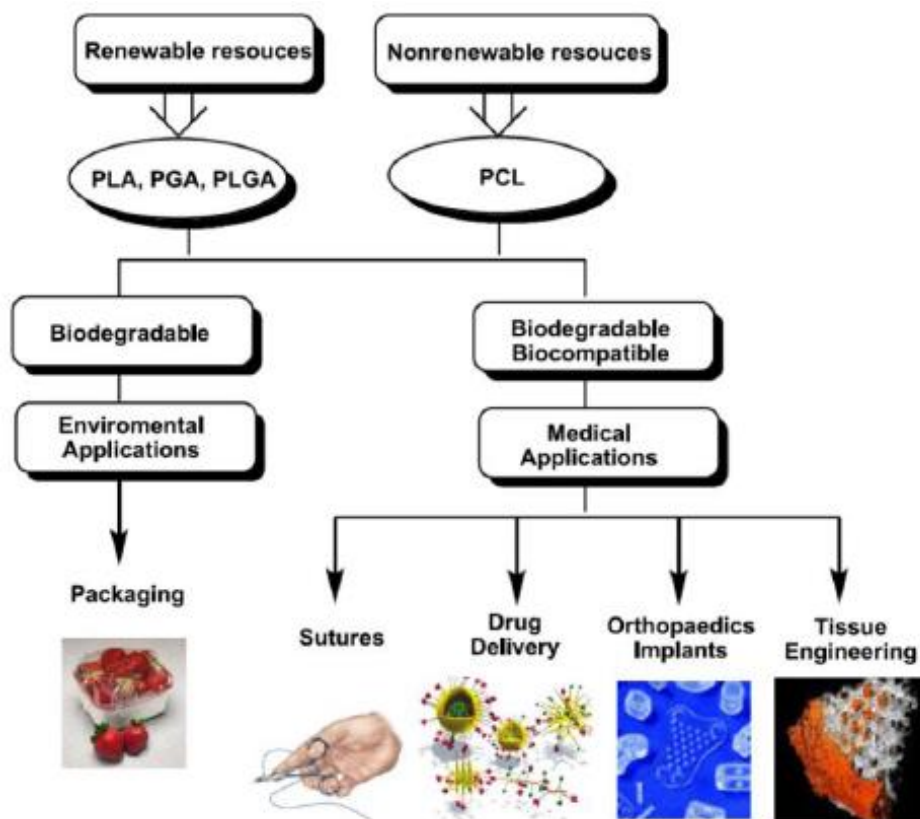
Figure 1.1: Potential applications of polymers obtained from (ε-caprolactone (ε-CL) and lactides (LAs)[7]

The major focus of this work was to synthesize biodegradable polymers, which could potentially be used in medical applications. For pharmacological applications, tailor-made polymers are designed which are proficient in delivering medicinal ingredients to the target tissues. The polymer nanomaterials can be designed into different structures such as nanoparticles,[8] polymeric micelles,[9-11] vesicles and nano-conjugates (Figure 1.2).[12-15] These approaches have improved drug efficacy by increasing drug water solubility, targeted delivery, improved pharmaceutical and pharmacological effects without transforming the drug molecules, enhanced half-lives and circulation times, and increased drug loading. Some technologies are already on the market and some are still under clinical trials. For example, Paxceed® a polymeric micellar formulation of paclitaxel (PTX) an anticancer drug encapsulated in poly(lactic acid-co-methoxypolyethylene) oxide (PLA-co-mPEO) di-block copolymers[16] effectively enhanced the maximum tolerated dose (MTD) and is still in clinical trials.
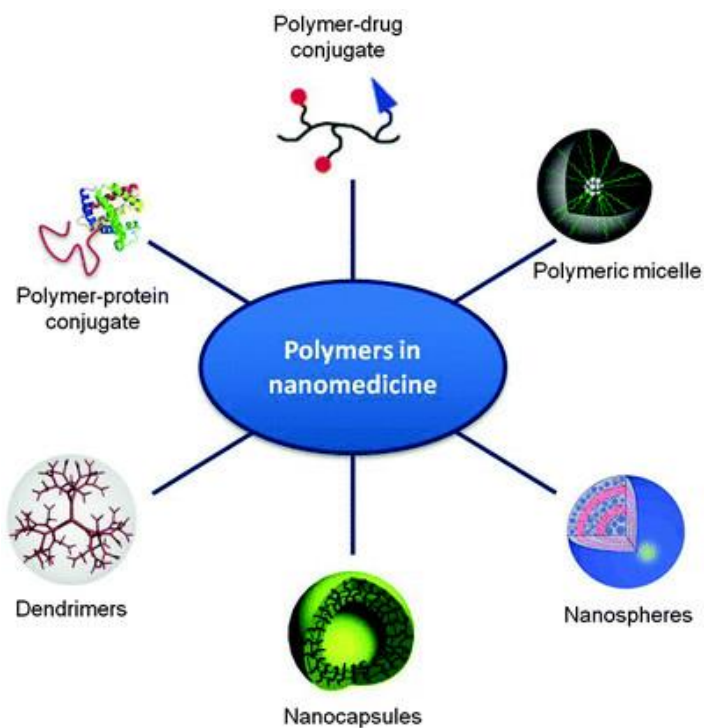
Figure 1.2: Polymer drug nano-carriers[17]

1.2 Synthesis of biomass-based monomers

Industrially, the most viable routes to produce monomers are from petroleum-based chemicals, which are facing extinction. In this context, research is geared toward the use of renewable biomass with complete replacement of petro-based monomers. Biomass-based polymers have majorly been derived from agricultural carbohydrate feedstocks. Some have argued that this threatens food security hence there is a need to use non-consumable biomass. The monomers are produced mainly from lignocellulosic biomass and other organic matter.[1] The innovations in biotechnology have been a significant breakthrough as lignocellulosic biomass transformation to usable fine chemicals and polymers is still a major area of research. Fermentation of glucose, obtained from lignocelluloses and starch, can be used to produce a variety of bio-based monomers (Figure 1.3 and 1.4).[18] Alternatively, enzymatic catalytic transformation of 5-(hydroxymethyl)furfural (5-HMF)[19] has yielded promising results.[20,21] Other monomers like δ-valerolactone, γ-butyrolactone can be similarly derived from renewable feedstocks[18] *via* microbial fermentation.

3

Predominantly, microbes such as *Escherichia coli*, *Lactobacillus casei*, *Anaerobiospirillium succiniciproducens* and *Actinobacillus succinogenes* have been systematically utilised in biomass transformation.[22]
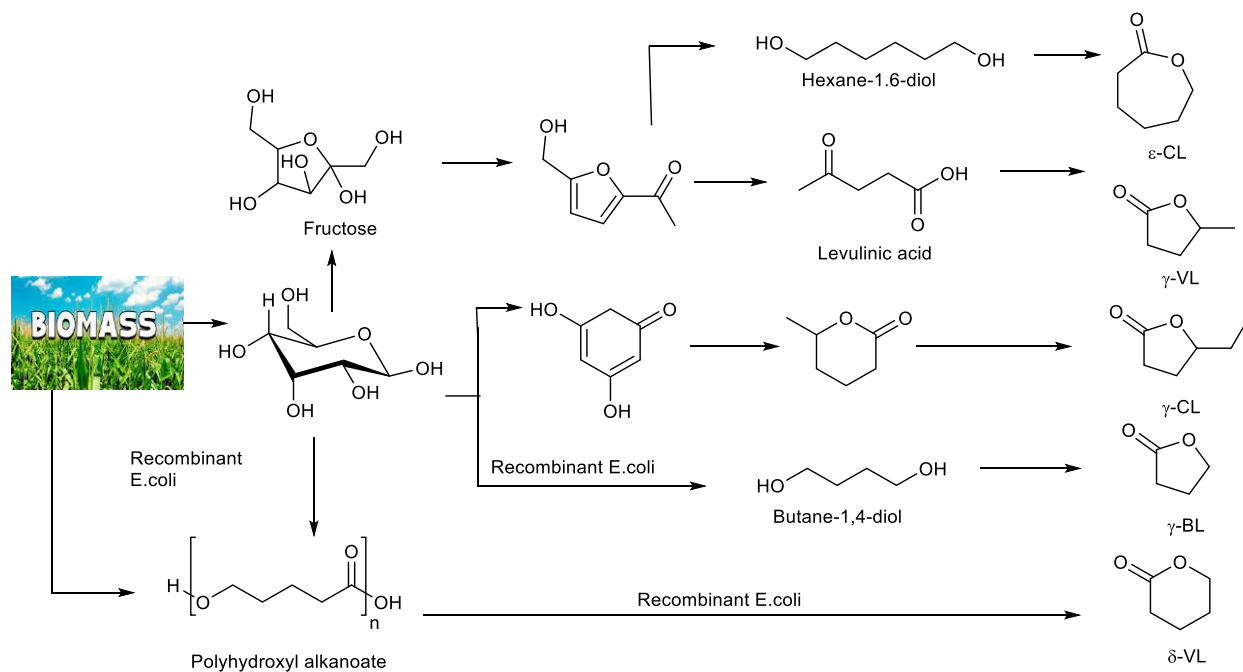
Figure 1.3: ε-Caprolactone (ε-CL), Ƴ-valerolactone (Ƴ-VL), Ƴ-caprolactone (Ƴ-CL), Ƴ-butyrolactone (Ƴ-BL) and σ-valerolactone (σ-VL)[22]
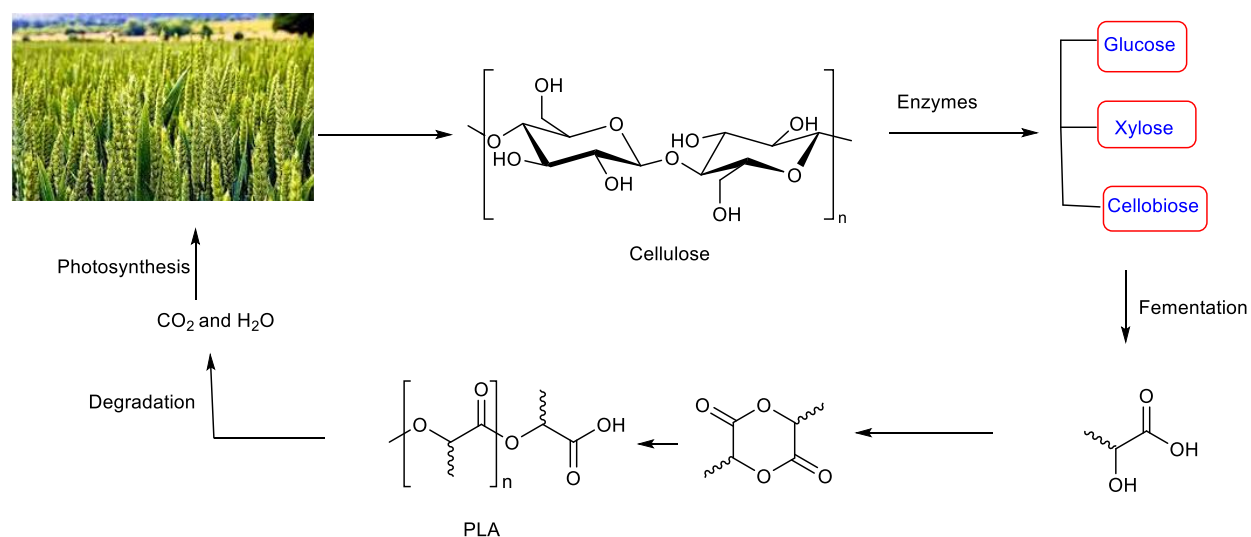
Figure 1.4: Biomass derived polylactic acid[22]

1.3 Ring-opening polymerization synthesis of polyesters

Polyesters can be synthesized with varying molar masses, architecture and stereochemical control through ring-opening polymerization (ROP) of cyclic esters monomers with the common being ε-caprolactone, (ε-CL) and lactides (LAs) (Figure 1.5). The ring-opening reaction is usually initiated by a catalyst. Alcohol can be added as co-initiators furnishing polymer with an alkoxy end group.
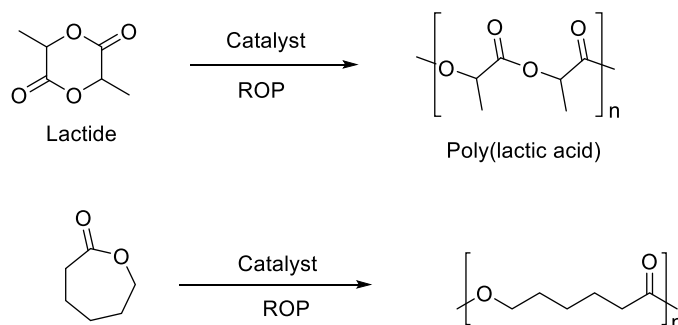
Figure 1.5: Lactides and lactone polymerization

1.4 The structures of lactides and poly(lactides)

Polymeric physical properties such as transition temperature, melting temperature, and tensile strength are dictated by the stereochemistry of the macromolecular backbone. Crystallinity is high in polymers with higher stereoregularity while random polymers are usually amorphous. Monomers with chiral centres polymerize to give polymers with variable microstructures referred to as the polymer tacticity. Lactides comprise of two stereogenic carbons which results in three isomeric forms, L-(*R,R*), D-(*S,S*), and *meso*-(*S,R*) as shown in Figure 1.6. The D/L system tags the entire molecule, while *R/S* classification labels the absolute configuration of each chiral point.
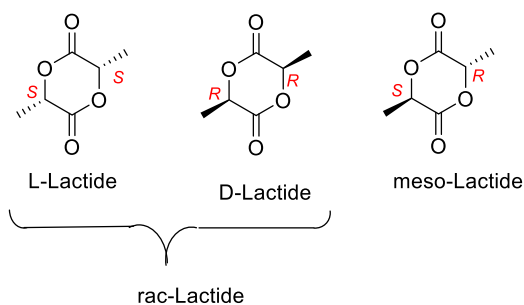
Figure 1.6: Lactic acid stereoisomers

Two head-to-head units in a polymer chain define a diad, and a tetrad, which results from four successive repeating units. Bovey interprets the tacticities as '*i*' (isotactic) or '*s*' (syndiotactic) for matching or interchanging sequences. The notation *meso* (*m*) and *racemic* (*r*) can also be used. Predominately isotactic polymers are obtained *via* polymerization of pure L- and D-lactide monomers. The methyl substituents on the carbon backbone have the same configuration resulting in (*RRRR*) or (*SSSS*) pattern along the chain. Syndiotactic polymers have an alternating methyl groups and the stereogenic carbon configuration alters (*RS* or *SR*).

The *rac*-lactide monomer results in heterotactic polymers where chain units are defined by *RRSS* or *SSRR* configuration. If the chain contains a large *R* and *S* block segments in sequence, then the polymer is referred to as stereo-block, which is a testimony that propagation of one stereoisomer is kinetically preferred. There are two scenarios which result in the formation of stereo-block polymers. The first, is when the other monomer is included in the growing chain after the consumption of the first one, and the second mechanism is when there is a monomer mismatch during formation of first block which is then propagated.

1.4.1   Stereo-controlled polymerization

The tacticity of the PLA is also affected by side reactions which are trans-esterification and epimerization. Trans-esterification can be classified into either inter- or intra-chain. Inter-chain trans-esterification is more profound when the monomers is depleted and this results in polymers with broad molecular weight distributions (PDI). Intra-chain trans-esterification results in cyclic oligomers, which also further diminishes the polymer molecular weights. These phenomena result in stereoirregularity of the growing polymer chains, and affect the polymer tacticity. Polymer tacticity is ellucidated with the help of homonuclear decoupled ^{1}H- and ^{13}C-NMR analysis of tetrad sequences. In the absence of the above mentioned side reactions ROP of lactide monomers results in well resolved tetrad sequences shown in Figure 1.7.
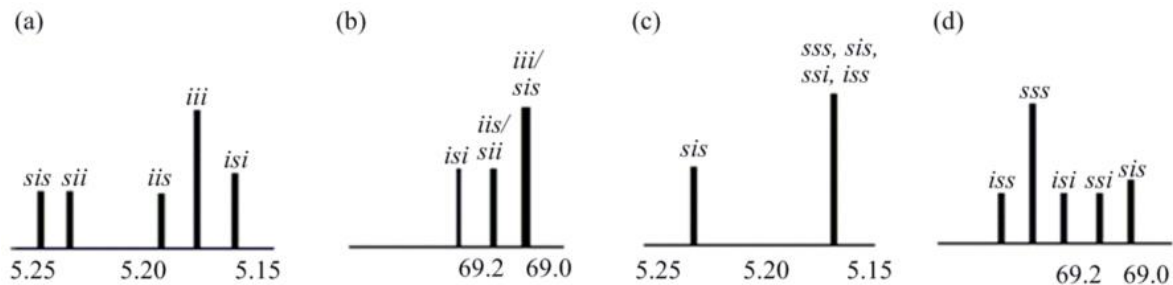
Figure 1.7: ^{1}H-NMR signal shifts (σ ppm) of polylactide tetrad sequences: (a) ^{1}H-NMR spectrum of poly(*rac*-lactide); (b) ^{13}C-NMR spectrum of poly(*rac*-lactide); (c) ^{1}H-NMR spectrum of poly(*meso*-lactide) and (d) ^{13}C-NMR spectrum of poly(*meso*-lactide)

The extent of stereoregularity in lactide polymerization is denoted as the probability of racemic (P_r) or *meso* (P_m) enrichment. The probabilities can be expresses as Bernoullian statistical mathematical expressions (Table 1.1).

Table 1.1: Bernoullian statistical mathematical expressions

	Probability	
Tetrad	*rac*-lactide	*meso*-lactide
[iii]	$P_m^2 + P_rP_m/2$	0
[iis]	$P_rP_m/2$	0
[sii]	$P_rP_m/2$	0
[isi]	$P_r^2/2$	$(P_m^2 + P_rP_m)/2$
[sss]	0	$P_r^2 + P_rP_m/2$
[ssi]	0	$P_rP_m/2$
[iss]	0	$P_rP_m/2$
[isi]	$(P_r + P_rP_m)/2$	$P_m^2/2$

For ROP of r*ac*- or *meso*-lactide, P_r or P_m = 0.5 specifies atactic polymer, while for *rac*-lactide P_r = 1.00 (P_m = 0.00) and P_m = 1.00 (P_r = 0.00) designates exclusive heterotactic and isotactic polymers, respectively. For ROP of *meso*-lactide probability values of P_r = 1.00 (P_m = 0.00) and P_m = 1.00 (P_r = 0.00) define pure syndiotactic and heterotactic polymers, respectively.

1.5   General ROP mechanisms

The most extensively researched ROP catalysts/initiators are organometallic complexes and their mechanism of operation has been a subject under review. Five mechanisms have been put forward and namely, cationic, anionic, activated monomer (AMM) anionic, and coordination-insertion (CIM) and they will be discussed in the following subsections.

1.5.1   Cationic ROP mechanism

The cationic ROP reaction mechanism (Figure 1.8) of cyclic esters involves the generation of positively charged intermediate species, which react with the monomer. The cyclic ring will open *via* an S_N^2 mechanism. The cationic polymerization transformation is poorly regulated, and polymers with low molecular weights are produced.[23] The initial step involves monomer activation by alkylation or protonation of the carbonyl oxygen generating a carbocation intermediate. Nucleophilic attack by an incoming monomer leads to ring-opening through scission of the C—O bond resulting in positively charged species. The propagation step occurs by successive addition of monomers until the polymerization is terminated by protonation.
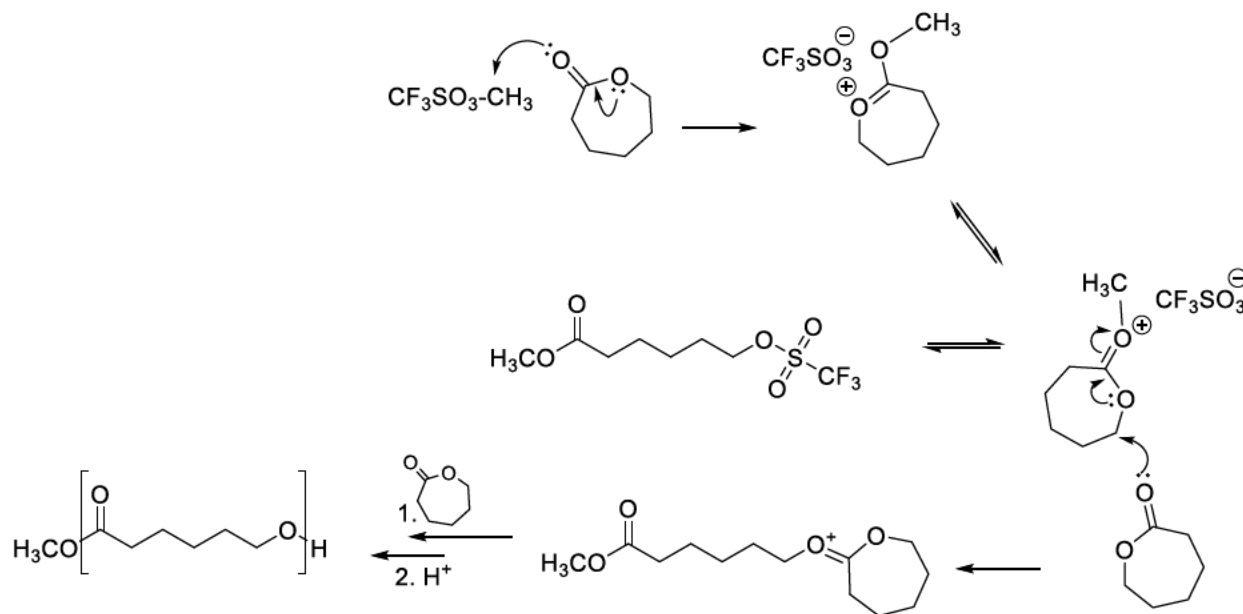
Figure 1.8: Cationic ring-opening polymerization mechanism

1.5.2 Anionic ROP mechanism

In anionic ROP of cyclic ester monomers, a negatively charged nucleophile attacks the carbon near the acyl-oxygen. The ruptured monomer then acts as a nucleophile and the replication of the same process occurs. The bonding of the metal alkoxide in the activated transition state shuttle between ionic and covalent. This depends on the chain end propagating species and the solvent (Figure 1.9).[23]
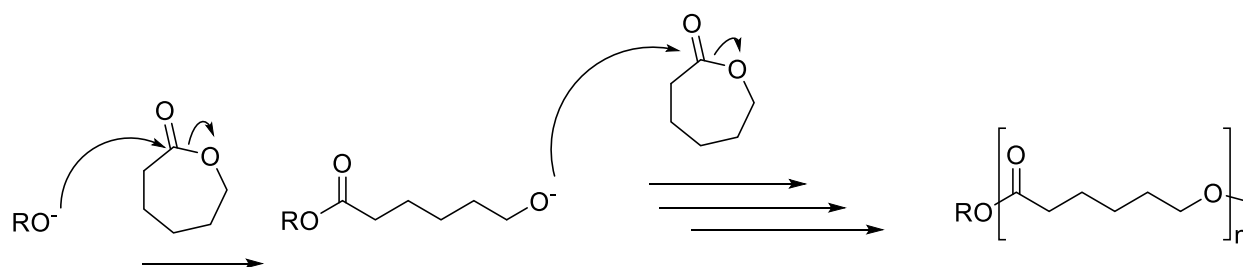
Figure 1.9: Anionic ring-opening polymerization mechanism

1.5.3 Coordination-insertion and activated monomer mechanisms

The coordination insertion mechanism (CIM) (Figure 1.10)[24] has been extensively studied, and is the mostly accepted mechanism. The mode of action has been supported by theoretically studies using density function theory (DFT) computations.[25-29] The first step has been proposed to be the complexation of the monomer *via* the carbonyl oxygen of the cyclic monomer. This enhance the monomer electrophilicity rendering scission of the oxygen-acyl link. The coordination insertion method is a controlled process which allow control of polymer molecular weight, molecular weight distributions (PDI) and epimerization reactions are hindered. Furthermore, it allows synthesis of stereo-regular polymers with well-defined end-group functionalities. In the activated monomer mechanism (AMM) (Figure 1.11)[30,31] an external nucleophile is added, while in CIM, the nucleophile is integrally attached to the active metal centre as an auxiliary ligand. In AMM the monomer is first coordinated to the metal centre for activation. An external nucleophile is then added, e.g. an alcohol (ROH), which then attack the electrophilic carbonyl carbon and initiate the polymerization resulting in the heterocyclic ring rapture of the oxygen–acyl bond.

9
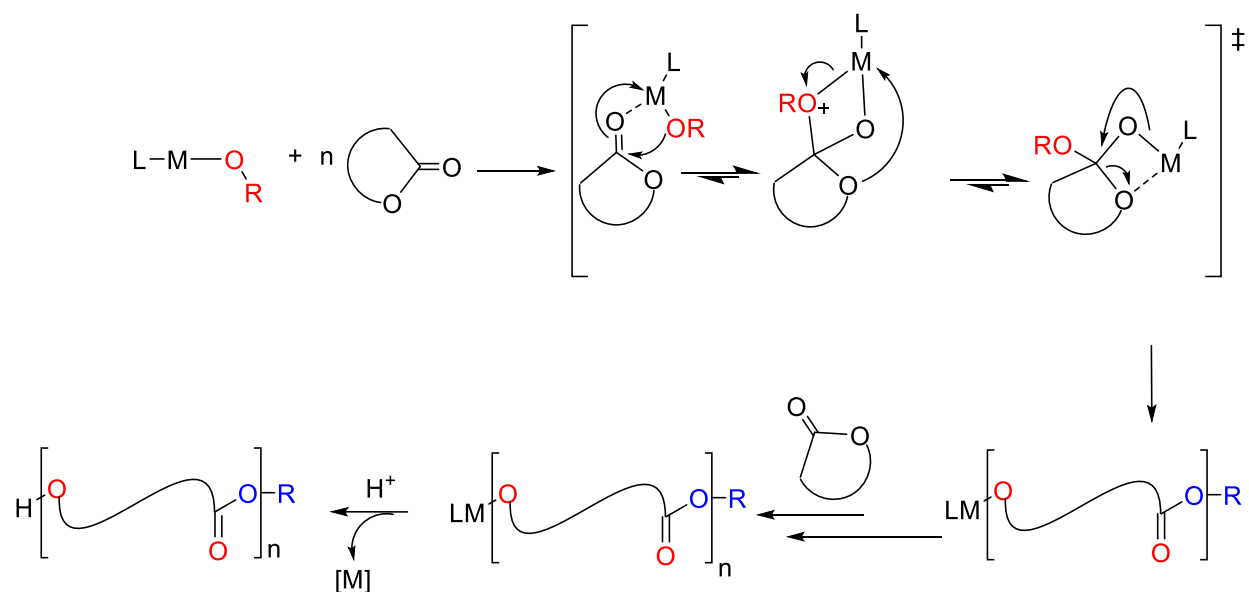
Figure 1.10: ROP coordination insertion mechanism[32]
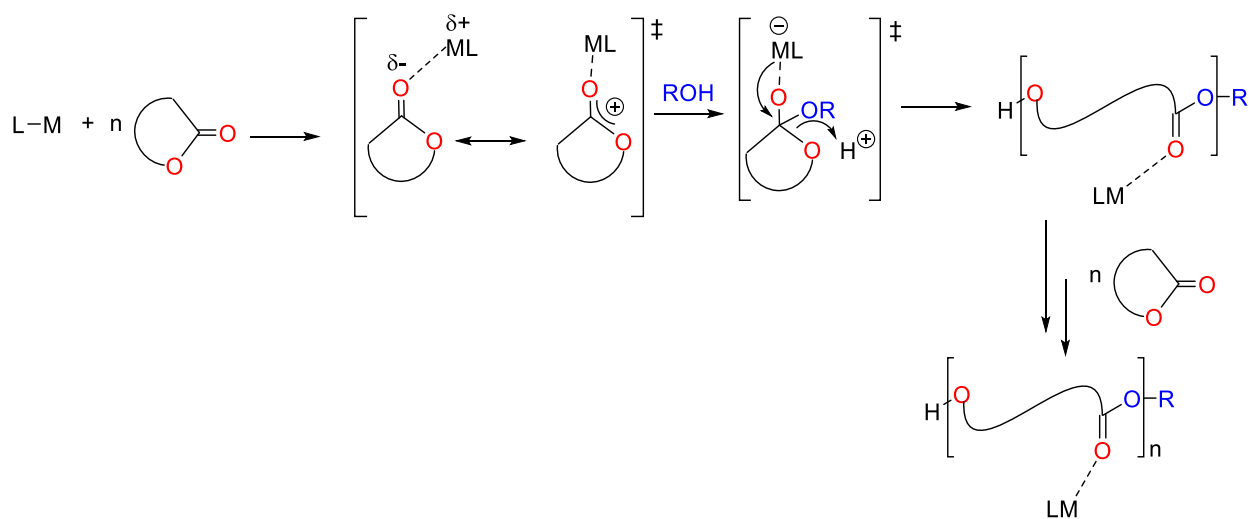
Figure 1.11: ROP activated monomer mechanism[32]

1.6 Thermodynamics and kinetics of ROP reactions

Macromolecules generally results from polymerization of small monomeric units associated with a reduction in entropy of the thermodynamic system. The polymerization process is promoted at low temperature while, the reverse process is only favoured at a higher temperature. The entropy change (ΔS_p) is typically negative and renders the $-T\Delta S_p$ term positive in the Gibb's free energy relationship equation (**1.1**),

$$\Delta G_p = \Delta H_p - T\Delta S_p \qquad (\mathbf{1.1})$$

where ΔH_p = enthalpy of polymerization, T = temperature and ΔG_p = Gibb's free energy

At comparatively elevated temperatures, $-T\Delta S$ is positive such that the overall chemical process becomes endergonic. The system temperature when, $\Delta G = 0$ is referred to as the ceiling temperature, T_c and defined by equation (**1.2**).[33,34]

$$T_c = \frac{\Delta H_p}{\Delta S_p} \qquad (\mathbf{1.2})$$

"T_c is the temperature at or above which the concentration of monomer in equilibrium with its polymer becomes essentially equal to the initial monomer concentration". The fundamental thermodynamic principles of this concept was explained by Dainton and Irvin, [35] who argued that this phenomenon is largely influenced by the initial monomer concentration. This leads to the derivation of Dainton's equation (**1.3**).[36]

$$T = \frac{H_p}{S_p + R\ln[M]_{eq}} \qquad (\mathbf{1.3})$$

Ring strain propels the polymerization process and is coupled to entropy reduction, owing to loss in translational degrees of motion. Disregarding the monomer-solvent interactions affects the enthalpy of polymerization can give an idea about the ring strain. The polymerization process becomes thermodynamically feasible only when the enthalpy contribution into ΔG dominates; hence larger ring strain corresponds to lower equilibrium monomer concentration ($[M]_{eq}$).

Polymerization reaction rates are defined by the change in monomer concentration as a function of time that is converted to a polymer. The change in monomer [M] and polymer [P] concentration per given time is expressed by rate equations **1.4** and **1.5**.

$$Rate = \frac{-d[M]}{dt} \qquad (\mathbf{1.4})$$

$$Rate = \frac{d[P]}{dt} \qquad (\mathbf{1.5})$$

Then polymerization rate for an nth order reaction can be expressed as shown in equation (**1.6**)

$$Rate = k[M]^n \qquad (\mathbf{1.6})$$

where $k = k_p[I]^x$; k_p = chain propagation rate, I = initiator; and x = order of reaction. The integrated rate law is expressed by equation (**1.7**).

$$In[M]_t - In[M]_0 = -kt \qquad (\mathbf{1.7})$$

Hence, the semi-logarithmic plots of $\ln([M]_0/[M]_t)$ *vs* time are linear and the rate constants can be extrapolated from the slope. Depending on the reaction time scale and monomer functionalities different instrumental techniques can be utilized to monitor the polymerization reaction. These include nuclear magnetic resonance (NMR),[37] infrared (IR),[38] Raman,[39] and ultraviolet–visible (UV/Vis)[40] spectroscopy techniques. Among these, NMR has proven to be a more powerful tool in polymerization reaction monitoring[41-43] and polymer characterization.[37,44-48]

1.7 Statement problem and rationale

Among the bulk materials, the usage of polymeric or plastics reached 322 million tons in 2015 and the trend is predicted to continue in comparison to conventional materials like glass and metal. The major concern is that most of the plastics are obtained from non-renewable, fossil fuel feedstocks. Also, the ever-increasing oil price, which is the main feedstock source, results in exorbitant production cost. In addition, waste management and environment destiny of these non-biodegradable materials is also a major concern. There is consensus among scientists and industrialists to move away from the use of petroleum based polymeric materials. Polyesters such as polylactic acid (PLA) and poly(ε-caprolactone) (PCL) have been listed as potential replacements. Commercially, tin(II) complexes have been used as initiators or catalysts for the synthesis of polyesters, but there are growing fears over its toxicity.

This poses a challenge toward their use in the production of polymers for medical applications, since, the elimination of residual catalyst from the polymer is a challenge.

1.8   Justification of study

Polyesters are biodegradable, bio-renewable and bio-derived and their applications range from medicine,[2,3] packaging,[4] and electronic devices,[6] among other applications. Owing to the toxicity of tin(II) compounds, complexes of metals such as zinc,[49-52] magnesium,[53-56] calcium[57-59] and copper[60-62] are now being investigated as alternatives because they are cheap and non-toxic. Metal-complex initiated ROP allows control over molecular parameters such as polydispersity index (*PDI*), molecular weight (*M_w*) and end-group functionality. The main aim of this project was to contribute toward the progress in search of non-toxic catalytic systems that will produce polymers with desirable physio-chemical properties.

The use of amidine and Schiff base ligand derivatives was necessitated by their modification flexibility and ease of synthesis. They are also capable of exhibiting different coordination modes and the ligand motifs have been found to greatly influence the catalytic behaviour of the organometallic catalyst. It was envisioned that careful modification of the electronic and steric environment around the ligand can intrinsically alter the polymerization behaviour and polymer microstructure.

The ligands of choice are the amidine (formamidines, type I and II) and imino-pyridinyl type ligands (III and IV) (Figure 1.12). These ligands are no strangers in the field of catalysis but their use in ROP has not been fully exploited. They are coined "privileged ligands" and are extensively used owing to their versatile synthesis, ability to stabilize many oxidation states and good solubility.   Stereogenic centres or chirality can be introduced thereby influencing observed molecular weights, molecular weight distributions and macromolecular backbone stereochemistry.

(I)   (II)

(III)   (IV)

R' = 2-furanyl, 2-thiophenyl, 2 or 4-pyridinyl
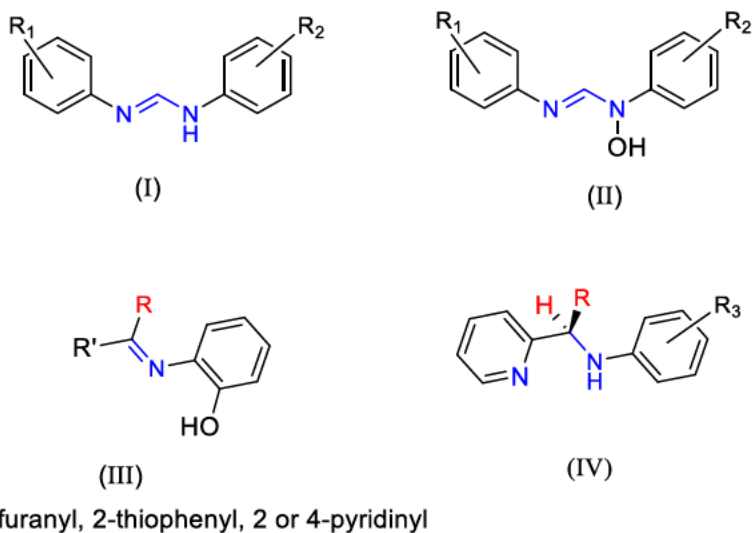
Figure 1.12: Types of ligands used in this study to support metal complexes

The chosen set of ligands also allow a comparative study to see the effect of varying the imine bridge. The span of the linking bridge between two donor atoms in bi-chelate ligands plays a fundamental part in catalysis and it is closely associated with the preferred coordination mode. Reported metal complexes of amidine ligands coordinating as a mono-dentate, bi-dentate through the nitrogen lone pairs and interestingly *via* π-electrons (Figure 1.13d).[63]

κN-monodentate κ^2N-chelate μ-κN,κN-bridging δ-π-coordination

a   b   c   d
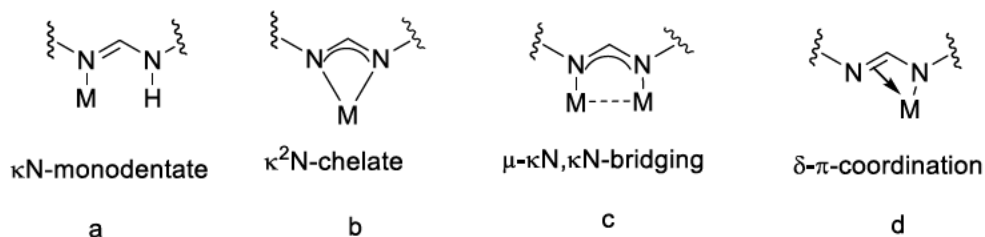
Figure 1.13: Amidine coordination modes

The resultant coordination mode is conferred by the steric and electronic environment around the ligand. Nitrogen and oxygen donor ligands and are usually strong σ-donors, while the π-character is hinged on the ligand skeleton. The introduction of other soft donor heteroatoms such as phosphorus and sulphur results in hemilabile ligands with outstanding coordination flexibility.[64]

14

1.9 Aim

The main objective of the project is to design and synthesize *N*-, and/or *O*-donor ligands and use them in the synthesis of complexes and evaluate their catalytic activity in ROP of cyclic esters.

1.10 Objectives

- To synthesis and characterize of *N,N′*-diarylformamidine ligands and their corresponding Zn(II) and Cu(II) complexes and to investigate the effect of ligand framework and synthesis method on coordination behaviour.
- To modify the structures from above to form *N,O*-type *N*-hydroxyl-*N′*-diarylformmidine ligands and use them in the synthesis of their Zn(II) and Cu(II) complexes.
- To synthesise and characterize Schiff base imino-pyridinyl derivatives and their respective Zn(II), Cu(II) and Mg(II) complexes.
- To apply the synthesized complexes as initiators or catalyst in ROP of cyclic esters.
- To study the polymerization kinetics and polymer microstructures of the resultant polymers.

1.11 Thesis outline

In this thesis we have designed and synthesised ROP metal complexes catalytic systems supported by different ligands. The studies are presented in four chapters based on four ligand systems.

Chapter 3 present the synthesis of formamidine Cu(II) and Zn(II) complexes and their application in ROP of *rac*-lactide and ε-caprolactone.

Chapter 4 details the synthesis of *N*-hydroxy-*N,N′*-diaryformamidine ligands, their corresponding Cu(II) and Zn(II) complexes. The application of the metal complexes in ROP of cyclic esters is also discussed.

Chapter 5 Discusses the synthesis of Mg(II) and Zn(II) pyridyl phenoxide complexes and their application in ROP.

Chapter 6 explores the use of chiral Zn(II) complexes in homo- and co-polymerization of ε-caprolactone and lactides

Finally, general conclusions on the key findings of this study and research prospects are presented in **Chapter 7**

References

1. R. T. Mathers and M. A. R. Meier, *Green polymerization methods: Renewable starting materials, catalysis and waste reduction*, Wiley-VCH Verlag, Weinheim, Germany, 2011.

2. M. Kashif, B.-m. Yun, K.-S. Lee and Y.-W. Chang, *Mater. Lett.*, **2016**, 166, 125.

3. K. Jelonek and J. Kasperczyk, *Polimery*, **2013**, 58, 858.

4. S. Hong, K.-D. Min, B.-U. Nam and O. O. Park, *Green Chem.*, **2016**, 18, 5142.

5. F. Carrión, L. Montalbán, J. I. Real and T. Real, *Sci. World J.*, **2014**, 2014, 526346.

6. N. Jürgensen, J. Zimmermann, A. J. Morfa and G. Hernandez-Sosa, *Sci. Rep.*, **2016**, 6, 36643.

7. B. P. Mooney, *Biochem. J*, **2009**, 418, 219.

8. B. Surnar, K. Sharma and M. Jayakannan, *Nanoscale*, **2015**, 7, 17964.

9. S. Sebastian Payyappilly, S. Dhara and S. Chattopadhyay, *Soft Matter*, **2014**, 10, 2150.

10. H. Gheybi and M. Adeli, *Polym. Chem.*, **2015**, 6, 2580.

11. Z. Ge and S. Liu, *Chem. Soc. Rev.*, **2013**, 42, 7289.

12. D. Zhou, S. He, Y. Cong, Z. Xie, X. Chen, X. Jing and Y. Huang, *J. Mater. Chem. B.*, **2015**, 3, 4913.

13. T. Eom, W. Yoo, Y.-D. Lee, J. H. Park, Y. Choe, J. Bang, S. Kim and A. Khan, *J. Mater. Chem. B.*, **2017**, 5, 4574.

14. A. Duro-Castano, J. Movellan and M. J. Vicent, *J. Biomater. Sci.*, **2015**, 3, 1321.

15. W. Chen, L. A. Shah, L. Yuan, M. Siddiq, J. Hu and D. Yang, *RSC Advances*, **2015**, 5, 7559.

16. A. Ehrlich, S. Booher, Y. Becerra, D. L. Borris, W. D. Figg, M. L. Turner and A. Blauvelt, *J. Am. Acad. Dermatol.*, **2004**, 50, 533.

17. R. Tong and J. Cheng, *Polym. Rev.*, **2007**, 47, 345.

18. F. H. Isikgor and C. R. Becer, *Polym. Chem.*, **2015**, 6, 4497.

19. M. Imteyaz Alam, S. De, S. Dutta and B. Saha, *RSC Advances*, **2012**, 2, 6890.

20. G. L. Gregory, E. M. Lopez-Vidal and A. Buchard, *Chem. Commun.*, **2017**, 53, 2198.

21. T. Buntara, S. Noel, P. H. Phua, I. Melián-Cabrera, J. G. de Vries and H. J. Heeres, *Angew. Chem. Int. Ed.*, **2011**, 50, 7083.

22. S. Gupta, R. Arora, N. Sinha, M. I. Alam and M. A. Haider, *RSC Advances*, **2016**, 6, 12932.

23. B. M. Mandal, *Fundamentals of polymerization*, World Scientific, New Jersey; London, 2013.

24. A. Kowalski, A. Duda and S. Penczek, *Macromolecules*, **2000**, 33, 7359.

25. I. del Rosal, P. Brignou, S. M. Guillaume, J.-F. Carpentier and L. Maron, *Polym. Chem.*, **2015**, 6, 3336.

26. J. Fang, I. Yu, P. Mehrkhodavandi and L. Maron, *Organometallics*, **2013**, 32, 6950.

27. J. Ling, J. Shen and T. E. Hogen-Esch, *Polymer*, **2009**, 50, 3575.

28. M. O. Miranda, Y. DePorre, H. Vazquez-Lima, M. A. Johnson, D. J. Marell, C. J. Cramer and W. B. Tolman, *Inorg. Chem.*, **2013**, 52, 13692.

29. I. D. Rosal, R. Poteau and L. Maron, *Dalton Trans.*, **2011**, 40, 11228.

30. H. R. Kricheldorf, I. Kreiser-Saunders and C. Boettcher, *Polymer*, **1995**, 36, 1253.

31. H. R. Kricheldorf, I. Kreiser-Saunders and A. Stricker, *Macromolecules*, **2000**, 33, 702.

32. N. Ajellal, J.-F. Carpentier, C. Guillaume, S. M. Guillaume, M. Helou, V. Poirier, Y. Sarazin and A. Trifonov, *Dalton Trans.*, **2010**, 39, 8363.

33. M. P. Stevens, *Polymer Chemistry: An Introduction*, Oxford University Press, New York, 1999.

34. A. Duda and A. Kowalski, in *Handbook of ring-opening polymerization*, Wiley-VCH Verlag GmbH & Co. KGaA, 2009,1.

35. F. Dainton and K. Ivin, *Nature*, **1948**, 162, 705.

36. S. Penczek, *J. Polym. Sci, Part A: Polym. Chem.*, **2002**, 40, 1665.

37. D. M. Savant, D. V. Reddy, E. F. McCord and P. L. Rinaldi, *Macromolecules*, **2007**, 40, 4199.

38. J.-N. Ollagnier, T. Tassaing, S. Harrisson and M. Destarac, *React. Chem. Eng.*, **2016**, 1, 372.

39. S. Parnell, K. Min and M. Cakmak, *Polymer*, **2003**, 44, 5137.

40. K. Kaastrup, A. Aguirre-Soto, C. Wang, C. N. Bowman, J. W. Stansbury and H. D. Sikes, *Polym. Chem.*, **2016**, 7, 592.

41. M. Duewel, N. Vogel, C. K. Weiss, K. Landfester, H.-W. Spiess and K. Münnemann, *Macromolecules*, **2012**, 45, 1839.

42.   J. B. McLeary, F. M. Calitz, J. M. McKenzie, M. P. Tonge, R. D. Sanderson and B. Klumperman, *Macromolecules*, **2004**, 37, 2383.

43.   M. A. Vargas, M. Cudaj, K. Hailu, K. Sachsenheimer and G. Guthausen, *Macromolecules*, **2010**, 43, 5561.

44.   D. R. Holycross and M. Chai, *Macromolecules*, **2013**, 46, 6891.

45.   J. U. Izunobi and C. L. Higginbotham, *J. Chem. Educ.*, **2011**, 88, 1098.

46.   S. C. Shit and S. Maiti, *Eur. Polym. J.*, **1986**, 22, 1001.

47.   K. A. M. Thakur, R. T. Kean, E. S. Hall, J. J. Kolstad, T. A. Lindgren, M. A. Doscotch, J. I. Siepmann and E. J. Munson, *Macromolecules*, **1997**, 30, 2422.

48.   K. A. M. Thakur, R. T. Kean, E. S. Hall, J. J. Kolstad and E. J. Munson, *Int. J. Polym. Anal. Charact.*, **1998**, 4, 379.

49.   L. Lin, Y. Xu, S. Wang, M. Xiao and Y. Meng, *Eur. Polym. J.*, **2016**, 74, 109.

50.   R. Petrus and P. Sobota, *Dalton Trans.*, **2013**, 42, 13838.

51.   G. Schwach, J. Coudane, R. Engel and M. Vert, *Polym. Int.*, **1998**, 46, 177.

52.   C.-H. Wang, C.-Y. Li, B.-H. Huang, C.-C. Lin and B.-T. Ko, *Dalton Trans.*, **2013**, 42, 10875.

53.   V. Balasanthiran, M. H. Chisholm, K. Choojun, C. B. Durr and P. M. Wambua, *Polyhedron*, **2016**, 103, Part B, 235.

54.   P.-S. Chen, Y.-C. Liu, C.-H. Lin and B.-T. Ko, *J. Polym. Sci, Part A: Polym. Chem.*, **2010**, 48, 3564.

55.   C. Jian, J. Zhang, Z. Dai, Y. Gao, N. Tang and J. Wu, *Eur. J. Inorg. Chem.*, **2013**, 2013, 3533.

56.   J.-C. Wu, B.-H. Huang, M.-L. Hsueh, S.-L. Lai and C.-C. Lin, *Polymer*, **2005**, 46, 9784.

57.   J. M. Colwell, E. Wentrup-Byrne, G. A. George and F. Schué, *Polym. Int.*, **2015**, 64, 654.

58.   L. Piao, Z. Dai, M. Deng, X. Chen and X. Jing, *Polymer*, **2003**, 44, 2025.

59.   Z. Zhong, P. J. Dijkstra, C. Birg, M. Westerhausen and J. Feijen, *Macromolecules*, **2001**, 34, 3863.

60.   S. H. Ahn, M. K. Chun, E. Kim, J. H. Jeong, S. Nayab and H. Lee, *Polyhedron*, 127, 51.

61.   D. Appavoo, B. Omondi, I. A. Guzei, J. L. van Wyk, O. Zinyemba and J. Darkwa, *Polyhedron*, **2014**, 69, 55.

62. J. Cho, S. Nayab and J. H. Jeong, *Polyhedron*, **2016**, 113, 81.

63. F. T. Edelmann, *Advances in the coordination chemistry of amidinate and guanidinate Ligands*, Anthony F. Hill and Mark J. Fink. The Netherlands: Elsevier, 2008.

64. J. C. Jeffrey and T. B. Rauchfuss, *Inorg. Chem.*, **1979**, 18, 2658.

Chapter 2   Literature review

A perspective into ring-opening polymerization of ε-caprolactone and lactides: Effects of, ligand, catalyst structure and system dynamics, on activity and polymer properties

Abstract

Catalysts are at the core of many chemical transformations and research is dedicated toward innovation of more efficient and selective catalysts. Catalyst structural features greatly influence catalyst performance, and this review discusses the effects of ligand and catalyst structure and system dynamics, on activity and polymer properties. The effects of associated catalyst components such as initiating groups, ligand chirality and stereochemistry in relation to catalyst activity and polymer properties were also reviewed. The effects of metal nuclearity and catalyst flexibility on activity was also reviewed. The effect of solvent and temperature was briefly considered.

2   Introduction

Catalytic ring-opening polymerization (ROP) reactions have had incredible influence on the synthesis of polyesters with distinctive, molecular weights, microstructures, molecular weights distributions and end group functionalities. These processes have mostly been effectively mediated by metals complexes synthesised using alkali metals,[1-3] copper,[4,5] iron,[6,7] indium[8] magnesium,[9,10] tin[11,12] and zinc[13,14] among others. Among these, magnesium complexes have shown greater activity compared to the other systems.[10,15-17] In the reactions involving metal complexes, ROP reactions are normally multicomponent systems, consisting of the catalyst or initiator, monomer, and in some cases co-initiator. In industry currently, tin(II) complexes are mostly used because it is highly active commercially available, easy to handle. However, they come with the disadvantages of toxicity, and high polymerization temperatures which promote inter- and intra-molecular transesterification reactions compromising polymerization control.

To circumvent the above disadvantages, there is an increased interest in the design of ROP catalysts that are active, less toxic and selective hence, in the process a whole assortment of

catalytic systems were made. Of the designed catalysts, ligand-supported metal complexes show a lot of promise.[18-21] The ligand structures have a significant impact on the product composition, selectivity and productivity in polymerization reactions.[22-25] Current studies of ROP are focused on the use of *N*- and/or *O*-ligands stabilized metal-based catalysts.[13,26-29] Ligands with soft donor atoms such as *P* and *S* have however been seldom explored, regardless of their positive effect in ROP reaction processes.[14,30-32] Previous studies have shown the benefits of including such soft donor atoms in improving catalyst performance and polymer properties.[33-35]

Many polymer properties depend on molecular weights and molecular weight distributions. The molecular weights are usually expressed as the weight average-molecular weights (M_w) and number-average molecular weights (M_n). The ratio M_w/M_n (also called polydispersity index or PDI) define the molecular weight distribution and it approaches a unit for a controlled polymerization process.[36] There are few manipulations that can be used to increase the molecular weights and reduce the PDI values. One such manipulation is the reduction in the concentration of the initiating species to reduce the number of growing chains per centre, which then enables the chains to grow to full length. Another manipulation is to reduce transesterification reactions of which should reduce chain shuttling and subsequently the chain lengths.[37]

The focus of this review is to give an understanding of ring-opening polymerization process by correlating catalyst structure with activity and polymer structures. The selected examples were chosen to explain the principles under consideration, which will serve as a starting point. The influence of ligand structure on activity and polymer properties is highlighted with emphasis on steric and electronic properties, and chirality. The influence of general catalyst structural features such as initiation groups, nuclearity and rigidity as well as an analysis of reaction variables are considered.

2.1 ROP catalysts structural features

A complete structural characterization of ligands and complexes used in ROP can shed more light in unravelling reaction mechanisms and can provide important information about catalyst design and efficiency. A typical ROP metal-based catalyst is comprise of the metal centre ligated with reactive and auxiliary ligands. When only one metal centre is present, the catalysts are normally termed "single-site catalysts" and denoted with a general formula (L_n-M-X), where L is the auxiliary ligand and n the equivalents coordinated to the active metal centre (M) and X is the reactive initiating group. In literature, the words catalyst or initiator are interchangeably used. In principle, most compounds used perform both functions where one fragment (initiating group) of the molecule initiates the reaction while the other part act as the catalyses. The following subsection will discuss the correlation between the initiating groups/ligands types and activity.

2.2 Types of initiating ligands

Ring opening polymerization is characterised by three steps namely initiation, propagation and termination. The initiation step is paramount to the process hence, catalyst design must factor in the prerequisite condition for this process. Several initiating groups have been investigated which include, carboxylates,[38,39] alkoxides[40,41] and amides.[15,42] These groups can be integrated into the ligands system or they can be attached as separate auxiliary ligands. In other scenarios, they are added as external nucleophiles during the polymerization reaction where they are referred to as chain transfer agents. Alkoxides are the most effective initiators compared to the others, hence many studies are devoted to probing such systems. The following sub-sections will discuss in detail the mentioned initiating groups.

2.2.1 Carboxylate type initiating ligands

The carboxylate-based tin(II)bis-(2-ethylhexanoate) ($Sn(Oct)_2$), laid the foundation for metal complex based catalytic ROP since its conception. The tin(II) catalysts appear to be the most active and are predominant utilized in industrial production of aliphatic polyesters. The complexes display a variety of structures in which, the carboxylate ligands assume a range of bonding modes (Figure 2.1), which including monodentate (a), chelating (b), bridging (c), symmetric and asymmetric (d) and monodentate bridging (e).

The stereo-electronic environment hugely influences the bonding mode is of the carboxylate ligands. The various bonding modes generally results in varying initiation efficiencies. The chelate bridging modes are generally more binding which eventually results in slow initiation and polymerization rates. On the other hand, monodentate, symmetric and asymmetric modes are weakly binding hence more active.[18]
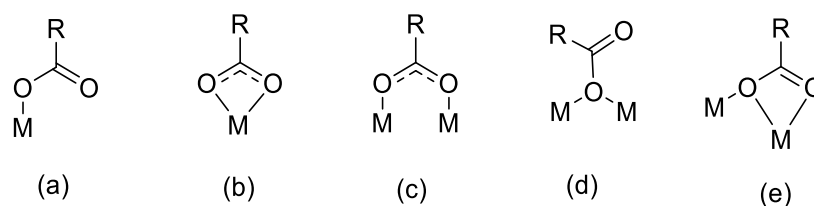
Figure 2.1: Carboxylate coordination modes

Research by our group[18,39] has investigated less toxic formamidine zinc and copper complexes with acetate and benzoate auxiliary ligands (Figure 2.2). Complex **2.0** exhibited a short induction period compared to complex **2.1** in ROP of ε-CL and L-LA. The same trend was observed in complexes **2.2** and **2.3**. The metal centres in complex **2.1** are arguably slightly crowded because of low repulsion of the methyl groups, which cause the ligands to approach more towards the metal compared to the bulk isopropyl groups. Presumably, the steric factors are comparable in both cases and the activities depend on the difference in the coordination modes of the acetate groups. Complex **2.1** with acetate groups was less active than complex **2.3** with benzoate groups. These findings resonance with the principle that benzoates are generally loosely bound to the metal centre, hence making them more reactive that the acetates.
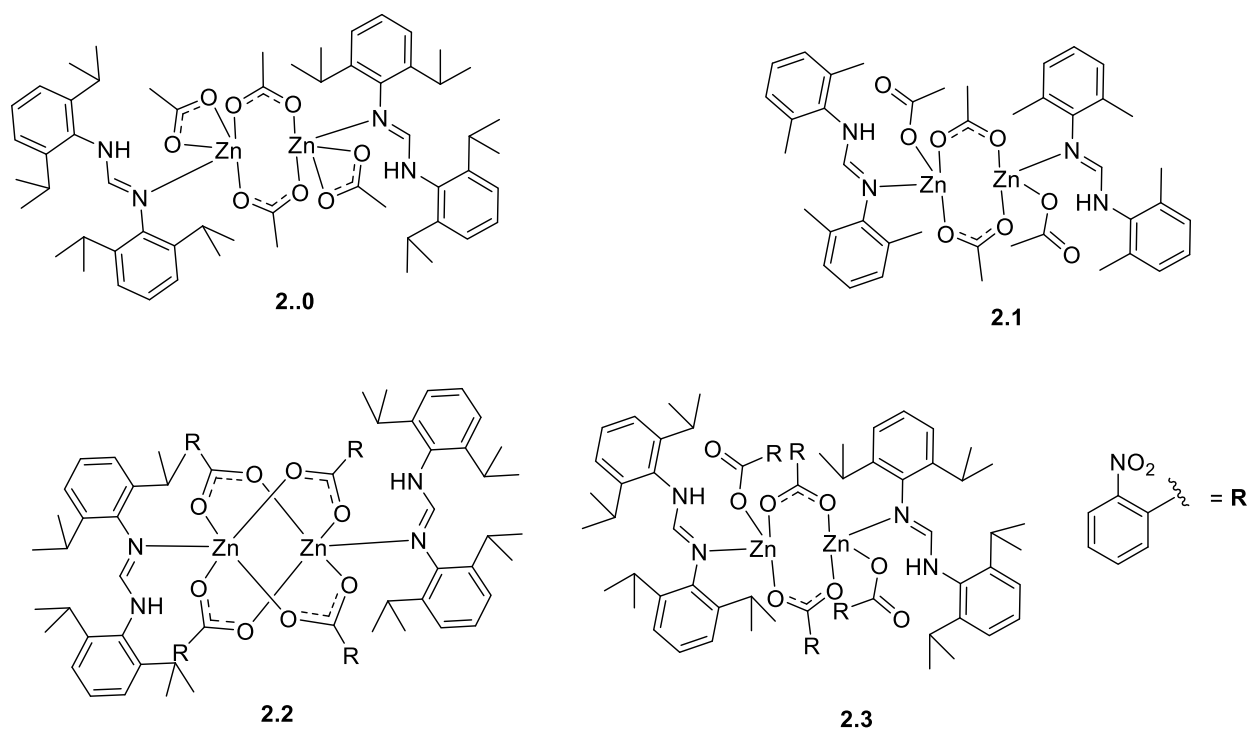
Figure 2.2: Formamidine zinc acetate and benzoate complexes

2.2.2 Alkoxy, alkyl and amide initiating ligands

Alkoxy, alkyls and amides are the most studied initiating groups and have proved to be more effective. Among these the alkoxy are the most active and they result in a controlled polymerization processes.[40,41] Alkyl complexes are seldom used due to their instability and difficulty in isolation. In most cases, they are used as intermediates to generate alkoxy species *in-situ*.[43] The difference in initiation efficiency and activity of alkoxides, alkyls and amides lies in the variation between the polarities of the metal-oxygen, metal-carbon and metal-nitrogen bonds, which are broken during the initiation step.

The effect of integrating the oxygen in the ligand framework together with alkoxyl was investigated by Fliedel *et al*[14] using phosphino phenolates alkoxides in ROP of ε-CL (Figure 2.3). Under similar conditions complex **2.4** was active while **2.5** did not show any activity eliminating the possibility of initiation through metal-O_{ligand} (Zn-O_{ligand}) bond. This implies that in this instance, the oxygen binds strongly for the bond to be activated for initiation. However, the addition of benzyl alcohol to generate the benzyl alkoxide species *in-situ* resulted in increased

24

activity for complex **2.5**. Other catalytic systems have been reported which are capable of initiation *via* the M—O$_{ligand}$ bond. One such examples is the zinc guanidine complexes reported by Schafer *et al*[44] (Figure 2.3). Complexes **2.6** and **2.7** showed similar activities despite the different auxiliary halides ligands. The guanidine ligand fragment was part of the polymers isolated confirming its involvement in the initiation step.

R = Me, ^{t}Bu
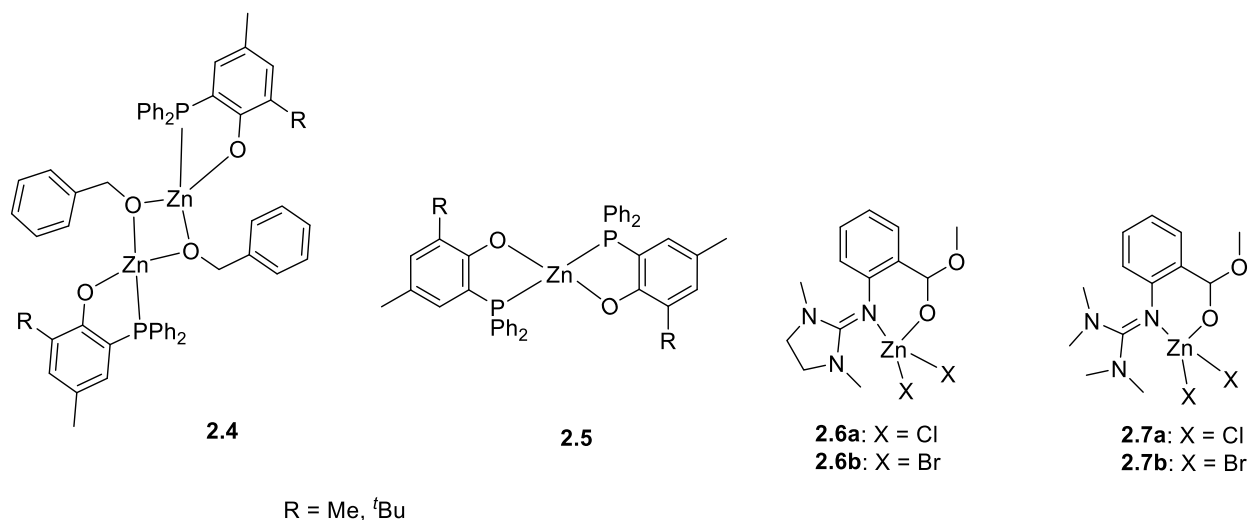
Figure 2.3: Zinc phenoxide and guanidine complexes for ROP

In principle, alkoxides are more active than the amide analogues a trend exhibited by many catalytic systems[45-47] due to the diffrence in nucleophilicity of the M—N and M—O bonds. However, a contrasting trend was observed by Thevenon *et al*[48] using zinc complexes supported by Schiff base ligands (Figure 2.4). Extremely high activities were realised using the amide complex **2.9** compared to **2.8**. The crystal structures analysis of complexes **2.8** and **2.9**, showed that the M—O and M—N bond distances are almost similar and in **2.8** the alkoxide bridge the two metals. Therefore, the difference in activity was attributed to the structural geometry, where the ligand framework in **2.9** is folded exposing the metal centres in contrast to **2.8** where the bridging alkoxide maintains a planar ligand conformation. It appears that the initiator bond strength is not the only factor that determine initiation efficiency but also structural effects.
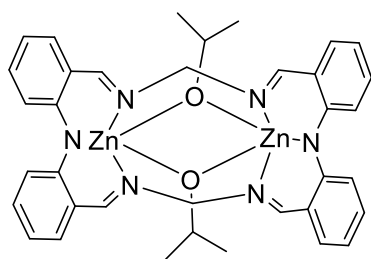
2.8
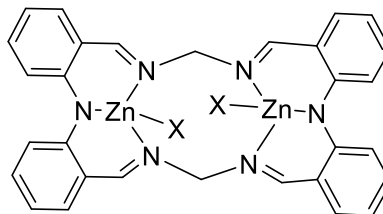
2.9: X = N(SiMe₃)₂

Figure 2.4: Schiff base zinc amide and alkoxide complexes

The nature of the alkoxide also influences the activity as well as polymer properties. The use of aromatic and phenoxy as initiating groups in ROP is seldom explored due to their low nucleophilicity compared to alkoxyl counterparts. Hao *et al*[47] studies the effect of three different initiating groups in complexes **2.10** – **2.12** (Figure 2.5) having 2-aminobenzyl, 9-hydroxyfluorenyl, and trans-4-aminocyclohexyl moieties, respectively. Complex **2.10** with 2-aminobenzyl alkoxide was the most active compared to complexes **2.11** and **2.12** bearing 9-hydroxyfluorenyl, and trans-4-aminocyclohexyl groups, respectively. Looking at the Al—O bonds range between 1.701 and 1.709 Å and are almost similar, which seems to suggest that the activity is comparable. Therefore, the difference in activity can be attributed to structural dynamics. The fluorenyl derivative complex **2.11** gave low molecular weight polymers with a value of 7271 compared to 17 650 and 12 684 g mol⁻¹ for complexes **2.10** and **2.12**, respectively. This reduction can be associated to greater steric hinderance of the fluorenyl group which can inhibit monomer approach towards the metal centre.
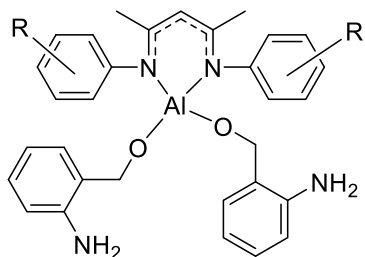
2.10
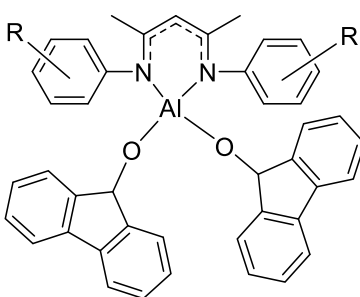
2.11
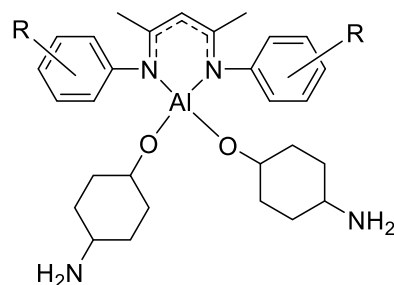
2.12

R = 2.6-*i*Pr

Figure 2.5: Aluminium diketiminato complexes

In an effort to understand the correlation between initiator structural effects with activity Chile *et al*[49] studied an indium system with alkoxyl and aromatic initiating groups (Figure 2.6). As expected, the polymerization for the alkoxy derivative complex **2.13** was higher than that of the aromatic derivatives complexes **1.14a** -**1.14e**. For the *para* substituted aromatic series rates decreased as the electron-withdrawing potency increased. Noteworthy, the complex with a *para* substituted nitro phenoxy group was virtually inactive. This trend is attributed to reduced nucleophilicity associated with low electron density induced by the electron withdrawing groups. The study was extended by investigating the effect of adding diol compounds **2.16** – **2.19** to complex **2.13**. Activity was only observed for 1,5-naphthalenediol (**2.19**), while the rest completely prevented polymerization. The crystal structure of isolated complex after adding compound **2.17** showed that the diol chelates one of the indium metal centre, which hinders monomer coordination as both metals are involved in polymerization.

R = **a** = H, **b** = Me, **c** = OMe, **d** = Br, **e** = NO$_2$
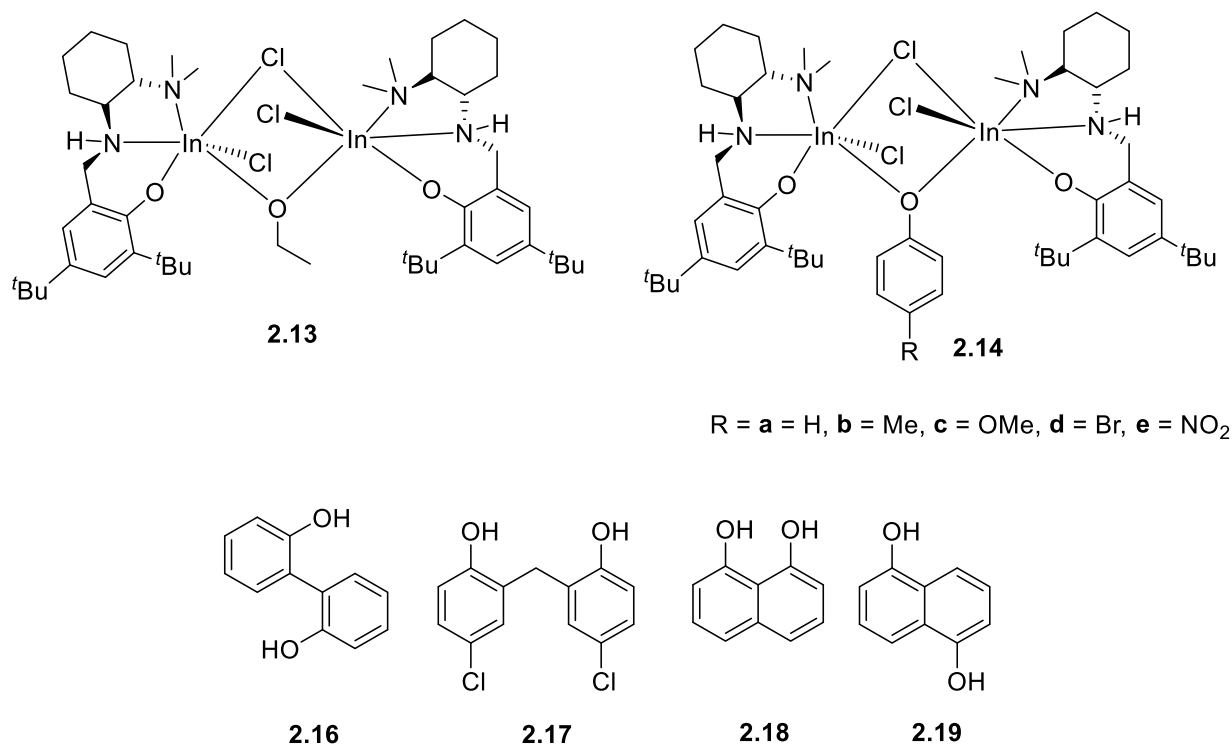
Figure 2.6: Indium amino phenolate complexes and aromatic diols

27

2.3 Ligand chirality and stereochemical polymerization

Monomers with chiral centres polymerize to give polymers with variable microstructures referred to as the polymer tacticity. Lactides (LAs) comprise of two stereogenic carbons which results in three isomeric forms i.e. L-(R,R)-, D-(S,S)-, and *meso*-(S,R)-lactide (Figure 2.7). The D/L system refers to the entire molecule, while R/S classification labels the absolute configuration of each stereocentre. Probable polylactide microstructures are illustrated in Figure 2.7.
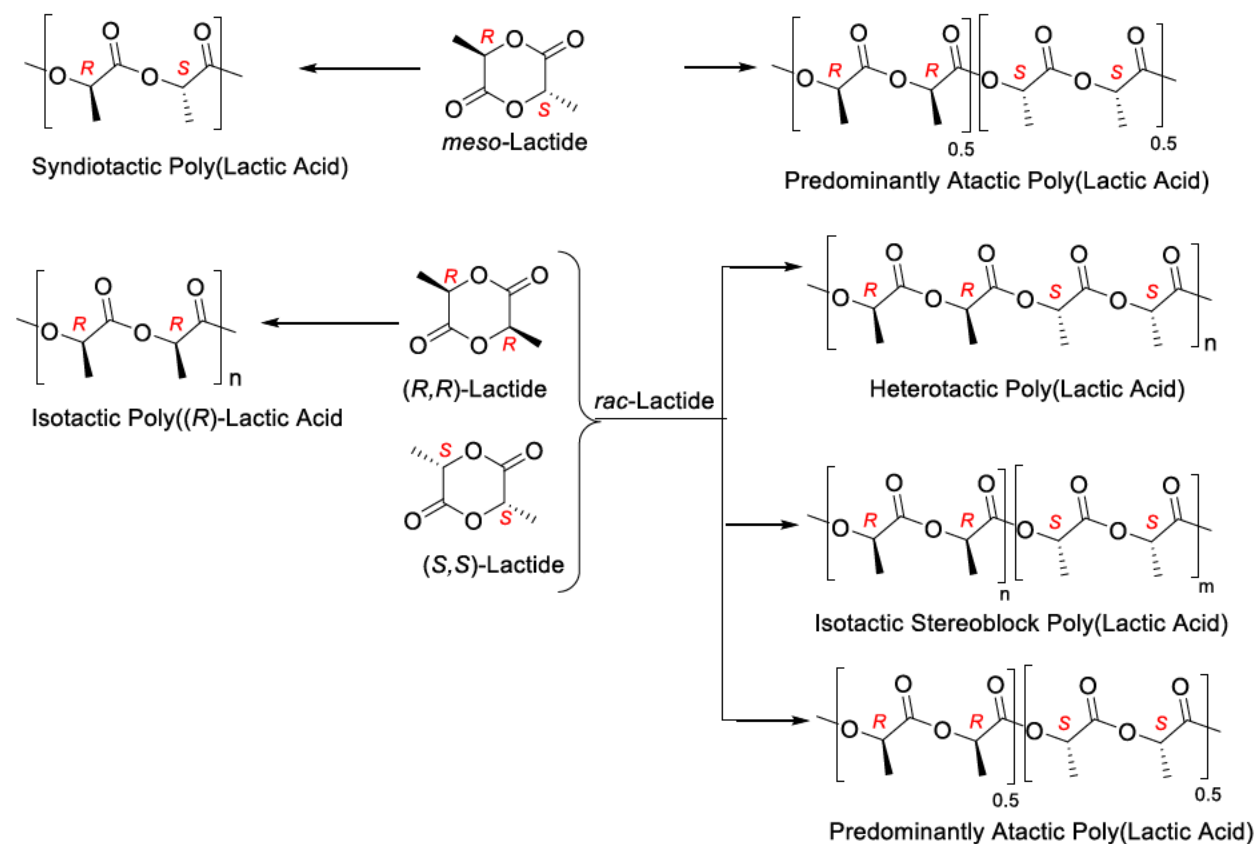
Figure 2.7: Polylactide polymer tacticities

Polymerization of *rac*-LA results in heterotactic or atactic polymers where by *RRSS* or *SSRR* configurations define the chain units. If the chain contains a large R and S block segments in sequence, then the polymer is referred to as stereo-block, which is a testimony that propagation of one stereoisomer is kinetically preferred. The extent of stereoregularity in lactide polymerization is denoted as the probability of *racemic* (P_r) or *meso* (P_m) enrichment.

28

Polymer microstructure and stereochemistry can be dictated by the operational propagation mechanism. There are two mechanisms which have been projected namely chain-end control mechanism (CECM)[11,50] and enantiomorphic site control mechanism (ESCM).[51] In the CECM, the stereogenic point of the last inserted repeating unit controls the polymer stereochemistry of the growing macromolecule while in ESCM the monomer arrangement is communicated from the chiral centre on the ligand framework of the catalyst. Therefore, careful design of ligands motifs can serve as a tool to prepare polymers with varying properties.

Salen-type ligands have been extensively used in ring opening polymerization.[52-54] A small variation in their backbone usually results in a significant change in their catalytic activity as well as polymer characteristics. Luo *et al*[24] have illustrated this by varying the symmetry and substituents on the ligand framework (Figure 2.8). They investigated the polymerization of *rac*-LA using complexes **2.20a** – **2.20c**. Catalysis using unsymmetrical complexes **2.20a** – **2.20c** resulted in isoselective polymerization furnishing isotactic polymers (P_m = 77) compared to a value of 66 for symmetrical *t*-butyl substituted complex **2.20b**. However, it was comparable to that of symmetrical phenyl substituted complex **2.20c** (P_m = 78). This phenomenon was attributed to the bulky phenyl groups, which induce greater repulsion, hence creating greater space around the metal centre, which affects monomer selectivity hence compromising isotacticity. Research has shown that ligand chirality can also result in increased isotactic enrichment.[55] Using chiral (*R,R*)-1,2-diammonium cyclohexane salen-complexes Feijin *et al*[52] and Gao *et al*[53] achieved enriched isotactic polylactide with P_m of values 0.88 and 0.91 for complexes **2.21** and **2.22**, respectively. The slight difference was attributed to symmetry and different substituents of the ligands. However, one has to bear in mind that polymer end groups as well the choice of solvent can result in complexity of the polymerization mechanism controlling the stereochemistry.[56-58]

2.20a: R$_1$ = R$_2$ = R$_3$ = R$_4$ = ^{t}Bu
2.20b: R$_1$ = R$_2$ = ^{t}Bu; R$_3$ = H; R$_4$ = Ph
2.20c: R$_1$ = R$_3$ = H; R$_2$ = R$_4$ = Ph

2.21

2.22
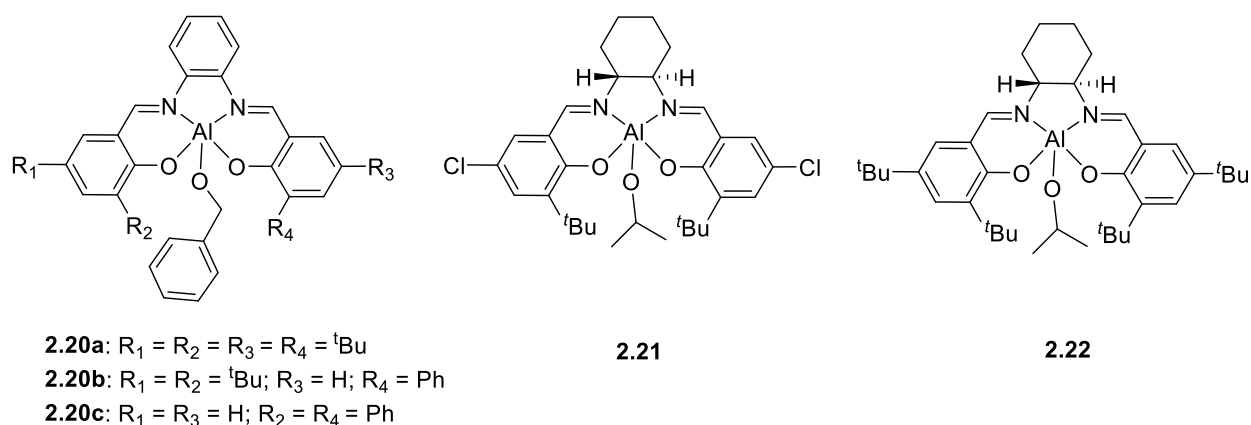
Figure 2.8: Aluminium *N,O*-salen-type complexes

Aluminium complexes have remarkably, exhibited supreme stereo-control in *rac*-lactide polymerization.[59-61]   A comparative study by Normand *et al*[62] using aluminium and indium complexes **2.23** and **2.24** (Figure 2.9).   The aluminium complex **2.23** resulted in isotactic enrichment while, indium complex **2.24** furnished atactic polymers.   This manifestation was alluded to the different operational mechanisms where aluminium complexes reacted *via* a CIM, while indium complexes proceeded through AMM.

2.23

2.24
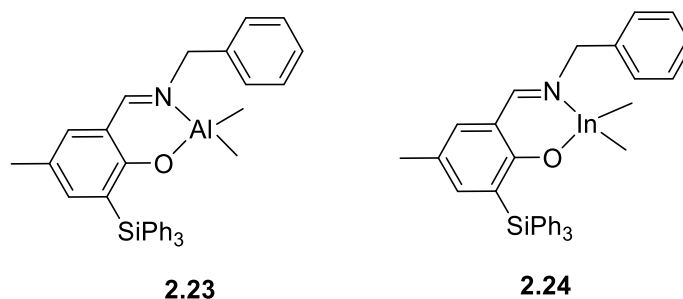
Figure 2.9: Aluminium and indium Schiff base complexes

2.4   Effect of the nature of the hetero-donor atoms on ROP activity

The apparent rate constants depend on the ligand architecture, i.e. nature and denticity of the hetero-donor atoms, stereo-electronic environment and linking atoms between the hetero-donor atoms. The atomic hybridization and substituent groups determine the electron donating potency of the heteroatoms. A combination of hard *P*-donor and soft *N*- and/or *O*-donor atoms result in an interesting class termed hemilabile ligands.[63]   The weak metal to hard donor atom interactions

30

cause the ligand to be easily substituted with the incoming substrate.[64] This characteristic promotes stabilization of low valence metal states and oxidative addition reactions.[65] Hemilability can also help to stabilize catalytic species produced during the catalytic cycle.[66]

A study by Tschan *et al*[67] demonstrated the effect of changing the donor-atoms on catalytic performance using complexes **2.25 – 2.28** (Figure 2.10). They observe a drastic change in activity when the tetradentate system was changed from N_3O in complex **2.25** to N_2PO in complex **2.26**. The turnover frequency increased from 43 to 418 h^{-1} for complex **2.25** and **2.26**, respectively. The same trend was also noticed for complexes **2.27** (N_2P_2) and **2.28** (NP_3) as evidenced by the change in activity from 218 to 770 h^{-1}. This behaviour is a clear testimony of the advantage inherited from hemilability of the ligand system, which makes the metal centre more accessible in the presence of phosphorus donor atoms.

2.25, [N_3O]   **2.26,** [N_2PO]   **2.27,** [P_2N_2]   **2.28**, [NP_3]

R = Ph
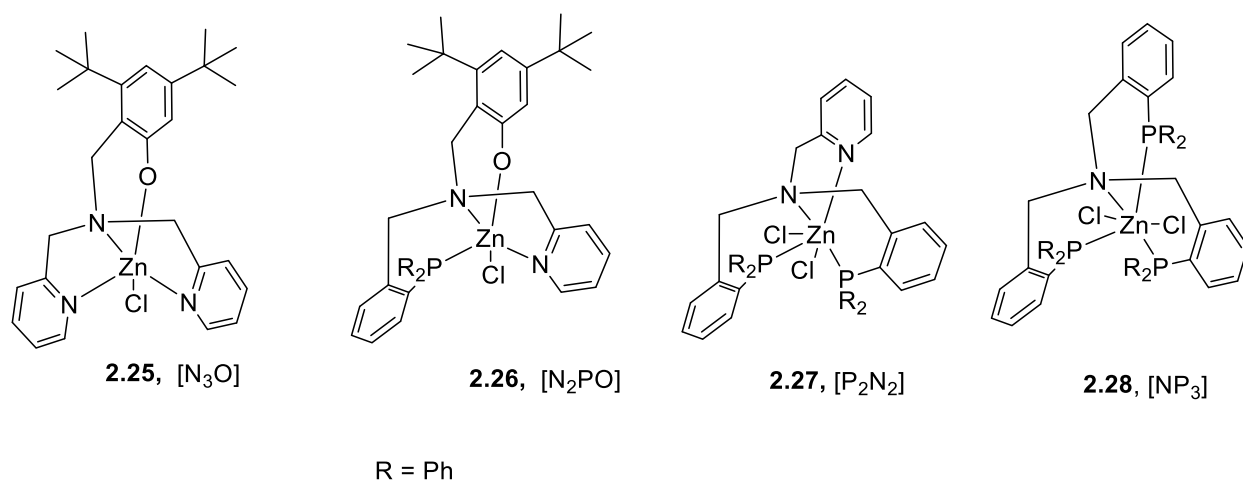
Figure 2.10: Zinc complexes supported by *N,O*, *NOP* and *N,P* ligands

Another effective way to fine tune the catalytic activity is to change the nucleophilicity of the hetero-donor atoms. Fortun *et al*.[68] studied the effect of N_{amine} compared to $N_{pyridyl}$ in ROP of lactides using complexes **2.29** and **2.30** (Figure 2.11). Complex **2.29** with pyridyl methoxy-bridge was less active compared **2.30**. This behaviour was explained by the coordination tenacity of pyridyl methoxy as compared to an amino ethoxyl group, which makes the complex easily dissociated into active monomeric species.
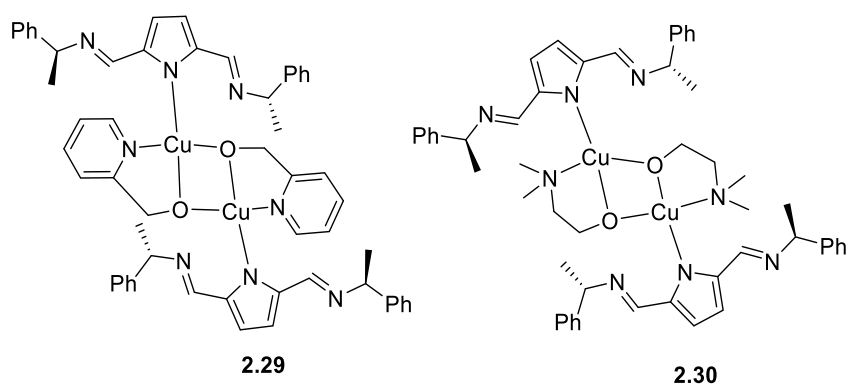
Figure 2.11: Copper alkoxide complexes

Hybridization of nitrogen hetero-donor atoms also affects the basicity, which in turn affects the redox potential of the metal centre. The redox potential of the metal centre interferes with monomer catalyst interaction, which in turn influences activity. Ebrahim *et al*[13] explored the effect of nitrogen hybridization on the polymerization of lactides using complexes **2.31** - **2.33** (Figure 2.12). All the complexes could polymerize *rac*-LA within 10 min. Complex **2.31** was less active than complex **2.32** although they were all more active than the mononuclear complex **2.33**. The binuclear species exhibit the same structure and the differences in activity is mainly due to nitrogen hybridization. The differences can be accounted for by the differences in basicity of the nitrogen atoms where the imine nitrogen reduces the electron density of the metal hence increasing monomer coordination compared to the amine nitrogen. N-alkylation resulted in the lowest rate as complex **2.33** was the least active, and the electron donating nature of the methyl substituent renders the metal centre less nucleophilic, hence reducing the probability of monomer binding. All complexes displayed higher molecular weights between (27.1 – 157.8 kDa) and a controllable living polymerization process shown by narrow PDIs (1.02 - 1.19). The binuclear complexes **2.31** and **2.32** showed good heterotacticity displaying P_r values of up to 80, which improved slightly at low temperature. In contrast, the mononuclear complex **2.33** furnished mainly atactic polylactide polymers.

2.31 **2.32** **2.33**
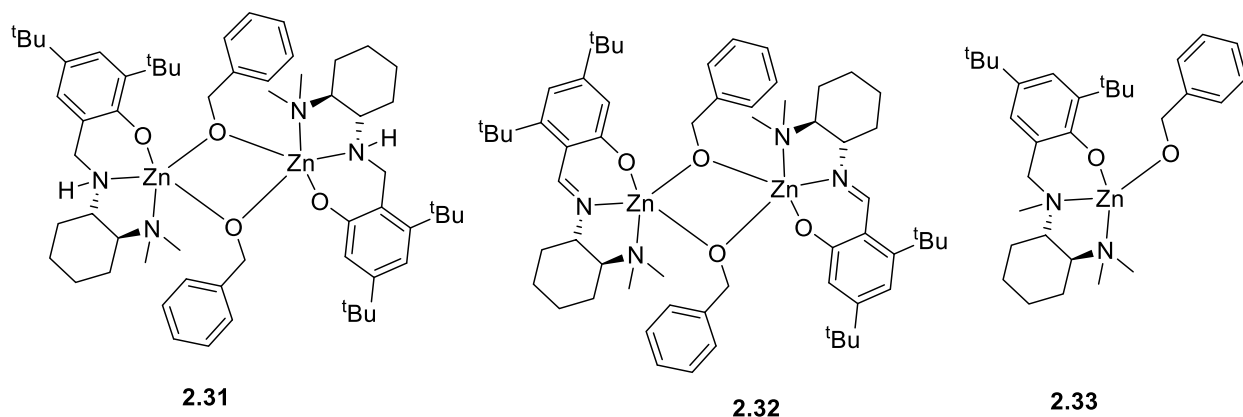
Figure 2.12: *N,O*-zinc alkoxide complexes

Typically, phosphorous is modified by changing the substituent groups attached to the hetero-donor atom, while sulphur and oxygen are usually etherified. The effect of substituents on phosphorus hetero-donor atom on ROP was put forward by D'Auria *et al*[69] using diphosphino pincer aluminium complexes **2.34a** – **2.34b** (Figure 2.13). Complexes **2.34a** and **2.34c** bearing phenyl phosphine showed increased activity in ROP of ε-CL and L-LA compared to the isopropyl phosphine analogue (**2.34b**). This modification offered greater positive inductive effect of the isopropyl group compared to phenyl group, which renders the metal more nucleophilic thereby retarding monomer activation.

2.34

2.34a: R = Ph, R' = Me
2.34b: R = ^{i}Pr, R' = Me
2.34c: R = Ph, R' = ^{i}Bu

2.35

2.35a: X = S
2.35b: X = O
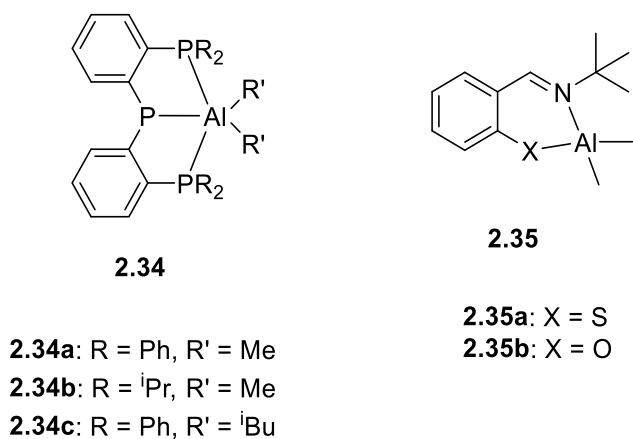
Figure 2.13: Diphosphino pincer and Schiff base aluminium complexes

In a related study Chang *et al*[19] studied the effect of *N,S*- and *N,O*-Schiff base aluminium complexes **2.35a** and **2.35b** (Figure 2.13) in ROP of ε-CL and LAs The thio-based complexes showed greater activity compared to the oxygen-based. Using density functional theory (DFT) calculations the authors showed that complex **2.35a** with the thio hetero-donor has a lower activation energy barrier (17.6 kcal/mol) compared to complex **2.35b** (19.0 kcal/mol) which possess an oxygen hetero-donor atom.

2.5   Effect of catalytic system rigidity and flexibility on ROP

The ring opening reaction is proceeds *via* the most accessible transition state. The resting state of the catalyst is not necessarily the active state but rather there is reorganisation after monomer coordination to generate the reactive transition state. Therefore, the structural features of the complex must allow free rotation to permit monomer access to the metal centre. Hence flexibility is an important aspect of catalyst design. In further understanding the effect of catalyst rigidity, Chen *et al*.[70] studied the ROP of LAs using alkali earth metals supported by mono-4,6-di-tert-butyl-phenol and 2,2-ethylidene-bis(4,6-di-tert-butyl- phenol) (EDBP) ligands (Figure 2.14). Complexes **2.35** and **2.36** showed greater activity compared to the chelate complex **2.37** of EDBP and the difference can be accounted for by steric and electronic considerations.[71] The authors explained the variation using DFT calculations.

They established that the freedom to rotate of the C_{ph}—O—M angle from linear to about 120° in complex **2.38** and **2.39** reduces the electrophilicity of the metal centre causing an increase in activity.   On the contrary, the chelate effect causes the metal complex to maintain its electrophilicity resulting in low catalytic activity.

2.35

2.36

2.37

2.38

2.39
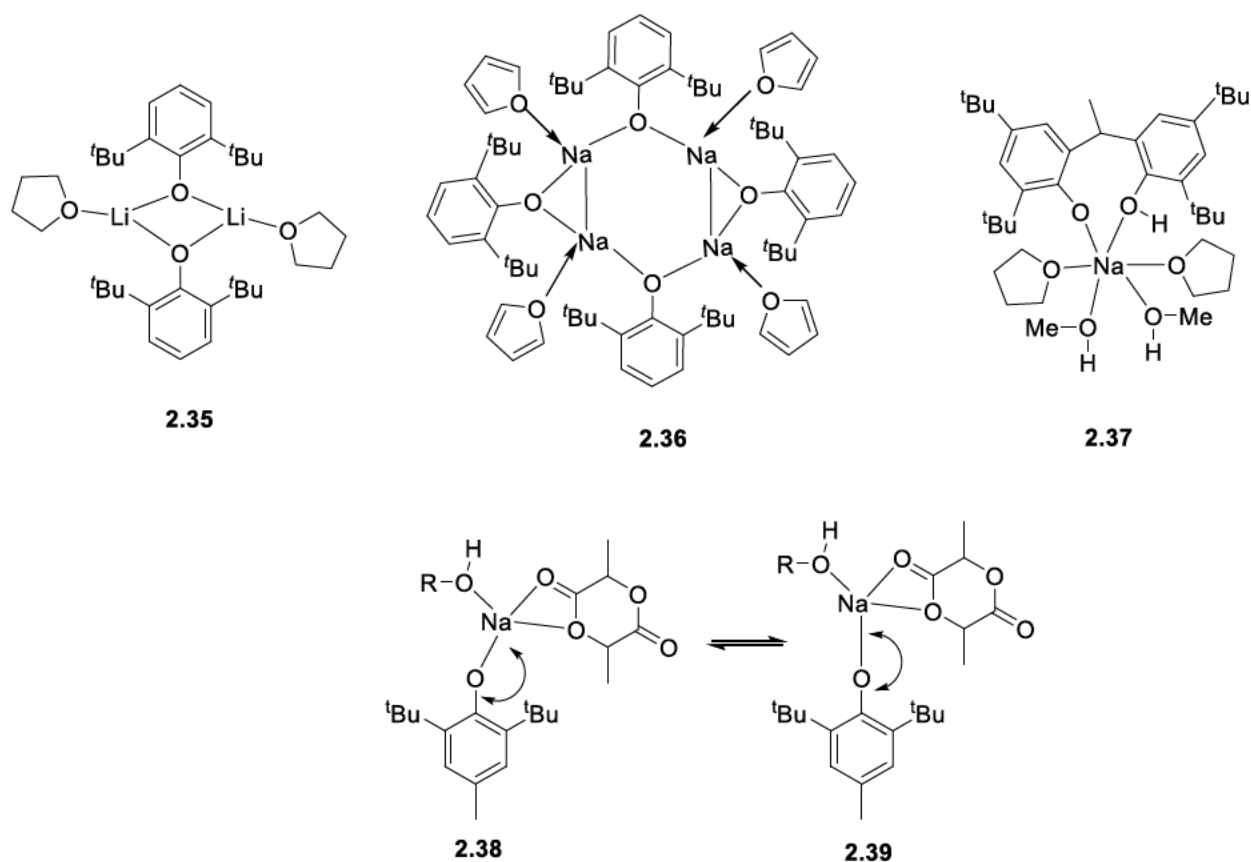
Figure 2.14: Alkali metals supported by oxygen containing ligands

Li *et al*[72] studied the flexibility and the rigidity of potassium calix[4]arene complexes **2.40** - **2.43** in ROP of *rac*-LA (Figure 2.15). The crown ether was introduced either as a separate ligand or integrated as part of the calix moiety. Complex **2.40** without the crown was the most active because the metal centre is expose to monomer coordination. However, introduction of the crown ether head resulted in reduced rates, which further decreased upon fixing it on the calix framework. Complex **2.42** was less active than complex **2.43** and this difference was attributed to hydrogen bonding. Hydrogen bonding interactions reduces the phenoxide nucleophilicity hence reducing monomer and co-initiator activation.

2.40 **2.41** **2.42** **2.43**
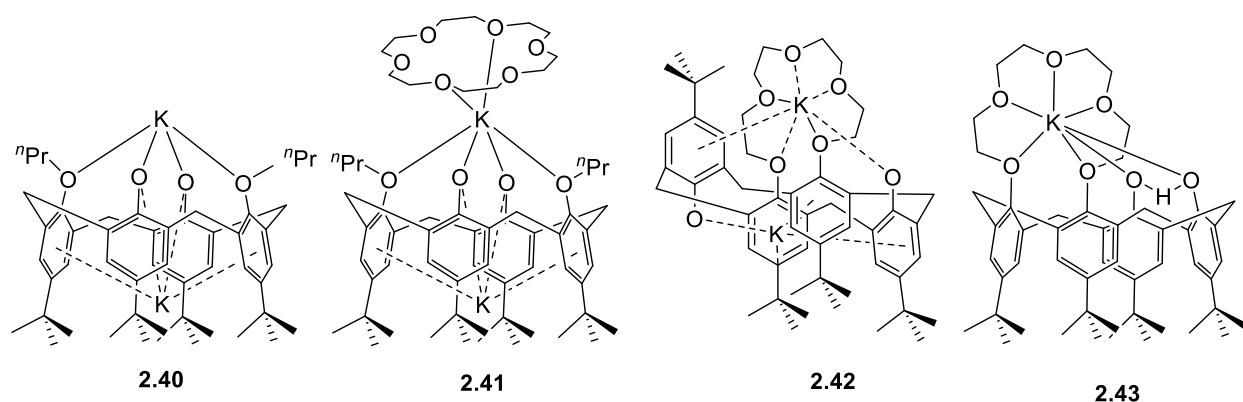
Figure 2.15: Potassium calix[4]arene complexes use in ROP of *rac*-lactide

2.6 Ligand steric and electronic effects in ROP

The prime role of ligands is to stabilise oxidation states and adjust ionic character of the metal centre. The presence of either electron donating or withdrawing groups, can further influence the metal redox potential, thereby affecting the catalyst activity and efficiency. Generally, in ring opening polymerization increased steric hindrance around the metal centre builds up repulsion in transition states raising the activation barrier thereby reducing reaction rates.[73] Electron withdrawing groups generally reduces the nucleophilicity of the metal centre and encourage monomer biding there by increasing reaction rates.[59]

A comparative study by Chen *et al*[74] using aluminium complexes presented the effects of ketimate ligand steric and electronic on catalytic activity in ROP of ε-CL and L-LA (Figure 2.16). Kinetic studies using alkyl-substituted complexes **2.44a** – **2.44b** showed that steric bulk substituents resulted in increased activity in polymerization of ε-CL, but an opposite trend was observed when the monomer was changed to L-LA. This trend is attributed to the repulsion between the monomer methyl groups with the substituents. The claim by the authors that it is due to greater ring size of L-LA compared to ε-CL, is rather invalid considering that ε-CL size is, greater than that of L-LA.

2.44

2.45

2.46

2.47

2.44a: $R_1 = R_2 = R_3 = H$
2.44b: $R_1 = R_2 = {}^iPr$, $R_3 = H$
2.44c: $R_1 = H$, $R_2 = {}^iPr$
2.44e: $R_1 = R_2 = R_3 = Me$

2.46a: R = Cl
2.46b: R = Br
2.46c: R = Me

2.47a = R = *p*-OMe
2.47b = R = *o*-F
2.47c = R = *p*-F
2.47d = R = *p*-Cl,
2.47e = R = *p*-NO$_2$
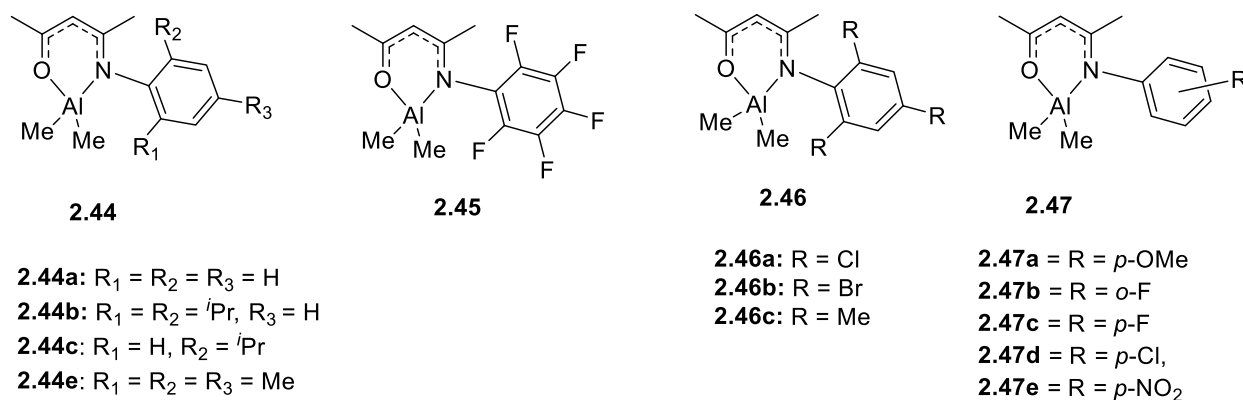
Figure 2.16: Dikitimate aluminium complexes

The same monomer dependence on the reactivity trend was also observed using the pentafluoro complex **2.45** and trisubstituted complexes **2.46a** – **2.46c**. The reactivity order was **2.45** >**2.46b** > **2.46a** > **2.46c** in L-LA polymerization which was reversed in ε-CL polymerization. This trend could be rationalised by the greater Lewis acidity induced by pentafluoro substituents compared to trichloro and tribromo groups. They also investigate the effect of *ortho*- and *para*-substitution on activity using complexes **2.47a** – **2.47e**. The substituents influenced the apparent rates in the following order *p*-NO$_2$ > *p*-F > *p*-Cl ~ *o*-F > H > OMe for ε-CL and *p*-F > *p*-NO$_2$ > *o*-F > *p*-Cl > H > OMe for L-LA. Generally, the activity decreased with a decrease in electron withdrawing effects because of reduced metal electrophilicity, which retarded monomer biding for activation. Related studies have also shown varying correlations between the substituents effects and activity using different ligands.[50,59,75] Hence, it is prudent to conclude that each ligand is unique, and it is difficult to assign the same trend across the whole spectrum of ligands.

In a related study by Wang *et al*,[76] the activity and induction time of β-quinolyl-enamino aluminium complexes was investigated and related to the substituted groups (Figure 2.17). Generally, the reaction rates decreased with reduction in electron donating ability of the substituent groups. As observed by Chen *et al*[74] the most substituted pentafluoro derivative complex **2.48a** showed the greatest activity. Of interest were the induction periods, for instance comparing complexes **2.48a** and **2.48b**, the induction time for complex **2.48a** is greater than that of complex **2.48b** although the former has a greater reaction rate post the induction period. This anomaly would suggest that these complexes are acting as both an initiators and catalysts with complex **2.48b** being a good initiator but a poor catalyst.
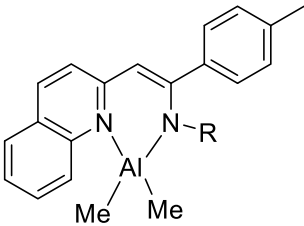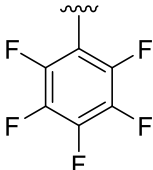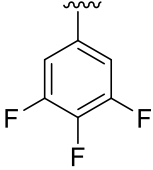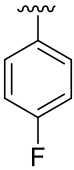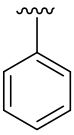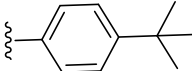
2.48

	2.48a	**2.48b**	**2.48c**	**2.48d**	**2.48e**
R =					
k_{obs}/min^{-1}	0.20654	0.18314	0.04918	0.04276	0.01314
Induction time/ min^{-1}	14.6	1.1	30.9	29.3	43.9

Figure 2.17: Aluminium β-quinolyl-enamino complexes

2.7 Catalyst metal nuclearity effects on ROP

Complexes comprising homo- or mono-multimetallic centers in close proximity can exhibit interesting properties compared to individual monometallic constituents. Multimetallic complexes generally have shown higher possibility of using adjacent metal centres to increase catalytic activity and selectivity.[77-80] It is believed that bimetallic complexes have the potential to result in stabilization of unusual ligand coordination modes, and multiple electron redox processes. This cooperative behaviour was reported by Chen *et al*[77] using phenolate aluminium complexes (Figure 2.18). The bimetallic species **2.49** were observed to be more active than the mononuclear species **2.50**. This superior behaviour was observed in other catalytic systems.[15,81]

2.49   **2.50**

$R_1 = Me, R_2 = {}^t Bu$ $R_3 = Me, Et$
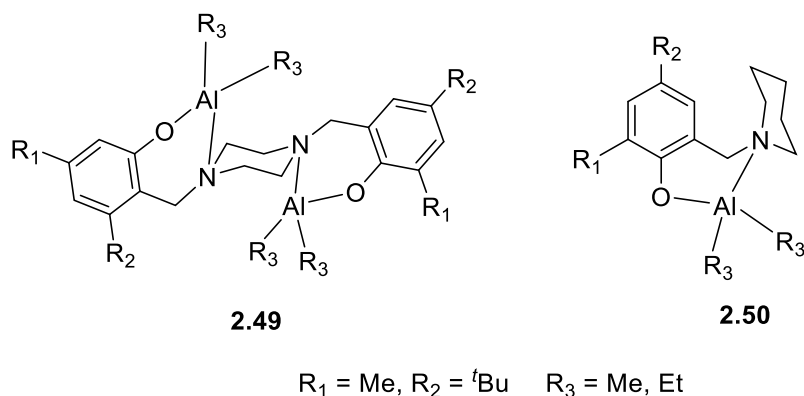
Figure 2.18: Aluminium salen-aminophenolate complexes

However, a contrasting trend was observed by Ding *et al*[54] in ROP of *rac*-LA using salan-ligated complexes (Figure 2.19). The heterobimetallic system **2.52,** assembled by adding a lanthanide ion to the nickel complex **2.51** showed no synergistic effects but rather a decline in activity was observed. Nevertheless, there was an improvement in molecular weights and polymerization controllability. The authors speculated that because the nitrate groups crowd the lanthanide metal in such a way that it prevents monomer access to the metal centre hence, excluding it from catalysis. The distortion in geometry because of the inclusion of the second metal ion also aided in increased Lewis acidity of the nickel centre, thereby reducing its affinity for the monomer hence slower rates. This finding might lead us to conclude that bond angle distortion, and steric interference factors need to be fine tuned to have maximum activity on the catalytic system.

2.51   **2.52**
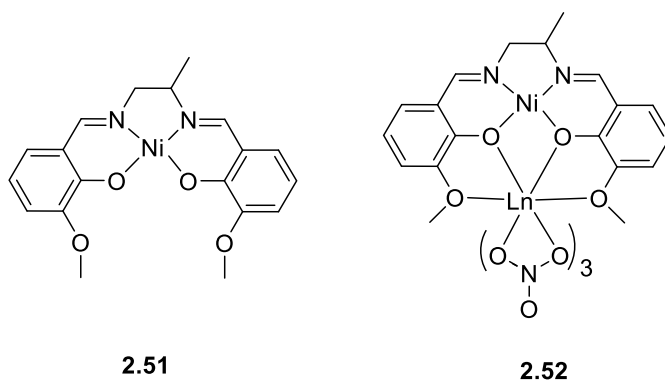
Ln = Ce, Nd, Sm, Eu, Tb, Ho, Tm

Figure 2.19: Mono nickel and heterobimetallic nickel-lanthanide complexes

2.8 Solvent and temperature effects on ROP

For a complete understanding of ROP reactions, one considers variables such as solvent and temperature. Industrially, ROP of ε-CL and LAs is done in bulk or melt conditions and activity is generally higher at higher temperatures. In academia, the use of solvents has been investigated and a correlation was established between the reaction medium and activity as well as polymer properties.[82,83] It has been shown that the activity is greater in high boiling temperatures solvents while, oxygen containing solvents compete with monomer binding resulting in slow rates. A contrasting temperature dependant activity was observed by Zhang and co-workers[3] using sodium and potassium complexes (**2.53**) for ROP of *rac*-LA (Figure 2.20). The initiator showed an interesting trend where higher catalytic activities were observed at a lower temperature. The authors speculate that the vibrations of the crown block the access of the monomer and co-initiator to the metal centre. As a result, the vibrations are minimised at lower temperature resulting in increased activity. PLA polymers with a P_m (0.86) were obtained which they claim to be superior over those other reported for alkali-metal complexes systems.

2.53a: M = Na
2.53b: M = Li
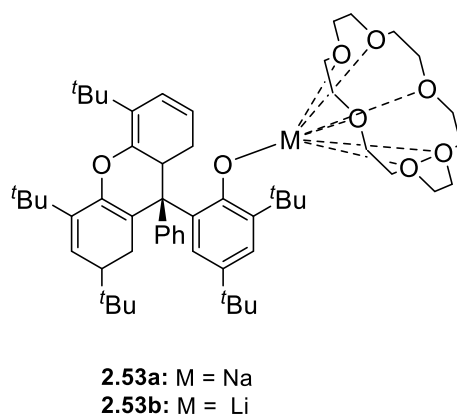
Figure 2.20: Sodium and lithium crown ether complexes

2.9   Conclusion

Structural features of some ROP catalyst focusing on ligand effects on activity and polymer properties were considered. The initiation groups, which are also central for the success of the polymerization process, were also reviewed.

It can be concluded from the discussion in the review that the ROP reaction is a complicated process such that it is difficult to solely pinpoint system dynamics on one variable. Each catalyst is distinctive and several factors such as ligand steric, chirality and electronic effects as well as metal identity regulate the polymerisation processes. In addition, experimental variables such as temperature and solvent also affect the polymerization reaction. Notwithstanding the progress made in search of active ROP catalyst/initiators, there is still a need to develop novel initiators/catalysts, which can control the polymerization process. Catalysts structural design and mechanistic studies have played an important role in development of ROP catalyst/initiators. Complexes and ligand structures have been discussed and correlated to the catalyst activity, selectivity and polymer properties.

References

1. D. Alhashmialameer, N. Ikpo, J. Collins, L. N. Dawe, K. Hattenhauer and F. M. Kerton, *Dalton Trans.*, **2015**, 44, 20216.

2. Z. Dai, Y. Sun, J. Xiong, X. Pan, N. Tang and J. Wu, *Catal. Sci. Technol.*, **2016**, 6, 515.

3. J. Zhang, J. Xiong, Y. Sun, N. Tang and J. Wu, *Macromolecules*, **2014**, 47, 7789.

4. S. H. Ahn, M. K. Chun, E. Kim, J. H. Jeong, S. Nayab and H. Lee, *Polyhedron*, 127, 51.

5. D. Appavoo, B. Omondi, I. A. Guzei, J. L. van Wyk, O. Zinyemba and J. Darkwa, *Polyhedron*, **2014**, 69, 55.

6. A. B. Biernesser, B. Li and J. A. Byers, *J. Am. Chem. Soc.*, **2013**, 135, 16553.

7. C. M. Manna, H. Z. Kaplan, B. Li and J. A. Byers, *Polyhedron*, **2014**, 84, 160.

8. K. M. Osten and P. Mehrkhodavandi, *Acc. Chem. Res.*, **2017**, 50, 2861.

9. Y. Wang, W. Zhao, D. Liu, S. Li, X. Liu, D. Cui and X. Chen, *Organometallics*, **2012**, 31, 4182.

10. H. Xie, Z. Mou, B. Liu, P. Li, W. Rong, S. Li and D. Cui, *Organometallics*, **2014**, 33, 722.

11. A. P. Dove, V. C. Gibson, E. L. Marshall, H. S. Rzepa, A. J. P. White and D. J. Williams, *J. Am. Chem. Soc.*, **2006**, 128, 9834.

12. A. Kowalski, A. Duda and S. Penczek, *Macromolecules*, **2000**, 33, 689.

13. T. Ebrahimi, E. Mamleeva, I. Yu, S. G. Hatzikiriakos and P. Mehrkhodavandi, *Inorg. Chem.*, **2016**, 55, 9445.

14. C. Fliedel, V. Rosa, F. M. Alves, A. M. Martins, T. Aviles and S. Dagorne, *Dalton Trans.*, **2015**, 44, 12376.

15. S. Range, D. F. J. Piesik and S. Harder, *Eur. J. Inorg. Chem.*, **2008**, 2008, 3442.

16. H. Wang, J. Guo, Y. Yang and H. Ma, *Dalton Trans.*, **2016**, 45, 10942.

17. H. Wang, Y. Yang and H. Ma, *Macromolecules*, **2014**, 47, 7750.

18. E. D. Akpan, S. O. Ojwach, B. Omondi and V. O. Nyamori, *New J. Chem.*, **2016**, 40, 3499.

19. M.-C. Chang, W.-Y. Lu, H.-Y. Chang, Y.-C. Lai, M. Y. Chiang, H.-Y. Chen and H.-Y. Chen, *Inorg. Chem.*, **2015**, 54, 11292.

20. H. Du, A. H. Velders, P. J. Dijkstra, Z. Zhong, X. Chen and J. Feijen, *Macromolecules*, **2009**, 42, 1058.

21. S. Gupta, R. Arora, N. Sinha, M. I. Alam and M. A. Haider, *RSC Advances*, **2016**, 6, 12932.

22. J. A. Castro-Osma, C. Alonso-Moreno, I. Márquez-Segovia, A. Otero, A. Lara-Sánchez, J. Fernández-Baeza, A. M. Rodríguez, L. F. Sánchez-Barba and J. C. García-Martínez, *Dalton Trans.*, **2013**, 42, 9325.

23. D. Li, Y. Peng, C. Geng, K. Liu and D. Kong, *Dalton Trans.*, **2013**, 42, 11295.

24. W. Luo, T. Shi, S. Liu, W. Zuo and Z. Li, *Organometallics*, **2017**, 36, 1736.

25. M.-C. Wu, T.-C. Hu, Y.-C. Lo, T.-Y. Lee, C.-H. Lin, W.-Y. Lu, C.-C. Lin, A. Datta and J.-H. Huang, *J. Organomet. Chem.*, **2015**, 791, 141.

26. Y. Han, Q. Feng, Y. Zhang, Y. Zhang and W. Yao, *Polyhedron*, **2017**, 121, 206.

27. W.-L. Kong, Z.-Y. Chai and Z.-X. Wang, *Dalton Trans.*, **2014**, 43, 14470.

28. W.-L. Kong and Z.-X. Wang, *Dalton Trans.*, **2014**, 43, 9126.

29. A. Otero, J. Fernández-Baeza, L. F. Sánchez-Barba, J. Tejeda, M. Honrado, A. Garcés, A. Lara-Sánchez and A. M. Rodríguez, *Organometallics*, **2012**, 31, 4191.

30. H.-M. Sun, H.-R. Li, C.-S. Yao, Y.-M. Yao, H.-T. Sheng and Q. Shen, *Chin. J. Chem.*, **2005**, 23, 1541.

31. L.-C. Liang, W.-Y. Lee, T.-L. Tsai, Y.-L. Hsu and T.-Y. Lee, *Dalton Trans.*, **2010**, 39, 8748.

32. A. Stopper, J. Okuda and M. Kol, *Macromolecules*, **2012**, 45, 698.

33. G.-J. M. Meppelder, H.-T. Fan, T. P. Spaniol and J. Okuda, *Inorg. Chem.*, **2009**, 48, 7378.

34. A.-Q. Jia and G.-X. Jin, *Organometallics*, **2009**, 28, 1872.

35. A.-Q. Jia, J.-Q. Wang, P. Hu and G.-X. Jin, *Dalton Trans.*, **2011**, 40, 7730.

36. M. P. Stevens, *Polymer Chemistry: An Introduction*, Oxford University Press, New York, 1999.

37. B. M. Mandal, *Fundamentals of polymerization*, World Scientific, New Jersey; London, 2013.

38. W. A. Munzeiwa, V. O. Nyamori and B. Omondi, *Appl. Organomet. Chem.*, e4247.

39. E. D. Akpan, S. O. Ojwach, B. Omondi and V. O. Nyamori, *Polyhedron*, **2016**, 110, 63.

40. C. Kan, J. Ge and H. Ma, *Dalton Trans.*, **2016**, 45, 6682.

41. C.-H. Wang, C.-Y. Li, B.-H. Huang, C.-C. Lin and B.-T. Ko, *Dalton Trans.*, **2013**, 42, 10875.

42. N. M. Rezayee, K. A. Gerling, A. L. Rheingold and J. M. Fritsch, *Dalton Trans.*, **2013**, 42, 5573.

43. J. Li, Y. Deng, S. Jie and B.-G. Li, *J. Organomet. Chem.*, **2015**, 797, 76.

44. P. M. Schäfer, M. Fuchs, A. Ohligschläger, R. Rittinghaus, P. McKeown, E. Akin, M. Schmidt, A. Hoffmann, M. A. Liauw, M. D. Jones and S. Herres-Pawlis, *ChemSusChem*, **2017**, 10, 3547.

45. M. H. Chisholm, J. C. Huffman and K. Phomphrai, *J. Chem. Soc., Dalton Trans.*, **2001**, 222.

46. P. Dubois, R. Jérǒme and P. Teyssié, *Makromol. Chem., Macromol. Symp.*, **1991**, 42-43, 103.

47. C. Jian, J. Zhang, Z. Dai, Y. Gao, N. Tang and J. Wu, *Eur. J. Inorg. Chem.*, **2013**, 2013, 3533.

48. A. Thevenon, C. Romain, M. S. Bennington, A. J. P. White, H. J. Davidson, S. Brooker and C. K. Williams, *Angew. Chem. Int. Ed.*, **2016**, 55, 8680.

49. L. E. Chile, T. Ebrahimi, A. Wong, D. C. Aluthge, S. G. Hatzikiriakos and P. Mehrkhodavandi, *Dalton Trans.*, **2017**, 46, 6723.

50. N. Nomura, R. Ishii, M. Akakura and K. Aoi, *J. Am. Chem. Soc.*, **2002**, 124, 5938.

51. M. H. Chisholm and E. E. Delbridge, *Chem. Commun.*, **2001**, 1308.

52. Z. Zhong, P. J. Dijkstra and J. Feijen, *Angew. Chem.*, **2002**, 114, 4692.

53. B. Gao, D. Li, Y. Li, Q. Duan, R. Duan and X. Pang, *New J. Chem.*, **2015**, 39, 4670.

54. L. Ding, W. Jin, Z. Chu, L. Chen, X. Lü, G. Yuan, J. Song, D. Fan and F. Bao, *Inorg. Chem. Commun.*, **2011**, 14, 1274.

55. T. M. Ovitt and G. W. Coates, *J. Am. Chem. Soc.*, **2002**, 124, 1316.

56. M. H. Chisholm and E. E. Delbridge, *New J. Chem.*, **2003**, 27, 1167.

57. M. H. Chisholm, J. Galucci, C. Krempner and C. Wiggenhorn, *Dalton Trans.*, **2006**, 846.

58. M. H. Chisholm, S. S. Iyer, D. G. McCollum, M. Pagel and U. Werner-Zwanziger, *Macromolecules*, **1999**, 32, 963.

59. P. Hormnirun, E. L. Marshall, V. C. Gibson, R. I. Pugh and A. J. P. White, *Proc. Natl. Acad. Sci.*, **2006**, 103, 15343.

60. P. Sumrit, P. Chuawong, T. Nanok, T. Duangthongyou and P. Hormnirun, *Dalton Trans.*, **2016**, 45, 9250.

61. P. Sumrit and P. Hormnirun, *Macromol. Chem. Phys.*, **2013**, 214, 1845.

62. M. Normand, V. Dorcet, E. Kirillov and J.-F. Carpentier, *Organometallics*, **2013**, 32, 1694.

63. J. C. Jeffrey and T. B. Rauchfuss, *Inorg. Chem.*, **1979**, 18, 2658.

64. P. Braunstein and F. Naud, *Angew. Chem. Int. Ed.*, **2001**, 40, 680.

65. K. Wajda-Hermanowicz, Z. Ciunik and A. Kochel, *Inorg. Chem.*, **2006**, 45, 3369.

66. P. Espinet and K. Soulantica, *Coordination Chemistry Reviews*, **1999**, 193–195, 499.

67. M. J. L. Tschan, J. Guo, S. K. Raman, E. Brulé, T. Roisnel, M.-N. Rager, R. Legay, G. Durieux, B. Rigaud and C. M. Thomas, *Dalton Trans.*, **2014**, 43, 4550.

68. S. Fortun, P. Daneshmand and F. Schaper, *Angew. Chem. Int. Ed.*, **2015**, 54, 13669.

69. I. D'Auria, M. Lamberti, M. Mazzeo, S. Milione and C. Pellecchia, *J. Polym. Sci, Part A: Polym. Chem.*, **2014**, 52, 49.

70. H.-Y. Chen, L. Mialon, K. A. Abboud and S. A. Miller, *Organometallics*, **2012**, 31, 5252.

71. H.-Y. Chen, J. Zhang, C.-C. Lin, J. H. Reibenspies and S. A. Miller, *Green Chem.*, **2007**, 9, 1038.

72. Y. Li, H. Zhao, X. Mao, X. Pan and J. Wu, *Dalton Trans.*, **2016**, 45, 9636.

73. I. del Rosal, P. Brignou, S. M. Guillaume, J.-F. Carpentier and L. Maron, *Polym. Chem.*, **2011**, 2, 2564.

74. Y.-H. Chen, Y.-J. Chen, H.-C. Tseng, C.-J. Lian, H.-Y. Tsai, Y.-C. Lai, S. C. N. Hsu, M. Y. Chiang and H.-Y. Chen, *RSC Advances*, **2015**, 5, 100272.

75. F. M. García-Valle, R. Estivill, C. Gallegos, T. Cuenca, M. E. G. Mosquera, V. Tabernero and J. Cano, *Organometallics*, **2015**, 34, 477.

76. P. Wang, J. Chao and X. Chen, *Dalton Trans.*, **2018**, DOI: 10.1039/C7DT04522K.

77. L. Chen, W. Li, D. Yuan, Y. Zhang, Q. Shen and Y. Yao, *Inorg. Chem.*, **2015**, 54, 4699.

78. H.-C. Huang, B. Wang, Y.-P. Zhang and Y.-S. Li, *Polym. Chem.*, **2016**, 7, 5819.

79. B. A. Rodriguez, M. Delferro and T. J. Marks, *J. Am. Chem. Soc.*, **2009**, 131, 5902.

80. S. Sun, K. Nie, Y. Tan, B. Zhao, Y. Zhang, Q. Shen and Y. Yao, *Dalton Trans.*, **2013**, 42, 2870.

81. Z. Sun, R. Duan, J. Yang, H. Zhang, S. Li, X. Pang, W. Chen and X. Chen, *RSC Advances*, **2016**, 6, 17531.

82. T. J. J. Whitehorne and F. Schaper, *Inorg. Chem.*, **2013**, 52, 13612.

83. X.-X. Zheng, C. Zhang and Z.-X. Wang, *J. Organomet. Chem.*, **2015**, 783, 105.

Chapter 3

Zn(II) and Cu(II) unsymmetrical formamidine complexes as effective initiators for ring-opening polymerization of cyclic esters

Abstract

A series of Zn(II) and Cu(II) complexes were synthesized using unsymmetrical *N,N′*-diarylformamdine ligands, i.e. *N*-(2-methoxyphenyl)-*N′*-2,6-dichorophenyl)-formamidine (**L3.1**), *N*-(2-methoxyphenyl)-*N′*-phenyl)-formamidine (**L3.2**), *N*-(2-methoxyphenyl)-*N′*-(2,6-dimethylphenyl)-formamidine (**L3.3**) and *N*-(2-methoxyphenyl)-*N′*-(2,6-diisopropylphenyl)-formamidine (**L3.4**). The complexes, [Zn$_2$(**L3.1**)$_2$(OAc)$_4$] (**3.1**), [Zn$_2$(**L3.2**)$_2$(OAc)$_4$] (**3.2**), [Zn$_2$(**L3.3**)$_2$(OAc)$_4$] (**3.3**), [Zn$_2$(**L3.4**)$_2$(OAc)$_4$] (**3.4**), [Cu$_2$(**L3.1**)$_2$(OAc) (**3.5**), [Cu$_2$(**L3.2**)$_2$(OAc)$_4$] (**3.6**), [Cu$_2$(**L3.3**)$_2$(OAc)$_4$] (**3.7**) and [Cu$_2$(**L3.4**)$_2$(OAc)$_4$] (**3.8**), were prepared *via* mechanochemical method with excellent yields (98%) by reacting the metal acetates with corresponding ligands. Structural studies showed that complexes **3.3** and **3.7** are dimeric with a paddlewheel core structure in which the separation between the two metal centres are 2.9898(8) and 2.6653(7) Å in complexes **3.3** and **3.7**, respectively. Complexes **3.1** – **3.8** were used in ring-opening polymerization of ε-caprolactone (ε-CL) and *rac*-lactide *(rac*-LA). Zn(II) complexes were more active than Cu(II) complexes, with complex **3.1** bearing electron withdrawing chloro groups being the most active ($k_{app} = 0.0803$ h^{-1}). Low molecular weight poly(ε-CL) and poly(*rac*-LA) ranging from 1720 to 6042 g mol^{-1}, with broad molecular weight distribution (PDIs, 1.78 – 1.87) were obtained. Complex **3.2** gave a rate law with reaction orders of 0.56 and 1.52 with respect to ε-CL and *rac*-LA, respectively.

Keywords: Copper(II), ε-caprolactone, *N,N′*-diarylformamidine, *rac*-lactide, zinc(II)

3.1   Introduction

Polyesters are vital polymers with diverse applications in packaging, pharmaceutical and medical industries to name a few. For example, polylactides with attributes such as good tensile strength, biocompatibility and biodegradability are suitable for making materials used in wound dressing[1] restorable medical implants and controlled drug delivery nanomaterials.[2-4]

Industrially, ring-opening polymerization (ROP) of cyclic esters has successfully been carried out using ligand supported complexes as initiators or catalysts for the synthesis of polyesters. The use of organometallic complexes as catalysts or initiators *via* the "coordination-insertion mechanism" has been preferable since it furnishes polymers with predictable molecular weights and low polydispersity.[5] [6]

Traditionally, tin compounds and in particular tin octanoate ($Sn(Oct)_2$), are irrefutably the most applied catalysts due to their outstanding catalytic properties   and good thermostabilities[7] Nevertheless, some tin compounds have appreciable cytotoxicity and are susceptible to decomposition under atmospheric conditions which increases the production expense.[8] In this regard, research is now exploring the use of other organometallic compounds with lower toxicity such as alkali earth metals,[9] magnesium,[10,11] calcium,[12,13] zinc,[14-16] copper,[17,18] iron,[19] and aluminum[20] all of which have shown promising results.

It has also been demonstrated that the ligand used in organometallic complexes can influence polymerization reactions and products, and this is due to ease of modifying the backbone architecture. Prevalent ligand frameworks such as diketiminate,[21] salen[22-24] and phenolate,[10,25] have been widely tailored to regulate the steric and electronic properties, thereby affecting catalytic activity of ROP reaction initiators. We recently focused our attention on the opportunity to fine tune formamidine ligand architectures and study their effect on catalytic behaviour in ROP. The resonance-stabilized amidine metal complex, can act as dual conjugated Lewis-Brønsted combined acid catalyst[26,27] (Figure 3.1). Additionally, a neutral amidine ligand coordinated to a metal centre can be deprotonated giving the amidinato analogue complex which can also participate in inter- or intra-molecular hydrogen-bonding, hence, assist in substrate activation (Figure 3.1a, b and c).[26-28]
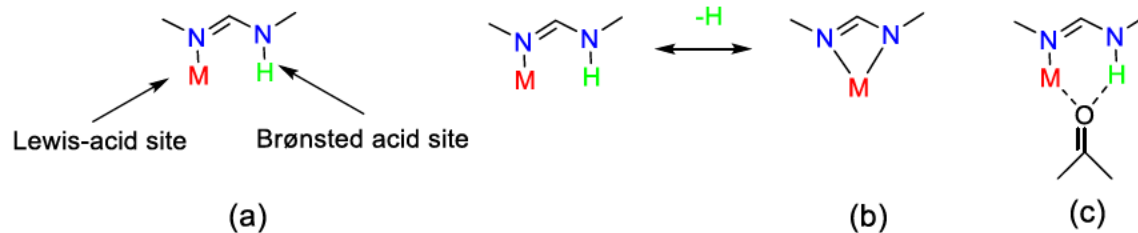
Figure 3.1: (a) Conjugated Lewis-Brønsted combined acid catalyst, (b) amidine deprotonation and (c) dual substrate activation

In recent published work from our group it was shown that symmetrical zinc and copper formamidine complexes (Figure 3.2) were active ROP initiators.[29,30] The complexes exhibited interesting coordination architectures which were dependent on substituents on the phenyl rings as well as the metal centre. In this work, we sought to investigate what effect there would be on using unsymmetrical formamidine complexes in ROP reactions and, also, what type of coordination the complexes would result.
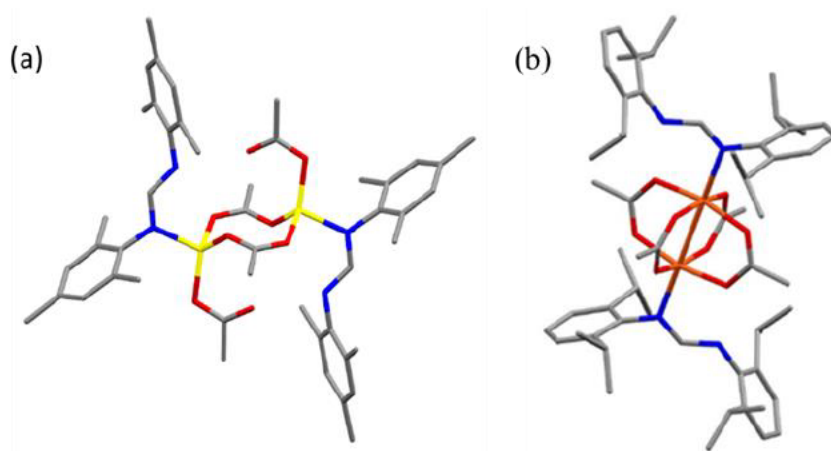
Figure 3.2: Selected complexes from previous work (a) Zn(II) complex and (b) Cu(II) complex.[30]

3.2 Experimental

3.2.1 Materials

All experiments were carried out under argon, 5.0 technical grade, (Airflex Industrial Gases, South Africa) using Schlenk techniques. All solvents were obtained from Sigma-Aldrich. Ethanol (99%) was distilled and dried from magnesium turnings while dichloromethane (DCM) (99%) and hexane (98%) were dried from a sodium-benzophenone mixture. Copper acetate (97%), zinc acetate (98%), ε-caprolactone (97%) and *rac*-lactide (98%) were obtained from Sigma-Aldrich.

3.2.2 Instrumentation

^{1}H- and ^{13}C-NMR spectra were measured at room temperature using a Bruker 400 MHz spectrometer. ^{1}H-NMR data were recorded in DMSO-d$_6$; chemical shifts were calibrated to the residual solvent signal of DMSO-d$_6$ (δ 2.5). Similarly, ^{13}C-NMR data were recorded in DMSO-d$_6$ and referenced to the residual solvent signal at δ 40.00. IR spectra were obtained on a PerkinElmer Universal ATR spectrum 100 FT-IR spectrometer. Mass spectra of compounds were obtained from a Water synapt GR electrospray positive spectrometer.

3.3 General methods

3.3.1 Synthesis of unsymmetrical formamidine ligands

Acetic acid (1.5 mmol) was added to a round-bottom flask charged with the first aniline (30 mmol, 1 equivalent) and triethyl orthoformate (30 mmol, 1 equivalent). The mixture was refluxed for 30 min with stirring to 140 °C. A distillation head was connected, and ethanol was distilled of until 60 mmol, 2 equivalent) were collected. The second aniline (30 mmol, 1 equivalent) was then added to the reaction mixture and heating continued until ethanol (1.75 ml, 30 mmol, 1 equivalent) was collected. Upon cooling to room temperature, the solution solidified. The crude product was triturated with cold hexane and collected by vacuum filtration. Solids were then dissolved in minimal hot acetone and recrystallized to remove traces of symmetric formamidine byproducts. The crystals were collected by vacuum filtration and dried *in vacuo*, providing *N*-(2-methoxyphenyl)-*N′*-(2,6-dichorophenyl)-formamidine (**L3.1**), *N*-(2-methoxyphenyl)-*N′*-(phenyl)-formamidine (**L3.2**), *N*-(2-methoxyphenyl)-*N′*-(2,6-dimethylphenyl)-formamidine (**L3.3**) and *N*-(2-methoxyphenyl)-*N′*-(2,6 diisopropylphenyl)-formamidine (**L3.4**) (74 - 89%) (Figure 3.3).

L3.1

L3.2

L3.3

L3.4
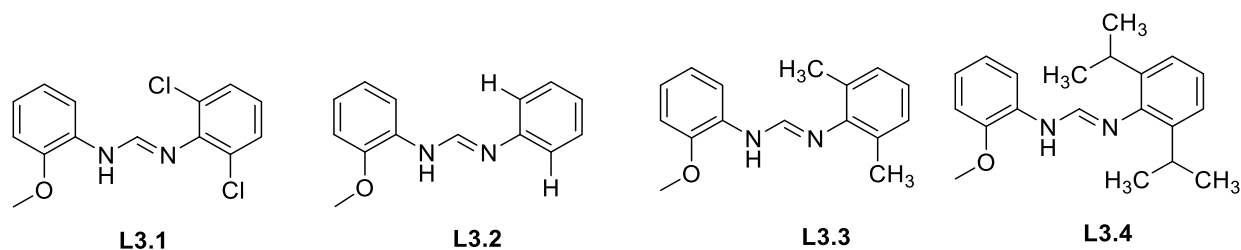
L3.1 = *N*-(2-methoxyphenyl)-*N'*-(2,6 dichlorophenyl)formamidine
L3.2 = *N*-(2-methoxyphenyl)-*N'*-(phenyl)formamidine
L3.3 = *N*-(2-methoxyphenyl)-*N'*-(2,6 dimethylphenyl)formamidine
L3.4 = *N*-(2-methoxyphenyl)-*N'*-(2,6 diisopropylphenyl)formamidine

Figure 3.3: Unsymmetrical formamidine ligands (**L3.1**- **L3.4**) used in this study

3.3.1.1   *N-(2-methoxyphenyl)-N'-(2,6-dichorophenyl)-formamidine (L3.1)*

Reaction of 2-methoxy aniline (2.5g, 20 mmol), triethylorthoformate (3.0g, 20 mmol) and 2,6-dicloroaniline (3.2g, 20 mmol) gave a white compound 4.3g, yield 74%. Mp = 92 °C. ^{1}H-NMR (CDCl$_3$, 400 MHz): δ (ppm) 3.92 (s, O-CH$_3$), 6.62 (t, H, Ar), 6.94 (q, 2H, Ar), 7.04 (t, H, Ar), 7.34 (d, 2H, Ar), 7.72 (s, 1H, CH=N), 8.08 (s, 2H, NH). ^{13}C-NMR (CDCl$_3$, 400 MHz): δ (ppm), 25.2, 25.6, 25.5, 27.8, 29.3, 123.1, 124, 129.8, 137.6, 144.5, 143.2, 145.4, 148.5. IR: v (cm^{-1}) 3220, v(N–H) stretching, 1620, v(C=N). ESI-TOF MS: m/z (%) = 317.43 [M+Na]$^+$. Anal. calcd for C$_{14}$H$_{12}$Cl$_2$N$_2$O: C, 56.97; H, 4.10; N, 9.49. Found: C, 56.45, H, 3.86, N, 9.55.

3.3.1.2   *N-(2-methoxyphenyl)-N'-(phenyl)-formamidine (L3.2)*

Reaction of 2-methoxy aniline (2.5g, 20 mmol), triethylorthoformate (3.0g, 20 mmol) and aniline (1.9g, 20 mmol) gave a white compound 3.2g, yield 74%. Mp = 68 °C, ^{1}H-NMR (CDCl$_3$, 400 MHz): δ (ppm) 3.89 (s, O-CH$_3$), 7.44 (m, 7H, Ar), 7.41(t, 2H, Ar), 7.75 (s, 1H, CH=N), 8.25 (s, 2H, NH). ^{13}C-NMR (CDCl$_3$, 400 MHz): δ (ppm), 28.3, 55.5, 113.9, 118.9, 122.2, 123.6, 123.7, 129.7, 135.9, 138.5, 147.2. IR: v (cm^{-1}) 3320, v(N–H) stretching, 1630, v(C=N). ESI-TOF MS: m/z (%) = 248.15 [M+Na]$^+$. Anal. calcd for C$_{14}$H$_{14}$N$_2$O: C, 74.31; H, 6.24; N, 12.38. Found: C 73.98, H, 5.90, N, 12.01.

3.3.1.3 N-(2-methoxyphenyl)-N'-(2,6-dimethylphenyl)-formamidine (L3.3)

Reaction of 2-methoxy aniline (2.5g, 20 mmol), triethyl orthoformate (3g, 20 mmol) and 2,6-dimethylaniline (2.4g, 20 mmol) gave a white compound 4.1 g yield 76%. Mp = 89 °C, ^{1}H-NMR (CDCl$_3$, 400 MHz): δ (ppm) 2.23 (s, 6H, CH$_3$), 3.89 (s, O-CH$_3$), 6.95 (m, 7H, Ar), 7.52 (s, 2H, NH), 7.88 (s, 1H, CH=N). ^{13}C-NMR (CDCl$_3$, 400 MHz): δ (ppm), 17.4, 18.5, 55.79, 126.2, 129, 130.3, 131.4, 132.7, 138.8, 139.8, 144.8, 146.8. IR: v (cm^{-1}) 3320, υ(N–H) stretching, 1596, υ(C=N). ESI-TOF MS: m/z (%) = 277.15 [M+Na]$^+$. Anal. calcd for C$_{16}$H$_{18}$N$_2$O: C, 75.56; H, 7.13; N, 11.01. Found: C 75.45., H, 6.88, N, 10.96.

3.3.1.4 N-(2-methoxyphenyl)-N'-(2,6 diisopropylphenyl)-formamidine (L3.4)

Reaction of 2-methoxy aniline (2.5g, 20 mmol), triethyl orthoformate (3g, 20 mmol) and 2,6-diisopropylaniline (3.5g, 20 mmol) gave a white compound 5.5 g yield 79%. Mp = 98 °C, ^{1}H-NMR (CDCl$_3$, 400 MHz): δ (ppm) 1.21 (d, 12H, ^{i}Pr-CH$_3$), 3.21 (qn, 2H, C(H)-^{i}Pr), 3.98 (3H, OCH$_3$), 6.93 (t, 3H, Ar), 7.00 (t, 3H, Ar) 7.12 (m, 3H, Ar), 7.85 (s, 2H, NH), 7.95 (s, 1H, CH=N). IR: v (cm^{-1}) 3320, υ(N–H) stretching, 1603, υ(C=N). ESI-TOF MS: m/z (%) = 311.21 [M]$^+$. Anal. calcd for C$_{20}$H$_{26}$N$_2$O: C, 77.38; H, 8.44; N, 9.02. Found: C 77.55., H, 8.30, N, 9.10.

3.3.1 *Synthesis of Zn(II) and Cu(II) complexes*

Ligand (1 equivalent) and the corresponding hydrated metal acetate (1 equivalent) was charged into a mortar and manually ground with pestle at room temperature for 20 min. The progress of the reaction was monitored using TLC. The crude reaction solid was then dissolved in ethanol and a pure product was precipitated using hexane. The desired products were obtained as solids.

3.3.1.1 [Zn$_2$(L3.1)$_2$] (3.1)

Reaction of ligand **L3.1** (0.3g, 1.0 mmol) and Zn(OAc)$_2$.2H$_2$O (0.22g, 1.02 mmol) gave complex **3.1** as a white powder after workup. Yield 90%. Mp 236-238 °C. ^{1}H-NMR (DMSO-d$_6$, 400 MHz): δ (ppm) 1.82 (s, 12H, OAc-CH$_3$), 3.87 (s, 6H, CH$_3$O), 6.92 (t, 4H, Ar), 7.03 (m, 10H, Ar), 7.42 (s, 2H, Ar), 7.44 (s, 1H, CH=N) 9.11 (s, 2H, NH). ^{13}C-NMR (DMSO-d$_6$, 400 MHz): δ (ppm) 160.6, 159.6, 148.4, 148.36, 146.3, 128.4, 127.2, 123.72, 123.0, 120.5, 111.1, 55.7, 28.10, 27.64, 22.52. IR: v (cm^{-1}) 3220, υ(N–H) stretching, 1634, υ(C=O) carbonyl. ESI-TOF MS: m/z (%); [M]$^+$ 958.03 Anal. calcd for C$_{36}$H$_{36}$Cl$_4$N$_4$O$_{10}$Zn$_2$: C, 45.17; H, 3.79; N, 5.85. Found: C, 45.48, H, 4.15, N, 6.13.

3.3.1.2 [Zn$_2$(L3.2)$_2$] (3.2)

Reaction of ligand **L3.2** (0.3g, 1.02 mmol) and Zn(OAc)$_2$.2H$_2$O (0.0.29g, 1.02 mmol) gave complex **3.2** as a white powder after workup. Yield 95%. Mp 227 – 231°C. ^{1}H-NMR (DMSO-d$_6$, 400 MHz): δ (ppm) 1.82 (s, 12H, OAc-CH$_3$),3.86 (s, 6H, CH$_3$O), 6.90 (sext, 6H, Ar), 7.10 (sept, 6H, Ar), 7.42 (s, 2H, Ar),7.60 (s, 2H, CH=N), 8.41 (s, H, NH). ^{13}C-NMR (DMSO-d$_6$, 400 MHz): δ (ppm) 149.9, 147.5, 145.8, 142.5, 139.1, 137.6, 129.8, 125.9, 123.2,55.72, 28.3, 27.8. IR: v (cm^{-1}) 3320 v(N–H) stretching, 1594 v(C=O) carbonyl. ESI-TOF MS: m/z (%); [M+Na]$^+$ 842.02. Anal. calcd for C$_{36}$H$_{40}$N$_4$O$_{10}$Zn$_2$: C, 52.76; H, 4.92, N, 6.84. Found C, 52. 89; H, 5.35, N, 7.08.

3.3.1.3 [Zn$_2$(L3.3)$_2$] (3.3)

The reaction of ligand **L3.3** (0.3g, 1.18 mmol) and Zn(OAc)$_2$.2H$_2$O (0.26g,1.18 mmol) gave complex **3.3** as a white powder after workup. Yield 90 %. Mp 218 – 220 °C. ^{1}H-NMR (DMSO-d$_6$, 400 MHz): δ (ppm) 1.82 (s, 12H OAc-CH$_3$), 2.10 (s, 6H, Ar-CH$_3$), 3.85 (s, 6H, CH$_3$O), 6.9 – 7.0 (m, 8H, Ar), 7.1 – 7.13 (m, 6H, Ar), 7.01 (s, 2H, CH=N), 8.34 (s, 2H, NH). ^{13}C-NMR (DMSO-d$_6$, 400 MHz): δ (ppm) 173.6, 160.6, 142.6, 134.0,130.2, 128.9, 127.6, 121.8, 118.1, 55.48, 27.8, 18.6, 17.6. IR: v (cm^{-1}) 3210 v(N–H) stretching, 1624 v(C=O) carbonyl. ESI-TOF MS: m/z (%); [M]$^+$ 874.29. Anal. calcd for C$_{40}$H$_{48}$N$_4$O$_{10}$Zn$_2$: C,54.8; H, 5.53, N, 6.40. Found: C, 55.18; H, 5.88; N, 6.67.

3.3.1.4 [Zn$_2$(L3.4)$_2$] (3.4)

The reaction of ligand **L3.4** (0.3 g, 0.97 mmols) and Zn(OAc)$_2$.2H$_2$O (0.21, 0.97 mmols) gave complex **3.4** as a white powder. Yield 95 %. Mp 209 – 213 °C. ^{1}H-NMR (DMSO-d$_6$, 400 MHz): δ (ppm) 1.12 (d, 24H ^{i}Pr-CH$_3$) 1.82 (s, 12H, OAc-CH$_3$), 3.02 (qn 4H CH-^{i}Pr), 3.86 (s, 6H, CH$_3$O), 6.96 (m, 12H, Ar), 7.62(s, 1H, CH=N), 8.30 (s, 1H, NH). ^{13}C-NMR (DMSO-d$_6$, 400 MHz): δ (ppm) 160.0, 148.5, 131.2, 126.8, 124.1, 122.5, 120.3, 116.5, 111.0, 55.6, 27.32, 23.5, 22.53. IR: selected: v (cm^{-1}) 3174 v(N–H) stretching, 1634 v(C=O) carbonyl. ESI-TOF MS: m/z (%); [M]$^+$ 988.14. Anal. calcd for C$_{48}$H$_{64}$N$_4$O$_{10}$Zn$_2$: C, 58.36; H, 6.53; N, 5.67. Found: C, 58.73; H, 6.72; N, 6.01.

3.3.1.5 [Cu₂(L3.1)₂] (3.5)

Reaction of ligand **L3.1** (0.3g, 1.02 mmol) and Cu(OAc)$_2$.2H$_2$O (0.20g, 1.02 mmol) gave complex **3.5** as green powder after workup. Yield 98 %. Decompose above 210 °C. IR: v (cm^{-1}) 3200 v(N–H) stretching, 1664 v(C=O) carbonyl. ESI-TOF MS: m/z (%); [M]$^+$ 954.37. Anal. calcd for C$_{36}$H$_{36}$Cl$_4$N$_4$O$_{10}$Cu$_2$: C, 45.17; H, 3.79; N, 5.85. Found: C, 45.58; H, 4.1; N, 5.96

3.3.1.6 [Cu₂(L3.2)₂)] (3.6)

Reaction of ligand **L3.2** (0.3g, 1.33 mmol) and Cu(OAc)$_2$.2H$_2$O (0.26g, 1.18 mmol) gave complex **3.6** as green powder after workup. Yield 96 %. Decompose above 205 °C. IR: v (cm^{-1}) 3320 v(N–H) stretching, 1590 v(C=O) carbonyl. ESI-TOF MS: m/z (%); [M+Na]$^+$ 837.16. Anal. calcd for C$_{36}$H$_{40}$N$_4$O$_{10}$Cu$_2$: C, 53.00; H, 4.94; N, 6.87. Found: C, 53.33; H, 5.23; N, 6.10.

3.3.1.7 [Cu₂(L3.3)₂] (3.7)

Reaction of ligand **L3.3** (0.03g, 1.18 mmol) and Cu(OAc)$_2$.2H$_2$O (0.24g, 1.02 mmol) gave complex **3.7** as a green powder after workup. Yield 98 %. Decompose above 205 °C. IR: v (cm^{-1}) 3209 v(N–H) stretching, 1666 v(C=O) carbonyl. IR: v (cm^{-1}) 3210 v(N–H) stretching, 1624 v(C=O) carbonyl. ESI-TOF MS: m/z (%); [M]$^+$ = 872.21. Anal. calcd for C$_{40}$H$_{48}$N$_4$O$_{10}$Cu$_2$: C, 55.10; H, 5.55; N, 6.43. Found C, 55.48; H, 5.89; N, 6.66.

3.3.1.8 [Cu₂(L3.4)₂] (3.8)

Reaction of ligand **L3.4** (0.03g, 0.96 mmol) and Cu(OAc)$_2$.2H$_2$O (0.20g, 1.02 mmol) gave complex **3.8** as a green powder after workup. Yield 99 %. Decompose above 203 °C. IR: v (cm^{-1}) 3180 v(N–H) stretching, 1606 v(C=O) carbonyl. ESI-TOF MS: m/z (%); [M]$^+$ 985.45. Anal. calcd for C$_{48}$H$_{64}$N$_4$O$_{10}$Cu$_2$: C, 58.58; H, 6.56; N, 5.69. Found: C, 58.89, H, 6.84, N, 5.8.

3.4 Polymerization of ε-caprolactone and rac-lactide

All manipulations were performed under an inert atmosphere (argon) using Schlenk techniques. The required amount of monomer ε-CL (bulk) and *rac*-LA (in 3 ml toluene) was added to a Schlenk tube and immersed in a preheated oil bath at 110 °C. The polymerization reaction was initiated by adding the required amount of the complex. Samples for kinetic experiments were withdrawn at regular intervals and quenched quickly by dissolving in cooled CDCl$_3$ in an NMR tube. The quenched samples were then analysed by ^{1}H-NMR spectroscopy to determine the extent of

polymerization. For PCL, the percentage conversion was obtained by considering the ε-CL monomer protons signal intensities at 4.2 ppm ($I_{4.2}$) and OCH$_2$ protons signal intensities at 4.0 ppm ($I_{4.0}$) and evaluated using equation (**3.1**).

$$\frac{[Polymer]_t}{[Monomer]_0} \times 100 = \frac{I_{4.0}}{(I_{4.2} + I_{4.0})} \times 100 \qquad (\textbf{3.1})$$

For PLA, the integration values of the methine proton of the monomer and that of the polymer were used to calculate the percentage conversion using the equation (**3.2**).

$$\frac{[Polymer]_t}{[Monomer]_0} \times 100 = \frac{I_{CH\ monomer}}{(I_{CH\ monomer} + I_{CH\ polymer})} \times 100 \qquad (\textbf{3.2})$$

The observed rate constants were extracted from the slope of the line of best fit from the plot of $\ln([M]_0/[M]_t)$ *vs t*

3.5 *Polymer characterization by size exclusion chromatography (SEC)*

Molecular weights and polydispersity indices were determined by size exclusion chromatography (SEC) at Stellenbosch University. The samples were dissolved in tetrahydrofuran (THF) stabilized with butylated hydroxytoluene (BHT) giving a sample with a concentration of 2 mg ml^{-1}. Sample solutions were filtered *via* a syringe through 0.45 mm nylon filters before being subjected to analysis. The SEC instrument consists of a Waters 1515 isocratic. HPLC pump, a Waters 717plus auto-sampler, a Waters 600E Paper system controller (run by Breeze Version 3.30 SPA) and a Waters in-line Degasser AF. A Waters 2414 differential refractometer was used at 30 °C in series along with a Waters 2487 dual wavelength absorbance UV/Vis detector operating at variable wavelengths. THF (HPLC grade stabilized with 0.125% BHT) was used as the eluent at flow rates of 1 ml min^{-1}. The column oven was kept at 30 °C and the injection volume was 100 ml. Two PLgel (Polymer Laboratories) 5 mm Mixed-C (300 x 7.5 mm) columns and a pre-column (PLgel 5 mm Guard, 50 x 7.5 mm) were used. Calibration was done using narrow poly-styrene standards ranging from 580 to 2 x 10^6 g mol^{-1}. All molecular weights were reported as polystyrene equivalents.

3.6 Single-crystal X-ray diffraction

Crystal evaluation and data collection was done on a Bruker Smart APEXII diffractometer with Mo Kα radiation (I = 0.71073 Å) equipped with an Oxford Cryostream low temperature apparatus operating at 100 K for all samples. Reflections were collected at different starting angles and the *APEX*II program suite was used to index the reflections.[31] Data reduction was performed using the *SAINT*[32] software and the scaling and absorption corrections were applied using the *SADABS*[33] multi-scan technique. The structures were solved by the direct method using the *SHELXS* program and refined using *SHELXL* program.[34] Graphics of the crystal structures were drawn using OLEX^2 software.[35] Non-hydrogen atoms were first refined isotropically and then by anisotropic refinement with the full-matrix least squares method based on F^2 using *SHELXL*.[34] The crystallographic data and structure refinement parameters for the complexes **3.3** and **3.7** are given in Table 3.1.

Table 3.1: The summary of X-ray crystal data collection and structure refinement parameters for complexes **3.3** and **3.7** and ligand **L3.1'**

Parameter	3.3	3.7	L3.1'
Empirical formula	$C_{24}H_{31}N_2O_6$ Zn	$C_{21}H_{26}Cl_2CuN_2O_5$	$C_{14}H_{12}Br_2N_2O$
Formula weight	508.88	520.88	384.08
T(K)	173(2)	173(2)	298(2)
λ(Å)	0.71073	0.71073	0.71073
Crystal system	Monoclinic	Monoclinic	Triclinic
Space group	$P2_1/n$	$P2_1/n$	P_{-1}
a (Å)	13.3875(10)	13.3645(10)	7.3470(3)
b (Å)	8.2952(6)	8.1503(6)	9.4435(4)
c (Å)	22.2506(16)	21.9480(18)	10.4335(4)
a, β, γ (°)	90, 105.9 (4), 90	90, 106.1 (3), 90	78.9(2), 85.4 (2), 86.384(2)
V (Å^3)	2376.2(3)	2295.8(3)	707.37(5)
Z	4	4	2
ρ_{calc} (mg/m^3)	1.422	1.507	1.803
μ (mm^{-1})	1.076	1.219	5.723
$F(000)$	1068	1076	376
Crystal size (mm)	0.41 x 0.38 x 0.22	0.250 x 0.230 x 0.130	0.33 x 0.25 x 0.28
θ range for data collection (°)	1.61 to 28.28.	1.611 to 28.554	707.37(5)
Index ranges	$-17 \leq h \leq 17$	$-17 \leq h \leq 17$	$-9 \leq h \leq 9$

	$-10 \leq k \leq 11$	$-8 \leq k \leq 10$	$-12 \leq k \leq 12$
	$-29 \leq l \leq 29$	$-29 \leq l \leq 29$	$-13 \leq l \leq 13$
Reflections collected	45974	21703	14686
Independent reflections	5852	5655	3439
	[R(int)= 0.0807]	[R(int) = 0.0262]	[R(int) = 0.0213]
Completeness to $\theta = 25.24°$ (%)	99.6	99.7	99.2
Data/restraints/parameters	5852/0/299	5655/0/280	3439/0/172
Goodness-of-fit (GOF) on F^2	1.039	1.053	1.295
Final R indices [$I > 2\sigma(I)$]	$R1 = 0.0552$,	$R1 = 0.0471$	$R_1 = 0.0335$,
	$wR_2 = 0.1373$	$wR_2 = 0.1185$	$wR_2 = 0.1038$
R indices (all data)	$R_1 = 0.0832$	$R_1 = 0.0573$	$R_1 = 0.0351$
	$wR_2 = 0.1512$	$wR_2 = 0.1231$	$wR_2 = 0.1045$
Largest diff. peak and hole (eÅ^{-3})	1.23 and -0.817	1.24 and -0.620	1.183 and -1.287

3.7 Results and discussion

3.7.1 Synthesis of N,N′-diarylformamidine ligands

The *N,N′*-diarylformamidine ligands **L3.1** – **L3.4** (Figure 3.3) were synthesized from a reported literature method and characterized by NMR and IR spectroscopy, mass spectrometry and elemental analysis. The unsymmetrical formamidines were synthesized in two steps and were isolated in excellent yields (74 - 79%). The reactions of the first portion of the aniline derivative with ethyl orthoformate and acid catalyst at 140 °C gave the intermediate (in blue) which was subsequently reacted with the second portion of the aniline to give the formamidine derivatives (Scheme 3.1).
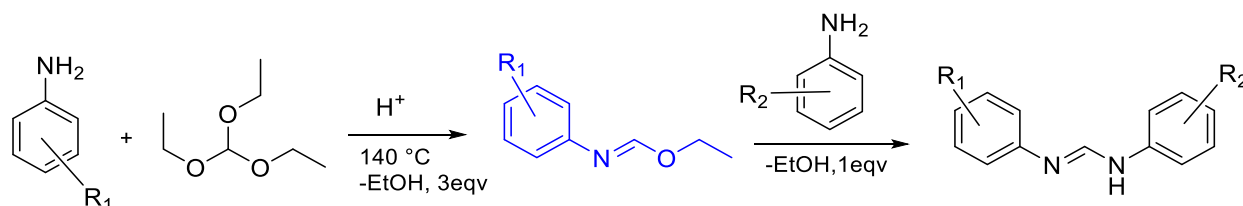
Scheme 3.1: Synthesis of *N,N′*-diarylformamidine ligands

The yield depended on the nature of the substituent groups. The positive inductive effect of the electron donating substituents renders the aniline to be more nucleophilic hence readily attack the carbocation. A plausible reaction mechanism involving electrophilic substitution to form the amidate intermediate with subsequent addition of the second the second aniline shown in Figure 3.4.
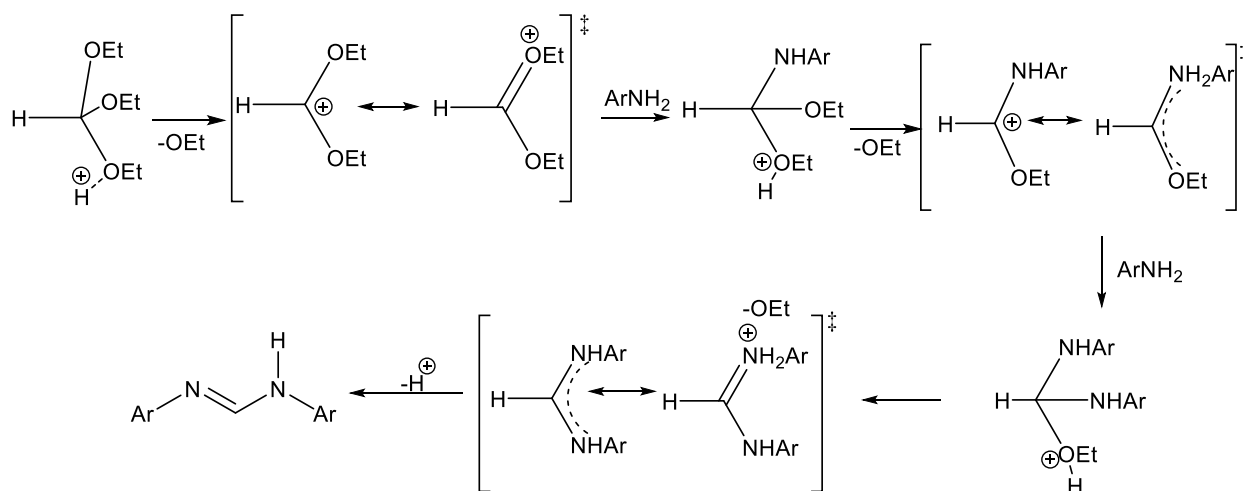
Figure 3.4: Reaction mechanism for synthesis of *N,N'*-diarylformamidine ligands

The presence of an acid can induce the conversion of unsymmetrical formamidines to the equivalent symmetrical formamidines, also elevated temperatures can cause a similar transformation. The mixture was separated by recrystallization in ethanol/acetone mixtures. Ligands **L3.1** – **L3.4** exhibited IR spectra showing the stretching frequency corresponding to ν(C=N), 1630 - 1666 cm^{-1} and ν(N—H), 3145 - 3200 cm^{-1}, respectively. These values agree with similar reported work for *N,N'*-diarylformamidine ligands.[36-38] The ligands were further characterised by ^{1}H- and ^{13}C-NMR. The ^{1}H-NMR spectra are characterized by azomethine (N-CH=N) proton resonate peaks between 7.45 – 9.00 ppm which further corroborate the formation of the amidine bridge. It is important to highlight that even though amidine compounds and their complexes are well studied, due to their isomeric nature, their solution NMR is sometimes complicated. This is attributed to their flexibility which results in rotational isomers that interconvert at rates restricted by the substituents and solvent.

For instance, for ligand **L3.4** two peaks were observed for the methoxy (OCH$_3$) and methine (Ha) protons with a ratio of 2:1 (Figure 3.5). The amine proton can also shuttle between the two nitrogens resulting in tautomerism and it can also participate in intermolecular H-bonding which further complicate their behaviour.
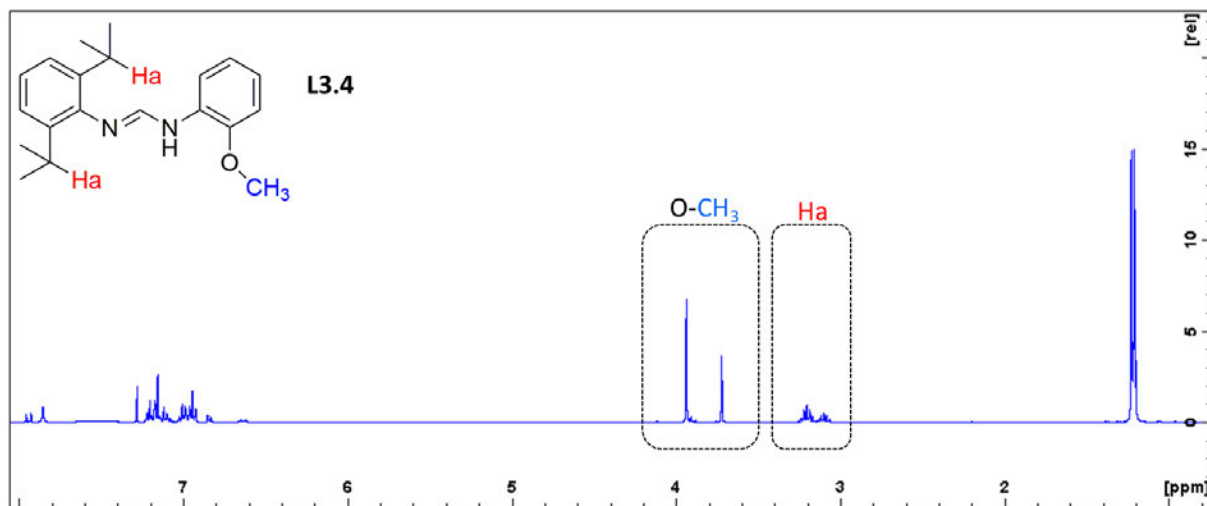
Figure 3.5: H^1-NMR spectrum of ligand **L3.4** at room temperature in CDCl$_3$ (400 MHz)

The isomeric forms are represented in Figure 3.6. The transformation between the isomers depends on the substituents with respect to the double bond. The isomers are assigned using the E/Z- and *syn/anti*-nomenclature relative to the C=N double bond and C—N single bond.
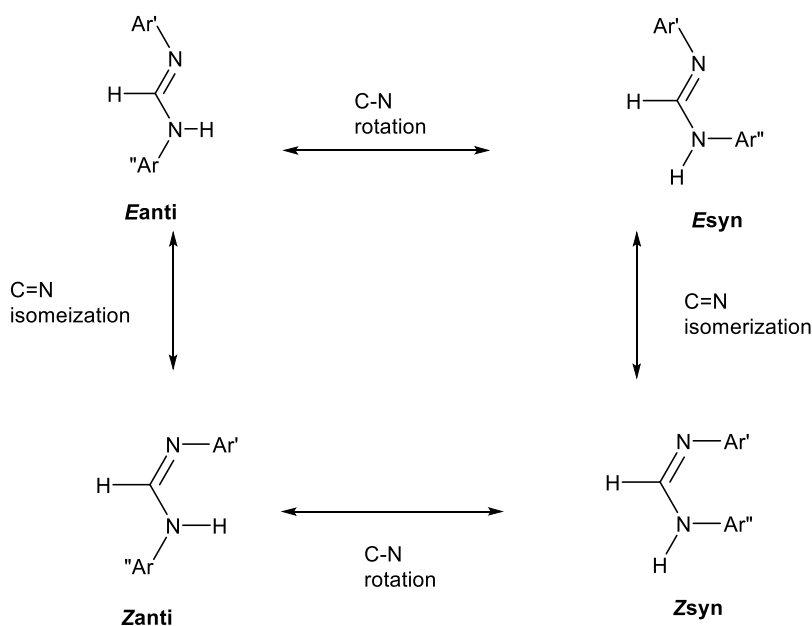
Figure 3.6: The *E/Z* and *syn/anti* nomenclature for *N,N'*-diarylformamidine

58

3.7.2 Synthesis of Zn(II) and Cu(II) complexes

Solvent-free mechanochemical grinding of appropriate ligand and metal acetate for 20 min resulted in Zn(II) and Cu(II) complexes **3.1** – **3.8** (see Scheme 3.2). The Zn(II) complexes were obtained as white solids while Cu(II) complexes were isolated as green solids in excellent yields (90 – 95%). The isolated powders were recrystallized in DCM and the complex stoichiometry corresponded to the elemental analysis and mass spectrometry data. For instance, complex **3.1** displayed a base ion peak at m/z 958.04 which correspond to $[Zn(\mathbf{L3.1})_2]^+$ (Figure 3.7). The results for the complexes **3.2** – **3.8** were consistent with their molecular structures, confirming their formation.

M = Zn, Cu

L3.1: R = Cl, **L3.2:** R = H, **L3.3:** R = Me, **L3.4:** R = ^{i}Pr,
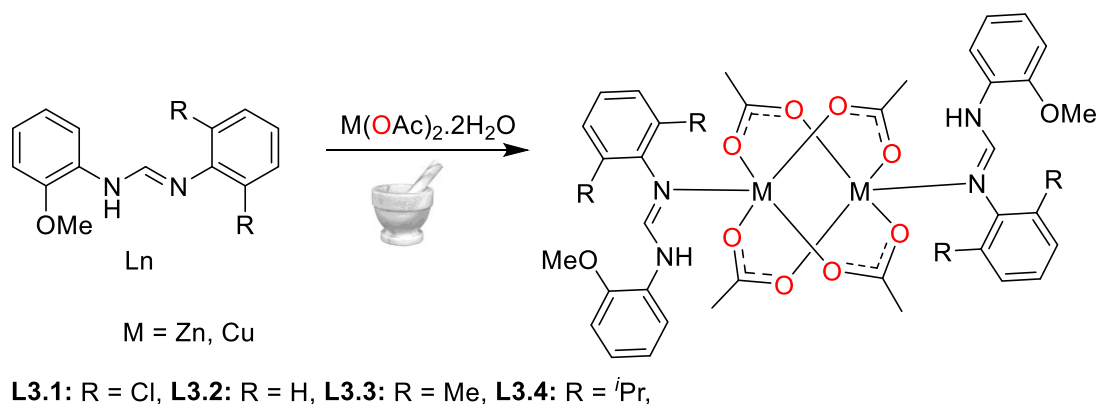
Scheme 3.2: Synthesis of Zn(II) and Cu(II) *N,N′*-diarylformamidine complexes
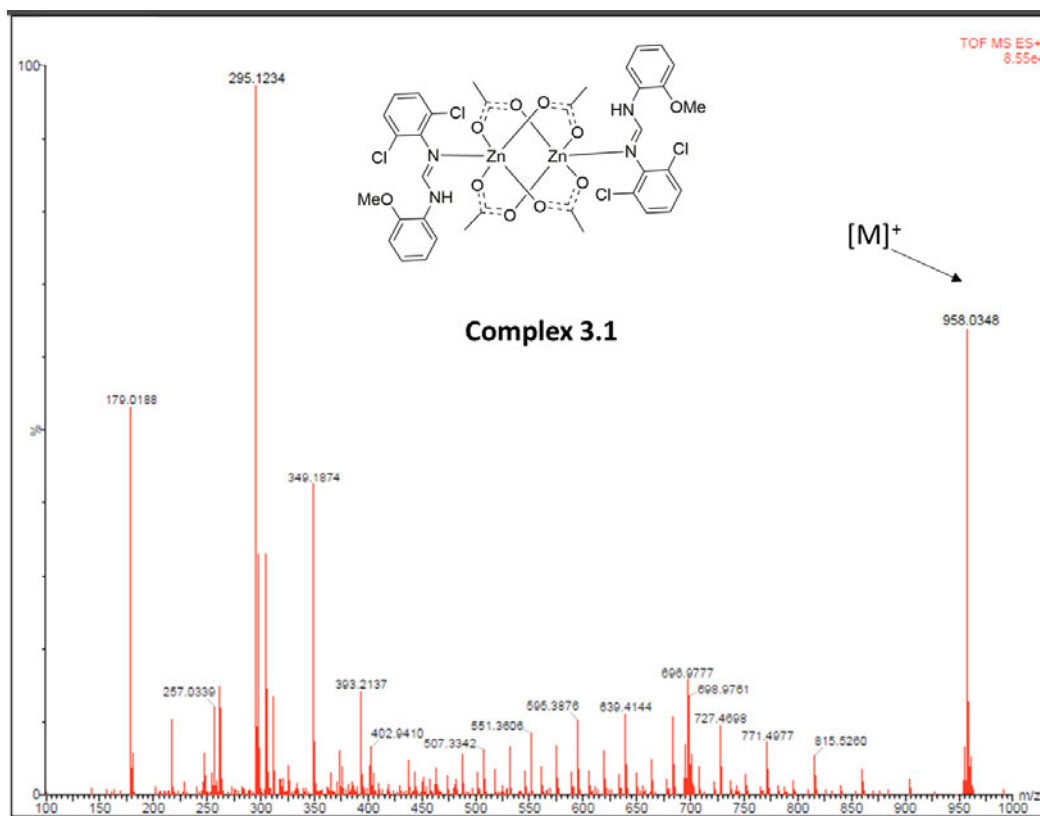
Figure 3.7: ESI-MS spectrum for complex **3.1**

3.7.3 IR and NMR spectroscopy analysis

The formation of complex **3.1** – **3.8** was also confirmed by IR spectroscopy where a sharp absorption peak at 3400 cm^{-1} was observed for all complexes assigned to N–H stretching frequency. In complexes **3.1** – **3.8**, the C=N band is red-shifted compared to ligands, due to the coordination through the imino nitrogen. They were also reasonably sharper in contrast to those observed in the spectra of ligands. For instance, the C=N symmetric stretching band in complex **3.1** resonate at 1620 cm^{-1} as compared to 1600 cm^{-1} in **L3.1**. The broad bands at about 1655 cm^{-1} and 1590 cm^{-1} match the symmetric and antisymmetric stretch of the carboxyl groups, respectively. Generally, carboxylates can coordinate in a mono- or bi-dentate manner. The peak at 1600 cm^{-1} is not split in all complexes, implying that the coordination mode is *syn-syn* bidentate. The parameter $\Delta\upsilon$ ($\upsilon(COO)_{sym} - \upsilon(COO))_{asym}$ is an indicator of the coordination mode of carboxylate ligand in metal–carboxylates complexes. In all complexes, the $\Delta\upsilon(COO)$ value are comparable to those of reported complexes that exhibited bidentate carboxylate coordination.[29,30]

60

Table 3.2: IR azomethine C=N and C=O symmetry stretch frequency and shift for ligands and complexes

Complex	IR v(C=N) cm^{-1}			IR v(C=O)		
	Ligand	Complex	Δv	Sym	Asym	Δv
3.1	1620	1600	20	1657	1586	71
3.2	1630	1618	12	1656	1594	62
3.3	1596	1591	5	1654	1593	61
3.4	1603	1583	20	1649	1584	65
3.5	1620	1597	23	1652	1585	67
3.6	1630	1612	18	1653	1590	63
3.7	1596	1592	4	1653	1592	60
3.8	1590	1587	3	1651	1586	65

The Zn(II) series of complex was further analysed with NMR spectroscopy and proton peaks that are consistent with the ligand motif were observed. For example, complex **3.1** ^{1}H- and ^{13}C-NMR spectra are shown in Figure 3.8 and 3.9. A slight shift in the azomethine proton of the complexes with respect to the ligands and the presence of the acetate CH$_3$ proton signals at around 1.82 ppm confirmed the formation of the complexes. The ^{13}C-NMR spectrum showed the presence of two extra carbon signals at 22.0 and 160 ppm, which are ascribed to the acetate methyl and carbonyl carbons. The ^{1}H- and ^{13}C-NMR spectra for other complexes appear in appendix A.
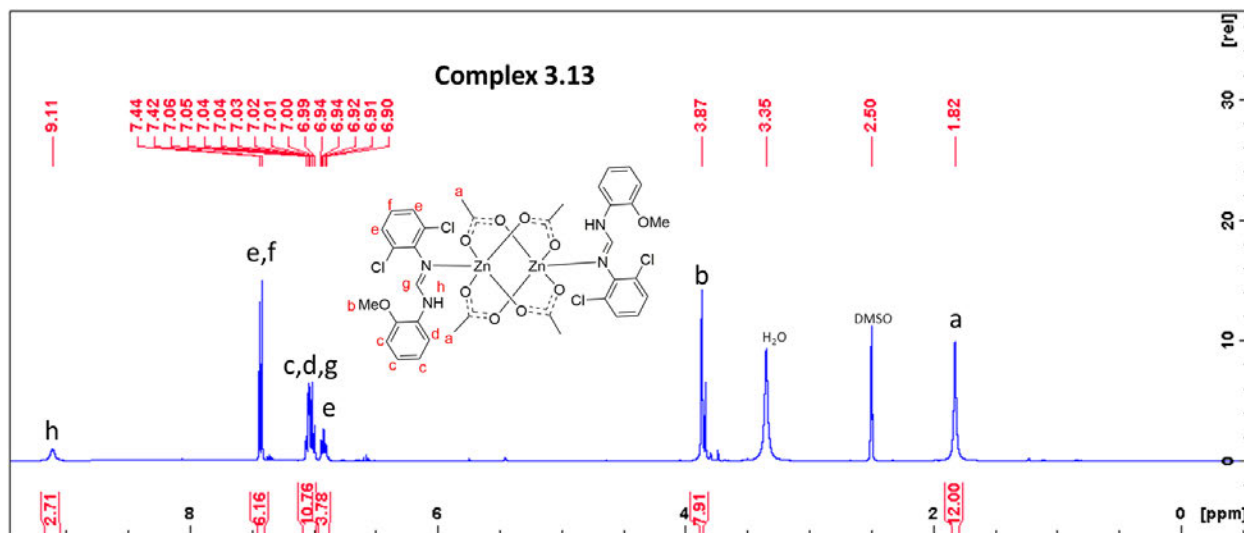
Figure 3.8: H^1-NMR spectrum of complex **3.1** at room temperature in DMSO-d$_6$ (400 MHz)
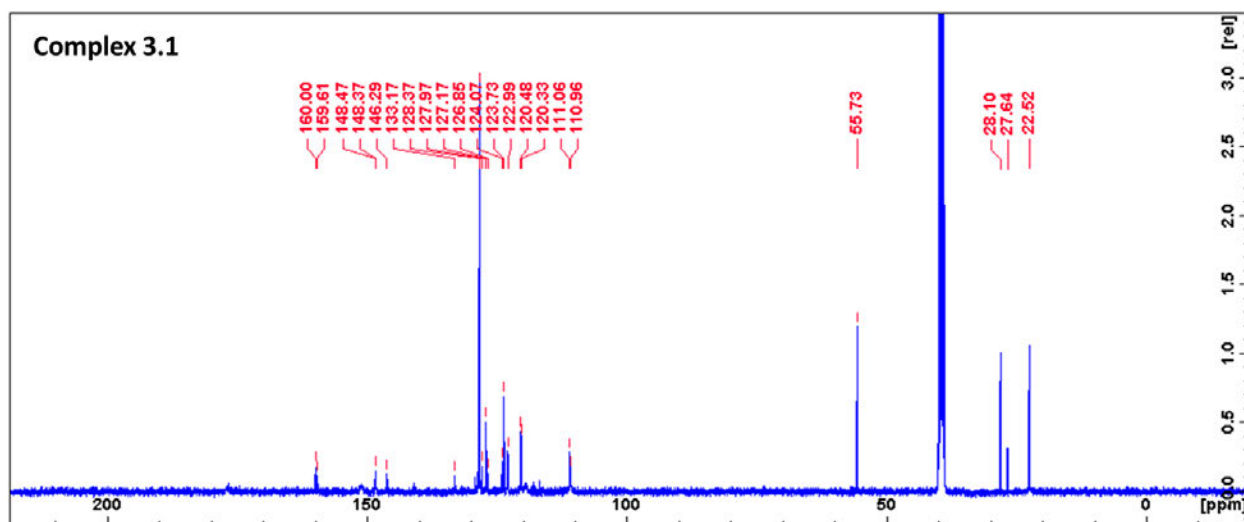
Figure 3.9: ^{13}C-NMR spectrum of complex **3.1** at room temperature in DMSO-d$_6$ (400 MHz)

3.7.4 *Uv-Vis spectroscopy*

The absorption spectra of all compounds in DCM were recorded in the 200 – 450 nm range solutions at concentrations of $\sim 10^{-5}$ M. The UV-visible absorption spectra of **L3.1 - L3.4** and complex **3.1 – 3.8** showed identical bands as anticipated at 270–277 nm and 327–334 nm regions, respectively, which are mainly due to intra-ligand (IL) π-π* and n-π* electronic transitions (Figure 3.10 and 3.11). The complex spectra almost match those of free ligand although there are minor shifts in some cases.

The presence of electron donating groups in complexes **3.3**, **3.4**, **2.7** and **3.8** resulted in higher π-π* absorption coefficient and this is due to the positive inductive effect. In contrast to complexes **3.1** and **3.5**, the negative inductive effect of the halogen removed the electron from the pi-system causing a reduction in π-π* absorption band. This also resulted in bathochromic shift of absorption maxima to lower extinction coefficients for complex **3.1**.
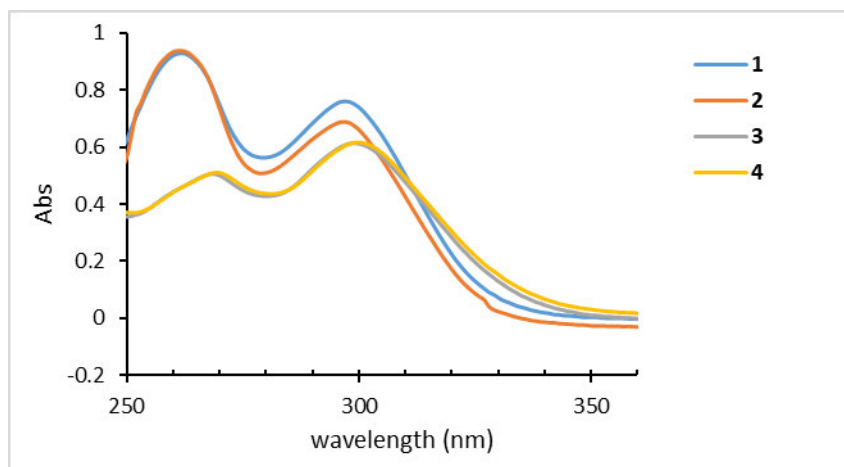
Figure 3.10: UV–Vis spectra of complexes **3.1** – **3.4** in DCM
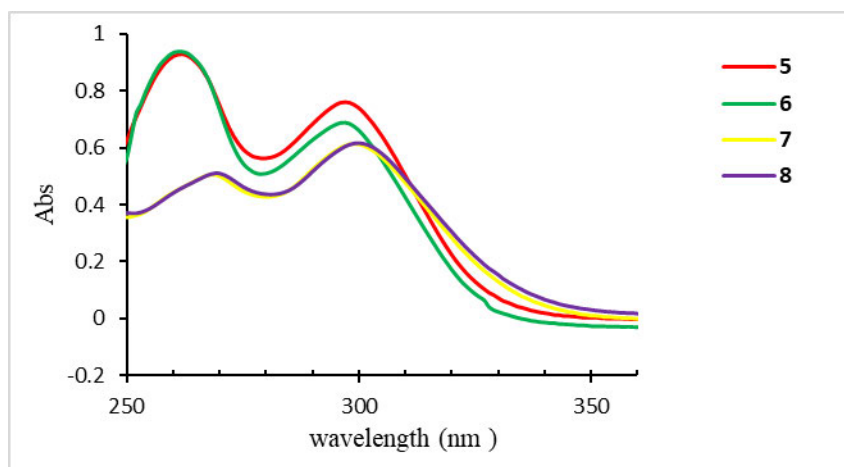
Figure 3.11: UV–Vis spectra of complexes **3.4** – **3.8** in DCM

3.7.5 Single-crystal X-ray analysis

3.7.5.1 Molecular structure of ligand L3.1'

The molecular structures of ligand **L3.1'** was determined by single crystal X-ray diffraction. The crystals were obtained by slow evaporation from DCM solution. The molecular structure is shown in Figure 3.12. The asymmetric unit of **L3.1'**contains one molecule and it preferably adopts the *trans* conformation. The C—N bonds length is between 1.290(5) - 1.343(5) Å with the two N atoms at an angle of 122.24(10)° with respect to azomethine carbon. These values agree with literature values.[36,39] The torsional angles of the bromo and methoxy substituted phenyl rings planes is 48°.

The unit cell contains a centrosymmetric dimers due weak intermolecular H-bonding with D···A distance of 2.9140 (1 2) Å and (D-H···A) angle of 163 (2)° and the deviation from linearity points to weaker interactions.
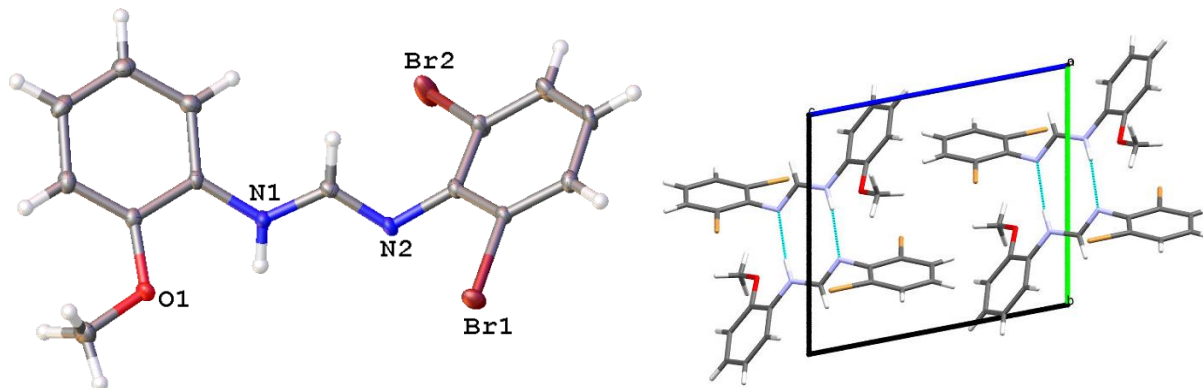
Figure 3.12: (a) X-ray crystal structure of ligand **L3.1'** with thermal ellipsoids drawn at 50% probability level and (b) Packing diagram of ligand as viewed down the crystallographic b-axis. The N—H···N hydrogen bonds are shown as dashed green line

3.7.5.2 Molecular structure of complexes 3.3 and 3.7

The molecular structures of complexes **3.3** and **3.7** were determined by single crystal X-ray diffraction. The crystals were obtained by slow evaporation THF and dichloromethane complex solutions, respectively. The molecular structures are shown in Figure 3.13 and 3.14 while selected bond distances and angles are listed in Table 3.3.
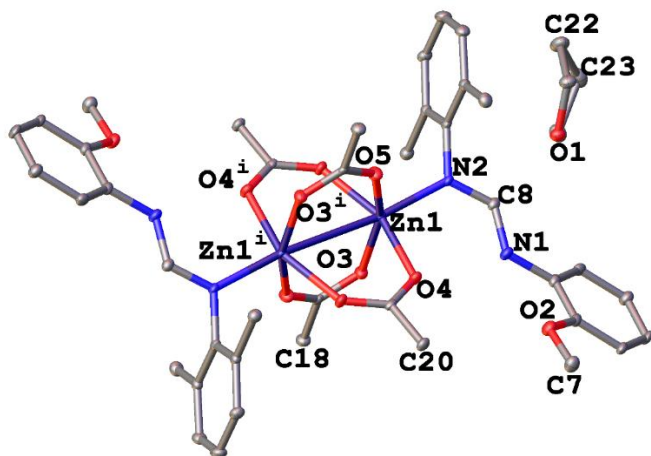
Figure 3.13: X-ray crystal structure of complex **3.3** with thermal ellipsoids drawn at 50% probability level. Hydrogen atoms have been omitted for clarity
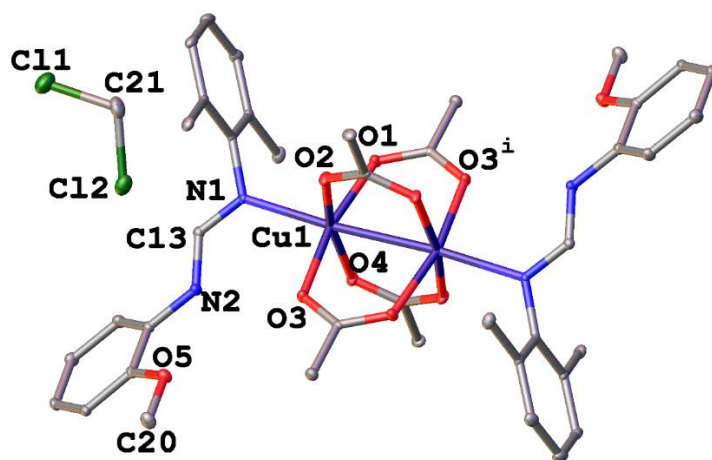
Figure 3.14: X-ray crystal structure of complex **3.7** with thermal ellipsoids drawn at 50% probability level. Hydrogen atoms have been omitted for clarity

Complexes **3** and **7** could, by virtue of similar unit cell parameters be isomorphous with the unit-cell volume of complex **3** slightly larger than that of complex **7** (Table 3.1). The asymmetric unit of each complex has a solvent molecule (tetrahydrofuran in complex **3** and dichloromethane in complex **7**) and only half a molecule of the complex. The molecular packing is different in the centring where we have *C* in **3** and *B* in **7** (Figure 3.15).

However, an overlay of the two complex molecules gives a root mean square deviation (RMSD) of only 0.0506 Å and as such the centring differences could be because of solvent molecule interactions with the complex (Figure 3.16).
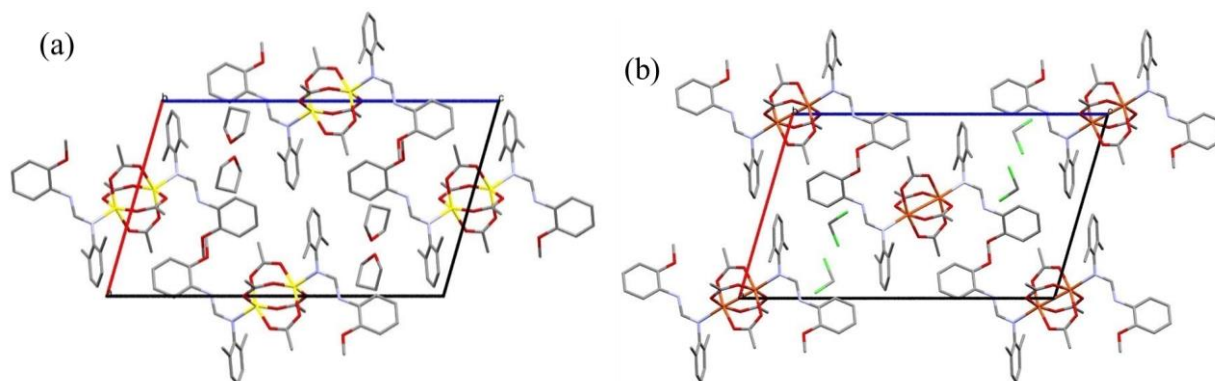
Figure 3.15:   Packing diagram of complexes (a) **3.3** and (b) **3.7** as viewed down the crystallographic b-axis direction. Hydrogen atoms have been omitted for clarity
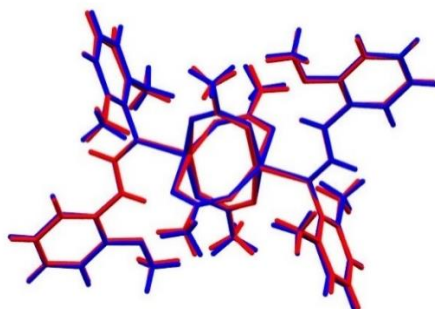
Figure 3.16: An overlay of complex **3.3** (blue) and complex **3.7** (red)

Complexes **3** and **7** are centro-symmetrical dimers with an inversion centre situated at the centre of a paddlewheel core-structure. The metal ions in both complexes are penta-coordinated resulting in distorted square-pyramidal geometries around them. Coordination is by auxiliary acetates *O* atoms in the base of the pyramid and the formamidine imino-nitrogen at the apical position of the pyramid. The O—M—O bond angles are orthogonal an arrangement that has the acetate anions bridging the two Zn(II) and two Cu(II) ions in a *syn-syn* arrangement in complexes **3** and **7**, respectively.

The Zn—O$_{eq}$ bond distances are 2.043(2) and 2.066(2) Å while the Cu—O$_{eq}$ bond distances are 1.972(2) and 1.975(2) Å while the Zn—N and the Cu—N bond distances are 2.042(3) and 2.197(2) Å and are comparable to similar complexes in literature.[40-42] While **7** exhibits a metal-to-metal interaction with a Cu⋯Cu separation of 2.6653(7) Å, less than the sum of van der Waals radii of about 2.8 Å, **3** has a Zn⋯Zn separation at 2.9898(8) Å, a distance larger than the sum of the van der Waals radii of Zn atoms (1.39 Å), hence no Zn⋯Zn interaction. These metal to metal distances are consistent with other reported structures.[29,30,43]

Table 3.3: Selected bond lengths and angles for complexes **3.3** and **3.7**

	3.3	3.7
Bond length [Å]		
M—M	2.9898(8)	2.6653(7)
M—N	2.042(3)	2.197(2)
M—O	2.043(2) -2.066(2)	1.972(2) – 1.975(2)
Angles [°]		
N—M—O	99.02(11) – 101.45(10)	95.15(9) – 97.58(9)
O—M—O	87.04(10) – 89.14(10)	88.61(8) – 90.85(8)
2,6MePh(NCN)		171.9(3)
2-MeOPh(NCN)		175.0(3)

3.7.6   Ring-opening polymerization of ε-caprolactone and ʟ-lactide

The polymerization performance of complexes **3.1** – **3.8** for caprolactone and *rac*-lactide polymerization was studied.   Preliminary investigations were done in bulk using monomer/initiator, [M]/[I] mole ratio of 200:1. Monomer conversion was monitored using ^{1}H-NMR and preliminary data showed that complexes **3.1** – 3.**8** could initiate ROP of ε-CL and *rac*-lactide attaining 99% monomer conversion within 28 – 120 h. Complexes **3.1** and **3.2** were further used to probe the effect of varying initiator concentration. The polymerization summary results of are recorded in Table 3.4 and 3.5. Zn(II) complexes showed superior activity over the Cu(II) analogues. Induction periods of about 6 h were observed for Zn(II) complexes while for Cu(II) complexes they range from 10 – 20 h. Low activity and slow onset of initiation in Cu(II) complexes can be attributed to the paddle-wheel structure commonly formed by Cu-carboxylate complexes that are normally very stable.

Even though the same paddle-wheel structure is observed in the Zn(II) complexes reported herein, it seems like the Zn—O bonds are slightly more labile in addition to greater nucleophilicity of Zn(II) acetates compared to Cu(II) acetates, hence a shorter induction period. Comparatively, the square planar complexes reported by in chapter 4 promoted faster monomer conversion with the most active taking 24 h for complete monomer conversion. The slower induction period in the paddlewheel structures can be attributed to structural rearrangement to generate the reactive catalytic species.[8] In such an instance, the complexes are said to be acting as both initiators and catalysts, a reason for the use of the terms interchangeably (v*ide infra*).

Table 3.4: Summary of polymerization data of ε -CL catalysed by complexes **3.1 – 3.8**

Entry	Complex	[M/I]	Time (h)	[b]Conv (%)	[c]$M_{w(cal)}$	[d]$M_{w(NMR)}$	k_{app}(h[-1])
1	**3.1**	100:1	48	98	11181.8	7345	0.0812
2	**3.2**	100:1	56	98	11067.7	7023	0.0721
3	**3.3**	100:1	66	99	11295.9	6822	0.0638
4	**3.4**	100:1	68	98	11181.8	5234	0.0627
5	**3.5**	100:1	72	98	11181.8	6345	0.0589
6	**3.6**	100:1	73	99	11295.9	6021	0.0551
7	**3.7**	100:1	78	98	11181.8	5673	0.0496
8	**3.8**	100:1	80	99	11295.9	4982	0.0462

[a]Polymerization conditions: 110 °C, Bulk. [b,d]Determined from NMR. [c]Calculated theoretical M_w

3.7.7   *Molecular weight and molecular weight distribution of polymers*

Increasing the monomer concentration resulted in increased molecular weights (see Table 3.5). This can be rationalized by the fact that there are few polymer chains propagating per initiating specie. Increasing the monomer:initiator ratio from 100:1 – 400:1, the $M_{n(GPC)}$ of poly(ε-CL) increased from 1720 g mol^{-1} to 6042 g mol^{-1} while those for poly(*rac*-LA) improved from 2292 to 7000 g mol^{-1}. Also, the GPC molecular weights are close to those obtained from NMR spectroscopy analysis and the discrepancies may be because the separation in GPC is mainly due to hydrodynamic volume assumed in solution.

Table 3.5: Effect of monomer concentration on rates and polymer M_w for complexes **3.1** and **3.2**

Entry	Complex	[M/I]	Time (h)	[c]Conv (%)	[d]$M_{w(calc)}$	[e]$M_{w(GPC)}$	[f]PDI	k_{app} (h⁻¹)	[g]IE
1	[a]**3.1**	100:1	42	98	11185.7	1720.9	2.00	0.0973	0.15
2	[a]**3.1**	200:1	50	98	22344.2	2511.0	1.89	0.0790	0.22
3	[a]**3.1**	300:1	56	97	33174.2	3035.8	1.99	0.0583	0.27
4	[a]**3.1**	400:1	62	95	43320.2	6043.0	1.76	0.0439	0.61
5	[b]**3.2**	100:1	6	98	14112.2	2292.7	1.87	0.5795	0.16
6	[b]**3.2**	200:1	24	98	28224.2	2793.3	1.78	0.1643	0.20
7	[b]**3.2**	300:1	30	98	42336.2	3796.1	1.78	0.1363	0.27
8	[b]**3.2**	400:1	34	87	50112.2	7000.0	1.82	0.0610	0.51

Polymerization conditions: 110 °C. [a]Bulk (ε-CL). [b]*rac*-LA, 3.0 ml of toluene as the solvent. [c]Determined from NMR. [d]Calculated theoretical Mw. [e,f]Determined by GPC relative to polystyrene standards in THF. [e]Experimental M_w was calculated considering Mark–Houwink's corrections of 0.56 for (PCL) and 0.58 for (PLA)
[g]Initiator efficiency (IE) = $M_{w(exp)}/M_{w(calc)}$

Generally, the molecular weight values obtained from NMR spectroscopy were influenced by the steric hindrance around the metal centre. In changing from H atom to ^{i}Pr substituent on the phenyl rings, there seems to be a reduction of the molecular weights of the polymers produced. This can be attributed to monomer inhibition, to access the catalytic centre, by the bulkier groups. The molecular weights for both monomers are comparable with broad molecular weight distributions ranging between 1.76 - 2.0 for poly(ε-CL) and 1.78 – 1.87 for poly(*rac*-LA). The broadness in molecular weight distribution is a testimony that the polymerization deviated from the ideal "living" ROP behaviour. This tendency also points to the occurrence of inter- and intramolecular transesterification and chain-transfer reactions which results in cyclic polymers. The ''non-living'' polymerization behaviour was also affirmed by the observed slight increase in molecular weight and PDI for complex **3.1** from 2559.5 g mol⁻¹ (Run 1, PDI = 2.6) to 3207.4 g mol⁻¹ (Run 2, PDI = 2.1) when a second equivalent amount monomer was added after the first run (Figure 3.17).
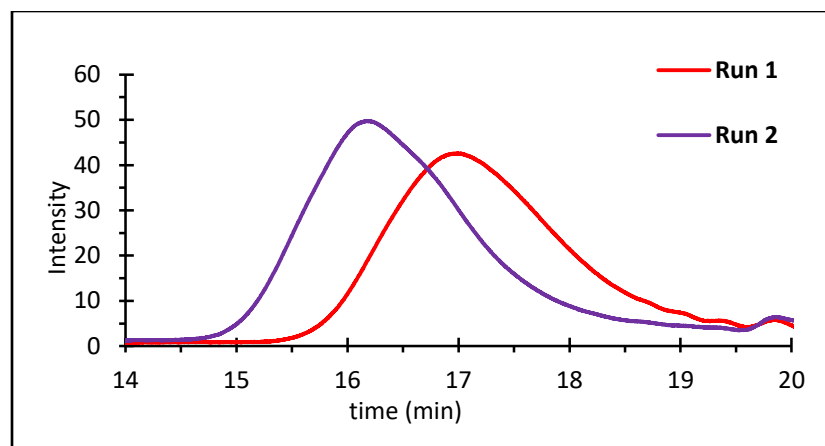
Figure 3.17: GPC chromatogram overlay for PCL recovered for complex **3.1**

Two distributions of peaks were observed in the EIS-MS spectrum of poly(ε-CL) (Figure 3.18) with the sets having a peak difference of 114 *m/z*, which agrees to the molecular weight of the ε-CL monomer unit. The second pattern of peaks is offset by 18 *m/z* corresponding to the loss of water which confirms the presence of cyclic polymers. The signals in ESI-MS spectrum (Figure 3.19) of poly(rac-LA) showed main peaks of the lactide repeat unit (144.0 g mol^{-1}) with small additional peaks. However, bimetallic nature cannot be excluded as it potentially presents many initiating sites.
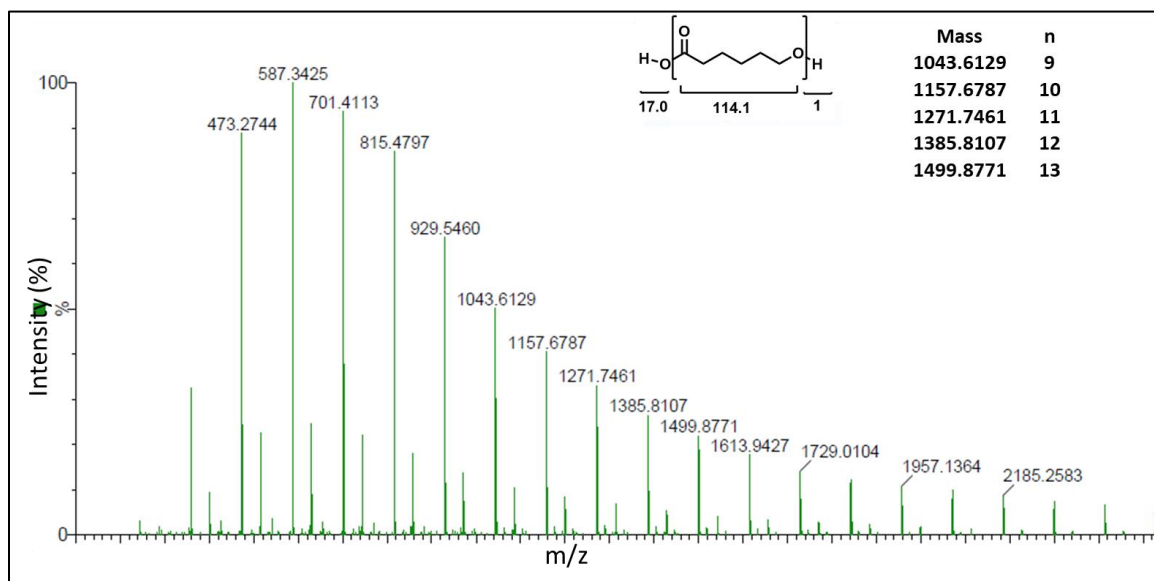
Figure 3.18: ESI-MS spectrum of poly(ε-CL) obtained from complex **3.1**, $[CL]_0:[I]_0 = 100:1$, t = 32 h

70
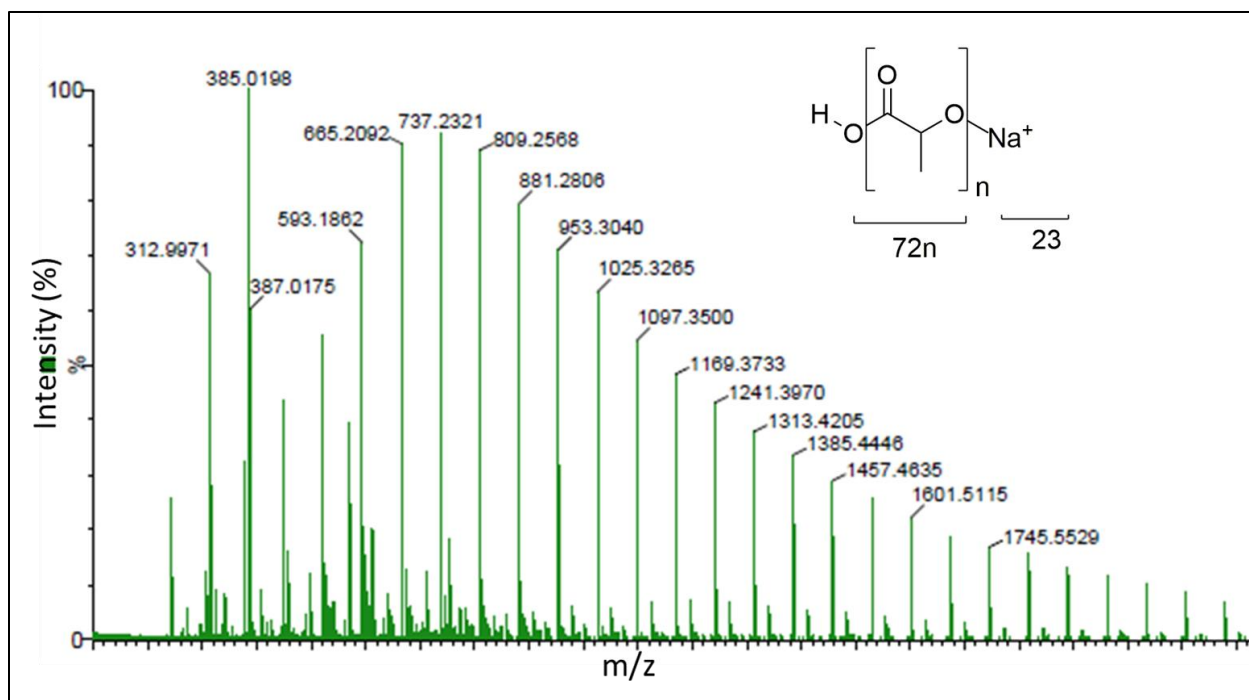
Figure 3.19: ESI-MS spectrum of poly(*rac*-PLA) obtained from complex **3.3**, $[CL]_0:[3.3]_0 = 100:1$, t = 56 h

3.7.8   Kinetics of ROP reactions of ε-CL and rac-LA

The ROP processes of ε-CL were investigated at 110 °C by kinetic studies using complexes **3.1** – **3.8** whereby complex **3.1** was found to be more active and it was used for *rac*-LA. The semi-logarithmic plots of $\ln([M]_0/[M]_t)$ *vs t* are shown in Figure 3.20 and 3.21. In both cases, an induction period *c.a.* 6 - 12 h and *pseudo* first-order kinetics dependency in monomer conversion is observed. Above the induction periods, the plots of $\ln([M]_0/[M]_t)$ *vs t* for Zn(II) complexes showed a linear relationship. However, the data for Cu(II) complexes deviated from fitted first order kinetics plot over the entire reaction time pointing to a *pseudo* first order kinetics behaviour. This trend can also be rationalized by the higher activation required to generate the active species. The apparent rate constant (k_{app}) for each complex was obtained from the slope of $\ln([M]_0/[M]_t)$ *vs t* and are summarized in Table 3.4. The monomer polymerization reaction using complexes **3.1** – **3.8** proceeded according to equation (**3.3**),

$$-\frac{d[M]}{dt} = k[M] \qquad (3.3)$$

where $k_p = k[I]^x$; k_p = rate of chain propagation and I = initiator/catalyst; x = order of reaction.

71

The rate of polymerization was also influenced by metal identity, with Zn(II) initiators being more active that Cu(II) initiators (Table 3.4). For instance, $k_{app} = 0.0608$ h^{-1} by complex **3.3** is greater than that of complex **3.6** ($k_{app} = 0.0384$ h^{-1}). Zn(II) has a greater electrophilicity which promotes monomer coordination, hence greater activity. The inductive tendency of the substituent also influences the activity of the complexes.[44] The Zn(II) complex possessing electron withdrawing chloro-substituents was the most active ($k_{app} = 0.0803$ h^{-1}) while the introduction of electron donating groups resulted in reduced activity.
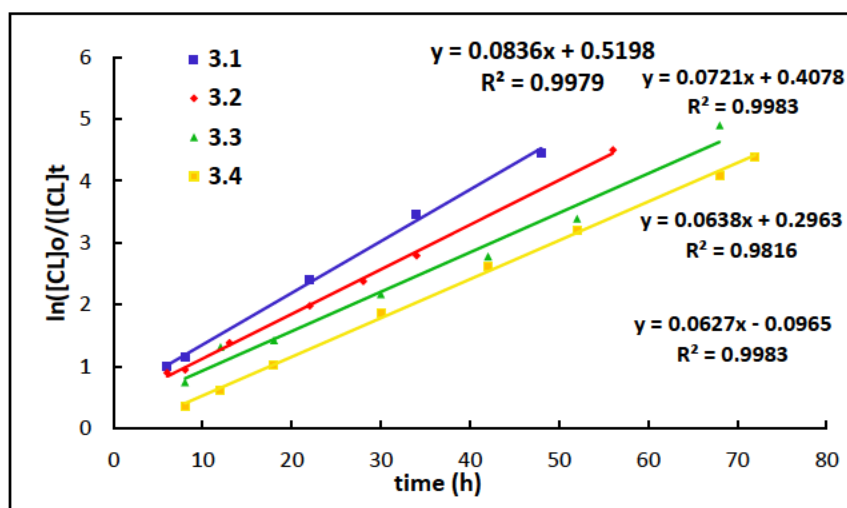
Figure 3.20: Plots of $\ln([CL]_0/[CL]_t)$ *vs* *t* catalysed by complexes **3.1 – 3.4**. Reaction conditions: $[M]_0 = 100{:}1$ bulk, T = 110 °C
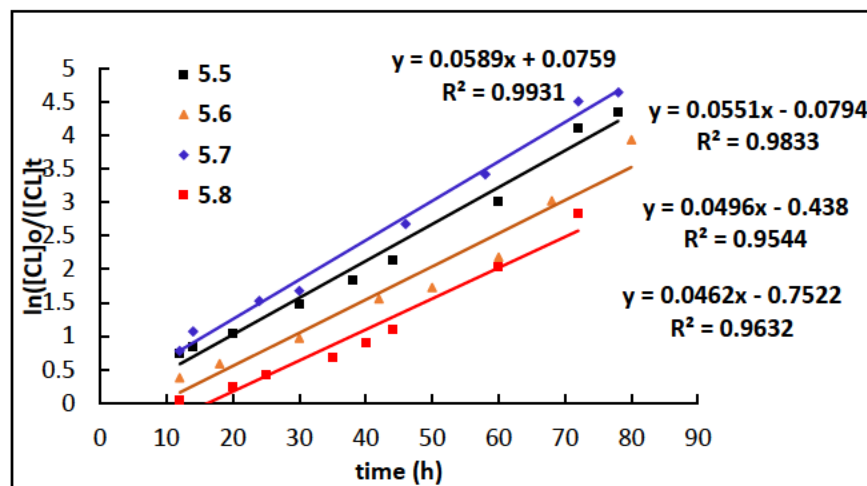
Figure 3.21: Plots of $\ln([CL]_0/[CL]_t)$ *vs* *t* catalysed by **3.5 – 3.8**. Reaction conditions: $[M]_0{:}[I]_0 = 100{:}1$; T = 110 °C

72

The steric effects can be noticed from the decreasing trend of apparent rate constant from unsubstituted complex **3.2** (k_{app} = 0.0696 h^{-1}) to bulk methyl and isopropyl groups complex **3.3** (k_{app} = 0.0608 h^{-1}) and complex **3.4** (k_{app} = 0.0543 h^{-1}), respectively. This considerable change in reactivity is due to the positive inductive effect which reduces the metal Lewis acidity making it less susceptible to coordinate to the monomer. The same trends have also been reported in literature.[45,46] The increase in bulkiness most likely retards rate of binding of the incoming monomer to the metal site. Even though literature has suggested that symmetry affects the catalytic activity,[47] the activities of the unsymmetrical complexes reported in this work are comparable to our previous work using symmetrical formamidine ligands.[29,30] For instance, a similar paddlewheel Cu(II) complex with symmetrical ligands (k_{app} = 0.0441 h^{-1})[30] is comparable to the unsymmetrical complex **3.3** (k_{app} = 0.0543 h^{-1}). Therefore, we conclude that the coordination mode of the auxiliary acetates ligands plays a bigger role on the catalytic activity than symmetry does. On the other hand, the apparent rate constants for complexes **3.1** – **3.8** are inferior to initiators containing alkoxides. However, they are comparable to similar metal catalyst containing carboxylate initiating groups.[48-50]

To determine the order of reaction of complex **3.2** with respect ε-CL and *rac*-LA, polymerizations at different initial initiator concentrations were done. The semi-logarithmic plots of lnk_{app} vs ln [**3.2**] for ε-CL and *rac*-LA are shown in Figure 3.22. The slopes obtained were 0.56 and 1.52 for complex **3.2** with respect to ε-CL and *rac*-LA, respectively. These results are similar to other reported initiator systems and symmetrical formamidine initiators from our earlier report.[29] However, they contrast results obtained for reported alkoxide initiators which exhibited a first order reliance on both monomer and catalyst.[51,52] Fractional reaction orders with respect to initiators have also been displayed in bulk polymerization process and this is due to initiator clustering and dissociation during polymerization.[53,54]
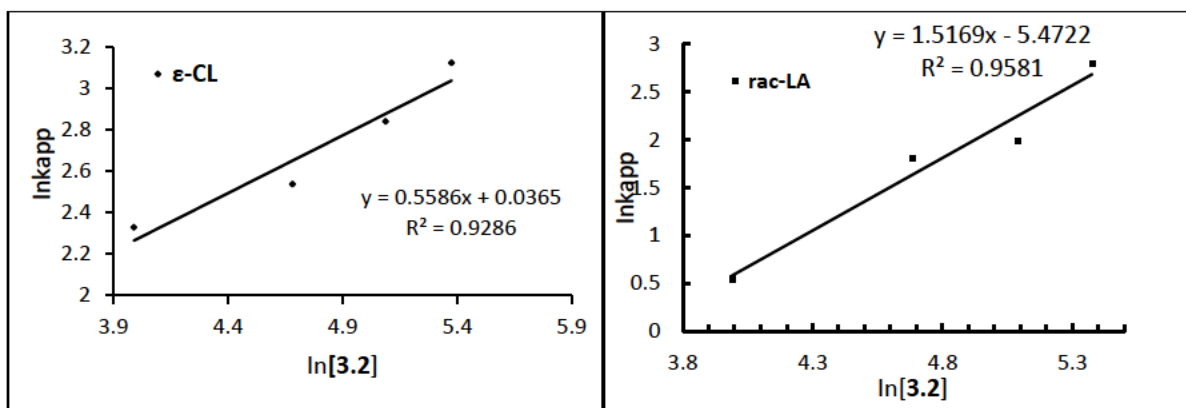
Figure 3.22: Plot of $\ln k_{app}$ vs $\ln[3.2]_0$ for determining the order of reaction with respect ε-CL and *rac*-LA

3.7.9 Effect of temperature and activation parameters

To further understand the polymerization process, kinetic experiments were done between 90 – 120 °C with complex **3.3** as the choice catalyst. Low activity was exhibited at 90 °C, with a longer induction period however the rate increased with temperature. The logarithmic plots of for $\ln([M]_0/[M]_t)$ *vs* t (Figure 3.23) were linear after the induction period for all temperatures studied which reveals a *pseudo*-first order kinetics and the apparent rate constant (k_{app}) increased with temperature.
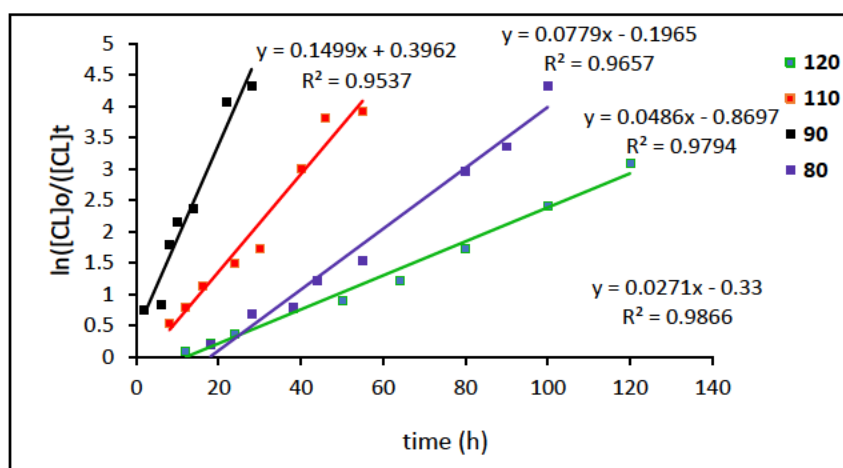
Figure 3.23: Plots of $\ln([CL]_0/[CL]_t)$ *vs* t catalysed by **3.2**. Reaction conditions: $[M]_0:[I] = 100:1$. T = 80 – 120 °C

74

It has been shown by several authors, through DFT analysis, that the reaction involves transition states exhibiting varying activation barriers.[55-57] The initiation and propagation proceeds *via* the most accessible pathway. For complex **3.3**, the overall activation barrier deduced from the slope of the Arrhenius plot of lnk_{app} vs T^{-1} (Figure 3.24a) and was found to be 60.12 KJ mol^{-1}. This value is twice (E_a = 28.05 kJ mol^{-1}) reported in our previous work on symmetrical formamidine ligands.[30] This difference is mainly attributed to the coordination geometry of the acetates to the Zn(II) and Cu(II) centres. The bridging mode *vs* the monodentate of the acetates as reported earlier renders the M—O bond in complex **3.3** to be stronger hence a larger activation barrier is involved to generate the active species. Activation parameters were inferred from the Eyring plots where the linear lines were fitted using equation (3.4).

$$In\frac{kapp}{T} = \frac{\Delta H^\#}{R}\frac{1}{T} + In\frac{kb}{h} + \frac{\Delta S^\#}{R} \qquad (3.4)$$

The enthalpy of activation ($\Delta H^\#$) and the entropy of activation ($\Delta S^\#$) were obtained as 56.97 kJ mol^{-1} and -118.35 JK^{-1} mol^{-1}, respectively, for complex **3.3** at [M]$_0$:[I] = 100:1 (Figure 3.24b). These typically higher values compared to other reported for ROP,[58,59] points to a highly ordered transition state.
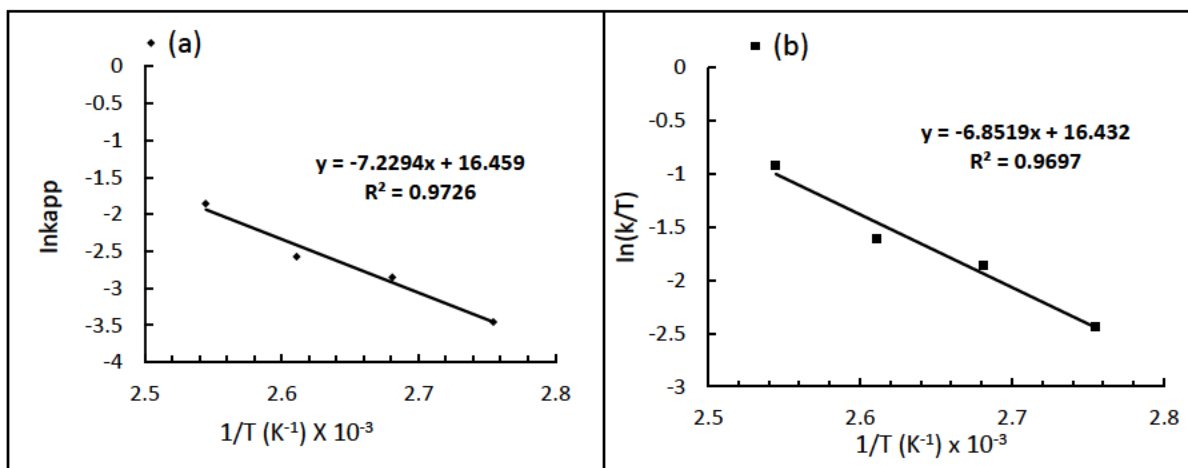
Figure 3.24: (a) Arrhenius plot of lnk_{app} vs T^{-1} for the bulk polymerization of ε-CL initiated by complex **3.3**, M/I = 200 and (b) Eyring plot of temperature dependence of the rate constant

3.7.10 Reaction mechanism

On the premise of results explained above, a plausible coordination–insertion mechanism into the M—O bond has been proposed (Scheme 3.3).[60] Initially, the monomer is activated by the metal centre forming a monomer-catalyst activated complex. Then the second step involves insertion of ε-CL/*rac*-LA monomer into the M–O bond; to furnish the first generation macroinitiator polymer bearing an active M–O bond on one side and an acetate (-OAc) at the other end. Repeated addition of the monomer will result in extension of the polymer chain *via* propagation. Hydrolysis would generate a polymer end capped with a hydroxy and an acetate (HO-(polymer)-OAc).

The observations made form ^{1}H-NMR (Figure 3.25 and 3.26) and EIS-MS and (Figure 3.18 and 19) for poly(ε-CL) and poly(*rac*-LA), respectively, all point to a "coordination insertion mechanism". Besides the polymer signals, two extra peaks of low intensity at σ = 2.3 and 3.2 ppm due to acetate methyl protons and methylene protons adjacent to the hydroxy end were present. Similar, polymers were also obtained using monocarboxylate iron complexes.[61] Low intensity of the signal is a result of less concentration of these species on the polymer chain. The acetate moiety could not be accounted for in ESI-MS (Figure 3.18 and 19) for both polymers and we presume that the acetate hydrolyses giving carboxylate end capped polymer during the analysis. The anhydride end can easily hydrolyse giving a carboxylate terminus due to the presence of adventurous water that could have been present in solvents used. This was supported by *m/z* peaks represented by (n(monomer) + 17) showing a polymer with OH terminal groups.
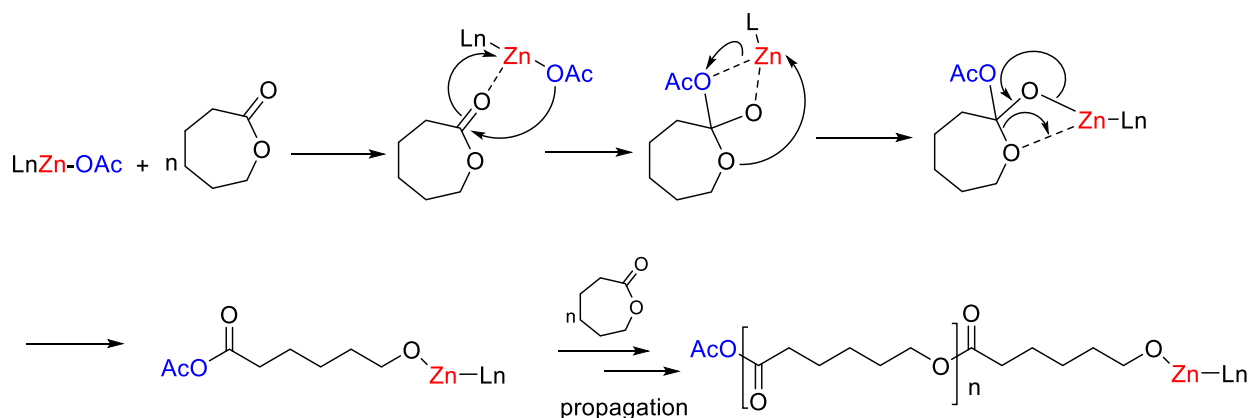
Scheme 3.3: Proposed mechanism for the ROP of ε-caprolactone
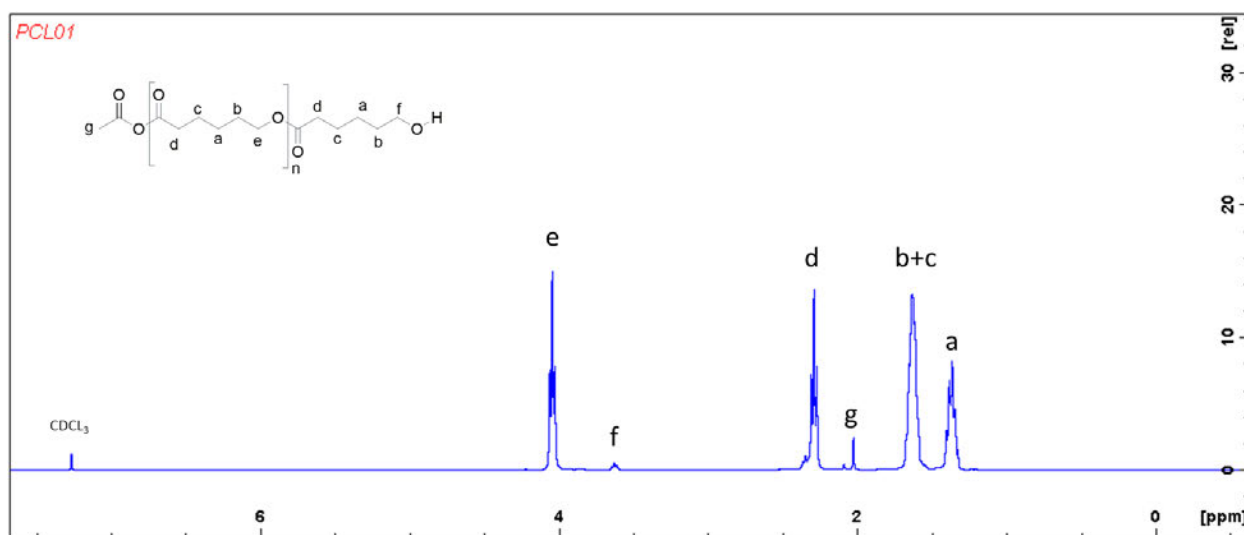
Figure 3.25: The ^{1}H-NMR spectrum of poly(ε-CL) initiated by complex **3.1** at room temperature in CDCl$_3$ (400 MHz). Reaction conditions: [CL]$_0$:[I]$_0$ = 100:1, bulk, T = 110 °C
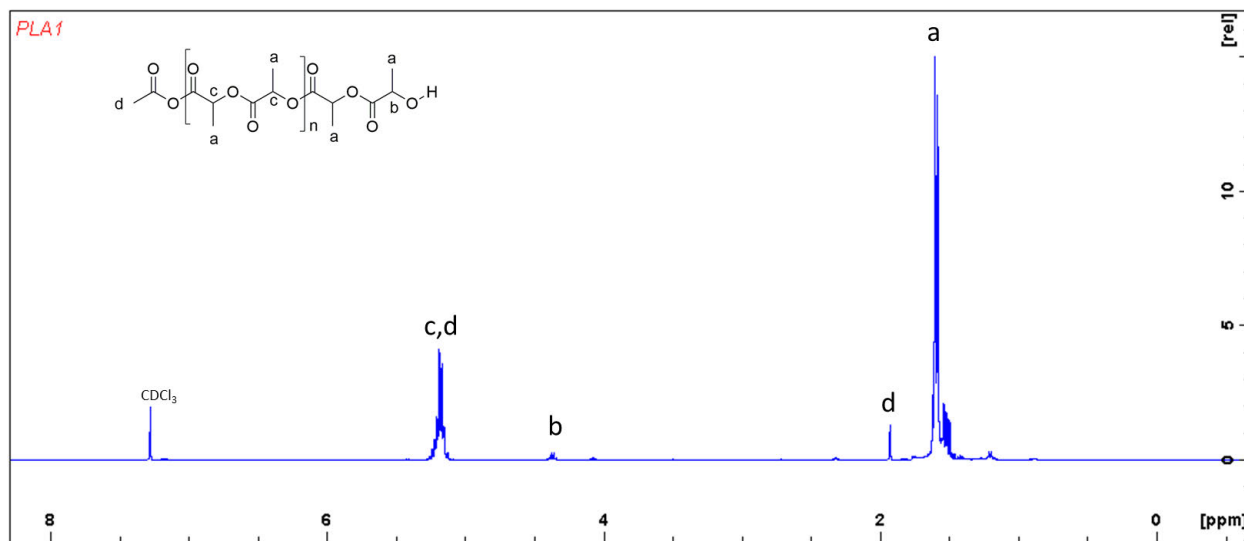
Figure 3.26: H^1 NMR spectrum of poly(*rac*-LA) initiated by complex **3.2** at room temperature in CDCl$_3$ (400 MHz). Reaction conditions: [CL]$_0$:[I]$_0$ = 100:1, bulk, T = 110 °C

3.7.11 Copolymerization and microstructure analysis

High resolution NMR spectroscopy has demonstrated its strength in PLA polymers structural elucidation and characterization.[62-64] The stereosequence pattern can be assigned with certainty for non-overlapping resonances. Methine to methyl proton resonance coupling in the polymer backbone is eliminated by homonuclear decoupling ^{1}H-NMR. The stereosequence distribution

assignment from ^{13}C-NMR is inferior to ^{1}H-NMR due to low sensitivity of the carbon nucleus.[65] Figure 3.27a shows the ^{13}C-NMR methine region which consist of two peaks which are assigned to the triads. The carbonyl region (Figure 3.27b) has distinctive three peaks with the middle peak having shoulders as observed in other reported work[66,67] and these are assigned to the triads *ii*, (*is*,*si*) and *ss*.[67] The catalytic system does not exhibit stereoselictive polymerizstion due to the lact of stereocenters hence PLAs produced exhibit heterotacticity.

The relative percentage monomer composition in the copolymers were quantified by ^{1}H-NMR spectroscopy. The micro-structures of the copolymers were elucidated by ^{13}C-NMR analysis on diads and triads sequence. The amount of CL−LA heterojunction (heterodiads) were determined by contrasting, signals intensity of methylene protons adjacent to CL−CL homo-sequence methylene protons. The monomer compositions of the copolymers followed the feed ratio trend.

As anticipated, an increase in *rac*-LA in the feed resulted in a surge in the percentage of CL-LA heterodiads, which infer random copolymerization behaviour. Further studies are underway to fully understand the copolymerization behaviour.
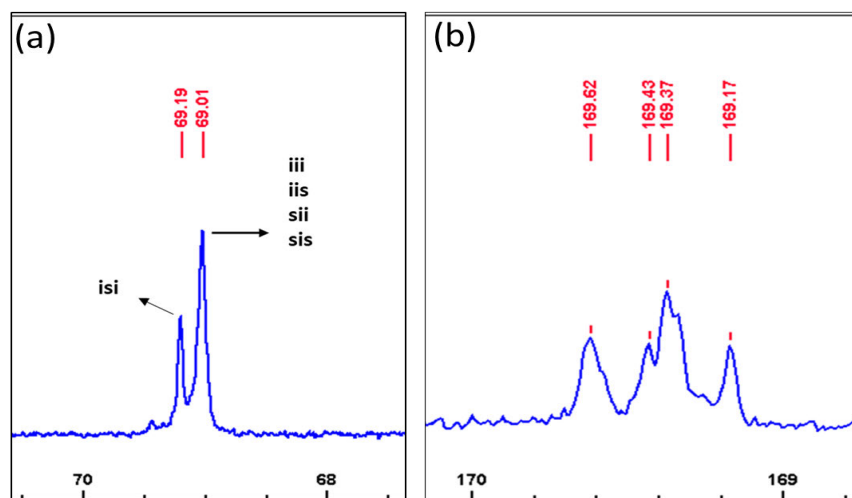
Figure 3.27: (a) ^{13}C-NMR methine region and (b) ^{13}C-NMR spectra carbonyl region of poly(*rac*-LA)

3.8 Conclusion

Zn(II) and Cu(II) complexes supported by unsymmetrical formamidine ligand were synthesized. Their identity was confirmed by IR, NMR, mass spectroscopy and elemental analysis. The molecular structures of complexes **3.3** and **3.7** were determined by single-crystal X-ray diffraction analyses. Both complexes are dimeric having a paddlewheel core structure supported by two ligands. In complex **3.3**, adjacent Zn(II) ions are separated by 2.9898(8) Å, greater than the van der Waals radii (1.39 Å) discounting meaningful metal-metal interactions. In complex **3.7**, Cu⋯Cu separation of 2.6653(7) Å is less the than the sum of the van der Waals radii 2.8 Å conferring a metal-metal bond. Complexes **3.1** – **3.8** were active initiators towards the ROP of ε-CL and *rac*-LA. The Zn(II) complex exhibited greater activity compared to Cu(II) complexes with complex **3.1** bearing electron withdrawing chloro groups showing greater catalytic activity. The experimental kinetics data indicates that the ring-opening polymerization of both monomers follows *pseudo* first order kinetics. Complex **3.2** exhibited reaction orders of 0.5 and 1.5 with respect to ε-CL and *rac*-LA monomers. Low molecular weight polymers ranging from 1720 to 6042 g mol^{-1} with PDIs between 1.78 – 1.87 were obtained which were influence by the steric crowding around the metal centre. The microstructure analysis of the resultant poly(*rac*-LA) exhibited isotactic-enriched chain.

The initial exploratory work in this chapter demonstrated successful synthesis and characterization of formamidine supported Zn(II) and Cu(II) complexes which showed catalytic activity in ROP. The research was extended further by modifying the ligands to *N,O* type and the investigations are described in **Chapter 4**.

References

1. B. Singh and A. Dhiman, *RSC Advances*, **2015**, 5, 44666.

2. A. Najer, D. Wu, M. G. Nussbaumer, G. Schwertz, A. Schwab, M. C. Witschel, A. Schafer, F. Diederich, M. Rottmann, C. G. Palivan, H.-P. Beck and W. Meier, *Nanoscale*, **2016**, 8, 14858.

3. J. Nicolas, S. Mura, D. Brambilla, N. Mackiewicz and P. Couvreur, *Chem. Soc. Rev.*, **2013**, 42, 1147.

4. P. Huang, C. Yang, J. Liu, W. Wang, S. Guo, J. Li, Y. Sun, H. Dong, L. Deng, J. Zhang, J. Liu and A. Dong, *J. Mater. Chem. B.*, **2014**, 2, 4021.

5. A. Hamitou, T. Ouhadi, R. Jerome and P. Teyssié, *J. Polym. Sci: Polym. Chem. Ed*, **1977**, 15, 865.

6. H. R. Kricheldorf, T. Mang and J. M. Jonte, *Macromolecules*, **1984**, 17, 2173.

7. O. Dechy-Cabaret, B. Martin-Vaca and D. Bourissou, *Chem. Rev.*, **2004**, 104, 6147.

8. R. F. Storey and J. W. Sherman, *Macromolecules*, **2002**, 35, 1504.

9. D. Alhashmialameer, N. Ikpo, J. Collins, L. N. Dawe, K. Hattenhauer and F. M. Kerton, *Dalton Trans.*, **2015**, 44, 20216.

10. K. Devaine-Pressing, J. H. Lehr, M. E. Pratt, L. N. Dawe, A. A. Sarjeant and C. M. Kozak, *Dalton Trans.*, **2015**, 44, 12365.

11. Y. Wang, W. Zhao, D. Liu, S. Li, X. Liu, D. Cui and X. Chen, *Organometallics*, **2012**, 31, 4182.

12. S. Range, D. F. J. Piesik and S. Harder, *Eur. J. Inorg. Chem.*, **2008**, 2008, 3442.

13. H.-Y. Chen, L. Mialon, K. A. Abboud and S. A. Miller, *Organometallics*, **2012**, 31, 5252.

14. Y. F. Al-Khafaji, M. R. J. Elsegood, J. W. A. Frese and C. Redshaw, *RSC Advances*, **2017**, 7, 4510.

15. X.-X. Zheng, C. Zhang and Z.-X. Wang, *J. Organomet. Chem.*, **2015**, 783, 105.

16. M. J. Walton, S. J. Lancaster, J. A. Wright, M. R. J. Elsegood and C. Redshaw, *Dalton Trans.*, **2014**, 43, 18001.

17. C.-Y. Li, S.-J. Hsu, C.-l. Lin, C.-Y. Tsai, J.-H. Wang, B.-T. Ko, C.-H. Lin and H.-Y. Huang, *J. Polym. Sci, Part A: Polym. Chem.*, **2013**, 51, 3840.

18. S. Fortun, P. Daneshmand and F. Schaper, *Angew. Chem. Int. Ed.*, **2015**, 54, 13669.

19. Y.-Y. Fang, W.-J. Gong, X.-J. Shang, H.-X. Li, J. Gao and J.-P. Lang, *Dalton Trans.*, **2014**, 43, 8282.

20. C.-Y. Li, D.-C. Liu and B.-T. Ko, *Dalton Trans.*, **2013**, 42, 11488.

21. T. J. J. Whitehorne and F. Schaper, *Inorg. Chem.*, **2013**, 52, 13612.

22. C. Kan, J. Ge and H. Ma, *Dalton Trans.*, **2016**, 45, 6682.

23. G. Xiao, B. Yan, R. Ma, W. J. Jin, X. Q. Lu, L. Q. Ding, C. Zeng, L. L. Chen and F. Bao, *Polym. Chem.*, **2011**, 2, 659.

24. M. P. F. Pepels, M. Bouyahyi, A. Heise and R. Duchateau, *Macromolecules*, **2013**, 46, 4324.

25. L. Chen, W. Li, D. Yuan, Y. Zhang, Q. Shen and Y. Yao, *Inorg. Chem.*, **2015**, 54, 4699.

26. D. Akalay, G. Dürner, J. W. Bats, M. Bolte and M. W. Göbel, *J. Org. Chem.*, **2007**, 72, 5618.

27. T. A. Davis, J. C. Wilt and J. N. Johnston, *J. Am. Chem. Soc.*, **2010**, 132, 2880.

28. R. Gotoh and M. Yamanaka, *Molecules*, **2012**, 17, 9010.

29. E. D. Akpan, S. O. Ojwach, B. Omondi and V. O. Nyamori, *Polyhedron*, **2016**, 110, 63.

30. E. D. Akpan, S. O. Ojwach, B. Omondi and V. O. Nyamori, *New J. Chem.*, **2016**, 40, 3499.

31. Bruker, ed., *APEXII*, APEXII Bruker AXS Inc, Madison, Wisconsin, USA, 2009.

32. Bruker, *SAINT*, SAINT Bruker AXS Inc, Madison, Wisconsin, USA, 2009.

33. Bruker, *SADABS*, Bruker SADABS Bruker AXS Inc, Madison,Wisconsin, USA, 2009.

34. G. Sheldrick, *Acta Crystallogr Sect. A: Found. Crystallogr.*, **2008**, 64, 112.

35. O. V. Dolomanov, L. J. Bourhis, R. J. Gildea, J. A. K. Howard and H. Puschmann, *J. Appl. Crystallogr.*, **2009**, 42, 339.

36. F. A. Cotton, P. Lei, C. A. Murillo and L.-S. Wang, *Inorg. Chim. Acta.*, **2003**, 349, 165.

37. C. Valdebenito, M. T. Garland, R. Quijada and R. Rojas, *J. Organomet. Chem.*, **2009**, 694, 717.

38. J. D. Masuda and D. W. Stephan, *Dalton Trans.*, **2006**, DOI: 10.1039/B513531A, 2089.

39. K. Gopi, B. Rathi and N. Thirupathi, *J. Chem. Sci.*, **2010**, 122, 157.

40. S. Vagin, A. K. Ott and B. Rieger, *Chem. Ing. Tech.*, **2007**, 79, 767.

41. Q.-Y. Zhu, Y. Liu, Z.-J. Lu, J.-P. Wang, L.-B. Huo, Y.-R. Qin and J. Dai, *Synth. Met.*, **2010**, 160, 713.

42. M. Luo, J. C. Zhang, W. M. Pang and K. K. Hii, *Chem. Cent. J.*, **2017**, 11, 81.

43. A. Motreff, R. Correa da Costa, H. Allouchi, M. Duttine, C. Mathonière, C. Duboc and J.-M. Vincent, *J. Fluor. Chem.*, **2012**, 134, 49.

44. H.-C. Huang, B. Wang, Y.-P. Zhang and Y.-S. Li, *Polym. Chem.*, **2016**, 7, 5819.

45. P. Hormnirun, E. L. Marshall, V. C. Gibson, R. I. Pugh and A. J. P. White, *Proc. Natl. Acad. Sci.*, **2006**, 103, 15343.

46. R. Takjoo, G. Dutkiewicz, M. Ahmadi and M. Kubicki, *Acta Crystallogr. Sect. E.*, **2012**, 68, 106.

47. W. Luo, T. Shi, S. Liu, W. Zuo and Z. Li, *Organometallics*, **2017**, 36, 1736.

48. C. Obuah, Y. Lochee, J. H. L. Jordaan, D. P. Otto, T. Nyokong and J. Darkwa, *Polyhedron*, **2015**, 90, 154.

49. S. O. Ojwach, T. T. Okemwa, N. W. Attandoh and B. Omondi, *Dalton Trans.*, **2013**, 42, 10735.

50. M. Zikode, S. O. Ojwach and M. P. Akerman, *J. Mol. Catal. A: Chem.*, **2016**, 413, 24.

51. H.-Y. Chen, H.-Y. Tang and C.-C. Lin, *Macromolecules*, **2006**, 39, 3745.

52. C. Jian, J. Zhang, Z. Dai, Y. Gao, N. Tang and J. Wu, *Eur. J. Inorg. Chem.*, **2013**, 2013, 3533.

53. P. Dubois, C. Jacobs, R. Jerome and P. Teyssie, *Macromolecules*, **1991**, 24, 2266.

54. Y. Huang, W. Wang, C.-C. Lin, M. P. Blake, L. Clark, A. D. Schwarz and P. Mountford, *Dalton Trans.*, **2013**, 42, 9313.

55. I. del Rosal, P. Brignou, S. M. Guillaume, J.-F. Carpentier and L. Maron, *Polym. Chem.*, **2011**, 2, 2564.

56. I. del Rosal, P. Brignou, S. M. Guillaume, J.-F. Carpentier and L. Maron, *Polym. Chem.*, **2015**, 6, 3336.

57. S. Gupta, R. Arora, N. Sinha, M. I. Alam and M. A. Haider, *RSC Advances*, **2016**, 6, 12932.

58. M. Oshimura, T. Tang and A. Takasu, *J. Polym. Sci, Part A: Polym. Chem.*, **2011**, 49, 1210.

59. A. Kapelski and J. Okuda, *J. Polym. Sci, Part A: Polym. Chem.*, **2013**, 51, 4983.

60. C. Fliedel, V. Rosa, F. M. Alves, A. M. Martins, T. Aviles and S. Dagorne, *Dalton Trans.*, **2015**, 44, 12376.

61. M. Stolt and A. Södergård, *Macromolecules*, **1999**, 32, 6412.

62. D. R. Holycross and M. Chai, *Macromolecules*, **2013**, 46, 6891.

63. J. E. Kasperczyk, *Polymer* **1999**, 40 5455.

64. K. A. M. Thakur, R. T. Kean, E. S. Hall, J. J. Kolstad, T. A. Lindgren, M. A. Doscotch, J. I. Siepmann and E. J. Munson, *Macromolecules*, **1997**, 30, 2422.

65. K. A. M. Thakur, R. T. Kean, E. S. Hall, J. J. Kolstad and E. J. Munson, *Int. J. Polym. Anal. Charact.*, **1998**, 4, 379.

66. F. Chabot, M. Vert, S. Chapelle and P. Granger, *Polymer*, **1983**, 24, 53.

67. M. H. Chisholm, S. S. Iyer, D. G. McCollum, M. Pagel and U. Werner-Zwanziger, *Macromolecules*, **1999**, 32, 963.

Chapter 4

Synthesis and polymerization kinetics of ε-caprolactone and ʟ-lactide to low molecular weight polyesters catalysed by Zn(II) and Cu(II) *N*-hydroxy-*N,N′*-diarylformamidine complexes

Because of catalytic activity which was showed by the catalytic in system in **Chapter 3**. To try and improve on the activity and polymer characteristics the ligand skeletons were modified to include an N—O bond which will introduce a metal-oxygen bond which is responsible for ROP initiation.

Abstract

Discrete Zn(II) and Cu(II) complexes were synthesis using *N*-hydroxy-*N,N′*-diarylformamidine ligands ,i.e. *N*-hydroxy-*N,N′*-bis(2,6-diisopropylphenyl)formamidine (**L4.1**), *N*-hydroxy-*N,N′*-bis(2,6-dimethyl)formamidine (**L4.2**), *N*-hydroxy-*N*-(2-methoxyphenyl)- *N′*-(2,6-diisopropylphenyl)formamidine (**L4.3**), and *N*-hydroxy-*N*-(2-methoxyphenyl)-*N′*-(2,6-dimethylphenyl)formamidine (**L4.4**). Reaction of ligands **L4.1 - L4.4** with either $ZnOAc_2.2H_2O$ or $CuOAc_2.2H_2O$ in aqueous ethanol gave mononuclear Zn(II) or Cu(II) complexes [Zn-(**L4.1**)$_2$] (**4.1**), [Zn-(**L4.2**)$_2$] (**4.2**), [Zn-(**L4.3**)$_2$] (**4.3**) and [Zn-(**L4.4**)$_2$] (**4.**) or [Cu-(**L4.1**)$_2$] (**4.5**), [Cu-(**L4.2**)$_2$] (**4.6**), [Cu-(**L4.3**)$_2$] (**4.7**) and [Cu-(**L4.4**)$_2$] (**4.8**), as complexes, respectively, with high yields of up to 84%. All the complexes were characterized by elemental analysis, IR and NMR spectroscopy and mass spectroscopy. Also, the molecular structures of complexes **4.3** and **4.7** were determined by single crystal X-ray diffraction analyses. The Zn(II) centre in complex **4.3** exhibited a distorted tetrahedral geometry while in complex **4.7**, the Cu(II) centre had a square planar geometry with near C_2 symmetry. In complex **4.3** and **4.7** structures, the coordination sites

are occupied by imino N and hydroxyl O donor atoms from the chelating ligands. All complexes showed catalytic activity and exhibited well-controlled living polymerization process in the ring-opening polymerization of ε-caprolactone and L-lactide in the presence of a co-initiator. The molecular weights of the polymers were found to be low ranging from 1855 to 3999 Da for polycaprolactone (PCL) and up to 1720 Da for polylactic acid (PLA). The Zn(II) catalysts were found to be more active than Cu(II) catalysts with complex **4.2** (k_{app} = 0.1751 h^{-1}) being the most active.

Keywords: Copper(II), ε-caprolactone, N-hydroxyl-N'-diarylformamidine, L-lactide, zinc(II)

4.1 Introduction

Petroleum based-polymers that are derived from non-renewable fossils have low biodegradability and on disposal cause environmental pollution.[1] In addressing these challenges, modern-day polymer research is geared towards developing economically viable, recyclable and biodegradable polymers derived from renewable resources. Aliphatic polyesters have emerged as better surrogates and they possess many favourable traits. In particular poly(lactic acid) (PLAs) and poly(ε-caprolactone) (PCLs) are interesting candidates because they are bio-compatible, bio-degradable and can be bio-derived. Owing to their diverse applications in the field of medicine,[2,3] packaging[4] and electronic devices,[5] their demand has increased over the past decades. Metal-based ring-opening polymerization (ROP) has indisputably proved to be a more proficient method for the synthesis of polyesters.

Commercially, tin(II) complexes are used as catalysts or initiators for the synthesis of PCLs and PLAs, however, their toxicities limit their use in the production of polymers for medical applications since the elimination of the remnant catalyst from the polymer is a challenge.[6] Coordination complexes of cheap and bio-compactable metals with reasonable toxicity are now being investigated as replacements. Complexes of metals such as zinc,[7-12] magnesium,[13-16] calcium,[17-20] aluminum[21-26] and copper[27,28] have been investigated and have shown promising results towards ROP of cyclic esters. Alkali earth metals[29,30] and lanthanides[31,32] have also been explored for catalytic activity in ROP.

More recently, silver complexes which are known to have antimicrobial[33] properties, have been found to be active towards ε-caprolactone (ε-CL) polymerization.[33]

A metal-oxygen bond is a prerequisite for effective initiation of the polymerization process. Many metal-based ROP systems are dominated by nitrogen and/or oxygen as metal stabilizing ligands which give a positive influence towards catalytic activity.[34] Ligand-supported single site metal alkoxide initiators have been shown to control the polymerization process and yield polymers with controlled molecular weights (M_w), polydispersity indices (PDIs), architecture and end groups.[35,36] This has attracted much interest and prompted researchers to design more ligands to support metal-alkoxide based catalyst for ROP. Salen-type ligand supported metal initiators have been systematically studied and used effectively in ROP of lactides with high stereo-control especially toward, either isotactic or heterotactic PLA polymers.[37-41]

Apart from the chemical properties, physical properties of auxiliary ligands also impact strongly on the catalytic activity of metal-based catalyst. Thus, it is paramount to probe the correlation between ligand structure and catalytic activity. From previous work reported by our group, *N,N'*-diarylformamidine ligands have been used to support Zn(II) and Cu(II) complexes which were active in ROP ε-CL and L-LA. Herein, the *N,N'*-diarylformamidines ligands were modified to *N*-hydroxy-*N,N'*-diarylformamidine ligands which potentially introduce M—O bonds as part of the catalyst. We hypothesized that the presence of M—O bonds will bring enhanced catalytic activity as well as interesting polymer characteristics.

4.2 Experimental section

4.2.1 *Materials*

All experiments were carried out under argon, 5.0 technical grade, (Airflex Industrial Gases, South Africa) using Schlenk techniques. All solvents were obtained from Sigma-Aldrich. Reagent grade absolute ethanol (98%) was distilled and dried from magnesium turnings; dichloromethane (DCM), (99%) and hexane (98%) were dried from sodium–benzophenone mixture. Reagents, $Cu(OAc)_2.H_2O$ (98%), $Zn(OAc)_2.2H_2O$ (97%), ε-caprolactone (ε-CL) (98%) - L-lactide (L-LA) (97%) and 3-chloroperoxybenzoic acid, (MCPBA) (77%) were also obtained from Sigma-Aldrich.

Anhydrous MgSO$_4$ (98%), NaOH (99%), anhydrous NaHCO$_3$ (97%) and anhydrous K$_2$CO$_3$ (99%) were obtained from Promark Chemicals, South Africa.

4.2.2 Instrumentation

^{1}H- and ^{13}C-NMR spectra were measured at room temperature on a Bruker Avance^{III} 400MHz spectrometer. Both ^{1}H- and ^{13}C-NMR data were recorded in CDCl$_3$ and referenced to the residual CDCl$_3$ peaks at δ 7.26 and δ 77.00, respectively. IR spectra were obtained on a PerkinElmer Universal ATR spectrum 100 FT-IR spectrometer. Mass spectra of complexes were obtained from a Water synapt GR electrospray positive spectrometer. EPR spectra were recorded on Bruker X Band ESR Spectrometer Electron Spin Resonance spectrometer (ESR).

4.3 General synthesis methods

4.3.1 Synthesis of N-hydroxy N,N' diarylformamidine ligands

Amidine (1.0 mmol) was dissolved in DCM and solid sodium hydrogen carbonate (1.0 mmol) was then added and the mixture cooled to 0 °C. Thereafter, *m*-MCPBA (1.2 mmol) in DCM was added dropwise and the reaction mixture was allowed to warm to room temperature with stirring for a further 1 h. The reaction mixture was then washed with a solution of potassium carbonate (5%; 2 × 25 ml) and the combined organic fractions were dried over anhydrous sodium sulphate and filtered. The solvent was then removed by evaporation to afford, N-hydroxy-*N,N′*-bis(2,6-diisopropylphenyl)formamidine (**L4.1**), *N*-hydroxy-*N,N′*-bis(2,6-dimethyl)formamidine (**L4.2**), and *N*-hydroxy-*N*-(2-methoxyphenyl)-*N′*-(2,6-dimethylphenyl)formamidine (**L4.4**) as solids whilst *N*-hydroxy-*N*-(2-methoxyphenyl)-*N′*-(2,6-diisopropylphenyl)formamidine (**L4.3**), was obtained an oil (Figure 4.1).
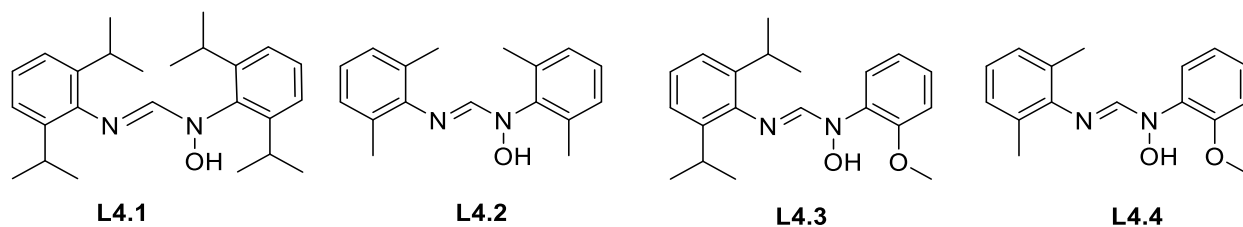
Figure 4.1: *N*-hydroxy-*N,N'*-diarylformamidine ligands employed in the synthesis of complexes reported herein

4.3.2 *Synthesis of Zn(II) and Cu(II) complexes*

The respective hydrated metal acetate salt (1 mmol) was dissolved in water and the pH adjusted to 8.0 using 1M NaOH solution. Thereafter, a solution of the ligand (2.0 mmol) in aqueous ethanol 90% was added. In each case a precipitate was formed immediately, and the reaction mixture was stirred at room temperature for 8 h. Deionized water (100 ml) was added and then the temperature lowered to 4 °C. There after the mixture was allowed to stir for further 2 h. The resultant solids were collected by filtration, washed with hot water and aqueous ethanol (50%). The complexes were then dissolved in DCM, dried with anhydrous $MgSO_4$, filtered and by slow evaporation of the solvent, the desired products were obtained as solids (see Scheme 4.1).

4.3.2.1 *[Zn-(L4.1)₂] (4.1)*

The reaction of **L4.1** (0.30 g, 0.788 mmol) and $Zn(OAc)_2.2H_2O$ (0.076 g, 0.394 mmol) in ethanol furnished complex **4.1** as a white powder. Yield 86%. Melting point 187 – 189 °C. ^{1}H-NMR (CDCl₃, 400 MHz): δ (ppm) 0.79 (d, $^3J_{H,H}$ = 6.84, 12H, [i]Pr-CH₃), 1.09 (dd, $^3J_{H,H}$ = 6.80 Hz, 12H, [i]Pr-CH₃), 1.20 (d, $^3J_{H,H}$ = 6.88 Hz, 12H, [i]Pr-CH₃), 1.35 (d, $^3J_{H,H}$ = 6.72 Hz, 12H, [i]Pr-CH₃), 3.24 (qn, $^3J_{H,H}$ = 4.80, 8H, CH [i]Pr-CH$_{methine}$), 7.02 (q, $^3J_{H,H}$ = 1.96 Hz, 4H, Ar), 7.19 (s, 2H, Ar), 7.11 - 7.15 (m, 2H, Ar), 7.20 (s, NC(H)N), 7.33 (t, $^3J_{HH}$ = 7.78 Hz, 2H, Ar). ^{13}C-NMR (CDCl₃, 400 MHz): δ (ppm) 23.6, 23.9, 24.2, 24.6, 25.5, 27.8, 28.3, 123.2, 124, 129.8, 137.6, 142.5, 143.2, 145.8, 147.5, 150.0. IR: *v* (cm⁻¹) 2961 (s), 2868 (w), 1663 (s), 1607 (s), 1441 (m), 1288 (w). ESI-TOF MS: m/z (%) 845.6 (100) [M + Na]⁺. Elemental analysis calcd (%) for $C_{50}H_{70}N_4O_2Zn$: C, 72.83; H, 8.56; N, 6.80. Found: C,72.70; H, 8.18; N, 6.87.

4.3.2.2 *[Zn-(L4.2)₂] (4.2)*

The reaction of ligand **L4.2** (0.30 g, 0.788 mmol) and $Zn(OAc)_2 \cdot 2H_2O$ (0.076 g, 0.394 mmol) in ethanol furnished complex **4.2** as a white powder. Yield 74%. Melting point: 242- 245 °C. ^1H-NMR (CDCl₃, 400 MHz): δ (ppm) 2.04 (s, 12H, CH₃), 2.29 (s, 12H, CH₃) 6.95 - 6.92 (m, $^3J_{H,H}$ = 4.91 Hz, 4H, Ar), 7.01 (d, $^3J_{H,H}$ = 7.4 Hz 4H, Ar), 7.07 (d, $^3J_{H,H}$ = 7.56 Hz, 4H, Ar), 7.31 (s, 2H, NCHN). ^{13}C-NMR (CDCl₃, 400 MHz): δ (ppm) 17.4, 18.5, 124.2, 128, 128.3, 129, 132.7, 136.8, 139.8, 144.8, 148.8. IR: v (cm⁻¹) 2964(w), 1610(s), 1598(s), 1471(w), 1206(s). ESI-TOF MS: m/z (%) 621.1 (100) [M + Na]⁺. Elemental analysis calcd (%) for $C_{34}H_{38}N_4O_2Zn$ C, 61.55; H, 6.22; N, 8.77. Found C, 61.37, H 5.89, N 8.18.

4.3.2.3 *[Zn-(L4.3)₂] (4.3)*

The reaction of ligand **L4.3** (0.30 g, 0.919 mmol) and $Zn(OAc)_2 \cdot 2H_2O$ (0.106 g, 0.483 mmol) in ethanol furnished complex **4.3** as a white powder. Yield 72%. Melting point: 228 – 230 °C. ^1H-NMR (CDCl₃, 400 MHz): δ (ppm) 1.19 (d, $^3J_{H,H}$ = 6.88 Hz, 12H, ^iPr-CH₃), 1.24 (d, $^3J_{H,H}$ = 6.68 Hz, 12H, ^iPr-CH₃), 3.21 (qn, $^3J_{H,H}$ = 6.61, 4H, ^iPr-CH$_{methine}$), 3.78 (s, 6H, OCH₃), 6.85 - 6.94 (m, 6H, Ar), 7.10 (dd, $^3J_{H,H}$ = 2.87 Hz 2H, Ar), 7.20 (d, $^3J_{H,H}$ = 7.72 Hz, 4H, Ar), 7.35 (d, $^3J_{H,H}$ = 7.74 Hz, 2H, Ar), 8.23 (s, 2H, NCHN). ^{13}C-NMR (CDCl₃, 400 MHz): δ (ppm) 24, 25, 28.3, 54.9, 110.9, 116.9, 121.2, 121.6, 123.7, 129.7, 135.9, 138.5, 145.2, 150.3. IR: v (cm⁻¹) 2963 (m), 1739 (m), 1582 (s), 1499 (m), 1462 (m), 1401 (w), 1312 (w), 1227 (m), ESI-TOF MS: m/z (%) 737.4 (100) [M + Na]⁺. Elemental analysis calcd (%) for $C_{40}H_{50}N_4O_4Zn$: C, 67.07; H, 7.04; N, 7.82. Found: C, 67.12; H, 6.88; N, 7.94.

4.3.2.4 *[Zn-(L4.4)₂] (4.4)*

The reaction of ligand **L4.4** (0.30 g, 0.919 mmol) and $Cu(OAc)_2 \cdot 2H_2O$ (0.078 g, 0.394 mmol) in ethanol furnished complex **4.4** as a white powder. Yield 60%. Melting point 240 – 243 °C. ^1H-NMR (CDCl₃, 400 MHz): δ (ppm) 2.32 (s, 6H, CH₃), 2.37 (s, 6H, CH₃), 3.78 (s, 6H, OCH₃),7.04 - 7.22 (m, 10H, Ar),7.71 -7.74 (d, $^3J_{H,H}$ = 9.8 Hz, 4H, Ar), 7.98 (s, 2H, NCHN). ^{13}C-NMR (CDCl₃, 400 MHz): δ (ppm) 17.7, 18.4, 23.9, 127.6, 128.5, 129.0, 144.7, 148.2.   IR*: v (cm⁻¹) 2949 (w), 1614 (s), 1579 (s), 1468 (m), 1228 (m), ESI-TOF MS: m/z (%) 626.34 (100) [M + Na]⁺. Elemental analysis calcd (%) for $C_{32}H_{34}N_4O_4Zn$, C, 63.63; H, 5.67; N, 9.28. Found C, 63.89, H 5.86, N, 9.66

4.3.2.5 [Cu-(L4.1)₂] (4.5)

The reaction of ligand **L4.1** (0.30 g, 0.919 mmol) and $Cu(OAc)_2.2H_2O$ (0.078 g, 0.394 mmol) in ethanol furnished complex **4.5** as a brown powder. Yield 76%. Melting point: decompose above 238 °C. IR v 3064 (w), 2960 (s), 2867 (w), 1664 (m), 1620 (s), 1461(m), 1326 (w), 1290 (w), 1254 (w). ESI-TOF MS: m/z (%) 844.6 (100) $[M + Na]^+$. Elemental analysis calcd (%) for $C_{50}H_{70}CuN_4O_2$: C, 73.00; H, 8.58; N, 6.81. Found: C,73.52; H, 8.39, N, 6.44.

4.3.2.6 [Cu-(L4.2)₂] (4.6)

The reaction of ligand **L4.2** (0.30 g, 0.788 mmol) and $Cu(OAc)_2.2H_2O$ (0.076 g, 0.394 mmol) in ethanol furnished complex **4.6** as a brown powder. Yield 76%. Melting point: decompose above 205 °C. IR v 3018 (w), 2918 (w), 1608 (s), 1583 (s), 1466 (m), 1390 (w), 1296 (w), 1205 (m), ESI-TOF MS: m/z (%) 621.32(100) $[M + Na]^+$. Elemental analysis calcd (%) for $C_{34}H_{38}N_4O_2Cu$, C, 63.05; H, 6.50; N, 8.40. Found C, 62.79, H 6.83, N 8.82

4.3.2.7 [Cu-(L4.3)₂] (4.7)

The reaction of ligand **L4.3** (0.30 g, 0.919 mmol) and $Cu(OAc)_2.2H_2O$ (0.096 g, 0.483 mmol) in ethanol furnished complex **4.8** as a brown powder. Yield 79%. Melting point: decompose at 235 °C. IR v 2962 (m), 2868 (w), 1620 (s), 1589 (m), 1494 (w), 1456 (m), 1405 (w), 1312 (w), 1224 (m). ESI-TOF MS: m/z (%) 736.4 (100), $[M + Na]^+$. Elemental analysis calcd (%) for $C_{40}H_{50}N_4O_4Cu$, C, 67.25; H, 7.05; N, 7.84. Found: C, 67.15; H, 6.75; N, 7.83.

4.3.2.8 [Cu-(L4)₂] (4.9)

The reaction of ligand **L4.4** (0.30 g, 0.919 mmol) and $Cu(OAc)_2.2H_2O$ (0.078 g, 0.394 mmol) in ethanol furnished complex **4.9** as a brown powder. Yield 66%. Melting point: decompose at 205 °C. IR v 2949 (w), 1612 (s), 1584 (s), 1469 (m), 1228 (m), ESI-TOF MS: m/z (%) 624.1 (100), $[M + Na]^+$. Elemental analysis calcd (%) for $C_{32}H_{34}N_4O_4Cu$, C, 61.97; H, 5.85; N, 9.03. Found C, 61.73, H 5.90, N, 8.84.

4.4   Polymerization of ε-caprolactone and ʟ-lactide

All manipulations were performed under an argon inert atmosphere using Schlenk techniques. The catalyst and benzyl alcohol as a co-initiator in a mole ratio of 1:1 were dissolved in toluene (2 ml) and the mixture stirred at 110 °C for 10 mins. Thereafter, the required amount of monomer (ε-CL or ʟ-LA) in toluene (1 ml) was then added. Samples for kinetic experiments were withdrawn at regular intervals and quenched quickly by dissolving in cooled $CDCl_3$ in an NMR tube. The quenched samples were then analysed by ^{1}H-NMR spectroscopy to determine the extent of polymerization. The percentage conversion was obtained by considering the ε-CL monomer protons signal intensities at 4.2 ppm ($I_{4.2}$) and OCH_2 protons signal intensities at 4.0 ppm ($I_{4.0}$) from PCL and evaluated using equation (**4.1**).

$$\frac{[Polymer]_t}{[Monomer]_0} \times 100 = \frac{I_{4.0}}{(I_{4.2} + I_{4.0})} \times 100 \qquad (\mathbf{4.1})$$

For PLA, the integration values of the methine proton of the monomer and that of the polymer were used to calculate the percentage conversion using the equation (**4.2**).

$$\frac{[Polymer]_t}{[Monomer]_0} \times 100 = \frac{I_{CH\ monomer}}{(I_{CH\ monomer} + I_{CH\ polymer})} \times 100 \qquad (\mathbf{4.2})$$

The observed rate constants were extracted from the slope of the line of best fit from the plot of $\ln([M]_0/[M]_t)$ *vs t*

4.5   Polymer characterization by size exclusion chromatography (SEC)

Molecular weights and polydispersity indexes were determined by size exclusion chromatography (SEC) at Stellenbosch University. The samples were dissolved in tetrahydrofuran (THF) stabilized with butylated hydroxytoluene (BHT) giving a sample with a concentration of 2 mg ml^{-1}. Sample solutions were filtered *via* a syringe through 0.45 mm nylon filters before being subjected to analysis. The SEC instrument consists of a Waters 1515 isocratic. HPCL pump, a Waters 717plus auto-sampler, a Waters 600E Paper system controller (run by Breeze Version 3.30 SPA) and a Waters in-line Degasser AF. A Waters 2414 differential refractometer was used at 30 °C in series along with a Waters 2487 dual wavelength absorbance UV/Vis detector operating at variable wavelengths. THF (HPLC grade stabilized with 0.125% BHT) was used as the eluent at flow rates of 1 ml min^{-1}. The column oven was kept at 30 °C and the injection volume was 100 ml. Two

PLgel (Polymer Laboratories) 5 mm Mixed-C (300 x 7.5 mm) columns and a pre-column (PLgel 5 mm Guard, 50 x 7.5 mm) were used. Calibration was done using narrow poly-styrene standards ranging from 580 to 2 x 10^6 g mol^{-1}. All molecular weights were reported as polystyrene equivalents.

4.6 Single-crystal X-ray diffraction

Crystal evaluation and data collection was done on a Bruker Smart APEXII diffractometer with Mo Kα radiation (I = 0.71073 Å) equipped with an Oxford Cryostream low temperature apparatus operating at 100 K for all samples. Reflections were collected at different starting angles and the *APEX*II program suite was used to index the reflections.[42] Data reduction was performed using the *SAINT*[43] software and the scaling and absorption corrections were applied using the *SADABS*[44] multi-scan technique. The structures were solved by the direct method using the *SHELXS* program and refined using *SHELXL* program.[45] Graphics of the crystal structures were drawn using *OLEX²* software.[46] Non-hydrogen atoms were first refined isotropically and then by anisotropic refinement with the full-matrix least squares method based on F^2 using *SHELXL*.[45] The crystallographic data and structure refinement parameters for complexes **4.3**, **4.5**, **4.6** and **4.7** is given in Table 4.1.

Table 4.1: The summary of X-ray crystal data collection and structure refinement parameters for complexes **4.3**, **4.5**, **4.6** and **4.7**

	4.3	4.5	4.6		4.7.CH$_2$Cl$_2$
Empirical formula	C$_{40}$H$_{50}$N$_4$O$_4$Zn	C$_{34}$H$_{38}$CuN$_4$O$_2$	C$_{50}$H$_{70}$CuN$_4$O$_2$		C$_{40}$H$_{52}$Cl$_2$CuN$_4$O$_4$
Formula weight	716.21	598.22	822.64		884.23
T(K)	173(2)	173(2)	173(2)		173(2)
λ(Å)	0.71073	0.71073	0.71073		0.71073
Crystal system	*Orthorhombic*	*Monoclinic*	*Triclinic*		*Monoclinic*
Space group	*Fdd2*	*P21$_{/c}$*	*P-1*		*P21/n*
a (Å)	33.4780(9)	8.6554(2)	10.5284(3)		10.1354(2)
b (Å)	46.5230(18)	8.4414(2)	10.8147(3)		11.1941(3)
c (Å)	9.8072(3)	20.6115(6)	11.7799(4)		19.1032(9)
α, β, γ (°)	90, 90, 90	90, 91.4330(10), 90	109.5950(10), 105.149(2), 99.928(3)		90, 90.1610(10), 90
V (Å3)	15274.7(9)	1505.48(7)	1168.75(6)		1645.06(19)
Z	16	2	1		2
ρcalc (mg/m3)	1.246	1.320	1.169		1.355
μ (mm-1)	0.687	0.762	0.508		0.795
F(000)	6080	630	443		926
Crystal size (mm)	0.190 × 0.170 × 0.130	0.320 x 0.230 x 0.140	0.240 x 0.220 x 0.130		0.290 × 0.250 × 0.220
θ range for data collection (°)	1.751 - 27.533	1.977 to 27.514	1.954 to 27.492		2.109 to 25.366
Index ranges	-43 ≤ h ≤ 43	-11≤ h ≤ 9	-13<=h<=13		-12 ≤ h ≤ 12
	60 ≤ k ≤ 60	-10 ≤ k ≤ 10	-13<=k<=14		-13 ≤ k ≤ 13
	-12 ≤ l ≤ 12	-22 ≤ l ≤ 26	-15<=l<=12		-21 ≤ l ≤ 21
Reflections collected	124701	19352	17575		40512
Independent reflections	8789	3425	5235		3860
	[Rint = 0.0234]	[R(int) = 0.0269]	[R(int) = 0.0173]		[Rint = 0.0173]
Completeness to theta= 25.24° (%)	99.9	99.6	99.9		97.2
Data/restraints/parameters	8789/1/442	3425/0/191	5235/0/267		3860/0/255
Goodness-of-fit (GOF) on *F2*	1.038	1.062	1.063		1.054
Final R indices [*I* >2σ(*I*)]	*R1* = 0.0202	*R1* = 0.0285	*R1* = 0.0284		*R1* = 0.0386
	wR$_2$ = 0.0531	*wR2* = 0.0760	*wR2* = 0.0737		w*R$_2$* = 0.0919
R indices (all data)	*R1* = 0.0218,	*R1* = 0.0331	*R1* = 0.0309		*R1* = 0.0401
	wR$_2$ = 0.0541	*wR$_2$* = 0.0781	*wR$_2$* = 0.0753		*wR$_2$* = 0.0930
Largest diff. peak and hole (e Å-3)	0.234d -0.278	0.338 and -0.428	0.365 and -0.307		0.3661.308 and -1.048

4.7   Results and discussion

4.7.1 Synthesis of N-hydroxy-N,N'-diarylformamidine ligands and their Zn(II) and Cu(II) complexes

The *N*-hydroxy-*N,N'*-diarylformamidine ligands **L4.1** - **L4.4** were synthesized from a previously reported method in which the *N, N'*-diarylformamidine precursors[47] were *N*-oxidized with *m*-MCPBA.[48] Their identity was confirmed using IR and NMR spectroscopy, mass spectrometry and elemental analysis. Reaction of **L4.1** - **L4.4** with hydrated Zn(II) and Cu(II) acetates gave metal complexes supported by two ligands where the acetate anions are displaced from the coordination sphere. The following complexes, [Zn-(**L4.1**)₂] (**4.1**), Zn-(**L4.2**)₂] (**4.2**), Zn-(**L4.3**)₂] (**4.3**), [Zn-(**L4.4**)₂] (**4.4**), [Cu-(**L4.1**)₂] (**4.5**), [Cu-(**L4.2**)₂] (**4.6**), [Cu-(**L4.3**)₂] (**4.7**), [Cu-(**L4.4**)₂] (**4.8**) were obtained as air stable solids in good yield (64 – 84%) (see Scheme 4.1).

L4.1: R = R₁ = R₂ = *i*Pr
L4.2: R = R₁ = R₂ = Me
L4.3: R = *i*Pr, R₁ = H, R₂ = OMe
L4.4: R = Me, R₁ = H, R₂ = OMe

M = Zn and Cu
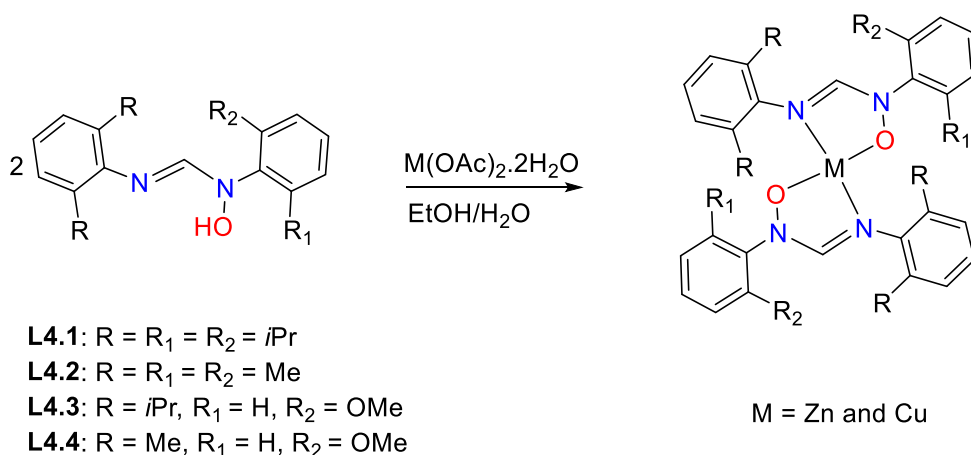
Scheme 4.1: Synthesis of Zn(II) and Cu(II) *N*-hydroxy-*N,N'*-diarylformamidine complexes

The Zn(II) complexes were obtained as white solids while Cu(II) complexes were obtained as brown solids. The melting points for Zn(II) complexes ranges from 189 – 245 °C compared to 130 – 154 °C for the ligands. Cu(II) complexes did not exhibit a defined melting points but rather, they decomposed between (205 – 245 °C). The general molecular formula of the complexes M(**L**)₂ (**L** = ligands **L4.1** - **L4.4**) was validated by microanalytical data which clearly showed that the metal:ligand ratio is 1:2. The stoichiometry was further corroborated by mass spectrometry data.

For example, complex **4.1** showed a base peak at *m/z* 847.59 which correspond to [Zn(**L4.1**)$_2$+Na]$^+$ (Figure 4.2). Similar results were also obtained for complexes **4.2** – **4.8** with spectra exhibiting m/z signals corresponding to the parent compounds as sodium adducts (see appendix B). It is noteworthy that monomeric forms of **4.1** and **4.2** with symmetrically 2,6-substituted *N*-hydroxy-*N,N'*-diarylformamidine ligands appear in literature and will not be discussed in detail.[49,50]
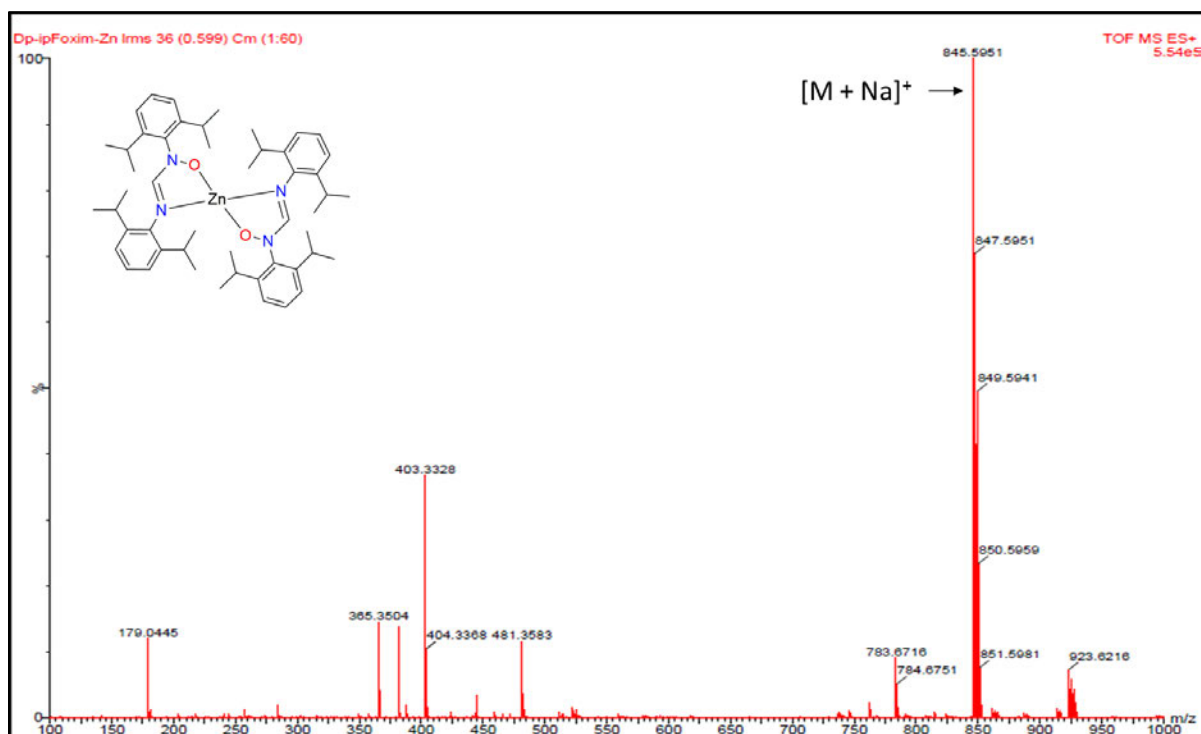
Figure 4.2: ESI-MS spectrum for complex **4.1**

4.7.2 *IR and NMR spectroscopy*

The IR spectra of complexes **4.1** – **4.8** display a general shift of the azomethine (C(H)=N) symmetric stretch toward lower frequencies as compared to free ligands indicative of imine nitrogen participation in coordination (see Table 4.2). For example, the C=N symmetric stretching frequency in complex **4.1** appeared at 1607 cm^{-1} as compared to 1610 cm^{-1} in ligand **L4.1**.

The observed shifts are due to reduced π-electron density upon coordination rendering the C=N bond to have a partial single bond character hence resonating at lower frequencies. The summarized data of shifts for other complexes are shown in Table 4.2.

Table 4.2: IR (azomethine C=N symmetry stretch frequency) and NMR (azomethine proton resonance peaks) for ligands and complexes, respectively

Complex	IR υ(C=N) cm^{-1}			NMR σ (ppm) NC(H)N		
	Ligand	Complex	$\Delta\upsilon$	Ligand	Complex	$\Delta\sigma$
4.1	1610	1607	3	7.22	7.20	0.01
4.2	1612	1598	14	7.34	7.31	0.03
4.3	1655	1582	73	8.90	8.33	0.57
4.4	1648	1579	69	8.42	8.25	0.20
4.5	1620	1610	10	-	-	
4.6	1612	1608	4	-	-	
4.7	1655	1620	35	-	-	
4.8	1648	1612	36	-	-	

The ^{1}H-NMR and ^{13}C-NMR spectra of Zn(II) complexes were recorded in CDCl$_3$ at room temperature. Typical aliphatic signals resonate in the region 1.0 - 2.29 ppm and could be seen for all Zn(II) complexes. In complex **4.1** the ^{i}Pr methyl signals appear as four doublets compared to the free ligand due to their stereochemical nature and interaction with the metal centre *(vide infra)*.
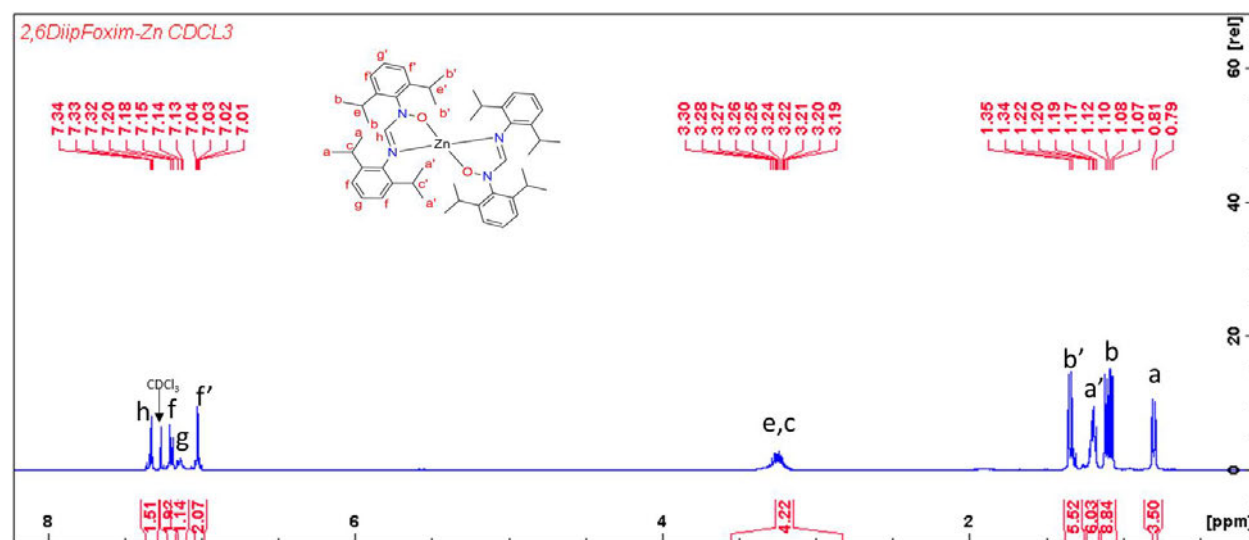
Figure 4.3: H^1-NMR spectrum of complex **4.1** at room temperature in CDCl$_3$ (400 MHz)

The azomethine proton NC(H)=N signals are shifted up field in complex **4.1** – **4.4** compared to the free ligands **L4.1** – **L4.4** (see Table 4.2) because they are shielded by the coordinating metal. The shielding is more pronounced with a significant proton resonance shift for unsymmetrical substituted complexes **4.3** and **4.4** as compared to complex **4.1** and **4.2**. Also, ^{13}C-NMR spectra for complex **4.1** (Figure 4.4) shows that azomethine carbon signal is shifted downfield due to metal coordination and appears around 150 ppm which contrasts with 147-148 ppm for free-ligand. A similar trend was also observed for complexes **4.2** - **4.4** (see appendix B).
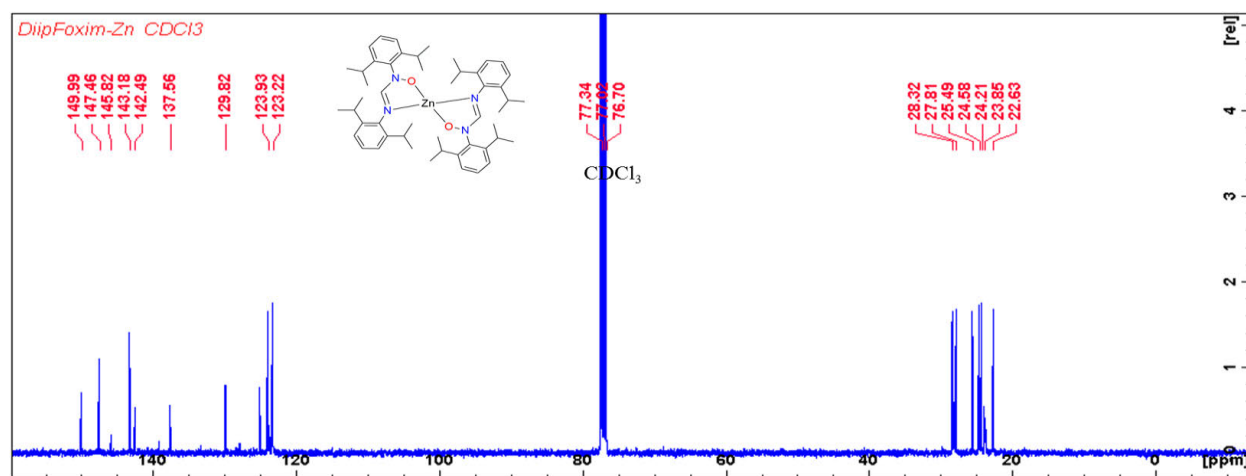
Figure 4.4: ^{13}C-NMR spectrum of complex **4.1** at room temperature in CDCl₃ (400 MHz)

Intermolecular contacts between metal centre and the ligand protons was confirmed by nuclear over-hauser effect spectroscopy (NOESY). For instance, the NOESY spectrum for complex 4.1 (Figure 4.5) showed cross peaks due interaction of the N-H and ^{i}Pr-methyl protons and the metal centre. Also, the other cross peaks are possibly due to adjacent protons in the ligand framework.
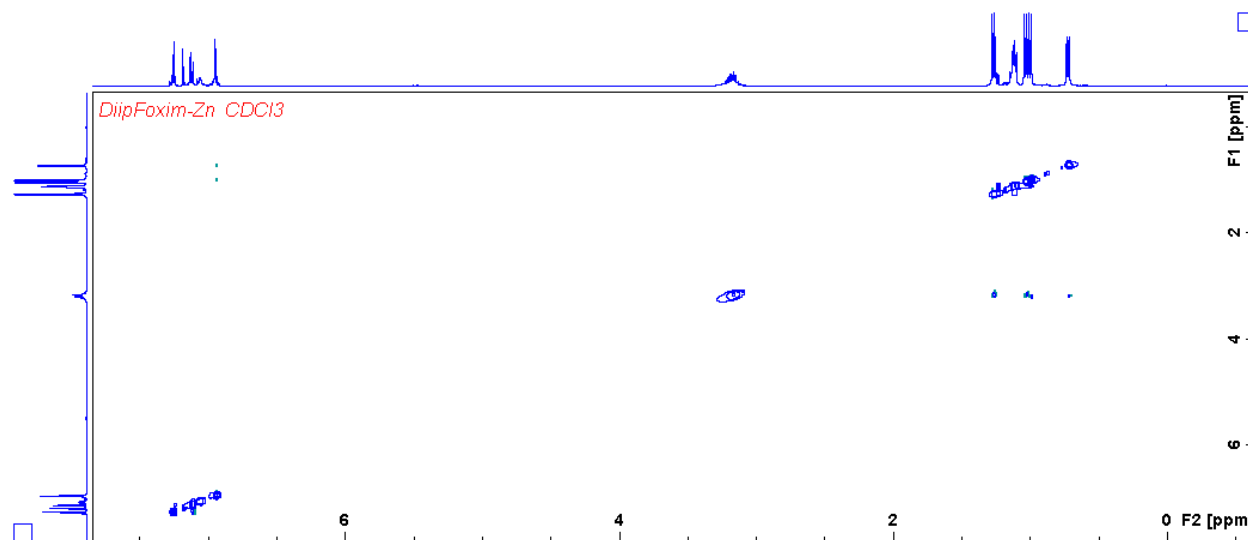
Figure 4.5: Two-dimensional 2D ^{1}H-^{1}H nuclear over-hauser effect spectroscopy (NOESY) NMR of complex **4.1** in CDCL3 (400 MHz) at room temperature

4.7.3   *EPR and magnetic studies of Cu(II) complexes*

To deduce the solid-state electronic structure of the copper complexes, X-band EPR spectra of the solid complexes were acquired at 295 K. The EPR spectra of complexes **4.5**, **4.7** and **4.8** are perfectly isotropic with a single line (g = 2.1082). This is normally an indication of a complete symmetric environment where the electrons in separate d-orbital interact in all directions with identical g-factors. The broad signals and slight deviation of the g-factors from the free electron value (2.0023) points to the $d_{(x^2-y^2)}$ orbital (*B1g*) ground state occupancy by the unpaired Cu(II) electrons. The g-values are comparable to those of other square-planar complexes reported in literature.[51] Complex **4.6** also showed axial symmetry with two magnetic parameters (g = 2.123 and g = 2.086). The ESR spectra also showed a resolved hyperfine structure in the perpendicular section due to the interaction of metal electrons with nitrogen atoms. In all complexes the spectra are devoid of $m_s = \pm 2$ transitions a half field signal ruling out any meaningful Cu$\cdots$Cu interactions.
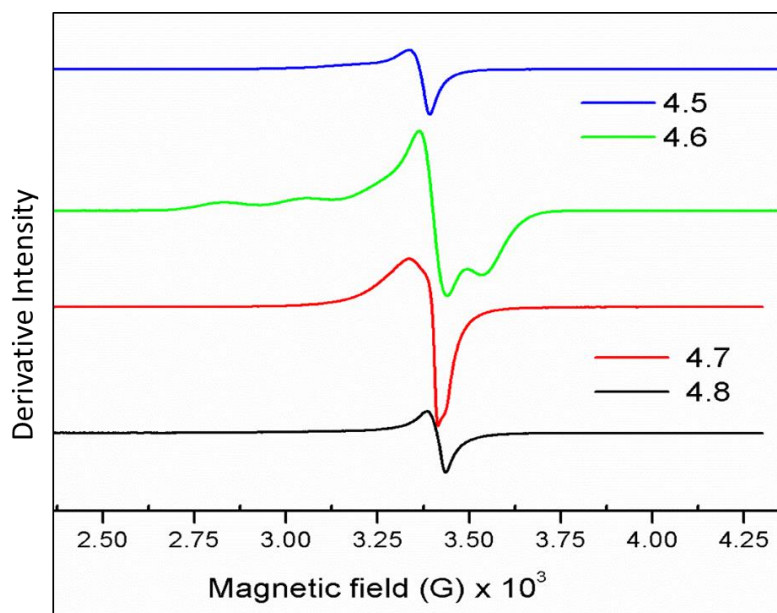
Figure 4.6: Solid state EPR spectra of complexes **4.5 – 4.8** (295K, 9.786GHz)

The paramagnetic nature of the Cu(II) complexes was further confirmed by magnetic studies. Figure 4.7 shows hysteresis loops which are almost linear and does not reach saturation at higher applied magnetic field. This is because of the paramagnetic nature of copper(II) ions and magnetic moments are aligned with the magnetic field.
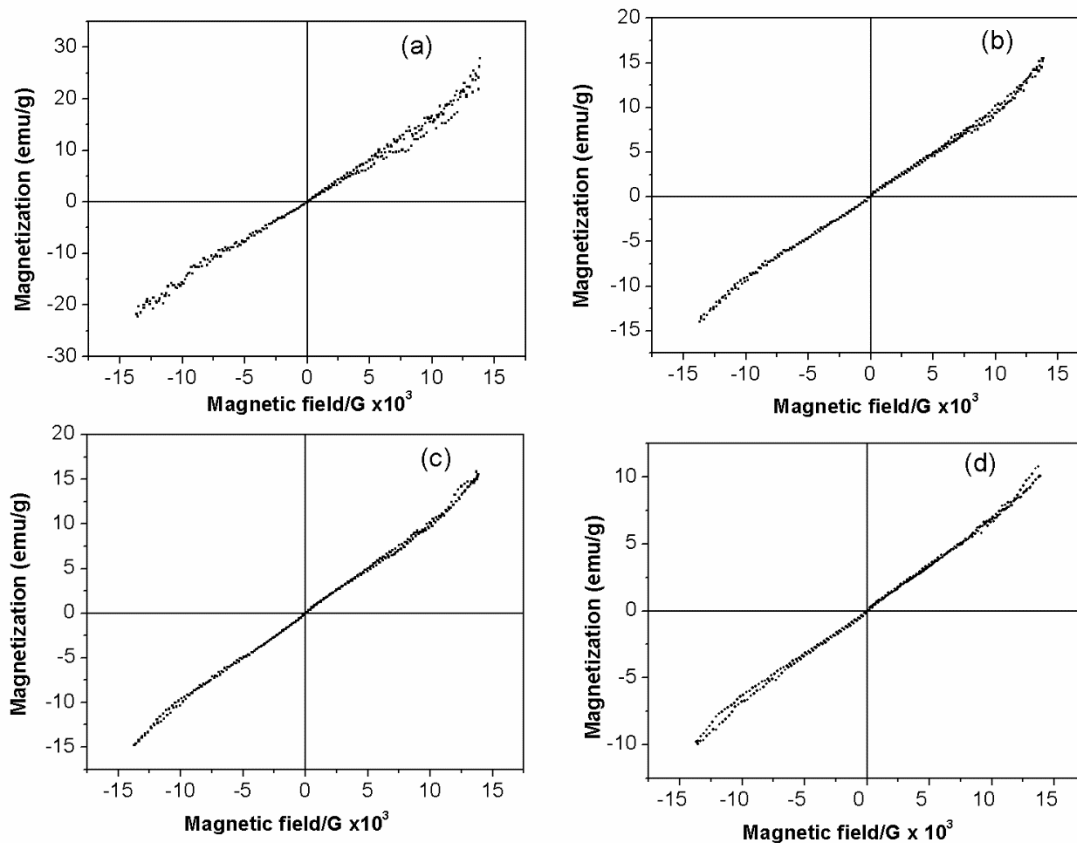
Figure 4.7: Magnetization behaviour of complexes (a) **4.5** – (d) **4.6**

Table 4.3: Magnetic parameters for complexes **4.5 – 4.8**

Parameter	**4.5**	**4.6**	**4.7**	**4.8**
Coercivity (H_{ci})	71.485	47.895	89.657	21.782
Magnetization (M_s)	14.777	15.290	10.350	25.090
M_s, Negative	-14.031	-14.744	-9.9445	-22.283
M_s, Positive	15.522	15.836	10.756	27.900
Squareness ($\times 10^{-3}$)	6.362	4.075	8.887	1.728

4.7.4 Single crystal X-ray structural analysis

Molecular structures of ligands **L4.3** and **L4.4** were determined by single crystal X-ray diffraction using good quality crystals grown from a solution of methanol at -4 °C. Complexes **4.3**, **4.5**, **4.6** and **4.7** were obtained by slow diffusion of diethyl ether to saturated dichloromethane complex solutions.

4.7.4.1 Molecular structures of ligands L4.3 and L4.4

The asymmetric unit of **L4.3** contains one ligand molecule together with a methanol solvent molecule while that of **L4.4** consist of one ligand molecule. In the molecules, the planes of the 2,6-substituted and the ortho-substituted phenyl rings are almost perpendicular with a tilt angles between 84 – 93°. The C—N bond distances in both ligands are almost similar and they range between 1.294(2) - 1.347(2) Å showing that the electrons are delocalised over the bridge. The bulky ^{i}Pr groups in **L4.4** results in slightly greater N—C—N cone angle (120.113°) due to greater repulsions. The bond distances and angles of both ligands agree well with reported values.[52] Both compounds exist as zwitterions with a negatively charged oxygen and the positively charge nitrogen. **L4.3** molecules are stabilised *via* H-bonding interactions O–H⋯O with the protic solvent.

.
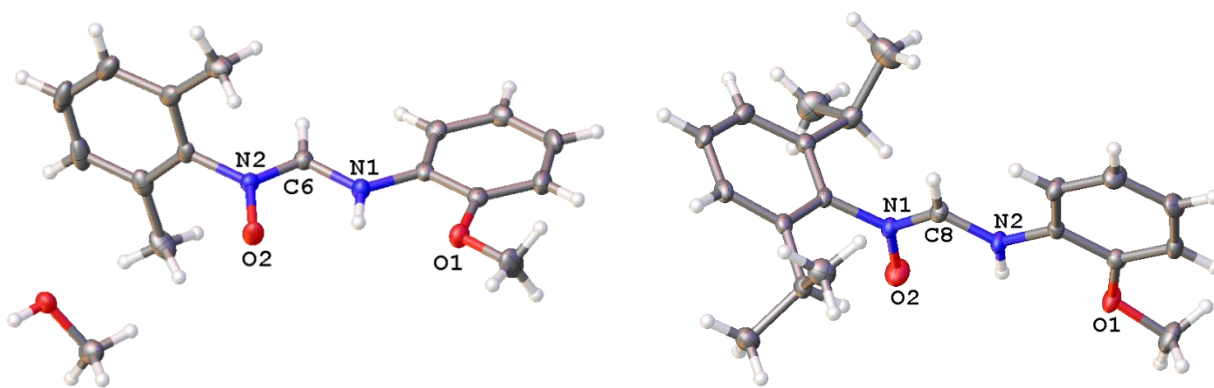
Figure 4.8: X-ray crystal structures of ligand **L4.3** and **L4.4** with thermal ellipsoids drawn at 50% probability. Selected bond length [Å] and angles [°]: (**L4.3**); C(6)-N(2) 1.2993(17); C(6)-N(1) 1.3418(17); N(2)-O(2) 1.3416(13); N(2)-C(6)-N(1) 117.57(11). (**L4.4**) N(1)-C(8) 1.294(2), N(2)-C(8) 1.347(2), O(2)-N(1), 1.3084(18); N(1)-C(8)-N(2) 120.13(16)

4.7.4.2 Molecular structures of complexes 4.3, 4.5, 4.6 and 4.7

The molecular structures are shown in Figure 4.9 - 4.10 while selected interatomic distances, and torsional angles for the complexes are listed in Table 4.4. The asymmetric unit of complex **4.3** contains one molecule of the complex while complex **4.7**, consist of one complex molecule and dichloromethane co-solvent. In both cases, the complex molecule consists of a metal ion coordinated to two ligands via the imine N and hydroxyl O and in doing so, the acetate anions from the metal salts are displaced from the coordination sphere. The coordination is in a bidentate fashion and results in pentacyclic metallacycles which are comparable to other *N,O* bidentate ligands.[53] In **4.3** a distorted tetrahedral geometry around the Zn(II)I s observed while a square planar geometry around the Cu(II) in 4.7 is observed. The bond angles around the metal centre in complex **4.3** range from 108.77(6) - 146.62(6)° while in complex **4.7** are 83.93(7) and 96.07(7)° (Table 4.4) and they deviate from those of regular tetrahedron and square planar geometries, respectively. Similar values have been reported in literature for related structures.[49,54]
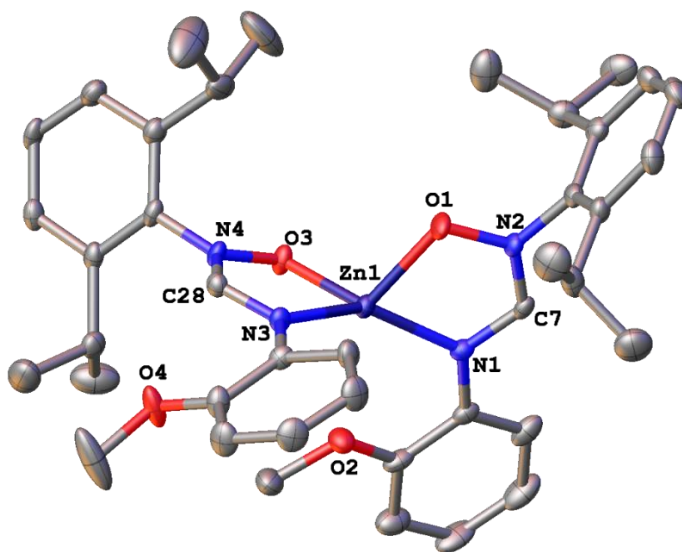
Figure 4.9: X-ray crystal structure of complex **4.3** with thermal ellipsoids drawn at 50% probability level and hydrogen atoms have been omitted for clarity
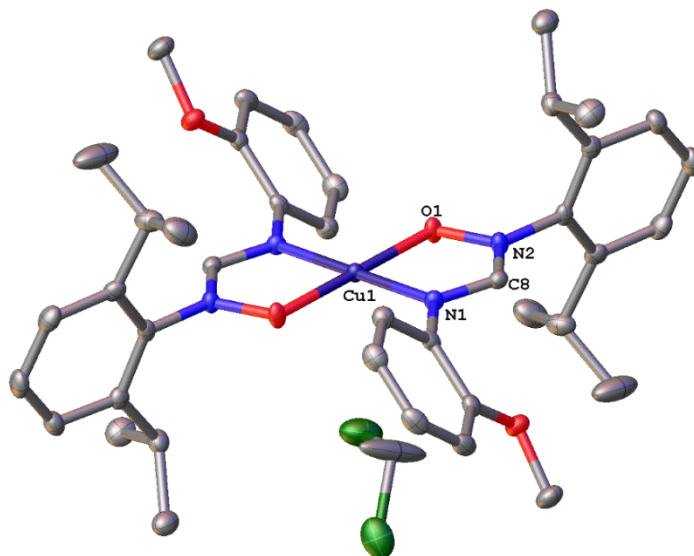
Figure 4.10: X-ray crystal structure of complex **4.7** with thermal ellipsoids drawn at 50% probability level and hydrogen atoms have been omitted for clarity

In complex **4.3**, the metallacycle plane is nearly perpendicular to the 2,6-disubstituted aromatic ring planes with dihedral angles between 79.9(3) - 92.5(3)° while nonplanar to the methoxy substituted rings with dihedral angles between 17.2(4) – 142.2(3)°. In complex **4.7**, the 2,6-disubstituted and methoxy substituted phenyl ring planes have dihedral angles of 82.7(2)° and 53.1(3)° with respect to the pentacyclic chelate rings. In both cases, the difference in dihedral angles between 2,6-^{i}Pr-and MeO- substituted rings is due to greater repulsions induced by bulk ^{i}Pr groups.

The mean Zn—O and Zn—N bond lengths in complex **4.3** are 1.998(2) and 1.984(2) Å, respectively which are consistent with reported structures coordinating through the imine nitrogen.[49] On the other hand, they are smaller compared to reported related Schiff base complexes.[55-57] For instance Wu *et al*[58] reported an average Zn—N$_{imine}$ bond length of 2.106(3) Å with Salen-type ligands. The Zn(1)—O(3)$_{methoxy}$ distance in complex **4.7** (2.477(2) Å) is slightly longer compared to other structures that have been reported in literature.[59]

In complex **4.7**, the Cu(1)—O(1)—N(1)—C(13) torsion angle confirms the out-of-plane displacement of 1.0(2)° from the chelate ring with respect to the N—O—Metal orbitals. The average bond distances of Cu—O (1.9264(14) Å) and Cu—N$_{imine}$ (1.9399(17) Å) are consistent

with other reported structures reported by Okazawa *et al*[60] for pyridyl nitroxide supported Cu(II) complexes with Cu—O bond distance between (1.9316(19) – 1.9491(18) Å) and Cu—N_{pyr} (1.9281) Å. The C—N bond distances are almost identical in both structures, indicative of delocalized π-electron density over the –N=C–N– backbone.

Complexes **4.5** and **4.6** are supported by symmetrical hydroxy formamidine ligands. The asymmetric units of both complexes contain half complex molecules with the other half generated through inversion centres or complexes **4.5** and **4.6** respectively. The mono metallic complexes are bis-ligated, and the ligands coordinate in the same fashion as discussed above. The Cu atoms also adopt a square planar geometry as witnessed in complex **4.7** with bond angles between 83.59(5) – 96.41(5)°. Steric repulsion between the bulky 2,6-*i*Pr groups resulted in greater tilt angles which lie between **4.6** as compared to **4.5**. The Cu—O and Cu—N bond distances are almost comparable in both complexes and they between 1.9139(10) – 1.9384(10) Å. These values are comparable to those reported in literature for related complexes.
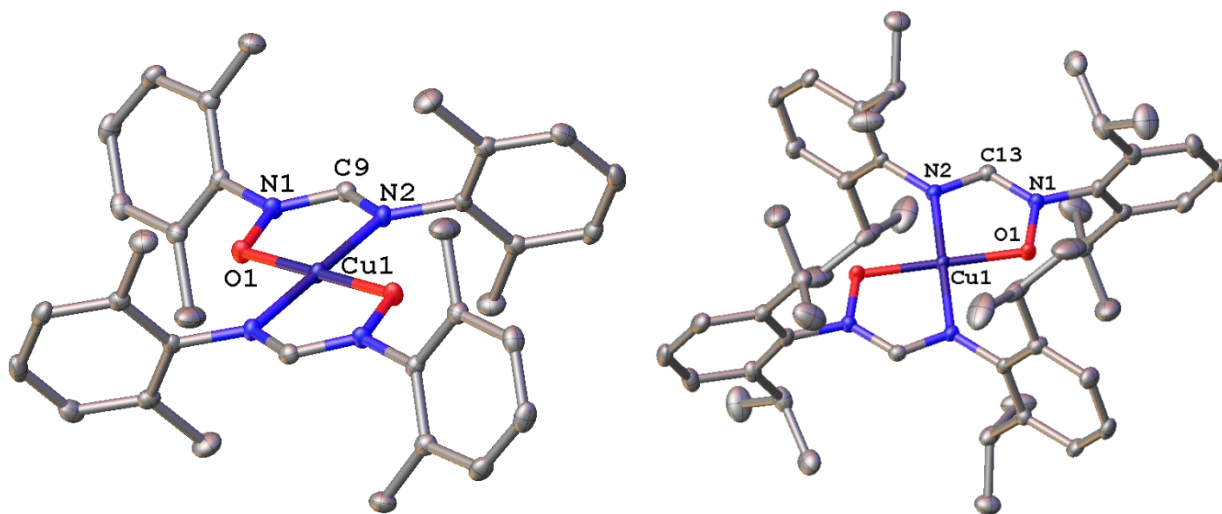
Figure 4.11: X-ray crystal structure of complexes **4.5** and **4.6** with thermal ellipsoids drawn at 50% probability level and hydrogen atoms have been omitted for clarity

Table 4.4: Selected bond lengths and angles for complexes **4.3**, **4.5**, **4.6** and **4.7**

	4.3	4.5	4.6	4.7
Bond lengths [Å]				
M—N	1.980(3) -1.988(2)	1.9138(10) -1.9385(12)	1.9350(10)- 1.9351(10)	1.9399(17)
M—O	1.982(2) - 2.014(2)	1.9138(10)	1.9185(9)	1.9264(14)
C—N	1.314(4) - 1.319(4)	1.9385(12)	1.3135(16)- 1.3119(16)	1.315(3) - 1.316(3)
Bond angles [°]				
O—M—N(cone)	81.48(5) - 83.84(5)	83.59(5) - 96.41(5)	95.96(4)- 84.04(4)	83.93(7) - 96.07(7)
O—M—O	112.27(6)	180.0	180.0	180(1)
N—M—N	146.62(6)	180.0	180.0	180(2)
O—M—N	108.77(6) –122.79(6)			
Dihedral angles [°]				
C—N—O—M	1.3(2) – 7.0(2)	-1.58(15)	-0.40(12)	1.0(2)
N—C—N—M	1.3(2) – 4.9(2)	0.23(17)	0.34(14)	-1.4(2)
2,6^{i}PrPh-(NO)	79.70(2) – 92.60(2)	60.21(17)	93.69(13)	82.7(2),
2-MeOPh-(NM))	17.2(2) – 141.85(16)	75.91(16)	92.19(13)	53.1(3)

4.7.5   *Ring-opening polymerization of ε-caprolactone and L-lactide*

Complexes **4.1** – **4.8** were investigated for their catalytic activity in polymerization of ε-caprolactone and L-lactide. Preliminary studies were done in bulk at 110 °C using 100:1 monomer to catalyst ratio. In bulk reactions, long induction periods, greater than 24 h, were observed for complexes **4.1** – **4.8** with complex **4.2** showing the greatest activity, achieving *ca.* 5% monomer

conversion. This can be attributed to three main reasons, namely catalyst conformational changes to form a monomer-catalyst transition state,[61,62] heat transfer and catalyst dissociation to less reactive species.[63] There were no further efforts to try and probe the nature of the induction periods in our system.

To speed up the initiation process an external nucleophile was then added as a co-initiator. The polymerization of ε-CL was then carried out in toluene at 110 °C using benzyl alcohol as a co-initiator with a [M/I/BnOH] mole ratio of 100:1:1. Complexes **4.1 – 4.8** showed increased catalytic activity with complex **4.2** still exhibiting superior activity. There was virtually no induction period for Zn(II) complexes **4.1 – 4.4** (Figure 4.12) in the presence of co-initiator, signifying the existence of reactive catalytic species from the start. However, for Cu(II) complexes **4.5 – 4.8** the induction period was reduced with complex **4.6** being the most active among the Cu(II) series having an induction period of about 10 h (Figure 4.12).
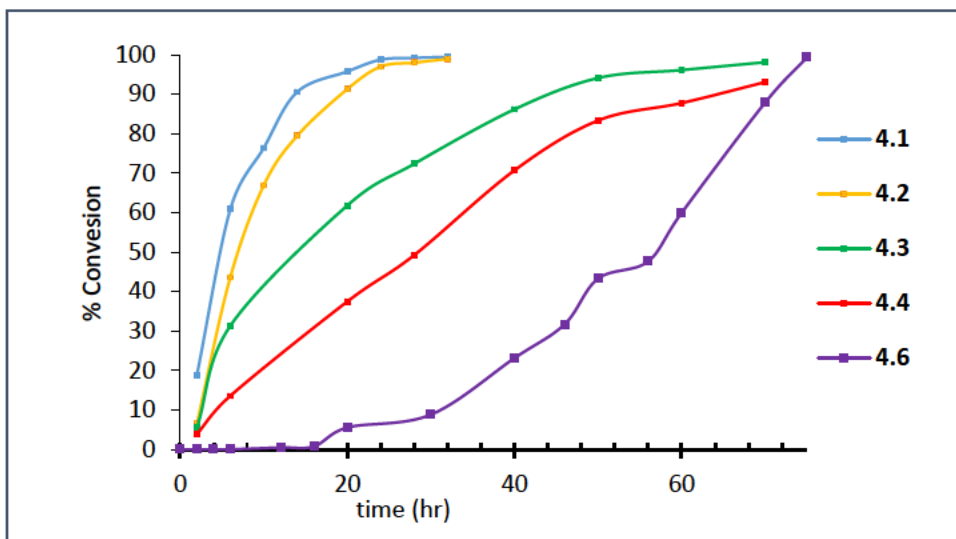
Figure 4.12: (a) Polymerization of ε-CL to PCL by complexes **4.1** - **4.4** and **4.6**. Reaction conditions: toluene, T = 110 °C

Complexes **4.1 – 4.8** can be referred to as catalyst since the induction periods involve monomer and co-initiator activation, therefore the complexes are interchangeably referred to as catalyst or initiators. Monomer conversions between 90 – 99% were observed within 22 – 125 h for complexes **4.1 – 4.8** (Table 4.5). Complex **4.2** which was the most active was used to probe the polymerization of ʟ-LA with monomer equivalent between 100 and 300.

Conversion of up 99% were achieved within 14 – 19 h for different L-LA monomer concentrations. The summary of results is presented in Tables 4.5 and 4.6.

Table 4.5: Summary of polymerization data of ε -CL by complexes **4.1 – 4.8**

Entry	Complex	[M/cat]	Time (h)	[b]Con(%)	[c]$M_{w(calc)}$	[d]$M_{w(GPC)}$	[e]PDI	k_{app}(h$^{-1)}$)
1	**4.1**	100:1	32	99	11286	1884	1.23	0.1519
2	**4.1**	300:1	36	97	33174	2667	1.45	-
3	**4.2**	100:1	24	98	11172	2239	1.30	0.1751
4	**4.2**	300:1	28	99	33858	2909	1.40	-
5	**4.3**	100:1	68	99	11286	2088	1.42	0.0693
6	**4.3**	300:1	80	99	33858	2184	1.24	-
7	**4.4**	100:1	73	96	10944	1512	1.22	0.0386
8	**4.4**	300:1	96	95	10830	1939	1.25	
9	**4.5**	100:1	94	90	10260	1506	1.38	
10	**4.6**	100:1	105	93	10602	2090	1.66	
11	**4.7**	100:1	115	97	11058	1039	1.20	
12	**4.8**	100:1	125	96	10944	1047	1.10	

[a]Polymerization conditions: 110 °C, 3.0 ml of toluene as the solvent, [M]$_0$:[catalyst]$_0$:[BnOH]$_0$ = 100:1:1. [b]Determined from NMR. [c]Calculated theoretical Mw. [d,e]Determined by GPC relative to polystyrene standards in THF. [d]Experimental M_w was calculated considering Mark–Houwink's corrections of 0.56.

The Zn(II) catalyst, complexes **4.1 – 4.4**, were more active than the Cu(II) analogues, complexes **4.5 – 4.8**, in solution polymerization of ε-CL. For example, in a relative comparison complexes **4.3** and **4.7** (entries 5 and 11 in Table 4.5) a conversion of about 99% was achieved within 68 h for complex **4.3** while complex **4.7**, 115 h of reaction time was needed. A more active Cu(II) diketimate system developed by Whiteborne *et al.*[64] is an exception where full conversion of lactides was obtained within 1 h at room temperature. There are two possible explanations for the difference in activity. Firstly, greater electrophilicity of Zn(II) result in increased monomer activation as compared to Cu(II), hence increased activity. Secondly, the stronger Cu—O bond compared to Zn—O (see Table 4.4), does not readily break to initiate the polymerization reaction. Although the M—O bond distances are comparable to those with auxiliary alkoxides and acetate ligands, which are normally active initiators,[35,64,65] inclusion of the oxygen in the ligand skeleton seem to make the bond less labile due to the chelating effect.

Table 4.6: Effect of complex **4.2** concentrations as a catalyst for polymerization of ʟ-lactide

Entry	[M/cat]	Time (h)	^{f}Conv (%)	$^g M_w$(calc)	$^h M_{w(GPC)}$	^{i}PDI
1	100:1	14	99	11286	1190	1.5
2	200:1	16	99	22572	1742	1.71
3	300:1	19	97	33174	2274	1.71

Polymerization conditions: 110 °C, 3.0 ml of toluene as the solvent, [catalyst]$_0$:[BnOH]$_0$ = 1:1. Percentage conversion from NMR. ^{g}Calculated theoretical Mw. ^{h,i}Determined by GPC relative to polystyrene standards in THF. Experimental M_w was calculated considering Mark–Houwink's corrections of 0.58.

4.7.6 *Kinetics of ROP reactions of ε-CL and ʟ-LA*

Kinetic studies to ascertain the dependence of reaction rates on monomer concentration were carried out at 110 °C with a [monomer]$_0$/[catalyst]$_0$ ratio of 100:1. Non-linear plots of ln([CL]$_0$/[CL]t) vs time were obtained for Cu(II) complexes suggesting a second order dependence on monomer concentration. Zn(II) complexes **4.1** – **4.4**, exhibited a linear relationship of ln ([M]$_0$/[M]$_t$) *vs* time and the apparent rate constants (k_{app}) of polymerization were obtained from the slopes (Figure 4.13).
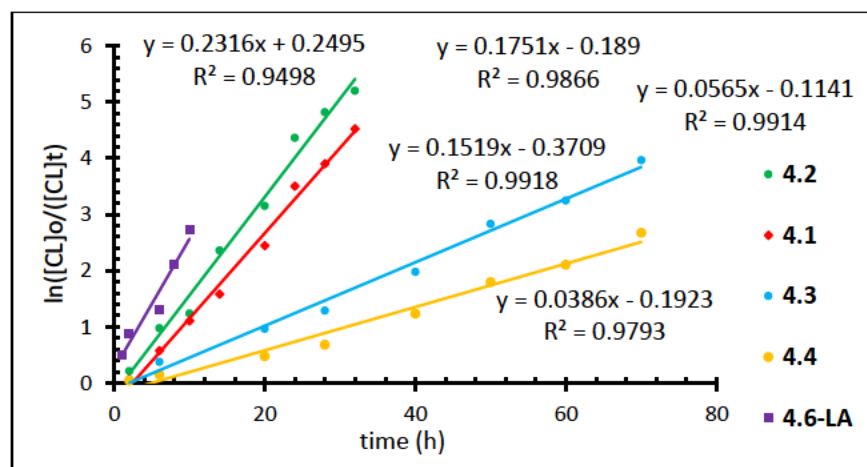
Figure 4.13: Plots of ln([M]$_0$/[M]$_t$) *vs t* for catalysed by complexes **4.1** - **4.4** and **4.6** for ε-CL and LA, respectively. Reaction conditions: [M]$_0$:[I]$_0$:[BnOH]$_0$ = 100:1:1 solvent: toluene; T = 110 °C

The linearity points to a *pseudo* first-order polymerization reaction with respect to ε-CL or ʟ-LA monomer concentrations. Hence, for *pseudo* first order kinetics, the rate of monomer polymerization can be calculated using equation (**4.3**).

$$-\frac{d[M]}{dt} = k[M] \qquad (\mathbf{4.3})$$

For a specific monomer concentration ([M]), and constant initial catalyst concentration ([Catalyst]$_0$), $k = k_p$,where k_p = rate of chain propagation, Cat = catalyst, and x is the order of reaction.

The overall propagation rate (R_p) is expressed a shown in equation (**4.4**).

$$R_p = \frac{d[M]}{dt} = k_p[M]_0^a[Cat]_0^x \qquad (\mathbf{4.4})$$

In the presence of a co-initiator, in case of benzyl alcohol (BnOH) with initial concentration [BnOH]$_0$, R_p is expressed as equation (**5**),

$$R_p = \frac{d[M]}{dt} = k_p[M]_0^a[BnOH]_0^b[Cat]_0^x \qquad (\mathbf{4.5})$$

where *a* and *b* are orders of reaction with respect to monomer and co-initiator, respectively. The rate of polymerization of ε-CL is comparable to that of L-LA. For instance, in the case of ε-CL complex **4.2** gave an apparent rate constant of 0.2036 h^{-1} compared to 0.1751 h^{-1} (Figure 4.13). Generally, the 6-membered L-LA heterocyclic ring is more strained as compared to the 7-membered ε-CL ring resulting in higher rates of polymerization. The observed low apparent rate constants were also depended on the steric and electronic effects of the catalyst. There was no drastic change in activity between complex **4.1** (0.1519 h^{-1}), bearing bulky isopropyl substituents and complex **4.2** (k_{app} = 0.1751 h^{-1}), with symmetric 2,6-methyl substituents. However, replacing 2,6-substituents with a single *ortho*-methoxyl group on the other phenyl ring resulted in a significant decrease in the activity (**4.3**, k_{app} = 0.0693 h^{-1} and **4.4**, k_{app} = 0.0386 h^{-1}). Metal to oxygen interactions of about 2.447(2) Å were detected in the molecular structure of complex **4.3** and can possibly be maintained in solution hence competing with monomer coordination resulting in lower polymerization rates. Generally the apparent rate constants obtained for the complexes **4.1** – **4.4** are slightly inferior to other reported systems bearing *N,N,O*-ligating ligands[7,66] but are comparable to Zn(II) and Cu(II) complexes supported by bis(3,5-dimethyl)pyrazole ligands with rates between 0.090 to 0.286 h^{-1} as reported by Appavoo *et al.*[27]

Reaction variables also influence the polymerization kinetics, hence the effect of varying the monomer concentration on the apparent rate constant was investigated for complex **2**. A constant [catalyst]$_0$/[BnOH]$_0$ mole ratio of 1:2 was used while the monomer ratio was varied from 150 to 300.

Increasing the monomer to catalyst ratio resulted in decreased rates without an induction period. The linearity of the plot of ln([CL]$_0$/[CL]$_t$) vs time for complexes **4.1 – 4.4** showed a *pseudo* first order dependence on the initial monomer concentration (Figure 4.14).
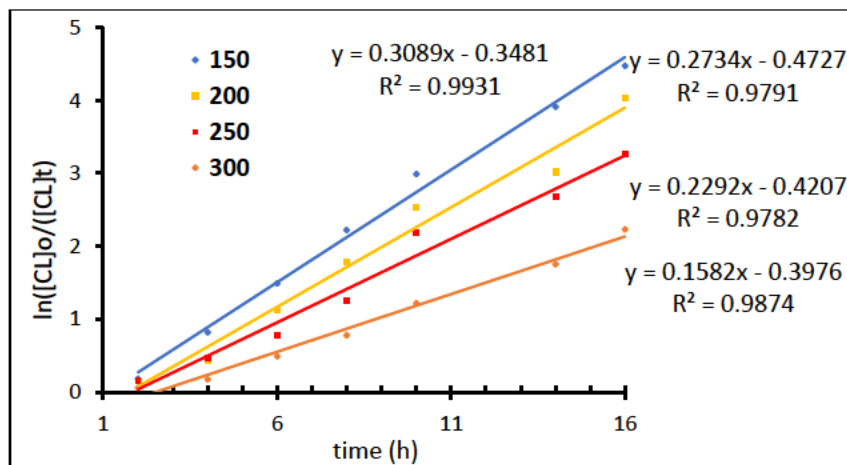
Figure 4.14: Plots of ln([CL]$_0$/[CL]$_t$) *vs t* catalysed by complex **4.2**/BnOH. Reaction conditions: [BnOH]$_0$ = [**4.2**]$_0$ 2:1 and [M]$_0$ between 150 - 300 solvent: toluene; T = 110 °C

4.7.7   *Reaction order for ROP of ε-CL with respect to co-initiator [BnOH]$_0$ and complex 4.2*

To establish the order of reaction with respect to the initial co-initiator (BnOH) concentration, the most active complex **4.2** was chosen and a constant monomer to catalyst ratio of 100:2 was used while varying the co-initiator concentration. The plot of ln(k_{app}) *vs* ln[BnOH]$_0$ (Figure 4.15, in black) permits the determination of reaction order with respect to benzyl alcohol concentration from the gradient. The extrapolated slope gave a fractional order of 0.49, which shows that multiple steps are involved. To obtain the order with respect to complex **4.2**, constant monomer to co-initiator ratio ([CL]:[BnOH]$_0$) of 100:2 was used and the catalyst was varied from 3 mM to 6 mM. The best fit logarithmic linear plot of ln(k_{app}) *vs* ln[**4.2**]$_0$ (Figure 4.15, in red) gave a slope of 1.1 indicating first order reliance on catalyst concentration and is comparable to the bis(pyrazolylmethyl)pyridine Zn(II) complex reported by Zikode *et a.l.*[67] In contrast, fractional reaction orders for the catalyst have also been observed in bulk polymerization due to catalyst aggregation, and dissociation to form reactive species.[68,69] In addition, a formamidine Zn(II) system showed 0.3 and 0.6 fractional reaction orders.[70] The overall rate equation for ε-CL polymerization can expressed as equation (**4.6**).

$$R_p = \frac{d[\varepsilon CL]}{dt} = k_p[\varepsilon CL]^1[\mathbf{BnOH}]^{0.5}[\mathbf{4.2}]^{1.1} \qquad (\mathbf{4.6})$$
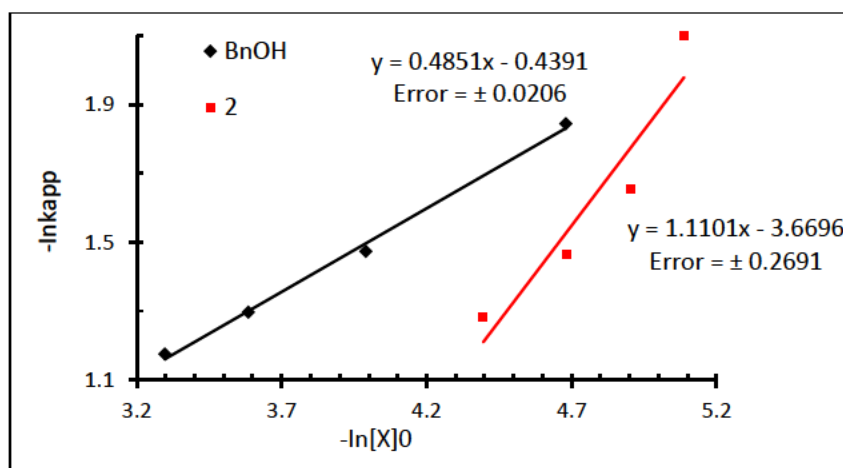
Figure 4.15: Plot of $\ln k_{app}$ vs $[\mathbf{BnOH}]_0$ (black) and complex **4.2** (red) for reaction order determination on with respect to co-initiator and catalyst

4.7.8   *Molecular weight and molecular weight distribution of polymers*

The molecular weight (M_w) and the molecular weight distributions (PDI = M_w/M_n) were determined by gel permeation chromatography (GPC) and compared to the theoretical values. Appropriate Mark–Houwink corrections 0.56 for PCLs and 0.58 PLAs were used. Lower molecular weights less than those obtained by NMR were obtained. The observed molecular weights ranged from 1855 - 3999 Da and 1190 - 2274 Da for PCLs and PLAs, respectively (Table 4.5 and 4.6). Increasing the monomer to catalyst ratio (having less initiating species) did not yield a significant increase in the molecular weight (Table 4.5, entries 2, 4, 6 and 8). For instance, complex **4** showed molecular weight increased from 1512 to 1939 Da (Table 4.5, entries 7 and 8), a 4% increase with respect to calculated molecular weight. Low molecular weights inferred that the catalysts are less efficient resulting in limited number of chains growing to reach the predicted molecular weights.[71]

The observed molecular weights for complexes **4.1** – **4.8** are inferior to those reported by Wang *et al*,[72] under similar conditions, which ranged from 1300 - 28800 Da. with PDIs less than 1.27. Obuah *et al.*,[73] also reported low molecular weights between 1480 to 7080 Da in bulk polymerization of ε-CL using ferrocenyl(pyrazolyl)- Zn(II) and Cu(II) complexes.

Two reasons are possible for the observed low molecular weights. Firstly, the co-initiator can act as a chain transfer agent causing premature chain termination.[74] Secondly, inter- and intra-molecular trans-esterification side reactions (back-biting) can result in cyclization and shortening of the propagating polymer chains[75] Our system appears to be influenced by both scenarios since a co-initiator was added and the presence of small peaks in the ESI-MS spectra of PCL and PLA (Figure 4.16 and 4.18) matching cyclic polymers were observed. Cyclization normally happens at extended reaction times when the monomer is almost completely depleted and at higher molecular weights where the chains can easily fold.[76] It has been reported that bulk ligands can help in selective coordination of the monomer than the polymer chains to the metal centre hence reducing transesterification.[77]

Although not significant, symmetry coupled with steric bulkiness of the ligand skeleton seem to have a bearing on the resultant polymer molecular weights. Bulky isopropyl groups in complex **4.1** and **4.5** (Table 4.5, entries ,1 and 9) resulted in slightly lower molecular weights as compared to complexes **4.2** and **4.6** (Table 4.5, entries 2 and 6) with methyl substituents. This is because bulky substituents inhibit monomer interaction with the metal centre for activation. This trend contrasts what was observed by Shen *et al.*,[78,79] in their study of steric effects in free ligand substituted phenolates samarium complex. They noted that *ortho* bulkier groups repel more and prevented close packing of phenyl rings towards the metal centre hence creating ample space for monomer coordination which resulted in increased catalytic activity.

Unsymmetrically substituted complexes **4.3**, **4.4**, **4.7** and **4.8** (Table 4.5, entries 5, 7, 11 and 12) have lower molecular weights as compared to symmetrically substituted complexes. This could be due to the methoxy oxygen which is weekly coordinating there by strongly competing with monomer coordination to the metal centre. Albeit catalytic activity shown by these complexes, the tendency to produce lower molecular weights polymers limits the system to produce polymers which can be applied in areas where toughness is a requirement.

However, they are suitable for drug delivery systems like hydrogels.[80,81] Polymers obtained from complexes **4.1** – **4.8** showed relatively narrow polydispersity indices which ranges between 1.2 and 1.45 and 1.5 and 1.7 for PCLs and PLAs, respectively. Relatively narrow polydispersity indices for PCLs as compared to the PLAs can infer that the polymerization is not well controlled

in case of PLAs. Although the polydispersity indices are higher than those anticipated for an ideally living polymerization, however, they are generally accepted for a controlled polymerization model in case of PCLs.
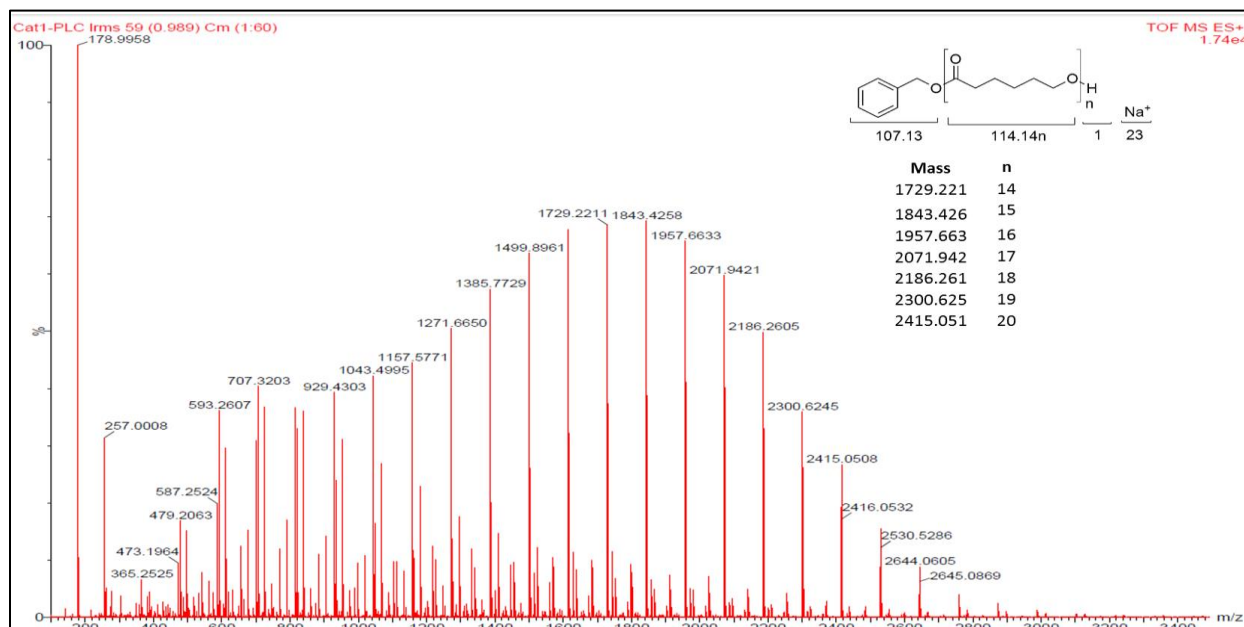
Figure 4.16: ESI-MS spectrum of PCL obtained for complex **4.1**, $[CL]_0:[BnOH]_0 = 100:1$, t = 32 h
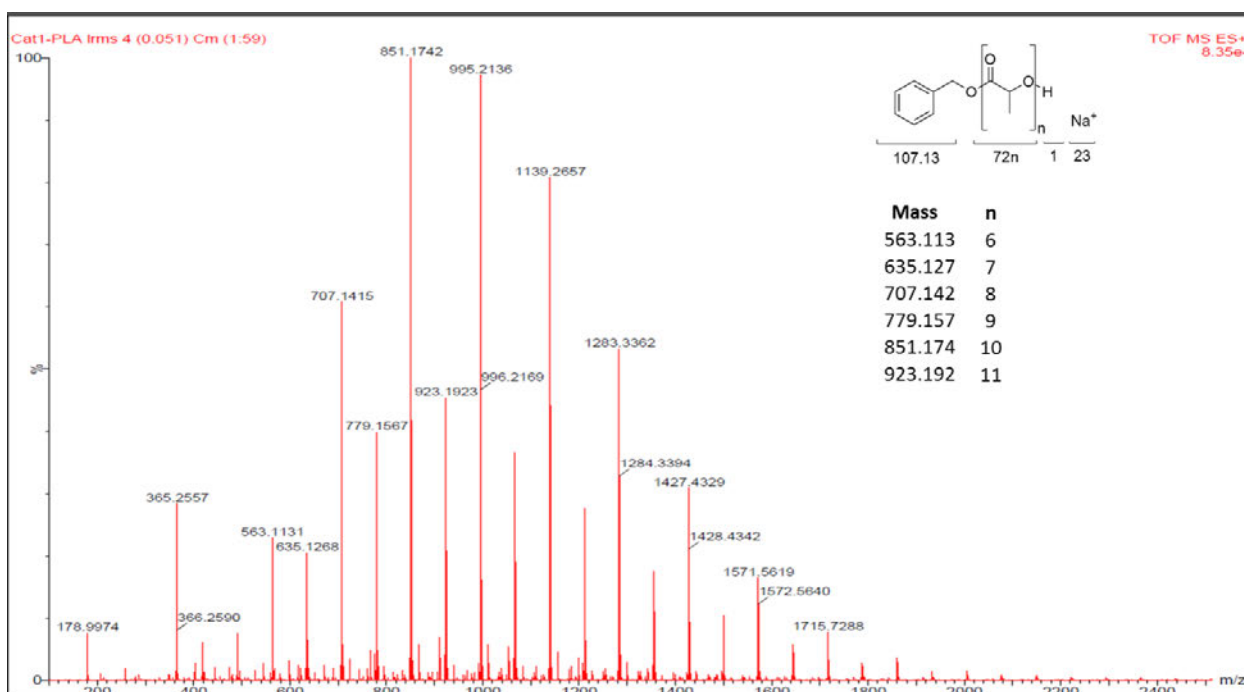
Figure 4.17: ESI-MS spectrum of PLA from complex **4.1**, $[LA]_0:[BnOH]_0 = 100:1$, t =12 h

4.7.9   Homo polymer structure, end group and mechanistic analysis

Two main mechanisms have been proposed for ROP of cyclic esters using metal alkoxide catalyst, namely coordination insertion (CIM) and activated monomer mechanisms (AMM).[82-84]   AMM utilizes an externally added nucleophile while in CIM the nucleophile is integrated as part of the catalyst through a covalent bond to the metal center.[84]   The system under study possess metal-oxygen bonds which are responsible for initiating in ROP therefore, initiation by coordinating ligands cannot be ruled out. NMR and mass spectroscopies were used for an in-depth analysis of the polymer microstructure to establish the initiating group.

Typical ESI-MS spectra for PCL and PLA are shown in Figure 4.16 and 4.17 and a monotone spreading peaks matching distinctive polymer topology were observed. The mass spectra are characterized by a collection of peaks separated by respective repeating unit molar masses. For PCLs peaks are differentiated by 114.1 Da (single caprolactone fragment, (Figure 4.16) and for PLA, a peak separation of 72 Da (single lactyl fragment, Figure 4.17) was observed. A peak difference of 72 Da points to significant transesterification during the polymerization of ʟ-LA. Analysis of PCL ESI-MS showed a polymer peak at $[M+Na]^+$, (1729.22 Da, Figure 4.17) with degree of polymerization (DP = 14) having BnO- and -OH terminal groups. From Figure 4.17 the ion peak at 817.15 Da ($[M+Na]^+$) matches a PLA polymer having DP of 10 with similar terminal groups.

H^1-NMR spectroscopy was used to further interpret and confirm the mechanism of polymerization. Analysis of the ^{1}H-NMR spectra of polymers (Figure 4.18 and 4.20) showed no signals of free *N-hydroxy-N,N′-*diarylformamidine ligand moiety. This is an indication that the ligand moiety was not part of the polymer chain hence it was not involved in the initiation step as was initially proposed. In contrast to amido ligands by Liu and Ma,[25] the chelating amido ligands were capable of initiation ROP and were part of the growing polymer chains. To get further insight about ligand lability in solution a mixture of complex **2** and BnOH was analysed by ^{1}H-NMR in C_6D_6. Two new singlet signals at 4.3 and 4.6 ppm were observed due to methylene protons of free and coordinated benzyl alcohol. No signals were observed of the free ligand hence the complex maintains its structure in solution.

The initiating and chain-end groups in the polymers, were deduced from ^{1}H-NMR and ESI-MS-data. Analysis of ^{1}H-NMR spectra (Figure 4.18 and 4.20) showed the presence of triplet signals at 3.66 and 4.88 ppm for PCL and PLA, respectively. The signals are ascribed to the methylene protons neighbouring the hydroxyl termini end. Also, the singlet at 5.2 ppm from the benzoyl methylene protons confirmed that the polymers were end capped with a benzyl ester. This supports that the propagation mechanism was *via* the insertion of a benzyloxy group into the oxygen-acyl bond of the monomer. Kinetics investigations together with NMR and ESI-MS data for the ROP of ε-CL for complex **4.2** and co-initiator lead us to conclude that an activated monomer mechanism is in operation as shown in Figure 4.20. This observation is consistent with other reported literature work.[69,84-86]
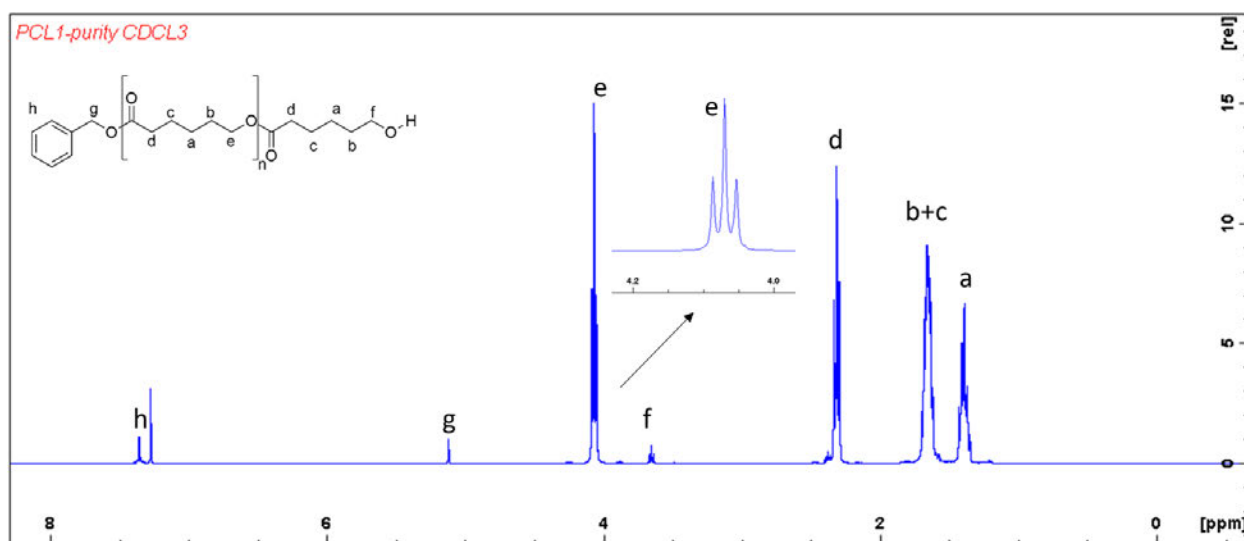
Figure 4.18: The ^{1}H-NMR spectrum of PCL initiated by complex **4.1**/BnOH. Reaction conditions: $[CL]_0:[BnOH]_0 = 100:1$, solvent: toluene, T = 110 °C
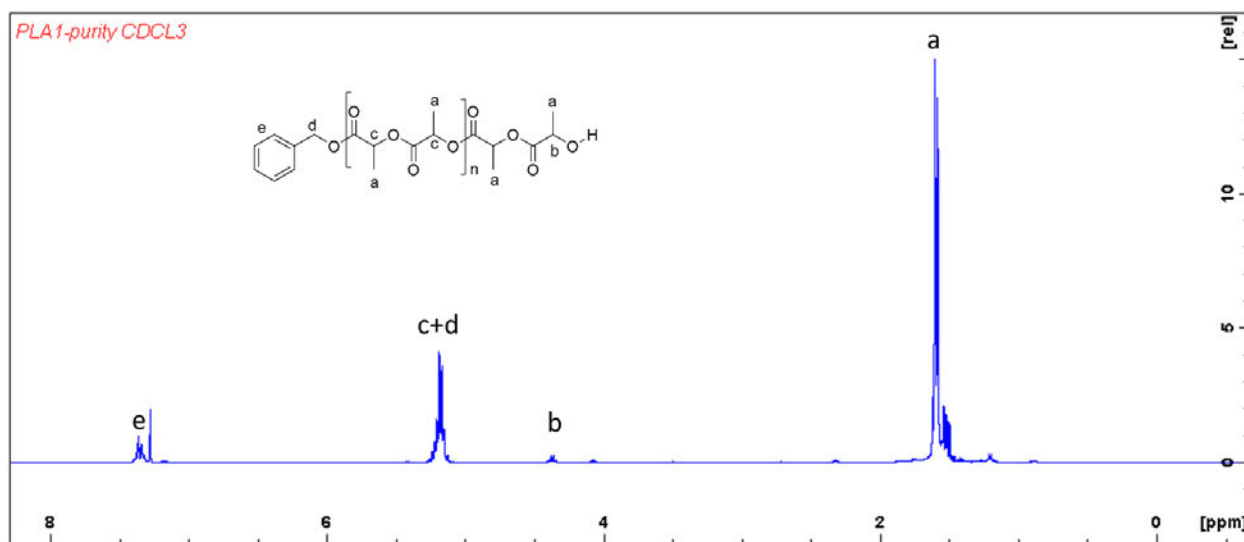
Figure 4.19: The ^{1}H-NMR spectrum of PLA initiated by complex **4.1**/BnOH. Reaction conditions: $[LA]_0:[BnOH]_0 = 100:1$, solvent: toluene, T = 110 °C
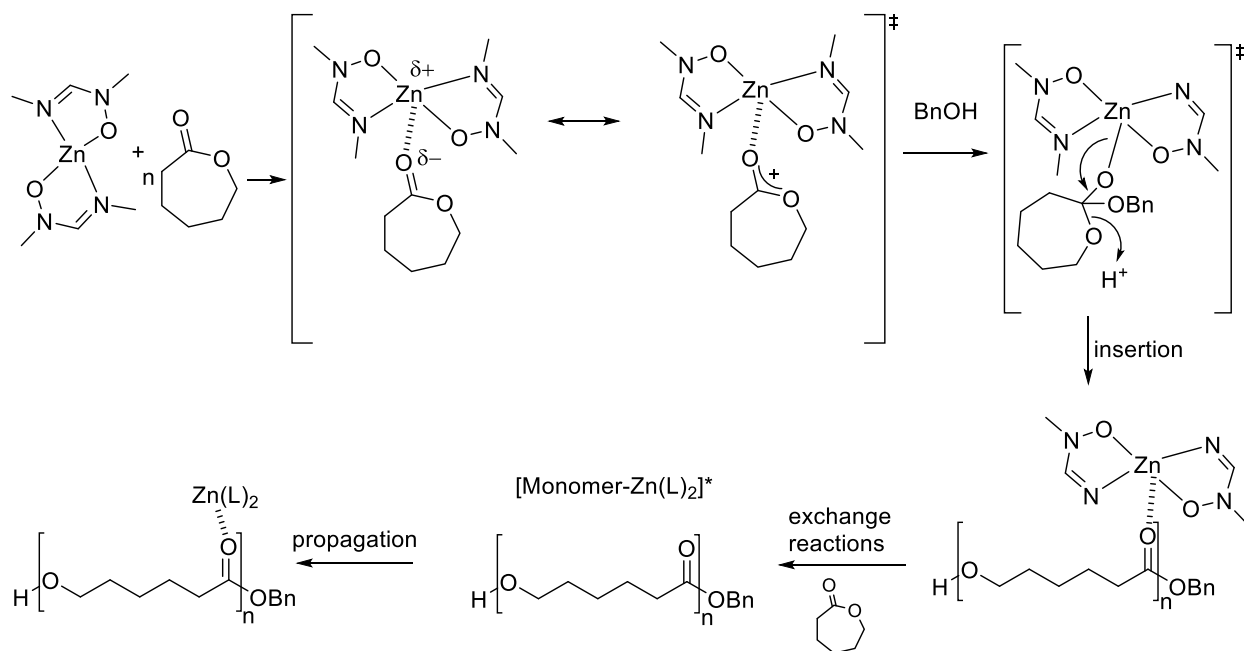
Figure 4.20: Proposed monomer activation mechanism for the polymerization of ε-caprolactone

4.7.10 *Copolymerization of ʟ-lactide and ε-caprolactone using complex 4.2 as catalyst*

The physical properties of polyesters derived homo-polymers can limit their applicability, thus require modification. One such strategy is copolymerization which results in block polymers with improved properties. Complex **4.2** was used in the co-polymerization of ε-CL and ʟ-LA and PCL-b-PLA block copolymers were obtained and characterized by NMR. The absence of a signal due to end group functionality methylene protons (HOCH$_2$-O-) at 3.65 ppm in ^{1}H-NMR spectra from the homo-polymer (Figure 4.18) showed that a block copolymer was formed. The two methylene proton signals at 4.16 and 4.06 ppm (Figure 4.21, inset) showed a CL-LA heterojunction compared to a CL-CL homojunction (4.06 ppm) (Figure 4.18 inset).
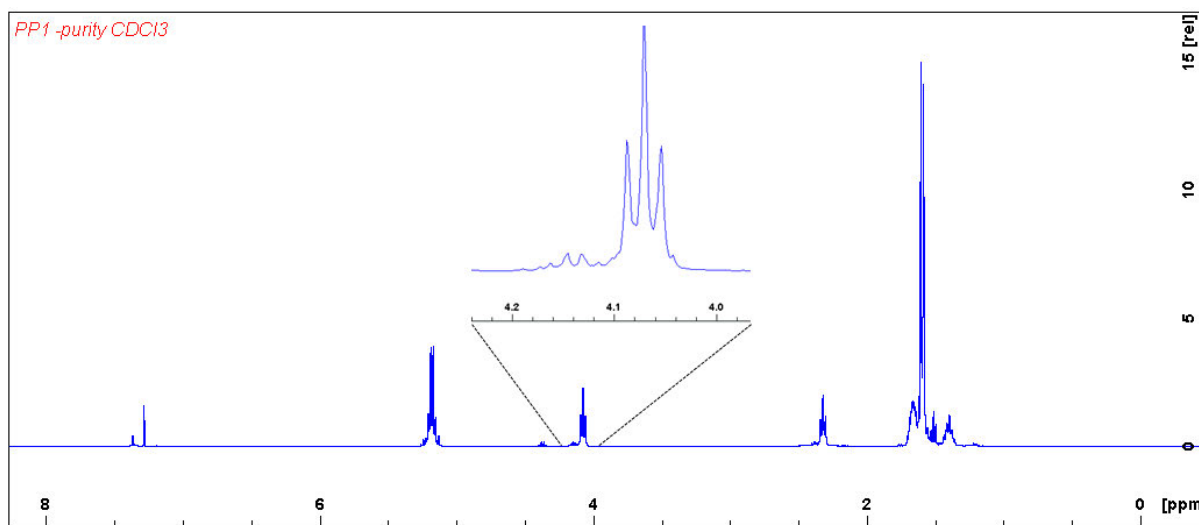
Figure 4.21: The ^{1}H NMR spectrum of PCL-b-PLA block copolymer catalysed by complex **4.2**/BnOH. Reaction conditions: [M]$_0$:[BnOH]$_0$ = 100: solvent: toluene, T = 110 °C

The PCL methylene protons in proximity to the PLA chain are slightly shifted giving two signals. This is corroborated by ^{13}C-NMR (Figure 4.22) where two carbonyl carbon signals at 169.5 and 173.6 ppm are present suggesting the sequences LLC and LCC originating from the homo-sequence LA-LA-LA and CL-CL-CL, respectively. Generally, it is more probable to form a PCL-b-PLA block copolymer than the PLA-b-PCL because the preformed PCL prepolymer is an effective co-initiator than the PLA, therefore, monomer addition sequence must be considered.
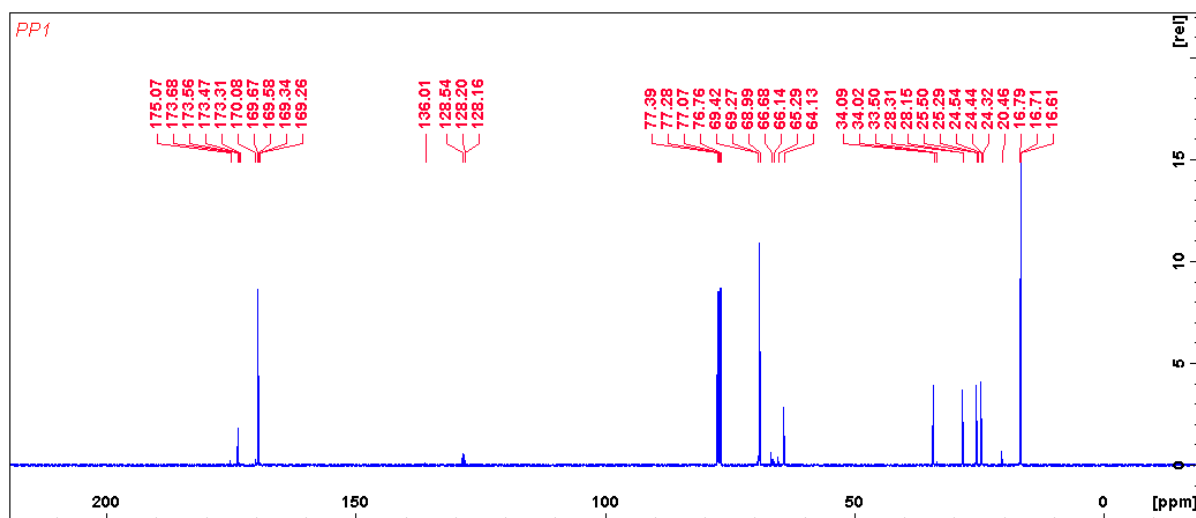
Figure 4.22: The ^{13}C NMR spectrum of PCL-b-PLA block copolymer catalyzed by **4.2**/BnOH. Reaction conditions: $[M]_0:[BnOH]_0 = 100$: solvent: toluene, T = 110 °C

4.8 Conclusion

Zn(II) and Cu(II) *N*-hydroxyformammidine complexes were effectively synthesizes and were obtained in reasonable yield (64 – 84%). All the complexes were characterized by IR and NMR spectroscopy, mass spectroscopy and elemental analysis. The molecular structures of complexes **4.7** and **4.7** were determined by single crystal X-ray diffraction analyses. In both structures, the coordination sites are occupied by imino *N*- and hydroxyl *O*-donor atoms from the chelating ligands. The geometry around the metal centre in complex **4.3** is distorted tetrahedral while in complex **4.7** is square planar. The ROP of ε-CL and L-LA catalysed by complexes **4.1 – 4.8** on their own showed longer induction periods with complex **4.2** achieving only 5% conversion within 24 h. Solution polymerization in toluene in the presence of a benzyl alcohol as co-initiator, complexes **4.1 – 4.8** proved to be active achieving monomer conversion upto 99% within 22 – 125 h. The more electrophilic Zn(II) complex were more active as compared to the Cu(II) analogues. The polymerization of ε-CL showed controllable characteristic as shown by relatively low PDIs ranging from 1.1 – 1.6 although low molecular weights less than 2909 Da were observed. The complexes exhibited low activity with complexes **4.1 – 4.4** achieving apparent rate constants (k_{app}) between 0.0386 – 0.1751 h^{-1}. Plots of $\ln([CL]_0/[CL]_t)$ vs time for complexes **4.5 – 4.8** were nonlinear showing the non-living characteristic of these systems. Symmetry coupled with steric effects seem to have an effect to the activities of the complexes. Complexes with symmetric 2,6-

substituents were more active than the unsymmetrical possessing 2-methoxy on the other phenyl ring. The substituents can also influence tacticity hence, but due lack of iso-selectivity heterotacticity is mainly observed in such systems. To improve the activity and polymer properties further studies might include dual catalytic approach where a Brønsted base is added to activate the catalyst/co-initiator[87] as well as ligand modification.

Another ligand system based on pyridyl moiety was introduced to attempt to control the ROP process and influence the molecular weights and polydispersity indices. Magnesium metal complexes were also investigated which are believed to have greater catalytic activity. The outcomes are presented in **Chapter 5**.

References

1. V. Mittal, *Renewable Polymers: Synthesis, Processing, and Technology*, John Wiley & Sons, Hoboken, NJ, 2012.

2. M. Kashif, B.-m. Yun, K.-S. Lee and Y.-W. Chang, *Mater. Lett.*, **2016**, 166, 125.

3. K. Jelonek and J. Kasperczyk, *Polimery*, **2013**, 58, 858.

4. S. Hong, K.-D. Min, B.-U. Nam and O. O. Park, *Green Chem.*, **2016**, 18, 5142.

5. N. Jürgensen, J. Zimmermann, A. J. Morfa and G. Hernandez-Sosa, *Scientific Reports*, **2016**, 6.

6. A. Kowalski, A. Duda and S. Penczek, *Macromolecules*, **2000**, 33, 689.

7. W.-L. Kong, Z.-Y. Chai and Z.-X. Wang, *Dalton Trans.*, **2014**, 43, 14470.

8. M. J. L. Tschan, J. Guo, S. K. Raman, E. Brulé, T. Roisnel, M.-N. Rager, R. Legay, G. Durieux, B. Rigaud and C. M. Thomas, *Dalton Trans.*, **2014**, 43, 4550.

9. M. J. Walton, S. J. Lancaster, J. A. Wright, M. R. J. Elsegood and C. Redshaw, *Dalton Trans.*, **2014**, 43, 18001.

10. C.-T. Chen, M.-C. Wang and T.-L. Huang, *Molecules*, **2015**, 20, 5313.

11. J. Li, Y. Deng, S. Jie and B.-G. Li, *J. Organomet. Chem.*, **2015**, 797, 76.

12. R. Petrus and P. Sobota, *Dalton Trans.*, **2013**, 42, 13838.

13. K. Devaine-Pressing, J. H. Lehr, M. E. Pratt, L. N. Dawe, A. A. Sarjeant and C. M. Kozak, *Dalton Trans.*, **2015**, 44, 12365.

14. Y. Wang, W. Zhao, D. Liu, S. Li, X. Liu, D. Cui and X. Chen, *Organometallics*, **2012**, 31, 4182.

15. P.-S. Chen, Y.-C. Liu, C.-H. Lin and B.-T. Ko, *J. Polym. Sci, Part A: Polym. Chem.*, **2010**, 48, 3564.

16. S. Range, D. F. J. Piesik and S. Harder, *Eur. J. Inorg. Chem.*, **2008**, 2008, 3442.

17. Z. Zhong, P. J. Dijkstra, C. Birg, M. Westerhausen and J. Feijen, *Macromolecules*, **2001**, 34, 3863.

18. L. Piao, Z. Dai, M. Deng, X. Chen and X. Jing, *Polymer*, **2003**, 44, 2025.

19. J. M. Colwell, E. Wentrup-Byrne, G. A. George and F. Schué, *Polym. Int.*, **2015**, 64, 654.

20. T.-L. Huang and C.-T. Chen, *Dalton Trans.*, **2013**, 42, 9255.

21. M. M. Kireenko, E. A. Kuchuk, K. V. Zaitsev, V. A. Tafeenko, Y. F. Oprunenko, A. V. Churakov, E. K. Lermontova, G. S. Zaitseva and S. S. Karlov, *Dalton Trans.*, **2015**, 44, 11963.

22. P. Sumrit, P. Chuawong, T. Nanok, T. Duangthongyou and P. Hormnirun, *Dalton Trans.*, **2016**, 45, 9250.

23. P.-H. Liu, F.-J. Chuang, C.-Y. Tu, C.-H. Hu, T.-W. Lin, Y.-T. Wang, C.-H. Lin, A. Datta and J.-H. Huang, *Dalton Trans.*, **2013**, 42, 13754.

24. Y. Zhang, A. Gao, Y. Zhang, Z. Xu and W. Yao, *Polyhedron*, **2016**, 112, 27.

25. J. Liu and H. Ma, *Dalton Trans.*, **2014**, 43, 9098.

26. C. Kan, J. Ge and H. Ma, *Dalton Trans.*, **2016**, 45, 6682.

27. D. Appavoo, B. Omondi, I. A. Guzei, J. L. van Wyk, O. Zinyemba and J. Darkwa, *Polyhedron*, **2014**, 69, 55.

28. S. H. Ahn, M. K. Chun, E. Kim, J. H. Jeong, S. Nayab and H. Lee, *Polyhedron*, 127, 51.

29. H.-W. Ou, K.-H. Lo, W.-T. Du, W.-Y. Lu, W.-J. Chuang, B.-H. Huang, H.-Y. Chen and C.-C. Lin, *Inorg. Chem.*, **2016**, 55, 1423.

30. F. M. García-Valle, R. Estivill, C. Gallegos, T. Cuenca, M. E. G. Mosquera, V. Tabernero and J. Cano, *Organometallics*, **2015**, 34, 477.

31. A. Otero, A. Lara-Sanchez, J. Fernandez-Baeza, C. Alonso-Moreno, I. Marquez-Segovia, L. F. Sanchez-Barba, J. A. Castro-Osma and A. M. Rodriguez, *Dalton Trans.*, **2011**, 40, 4687.

32. H.-M. Sun, H.-R. Li, C.-S. Yao, Y.-M. Yao, H.-T. Sheng and Q. Shen, *Chin. J. Chem.*, **2005**, 23, 1541.

33. E. M. Njogu, B. Omondi and V. O. Nyamori, *Inorg. Chim. Acta.*, **2017**, 457, 160.

34. C. Fliedel, V. Rosa, F. M. Alves, A. M. Martins, T. Aviles and S. Dagorne, *Dalton Trans.*, **2015**, 44, 12376.

35. W.-L. Kong and Z.-X. Wang, *Dalton Trans.*, **2014**, 43, 9126.

36. K. A. Gerling, N. M. Rezayee, A. L. Rheingold, D. B. Green and J. M. Fritsch, *Dalton Trans.*, **2014**, 43, 16498.

37. M. Mandal, D. Chakraborty and V. Ramkumar, *RSC Advances*, **2015**, 5, 28536.

38. A. Pilone, N. De Maio, K. Press, V. Venditto, D. Pappalardo, M. Mazzeo, C. Pellecchia, M. Kol and M. Lamberti, *Dalton Trans.*, **2015**, 44, 2157.

39. N. Nomura, R. Ishii, M. Akakura and K. Aoi, *J. Am. Chem. Soc.*, **2002**, 124, 5938.

40. M. Wisniewski, A. L. Borgne and N. Spassky, *Macromol. Chem. Phys.*, **1997**, 198, 1227.

41. N. Spassky, M. Wisniewski, C. Pluta and A. Le Borgne, *Macromol. Chem. Phys.*, **1996**, 197, 2627.

42. Bruker, ed., *APEXII*, APEXII Bruker AXS Inc, Madison, Wisconsin, USA, 2009.

43. Bruker, *SAINT*, SAINT Bruker AXS Inc, Madison, Wisconsin, USA, 2009.

44. Bruker, *SADABS*, Bruker SADABS Bruker AXS Inc, Madison,Wisconsin, USA, 2009.

45.   G. Sheldrick, *Acta Crystallogr Sect. A: Found. Crystallogr.*, **2008**, 64, 112.

46.   B. Dolomanov O. V, L. J. Gildea,R. J, HowardJ. A. K. Puschmann, H, *Appl. Crystallogr*, **2009**, 42, 339.

47.   M. L. Cole, G. B. Deacon, C. M. Forsyth, K. Konstas and P. C. Junk, *Dalton Trans.*, **2006**, 3360.

48.   M. Cibian, S. Derossi and G. S. Hanan, *Dalton Trans.*, **2011**, 40, 1038.

49.   M. Cibian, S. Langis-Barsetti, J. G. Ferreira and G. S. Hanan, *Eur. J. Inorg. Chem.*, **2016**, 2016, 177.

50.   M. Cibian, S. Langis-Barsetti, F. G. De Mendonça, S. Touaibia, S. Derossi, D. Spasyuk and G. S. Hanan, *Eur. J. Inorg. Chem.*, **2015**, 2015, 73.

51.   D. J. Hodgson, *Inorganica Chimica Acta*, **1983**, 75, 225.

52.   M. Cibian, S. Derossi and G. S. Hanan, *Acta Crystallogr. Sect. E.*, **2009**, 65, o2485.

53.   R. Murakami, T. Ishida, S. Yoshii and H. Nojiri, *Dalton Trans.*, **2013**, 42, 13968.

54.   A. Okazawa, Y. Nagaichi, T. Nogami and T. Ishida, *Inorg. Chem.*, **2008**, 47, 8859.

55.   O. Q. Munro, K. Gillham and M. P. Akerman, *Acta Crystallogr. Sect. C: Cryst. Struct. Commun.*, **2009**, 65, 317.

56.   M. Odoko, N. Tsuchida and N. Okabe, *Acta Crystallogr. Sect. E: Struct. Rep. Online*, **2006**, 62, 708.

57.   M. Gembický, P. Baran, R. Boča, H. Fuess, I. Svoboda and M. Valko, *Inorg. Chim. Acta.*, **2000**, 305, 75.

58.   J.-C. Wu, B.-H. Huang, M.-L. Hsueh, S.-L. Lai and C.-C. Lin, *Polymer*, **2005**, 46, 9784.

59.   T. S. Basu Baul, S. Kundu, A. Linden, N. Raviprakash, S. K. Manna and M. F. C. Guedes da Silva, *Dalton Transactions*, **2014**, 43, 1191.

60.   A. Okazawa, D. Hashizume and T. Ishida, *J. Am. Chem. Soc.*, **2010**, 132, 11516.

61.   H.-C. Tseng, M. Y. Chiang, W.-Y. Lu, Y.-J. Chen, C.-J. Lian, Y.-H. Chen, H.-Y. Tsai, Y.-C. Lai and H.-Y. Chen, *Dalton Trans.*, **2015**, 44, 11763.

62.   N. Buis, S. A. French, G. D. Ruggiero, B. Stengel, A. A. D. Tulloch and I. H. Williams, *J. Chem. Theory Comput.*, **2007**, 3, 146.

63.   R. F. Storey and J. W. Sherman, *Macromolecules*, **2002**, 35, 1504.

64.   T. J. J. Whitehorne and F. Schaper, *Inorg. Chem.*, **2013**, 52, 13612.

65.   E. D. Akpan, S. O. Ojwach, B. Omondi and V. O. Nyamori, *New J. Chem.*, **2016**, 40, 3499.

66.   J. A. Castro-Osma, C. Alonso-Moreno, I. Márquez-Segovia, A. Otero, A. Lara-Sánchez, J. Fernández-Baeza, A. M. Rodríguez, L. F. Sánchez-Barba and J. C. García-Martínez, *Dalton Trans.*, **2013**, 42, 9325.

67. M. Zikode, S. O. Ojwach and M. P. Akerman, *J. Mol. Catal. A: Chem.*, **2016**, 413, 24.

68. P. Dubois, C. Jacobs, R. Jerome and P. Teyssie, *Macromolecules*, **1991**, 24, 2266.

69. Y. Huang, W. Wang, C.-C. Lin, M. P. Blake, L. Clark, A. D. Schwarz and P. Mountford, *Dalton Trans.*, **2013**, 42, 9313.

70. E. D. Akpan, S. O. Ojwach, B. Omondi and V. O. Nyamori, *Polyhedron*, **2016**, 110, 63.

71. L. E. N. Allan, G. G. Briand, A. Decken, J. D. Marks, M. P. Shaver and R. G. Wareham, *J. Organomet. Chem.*, **2013**, 736, 55.

72. C.-H. Wang, C.-Y. Li, B.-H. Huang, C.-C. Lin and B.-T. Ko, *Dalton Trans.*, **2013**, 42, 10875.

73. C. Obuah, Y. Lochee, J. H. L. Jordaan, D. P. Otto, T. Nyokong and J. Darkwa, *Polyhedron*, **2015**, 90, 154.

74. Y.-C. Liu, B.-T. Ko and C.-C. Lin, *Macromolecules*, **2001**, 34, 6196.

75. M. Bero, B. Czapla, P. Dobrzyński, H. Janeczek and J. Kasperczyk, *Macromol. Chem. Phys.*, **1999**, 200, 911.

76. N. Spassky, V. Simic, M. S. Montaudo and L. G. Hubert-Pfalzgraf, *Macromol. Chem. Phys.*, **2000**, 201, 2432.

77. Y. Shen, Z. Shen, Y. Zhang and K. Yao, *Macromolecules*, **1996**, 29, 8289.

78. F. Peng and Z. Shen, *J. Appl. Polym. Sci.*, **2007**, 106, 1828.

79. M. P. F. Pepels, P. Souljé, R. Peters and R. Duchateau, *Macromolecules*, **2014**, 47, 5542.

80. A. Rai, S. Senapati, S. K. Saraf and P. Maiti, *J. Mater. Chem. B.*, **2016**, 4, 5151.

81. Z. Zhang, X. Chen, X. Gao, X. Yao, L. Chen, C. He and X. Chen, *RSC Advances*, **2015**, 5, 18593.

82. J. Liu, J. Ling, X. Li and Z. Shen, *J. Mol. Catal. A: Chem.*, **2009**, 300, 59.

83. E. E. Marlier, J. A. Macaranas, D. J. Marell, C. R. Dunbar, M. A. Johnson, Y. DePorre, M. O. Miranda, B. D. Neisen, C. J. Cramer, M. A. Hillmyer and W. B. Tolman, *ACS Catalysis*, **2016**, 6, 1215.

84. N. Ajellal, J.-F. Carpentier, C. Guillaume, S. M. Guillaume, M. Helou, V. Poirier, Y. Sarazin and A. Trifonov, *Dalton Trans.*, **2010**, 39, 8363.

85. D. Li, Y. Peng, C. Geng, K. Liu and D. Kong, *Dalton Trans.*, **2013**, 42, 11295.

86. T.-L. Yu, C.-C. Wu, C.-C. Chen, B.-H. Huang, J. Wu and C.-C. Lin, *Polymer*, **2005**, 46, 5909.

87. C. Thomas and B. Bibal, *Green Chem.*, **2014**, 16, 1687.

Chapter 5

N,O-Amino-phenolate Mg(II) and Zn(II) Schiff base complexes: Synthesis and application in ring-opening polymerization of ε-caprolactone and lactides

This chapter builds on the effect of changing the length of the spacer between the hetero-donor atoms as compared to ligand systems reported in prior chapters. The intention was to increase the size of the metallacycle so as to enhance catalytic activity. We have also introduced sulphur and oxygen five membered heterocyclic side arms to investigate the contribution of *S-* and *O*-donor atoms in comparison to the *N*-pyridyl. Magnesium metal centre was also introduced in a bid to increase the catalytic activity since it has been shown to be more active than zinc and copper. The ligand synthesis was also done in an eco-friendly way *via* solventless grinding.

Abstract

Solventless grinding of 2-aminophenol and the corresponding aldehyde furnished compounds 2-(pyridin-2-ylmethylene)aminophenol (**L5.1**), 2-(pyridin-4-ylmethylene)aminophenol (**L5.2**), 2-(thiophen-2-ylmethylene)aminophenol (**L5.3**) and 2-(furan-2-ylmethylene)aminophenol (**L5.4**), in excellent yields of 97 – 99%. Reaction of ligands **L5.1** – **L5.4** with zinc or magnesium alkyl solutions produced complexes [Mg(**L5.1**)$_2$] (**5.1**), [Mg(**L5.2**)$_2$] (**5.2**), [Mg(**L5.3**)$_2$] (**5.3**) and [Mg(**L5.4**)$_2$] (**5.4**) or [Zn(**L5.1**)$_2$] (**5.5**), [Zn(**L5.2**)$_2$] (**5.6**), [Zn(**L5.3**)$_2$] (**5.7**) and [Zn(**L5.4**)$_2$] (**5.8**). The complexes were characterized by ^{1}H-NMR, ^{13}C-NMR and IR spectroscopies, elemental analysis and mass spectrometry. Complexes **5.1** was further analysed by single-crystal X-ray crystallography. The complexes were investigated as catalysts/initiators in the ring-opening polymerization (ROP) of ε-caprolactone (ε-CL), L-lactide (L-LA) and *rac*-lactide (*rac*-LA). Mg(II) complexes **5.1** – **5.4** (k_{app} = 0.12 – 0.58 h^{-1}) were more efficient catalyst as compared to the Zn(II) complexes **5.5** – **5.8** (k_{app} = 0.04 – 0.24 h^{-1}). The catalytic activity was enhanced by adding of alcohol co-initiators. Comprehensive kinetic and mechanistic investigations revealed that the polymerization reaction follows *pseudo*-first-order kinetics. Moderate molecular weights increased from 1234 to 4567 g mol^{-1} with an increase in catalyst concentration with polydispersity (PDIs) ranging from 1.4 to 2.0. The enthalpy ΔH_p were found to be 23.5 and 63.9 kJ mol^{-1} while the entropy of activation (ΔS_p) values were -157 and -33 JK^{-1} mol^{-1} for ε-CL and L-LA monomers, respectively.

5.1 Introduction

The continuous use of non-degradable polyolefin-based products which have negative environmental impact is becoming a major concern. To resolve the potential environmental threat biodegradable polymers are gaining popularity and are foreshadowed as alternative replacements.[1] Among them polycaprolactone (PCL) and polylactides (PLA) have been successfully used in packaging and construction of biomedical devices, such as, tissue and bone engineering scaffolds,[2,3] surgical sutures,[4,5] and drug delivery systems.[6-8] Polyesters are produced *via* ring-opening polymerization (ROP) process using metal-based catalyst.[9-11]   Notwithstanding the dynamic research efforts dedicated to this field, there are still some challenges. For instance, in the case of lactides, a limited number of catalytic systems are capable of stereoselective polymerization. In addition, there is lack of control of the polymerization process due to side reactions which results in low molecular weights (M_w) with broad molecular weight distributions.

Recently, benign metal complexes such as zinc,[12-14] magnesium,[10,15,16] calcium,[17-19] alkali earth metals,[17,20] iron[21-24] and copper[25-27] have been a subject of many research articles. Above and beyond the choice of the catalytic metal-centre, the catalytic outcome can be influence by manipulating the ancillary ligands structural and electronic properties.

Many *N,N′*-bis-ligating ligands, such β-diketiminate,[28,29] pyrrolyl[30,31] pyrazoly[32] amidines[33] and guanidines[34] have been employed to stabilize metal complexes used as catalyst in ROP. This work involves the synthesis of *N,O*-Schiff base type ligands and corresponding Mg(II) and Zn(II) complexes.   It is envisioned that, the side pendant arms of pyridyl, furyl and thiophenyl heterocycles will present some interesting properties in coordination and catalytic activity. The lone pairs of *O* and *S* hetero atoms are part of the aromatic π-system, hence not freely accessible for coordination. The anticipated metal to *O/S* interactions should thus sufficiently stabilize the catalyst *via* coordination on the unoccupied site but appreciably labile to be dislodged by the incoming coordinating monomer.

5.2 Experimental

5.2.1 Materials

All experiments were carried out under argon, 5.0 technical grade, (Airflex Industrial Gases, South Africa) using Schlenk techniques. All the solvents were obtained from Sigma-Aldrich and this include trahydrofuran (THF) 98%, dichloromethane (DCM) (99%) and hexane (98%) were dried from a sodium-benzophenone mixture. 2-Thiophenecarboxaldehyde (98%), 2-furaldehyde (98%), 2-aminophenol (99%), benzyl alcohol (BnOH), *tert*-butanol (^{t}BuOH), *iso*-propyl alcohol (^{i}PrOH), Di-*n*-butylmagnesium (Mg(n-Bu)$_2$) solution 1.0 M in heptane, diethylzinc (ZnEt$_2$) solution 1.0 M in hexanes, ε-caprolactone (ε-CL) (97%), L-lactide (L-LA) (98 %) and *rac*-lactide (*rac*-LA)(98%) were also obtained from Sigma-Aldrich.

5.2.2 Instrumentation

^{1}H- and ^{13}C-NMR spectra were measured at room temperature using a Bruker 400 MHz spectrometer. ^{1}H-NMR data were recorded in DMSO-d$_6$; chemical shifts were calibrated to the residual solvent signal of DMSO-d$_6$ (δ 2.5). Similarly, ^{13}C-NMR data were recorded in DMSO-d$_6$ and referenced to the residual solvent signal at δ 40.00. IR spectra were obtained on a PerkinElmer Universal ATR spectrum 100 FT-IR spectrometer. Mass spectra of compounds were obtained from a Water synapt GR electrospray positive spectrometer.

5.3 General synthetic methods

5.3.1 Synthesis of Schiff base ligands

All ligands were synthesised using a solventless grinding method. The aniline, 2-aminophenol (1 mmol), together with corresponding carboxaldehyde (1 mmol) were added to a Pyrex tube fitted with a ground joint. Thereafter the mixtures ware ground for 10 – 15 min resulting in solid crude products. The solids were dried in *vacuo* to completely remove the water, furnishing 2-((pyridin-2-ylmethylene)amino)phenol (**L5.1**) (99%), 2-((pyridin-4-ylmethylene)amino)phenol (**L5.2**) (99%), 2-((thiophen-2-ylmethylene)amino)phenol (**L5.3**) (97%), 2-((furan-2-ylmethylene)amino)phenol, (**L5.4**) (98%) in excellent yields (Scheme 5.1).
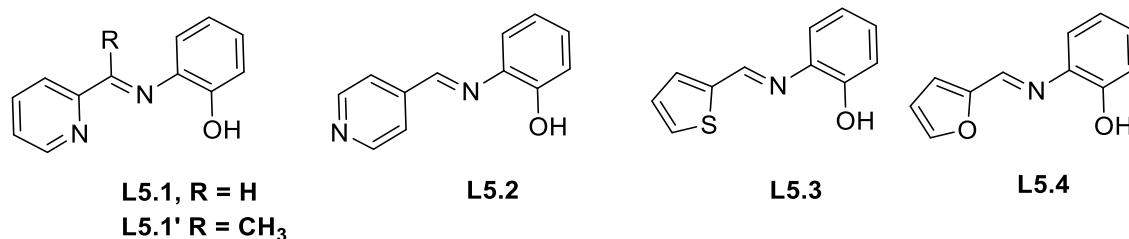
Scheme 5.1: Schiff base ligands used therein

5.3.2 Synthesis of Zn(II) and Mg(II) complexes

All manipulations were carried out under Schlenk conditions. The appropriated ligands (2 mmol equivalent) was dissolved in dry THF. There after the corresponding metal alky solution (1 mol equivalent) was added drop wise at 0 °C and the solution stirred for 4 h at room temperature. The solvent was removed in *vacuo* to furnish complexes **5.1 – 5.8** as solids (Yield 60 - 67%).

5.3.2.1 *[Mg(L5.1)₂] (5.1)*

Reaction of ligand **L5.1** (2 mmol) and Mg(n-Bu)$_2$ (1 mmol) gave complex **5.1** as a pure red powder after workup. Yield 65%. Decompose 253 °C. ^{1}H-NMR (DMSO-d$_6$, 400 MHz): δ (ppm) 7.31 (t, $^3J_{HH}$ = 7.60, 2H, Ar), 7.50 (m, 2H, Ar), 7.56 (d, $^3J_{HH}$ = 7.58, 1H, Ar), 7.75 (d, $^3J_{HH}$ = 2.79, 2, H, Ar), 7.76 (s, 2H, Ar), 7.92 (t, $^3J_{HH}$ = 7.78, 1H, Ar), 9.03 (s, HC=N). ^{13}C-NMR (DMSO-d$_6$, 400 MHz): δ (ppm) 161.1, 157.1, 147.2, 148.10, 147.3, 128.1, 126.9, 123.90, 123.0, 120.5, 111.1. IR: v (cm^{-1}) 1656 v(C=N) stretching. ESI-TOF MS: m/z (%); obtained [M+Na]$^+$ 441.1194, calculated 441.7216. Anal. calcd for C$_{24}$H$_{18}$N$_4$O$_2$Mg: C, 68.84; H, 4.33; N, 13.38. Found: C, 68.99, H, 4.11, N, 13.56.

5.3.2.2 *[Mg(L5.2)₂] (5.2)*

Reaction of ligand **L5.2** (2 mmol) and Mg(n-Bu)$_2$ (1 mmol) gave complex **5.2** as a pure red solid after workup. Yield 60%. Decompose 263 °C. ^{1}H-NMR (DMSO-d$_6$, 400 MHz): δ (ppm) 6.58 (t, $^3J_{HH}$ = 7.54, 1H, Ar), 7.10 (t, $^3J_{HH}$ = 7.79, 1H, Ar), 7.50 (d, $^3J_{HH}$ = 8.0, 1H, Ar), 8.6 (s, 1H, s, HC=N), 7.89 (d, $^3J_{HH}$ = 5.6, 1H, Ar). ^{13}C-NMR (DMSO-d$_6$, 400 MHz): δ (ppm) 163.1, 157.1, 150.9, 149.40, 147.3, 128.1, 127.3, 123.90, 123.0, 120.5, 111.1. IR: v (cm^{-1}) 1632 v(C=N) stretching. ESI-TOF MS: m/z (%); obtained [M+Na]$^+$ 442.1612, calculated 442.1234. Anal. calcd for C$_{24}$H$_{18}$N$_4$O$_2$Mg: C, 68.84; H, 4.33; N, 13.38. Found: 68.56; H 4.66; N 13.53.

5.3.2.3 [Mg(L5.3)₂] (5.3)

Reaction of ligand **L5.3** (2 mmol) and Mg(n-Bu)₂ (1 mmol) gave complex **5.3** as a pure red powder after workup. Yield 62%. Decompose 251 °C. ^{1}H-NMR (DMSO-d₆, 400 MHz): δ (ppm) 6.69 (dd, $^3J_{HH}$ = 4.06, 1H, Ar), 6.82 (dd, $^3J_{HH}$ = 2.89,1H, Ar), 6.88 (dd, $^3J_{HH}$ = 2.88, 1H, Ar), 7.04 (dd, $^3J_{HH}$ = 4.11, 1H, Thiop), 7.12 (dd, $^3J_{HH}$ = 4.40, 1H, Thiop), 7.17 (d, $^3J_{HH}$ = 5.52, 1H, Thiop), 7.90 (d, 1H, Ar), 8.47 (s, HC=N). ^{13}C-NMR (DMSO-d₆, 400 MHz): δ (ppm) 163.1, 158.1, 147.9, 148.40, 147.3, 128.1, 126.3, 123.30, 123.0, 121.5, 115.1. IR: v (cm^{-1}) 1598 v(C=N) stretching. ESI-TOF MS: m/z (%); obtained [M+Na]$^+$ 451.2390, calculated 451.7923, Anal. calcd for C₂₂H₁₆N₂O₂S₂Mg: C, 61.62; H, 3.76; N, 6.53 Found: C, 61.60, H, 3.52, N, 6.96.

5.3.2.4 [Mg(L5.4)₂] (5.4)

Reaction of ligand **L5.4** (2 mmol) and Mg(n-Bu)₂ (1 mmol) gave complex **5.4** as a pure red solid after workup. Yield 60%. Decompose 256 °C. ^{1}H-NMR (DMSO-d₆, 400 MHz): δ (ppm) 6.81 (td, $^3J_{HH}$ = 4.10, 1H, Fur), 6.89 (dd, $^3J_{HH}$ = 3.01, 1H, Ar), 7.04 (td, $^3J_{HH}$ = 2.88, 1H, Fur), 7.10 (dd, $^3J_{HH}$ = 4.22, 1H, Ar), 7.20 (dd, $^3J_{HH}$ = 3.08, 1H, Ar), 7.67 (dd, $^3J_{HH}$ = 3.46, 1H, Fur), 7.79 (dd, 1H, Ar), 8.87 (s, HC=N). ^{13}C-NMR (DMSO-d₆, 400 MHz): δ (ppm) 163.1, 158.1, 147.9, 148.40, 147.3, 128.1, 126.3, 123.30, 123.0, 121.5, 115.1. IR: v (cm^{-1}) 1614 v(C=N) stretching. ESI-TOF MS: m/z (%); obtained [M+Na]$^+$ 419.2719, calculated 419.6634, Anal. calcd for C₂₂H₁₆N₂O₄Mg: C, 66.61; H, 4.07; N, 7.06. Found: C, 66.75, H, 3.94, N, 6.98.

5.3.2.5 [Zn(L5.1)₂] (5.5)

Reaction of ligand **L5.1** (2 mmol) and ZnEt₂ (1 mmol) gave complex **5.5** as a pure red solid after workup. Yield 67%. Decompose 254 °C. ^{1}H-NMR (DMSO-d₆, 400 MHz): δ (ppm) 7.31 (t, $^3J_{HH}$ = 7.60, 2H, Ar), 7.50 (m, 2H, Ar), 7.56 (d, $^3J_{HH}$ = 7.58, 1H, Ar), 7.75 (d, $^3J_{HH}$ = 2.79, 2, H, Ar), 7.76 (s, 2H, Ar), 7.92 (t, $^3J_{HH}$ = 7.78, 1H, Ar), 9.03 (s, HC=N) 123.90, 123.0, 120.5, 111.1. IR: v (cm^{-1}) 1633 v(C=N) stretching. ESI-TOF MS: m/z (%); obtained: [M+Na$^+$] 480.0329, calculated: 480.0612, Anal. calcd for C₂₄H₁₈N₄O₂Zn: C, 62.69; H, 3.95; N, 12.18. Found: C, 63.48, H, 4.08, N, 12.36.

5.3.2.6 [Zn(L5.2)₂] (5.6)

Reaction of ligand **L5.2** (2 mmol) and ZnEt₂ (1 mmol) gave complex **5.6** as a pure red powder after workup. Yield 64%. Decompose 263 °C. ^{1}H-NMR (DMSO-d₆, 400 MHz): δ (ppm) 6.58 (t, $^3J_{HH}$ = 7.54, 1H, Ar), 7.10 (t, $^3J_{HH}$ = 7.79, 1H, Ar), 7.50 (d, $^3J_{HH}$ = 8.0, 1H, Ar), 8.6 (s, 1H, s, HC=N), 7.89 (d, $^3J_{HH}$ = 5.6, 1H, Ar) ^{13}C-NMR (DMSO-d₆, 400 MHz): δ (ppm) 162.1, 157.1, 147.9, 148.40, 147.3, 128.1, 127.3, 123.90, 123.0, 120.5, 111.1. IR: v (cm^{-1}) 1633 v(C=N) stretching. ESI-TOF MS: m/z (%); obtained: [M+Na]⁺ 480.1623, calculated: 481.0123. Anal. calcd for C₂₄H₁₈N₄O₂Zn: C, 62.69; H, 3.95; N, 12.18. Found: C; 63.02. H; 4.15 N, 12.40

5.3.2.7 [Zn(L5.3)₂] (5.7)

Reaction of ligand **L5.3** (2 mmol) and ZnEt₂ (1 mmol) gave complex **5.7** as a pure yellow solid after workup. Yield 65%. Decompose 253 °C. ^{1}H-NMR (DMSO-d₆, 400 MHz): δ (ppm) 6.69 (dd, $^3J_{HH}$ = 4.06, 1H, Ar), 6.82 (dd, $^3J_{HH}$ = 2.89, 1H, Ar), 6.88 (dd, , $^3J_{HH}$ = 2.88, 1H, Ar), 7.04 (dd, $^3J_{HH}$ = 4.11, 1H, Thiop), 7.12 (dd, , $^3J_{HH}$ = 4.40, 1H, Thiop), 7.17 (d, 1H, Thiop), 7.90 (d, 1H, Ar), 8.48 (s, HC=N). ^{13}C-NMR (DMSO-d₆, 400 MHz): δ (ppm) 163.1, 158.1, 147.9, 148.40, 147.3, 128.1, 126.3, 123.30, 123.0, 121.5, 115.1. IR: v (cm^{-1}) 1598 v(C=N) stretching. obtained: ESI-TOF MS: m/z (%); [M+Na]⁺ 480.1267, calculated: 481.0123. Anal. calcd for C₂₂H₁₆N₂O₄Zn: C, 56.24; H, 3.43; N, 5.96. Found: C, 56.45, H, 3.59, N, 6.04.

5.3.2.8 [Zn(L5.4)₂] (5.8)

Reaction of ligand **L5.4** (2 mmol) and ZnEt₂ (1 mmol) gave complex **5.8** as brown powder after workup. Yield 60%. Decompose 250 °C. ^{1}H-NMR (DMSO-d₆, 400 MHz): δ (ppm) 6.81 (td, $^3J_{HH}$ = 4.10, 1H, Fur), 6.89 (dd, $^3J_{HH}$ = 3.01, 1H, Ar), 7.04 (td, td, $^3J_{HH}$ = 2.88, 1H, Fur), 7.10 (dd, , $^3J_{HH}$ = 4.22, 1H, Ar), 7.20 (dd, , $^3J_{HH}$ = 3.08, 1H, Ar), 7.67 (dd, (dd, $^3J_{HH}$ = 3.46, 1H, Fur, 1H, Fur), 7.79 (dd, 1H, Ar), 8.87 (s, HC=N). ^{13}C-NMR (DMSO-d₆, 400 MHz): δ (ppm) 163.1, 158.1, 147.9, 148.40, 147.3, 128.1, 126.3, 123.30, 123.0, 121.5, 115.1. IR: v (cm^{-1}) 1592 v(C=N) stretching. ESI-TOF MS: m/z (%): obtained: [M+Na]⁺ 459.2567, calculated 459.0324. Anal. calcd for C₂₂H₁₆N₂O₄Zn: C, 60.36; H, 3.68; N, 6.40. Found: C, 60.65, H, 3.66, N, 6.78.

5.4 Polymerization of ε-caprolactone and lactides

All manipulations were performed under an inert atmosphere (argon) using Schlenk techniques. The required amount of monomer ε-CL (bulk) and LA (in 3 ml toluene or THF) was added to a Schlenk tube and immersed in a preheated oil bath at 110 °C. The polymerization reaction was initiated by adding the required amount of the complex. To study the effect of benzyl alcohol, isopropyl alcohol and t-butanol co-initiators a catalyst-to-mole ratio between 1 and 10 was used. Samples for kinetic experiments were withdrawn at regular intervals and quenched quickly by dissolving in cooled $CDCl_3$ in an NMR tube. The quenched samples were then analysed by ^{1}H-NMR spectroscopy to determine the extent of polymerization. For PCL, the percentage conversion was obtained by considering the signal intensities of ε-CL monomer protons at 4.2 ppm ($I_{4.2}$) and OCH_2 at 4.0 ppm ($I_{4.0}$) then evaluated using equation (**5.1**).

$$\frac{[Polymer]._t}{[Monomer]_0} \times 100 = \frac{I_{4.0}}{(I_{4.2} + I_{4.0})} \times 100 \qquad (5.1)$$

For PLA, the integration values of the methine proton of the monomer and that of the polymer were used to calculate the percentage conversion using the equation (**5.2**).

$$\frac{[Polymer]_t}{[Monomer]_0} \times 100 = \frac{I_{CH\ monomer}}{(I_{CH\ monomer} + I_{CH\ polymer})} \times 100 \qquad (5.2)$$

The observed rate constants were extracted from the slope of the line of best fit from the plot of $\ln([M]_0/[M]_t)$ *vs t*.

5.5 Polymer characterization by size exclusion chromatography (SEC)

Molecular weights and polydispersity indices were determined by size exclusion chromatography (SEC) at Stellenbosch University. The samples were dissolved in tetrahydrofuran (THF) stabilized with butylated hydroxytoluene (BHT) giving a sample with a concentration of 2 mg ml^{-1}. Sample solutions were filtered *via* a syringe through 0.45 mm nylon filters before being subjected to analysis. The SEC instrument consists of a Waters 1515 isocratic. HPLC pump, a Waters 717plus auto-sampler, a Waters 600E Paper system controller (run by Breeze Version 3.30 SPA) and a Waters in-line Degasser AF. A Waters 2414 differential refractometer was used at 30 °C, in series along with a Waters 2487 dual wavelength absorbance UV/Vis detector operating at variable wavelengths. THF (HPLC grade stabilized with 0.125% BHT) was used as the eluent at flow rates of 1 ml min^{-1}.

The temperature of the column oven was kept at 30 °C and the injection volume was 100 ml. Two PLgel (Polymer Laboratories) 5 mm Mixed-C (300 x 7.5 mm) columns and a pre-column (PLgel 5 mm Guard, 50 x 7.5 mm) were used. Calibration was done using narrow polystyrene standards ranging from 580 to 2 x 10^6 g mol^{-1}. All molecular weights were reported as polystyrene equivalents.

5.6 Single-crystal X-ray diffraction

Crystal evaluation and data collection was done on a Bruker Smart APEXII diffractometer with Mo Kα radiation (I = 0.71073 Å) equipped with an Oxford Cryostream low temperature apparatus operating at 100 K for all samples. Reflections were collected at different starting angles and the *APEX*II program suite was used to index the reflections.[35] Data reduction was performed using the *SAINT*[36] software and the scaling and absorption corrections were applied using the *SADABS*[37] multi-scan technique. The structures were solved by the direct method using the *SHELXS* program and refined using *SHELXL* program.[38] Graphics of the crystal structures were drawn using *OLEX*^{2} software.[39] Non-hydrogen atoms were first refined isotropically and then by anisotropic refinement with the full-matrix least squares method based on F^2 using *SHELXL*.[38] The crystallographic data and structure refinement parameters for the complexes **5.1** and **5.5** is given in Table 5.1.

Table 5.1: The summary of X-ray crystal data collection and structure refinement parameters for complexes **5.1** and **5.5**

Parameter	5.1	5.5
Empirical formula	$C_{24}H_{22}MgN_4O_2$	$C_{24}H_{18}N_4O_2Zn$
Formula weight	446.76	459.79
T(K)	296(2)	296(2)
λ(Å)	0.71073	0.71073
Crystal system	Monoclinic	Orthorhombic
Space group	*C2/c*	*P2/1*
a (Å)	23.136(2)	8.5977(3)
b (Å)	11.2849(9)	10.4811(3)
c (Å)	16.6718(13)	22.3983(7)
a, β, γ (°)	90, 103.239(5), 90	90, 90. 90
V (Å^3)	4237.1(6)	4
Z	1.513	8
ρ_{calc} (mg/m^3)	1.401	1.247
μ (mm^{-1})	0.122	0.122

F(000)	1872	944
Crystal size (mm)	0.196 x 0.193 x 0.122	0.246 x 0.218 x 0.202
θ range for data collection (°)	2.019 to 25.622	1.818 to 28.349
Index ranges	$-28 \leq h \leq 24$	$-10 \leq h \leq 11$
	$-12 \leq k \leq 13$	$-13 \leq k \leq 13$
	$-17 \leq l \leq 19$	$-29 \leq l \leq 23$
Reflections collected	22606	36209
Independent reflections	3545 [$R_{(int)}$ = 0.0603]	4781 [R(int) = 0.0560]
Completeness to (θ) = 25.24° (%)	91.9	99.4
Data/restraints/parameters	3545/6/306	4781/0/281
Goodness-of-fit (GOF) on F^2	1.042	1.119
Final R indices [$I > 2\sigma(I)$]	R_1 = 0.0463, wR_2 = 0.0940	R_1 = 0.0608, wR_2 = 0.1711
R indices (all data)	R_1 = 0.0754, wR_2 = 0.1029	R_1 = 0.0723, wR_2 = 0.1753
Largest diff. peak and hole (e Å^{-3})	0.219 and -0.451	2.017 and -0.630

5.7 Results and discussion

5.7.1 Synthesis of Schiff base ligands and their corresponding Zn(II) and Mg(II) complexes

The Schiff base ligands were designed to possess pyridyl, thiophenyl and furyl heterocycle rings side arms and the position of the pyridyl nitrogen was also varied. The Schiff base ligands, **L5.1 - L5.4**, were synthesised by solventfree mechanochemical grinding of 2-aminophenol with the corresponding aldehydes for 15 min (see Scheme 5.2). Reaction progression was monitored using FT-IR until there was complete disappearance of the aniline N—H and aldehyde carbonyl C=O signals. The development of the C=N stretching band signified the formation of the ligands. The ligands were obtained in excellent yields ranging between 97 - 99% and were characterised by elemental analysis, IR spectroscopy, NMR spectroscopy and mass spectrometry. The spectroscopic data matched those reported in literature.[40]

133
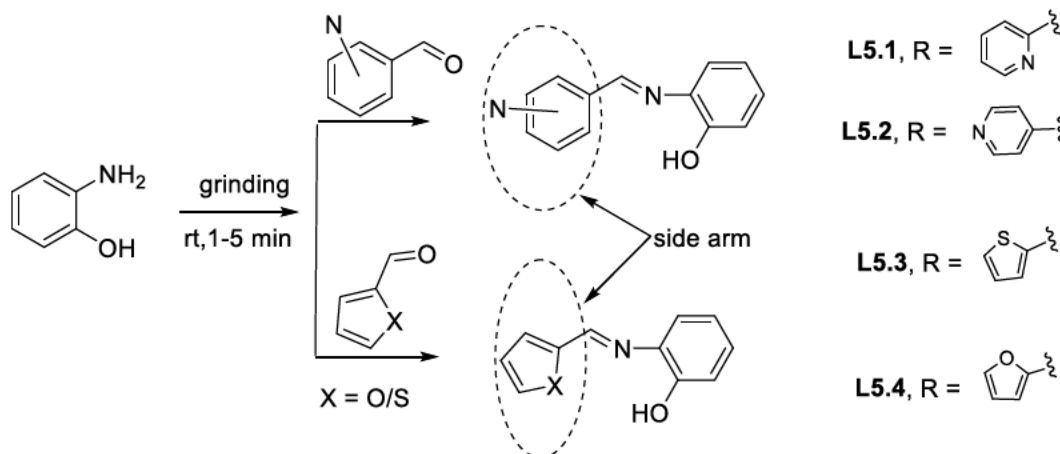
Scheme 5.2: Synthesis of Schiff base ligands **L5.1 – L5.4**

The synthesised ligands were reacted with appropriate metal alkyl solution in a 2:1 molar ratio to furnish a series of Mg(II) complexes, **5.1 – 5.2** and Zn(II) complexes **5.5 – 5.6** (Scheme 5.3). The complexes were obtained as red solids with yields between 60 – 67%. The imine bond is susceptible to hydrolysis which might have resulted in low yields. All complexes decomposed above 250 °C contrast to pure ligands which melt between 110 – 135 °C.

M = Mg; **5.1 - 5.4**
M = Zn; **5.5 - 5.8**
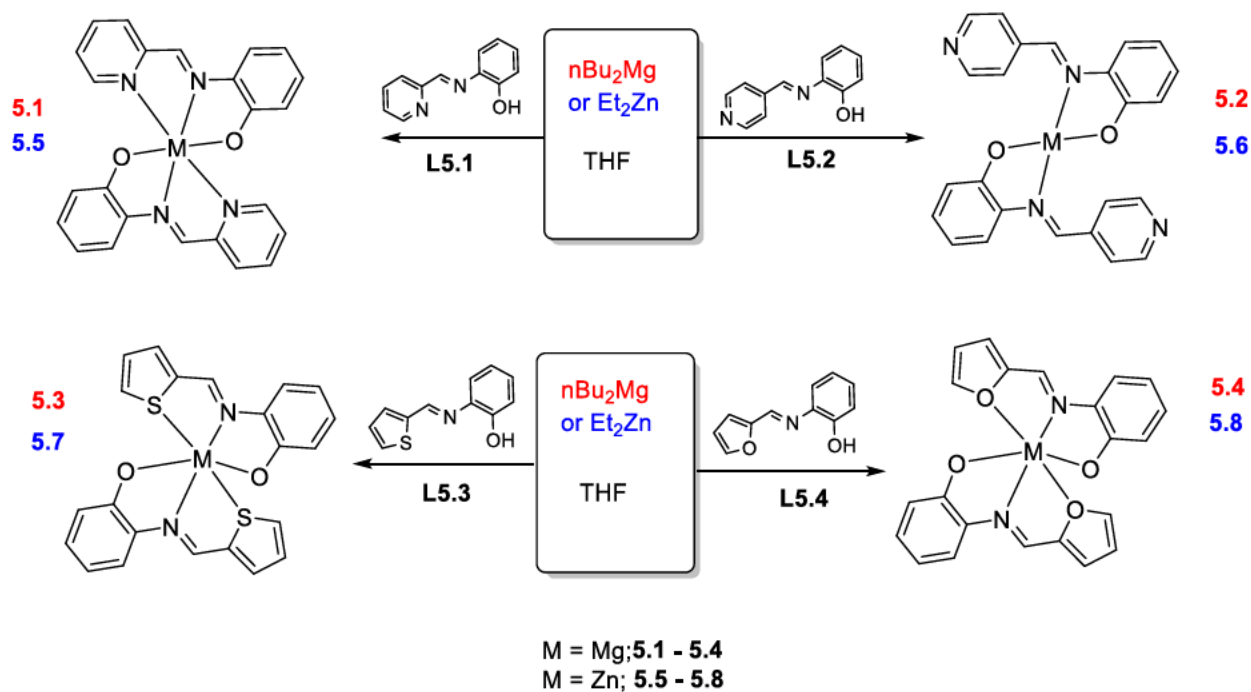
Scheme 5.3: Synthesis of Mg(II) and Zn(II) Schiff base complexes

5.7.2 *Spectroscopic analysis*

The metal to ligand ratio was affirmed by elemental and mass spectrometry to be ML_2 (M = metal). For example, the Mg(II) complex **5.1** gave a *m/z* peak at 441.1 which matched the molecular formula Mg(**L5.1**)$_2$. Matching the molecular peaks for complexes 5.2 – 5.8 were also obtained (see appendix C). The elemental analysis data was consistent with metal to ligand ration of 1:2.
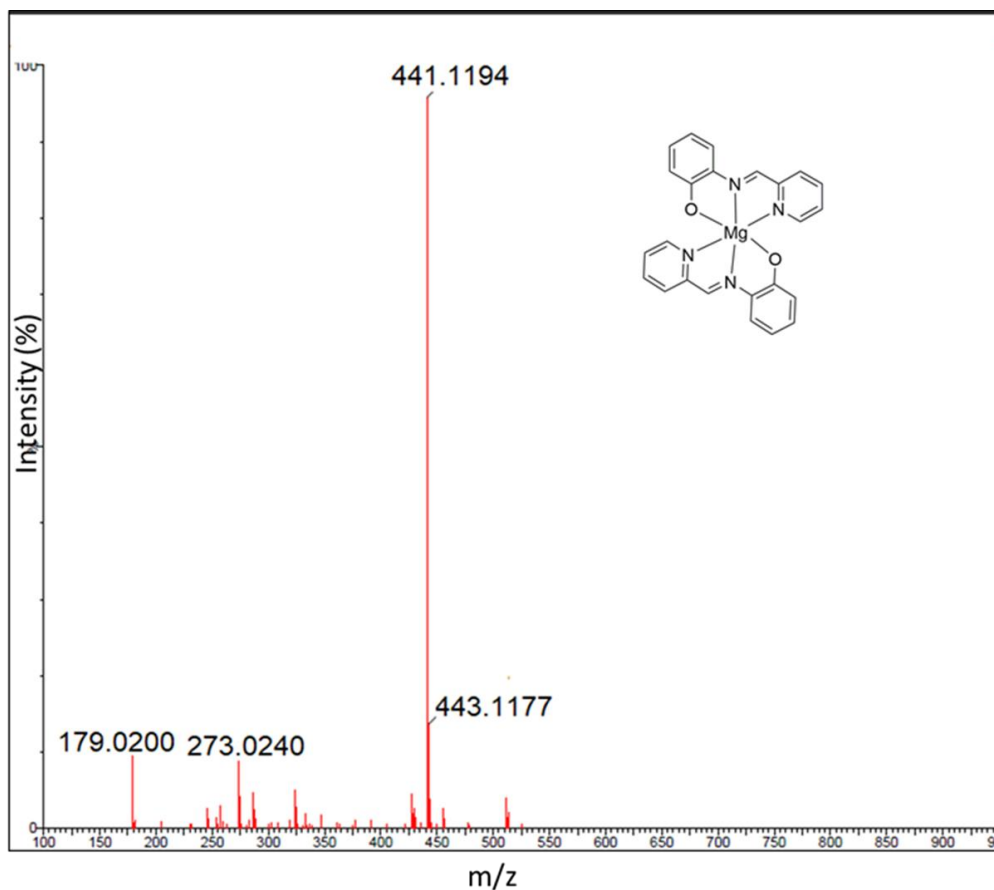
Figure 5.1: ESI-MS spectrum for complex **5.1**

The complexes were further analysed using FT-IR spectroscopy. The proton chemical shifts and stretching bands are comparable to those of the corresponding ligands. The selected analytical assignment shifts, and bands are listed in Table 5.2. The strong stretching bands characteristic of a C=N bond which lie between 1585 - 1630 cm^{-1} in free ligands experience a red shift of 3 – 35 cm^{-1} in complexes **5.1** to **5.8**. This is primarily attributed to the reduction in the π- character of the C=N bond due to coordination of the imine nitrogen. The presence of M—N stretching frequency ranging from 430 to 450 cm^{-1} also further support the formation of the complexes.

Table 5.2: IR azomethine C=N symmetry stretch frequency and azomethine proton (HN=N) shift for ligands and complexes

Complex	IR υ(C=N) cm^{-1}			NMR σ(N=C**H**) ppm		
	Ligand	Complex	$\Delta\upsilon$	Ligand	Complex	$\Delta\sigma$
5.1	1630	1656	26	8.51	9.03	0.52
5.2	1614	1632	18	8.32	9.15	0.83
5.3	1590	1598	8	8.22	8.47	0.25
5.4	1585	1614	29	8.24	8.87	0.63
5.5	1598	1633	35	8.52	9.04	0.52
5.6	1615	1633	18	8.32	9.15	0.83
5.7	1594	1598	4	8.22	8.48	0.26
5.8	1589	1592	3	8.24	8.87	0.63

The ^{1}H- and ^{13}C-NMR spectra were recorded in DMSO-d$_6$ at room temperature. The proton signals in the spectra are in conformity with the formation of the metal complexes. The ^{1}H-NMR spectra for complexes **5.1** – **5.8**, showed that the azomethine protons were shifted downfield because of the strain of the imine bridge induced by the coordinating metal. For example, typical ^{1}H- and ^{13}C-NMR spectra for complex **5.1** are shown in Figure 5.2 and 5.3. A signal shift difference of 0.52 ppm of the azomethine proton was observed in complex **5.1** with respect to **L5.1**. The proton shifts for other complexes are listed in Table 5.2. The α-protons with respect to the N$_{pyr}$ are shifted downfield in comparison to free ligands. This is because the protons are deshielded by the coordinated metal. On the other hand, α-protons in the 5-membered heterocycles are not significantly affected suggesting that *O* and *S* atoms are weakly coordinating. The ^{13}C-NMR spectra also showed a shift of the azomethine carbon due to the polarization effect of the metal ion. The ^{1}H- and ^{13}C-NMR spectra for complexes are given in appendix C.
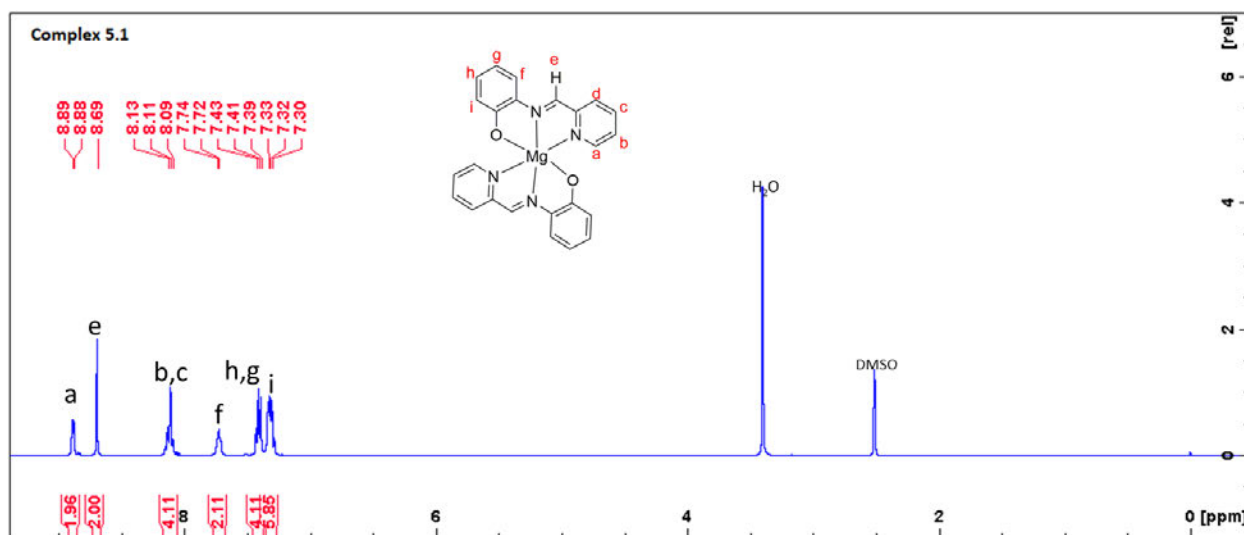
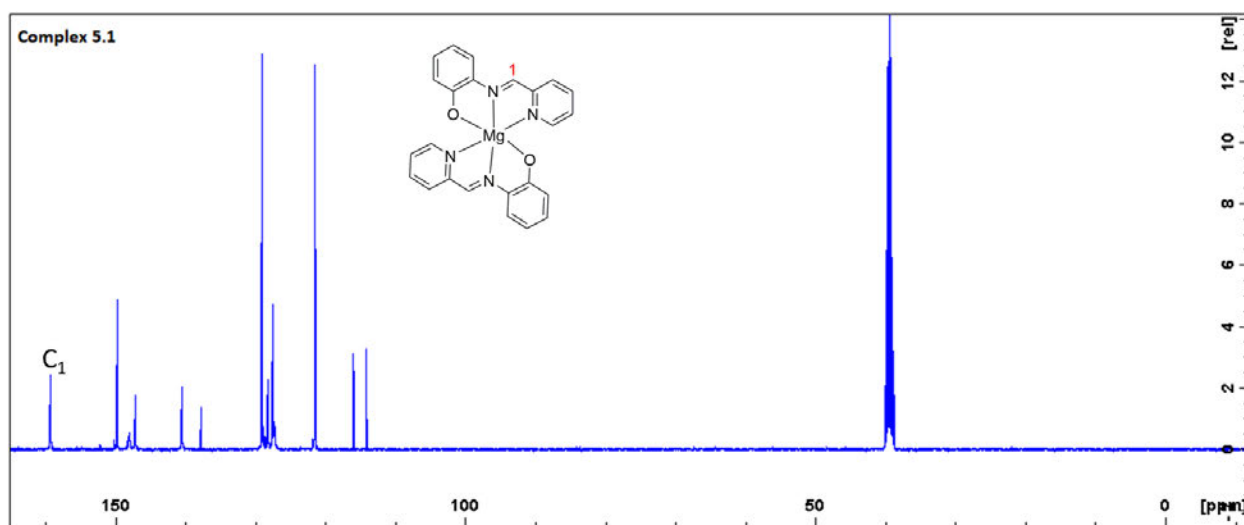**Figure 5.2**: H^1-NMR spectrum of complex **5.1** at room temperature in DMSO-d$_6$ (400 MHz)

Figure 5.3: ^{13}C-NMR spectrum of complex **5.1** at room temperature in DMSO-d$_6$ (400 MHz)

5.7.3   Molecular structures of complexes

Crystals for complexes **5.1** and **5.5** were obtained by slow evaporation of ethanol complex solutions. The molecular structures are shown in Figure 5.4 while selected bond distances and angles are listed in Table 5.3. Complex **5.5** exhibits the same geometry as **5.1** and is reported in literature.[41] Herein, it is presented to show the coordination and it will not be discussed in detail. The asymmetric unit of complex **5.1** contains one magnesium complex molecule and two water molecules which form hydrogen bonds with the ligand oxygen atoms. The Mg(II) centre assumes a distorted octahedral geometry built by two oxygen and four nitrogen atoms from the two tris-chelate ligands. The equatorial positions are occupied by *NNO* atoms of first ligand the N_{imine} of the second ligand while axial positions are occupied by N_{py} and *O* of the second ligand. The distortion from octahedral geometry is shown by the bite angles which range between 89.92 - 95.23°. The MgN$_2$O chelates rings are almost perpendicular with a dihedral angle of 5.0°. The average distance of Mg—N_{py} (2.280 Å) is greater than of Mg—N_{imine} (2.149 Å, a trend which is exhibited in related Mg(II) complexes.[42,43] This variation shows that the bonding tenacity of imine nitrogen is stronger than the pyridine nitrogen.
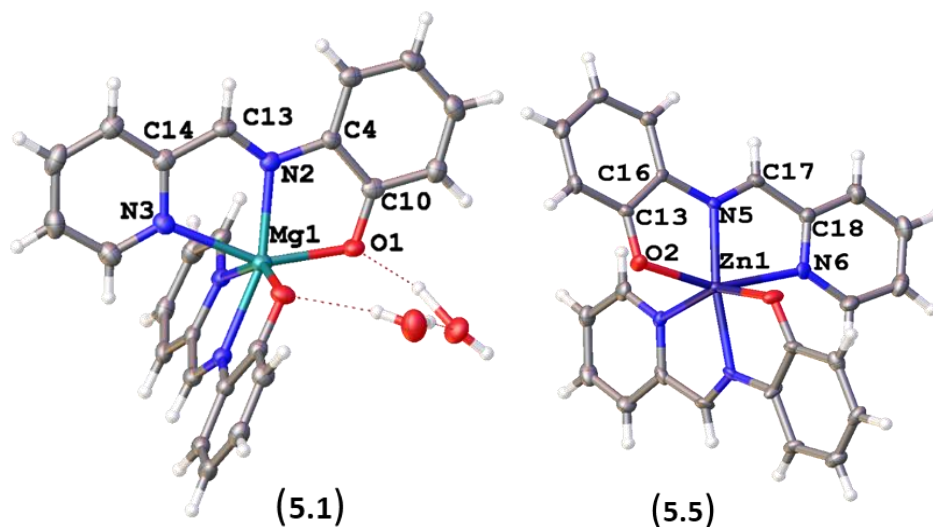

Figure 5.4: X-ray crystal structures of complexes **5.1** and **5.5** with thermal ellipsoids drawn at 50% probability level

Table 5.3: Selected bond lengths and angles for complexes **5.1** and **5.5**

	5.1	5.5
Bond length [Å]		
M—Npy	2.280(11)	2.259(7) - 2.359(7)
M—Nimine	2.149(2)	2.098(7) - 2.082(7)
M—O	2.063(16)	2.046(6), 2.055(6)
Angles [°]		
N—M—N	72.85(7), 73.53(7), 88.92(7)	74.7(3), 73.3(3), 91.5(3), 93.3(2)
N—M—O	77.71(7), 77.54(7), 95.23(7)	80.0(2), 79.3(3), 93.0(2), 88.5(3)
O—M—O	97.94(7)	97.1(3)

5.7.4 *Ring-opening polymerization of ε-caprolactone*

The ability of complexes **5.1** - **5.8** to initiate the ROP of ε-CL and ʟ/*rac*-lactide and was studied. Pilot studies were done on ε-CL in bulk using monomer to initiator ([M]/[I]) ratio of 100:1 at 110 °C. Complexes **5.1** to **5.8** proved to be effective initiators attaining 98% monomer conversion between 6 – 55 h. The corresponding data is presented in Table 5.4. Induction time of about *ca* 3 h was observed for complexes **5.1** – **5.8** with complex **5.3** demonstrating superior activity attaining full monomer conversion within 12 h. The induction time is ascribed to three main reasons, specifically catalyst conformational transformation to attain a reactive transition state,[44,45] heat current distribution and catalyst degradation to less reactive species.[46] There were no additional attempts to investigate the type of induction periods in the system.

Generally, the Mg(II) complexes were more active as compared to the Zn(II) complexes, a trend that correlates to similar work in literature.[10,47] The trend is attributed to the difference in ionic or polarity character of the M—O bond in these metal complexes.[48] The induction phases involves monomer activation and initiation, therefore the complexes are interchangeably referred to as catalysts or initiators. Complexes **5.1** and **5.5** bearing 2-pyridyl moiety were the least active for the series. The low activity can be accounted for by two plausible explanations. Firstly, it can be ascribed to low solubility of the catalyst in the monomer which might retard the polymerization reaction.

Secondly, the metal pocket of the six-coordinated metal centre is crowded thereby retarding monomer coordination, hence, reducing the catalytic activity. Monomer coordination to the metal centre is possible only after dechelation of N_{py} atom in the six-coordinated complexes. This hypothesis is supported by the improved activity when the N_{py} heteroatom is moved away from the coordination sphere.

Table 5.4: Summary of polymerization data of ε -CL catalysed by complexes **5.1** – **5.8**

Entry	Complex	Time (h)	[b]Conv (%)	[c]Mw (calc)	[d]Mw (NMR)	k_{app} (h^{-1})
1	**5.1**	32	97	11181.8	4034	0.131
2	**5.2**	14	99	11395.9	5043	0.231
3	**5.3**	6	98	11281.8	4673	0.382
4	**5.4**	8	98	11295.9	5982	0.358
5	**5.5**	55	99	11581.8	4445	0.042
6	**5.6**	32	98	11567.7	4023	0.086
7	**5.7**	24	97	11395.9	4822	0.192
8	**5.8**	30	99	11181.8	5234	0.128

[a]Polymerization conditions: 110 °C, Bulk, $[M]_0:[initiator]_0 = 100:1$. [b,d]Determined from NMR. [c]Calculated theoretical M_w.

5.7.5   *Ring-opening polymerization of rac-lactide and L-lactide*

The most active Mg(II) complexes **5.3** and **5.4** were further used as representatives to assess the ROP of L-lactide and *rac*-lactide with monomer-to-initiator ratio of 100:1 and 200:1 in toluene at 110 °C. The summary of results is presented in Table 5.5. Monomer conversion of up to 99% were achieved within 8 – 30 h and an induction period of *ca*. 30 min was observed. The shorter induction period compared to that of ε-CL is attributed to the greater reactivity of lactides which is linked to ring strain differences. An increase in monomer concentration resulted in longer polymerization time because of few initiation species.

Table 5.5: Summary of ROP data of L-LA and *rac*-LA catalysed by complexes **5.3** and **5.4**

Entry	Complex	[M/I]	Time (h)	[b]Conv (%)	[c]M_w (calc)	[d]M_w (NMR)	[e]M_w (GPC)	[f]PDI	k_{app} (h^{-1})
rac-LA	**5.3**	100:1	8	99	12581.8	7326	3323	1.40	0.709
L-LA	**5.4**	100:1	10	98	12567.7	8003	3284	1.40	0.689
rac-LA	**5.3**	200:1	25	97	30791.8	7445	-	-	0.170
L-LA	**5.4**	200:1	30	99	31621.6	8223	-	-	0.129

[a]Polymerization conditions: T = 110 °C, toluene, $[M]_0:[initiator]_0$ = 100:1. [b,d]Determined from NMR. [c]Calculated theoretical Mw. [e,f]Determined by GPC relative to polystyrene standards in THF. [e]Experimental M_w was calculated considering Mark–Houwink's corrections of 0.58.

5.7.6 *Molecular weight and molecular weight distribution of polymers*

The weight average molecular weight (M_w), number average molecular weight (M_n) and the molecular weight distributions (PDI = M_w/M_n) were determined by gel permeation chromatography (GPC) and NMR spectroscopy. The experimental values were further compared with theoretical values while applying the Mark–Houwink corrections, i.e. 0.56 and 0.58 for PCLs and PLAs, respectively.

The calculated molecular weights of the polymers obtained are higher than the experimental values from GPC and NMR analysis. This can be ascribed to intermolecular transesterification chain transfer reactions (*vide infra)* which result in dormant chains as the reaction progresses. Molecular weights obtained from GPC are similar to those from NMR analysis. For instance, complex **5.3** furnished polymers with $M_{w(NMR)}$ of 3067 g mol^{-1} and $M_{w(GPC)}$ 2989 g mol^{-1} while, the divergences lie in the analytical principle of these two techniques. In GPC analysis, separation is due to polymer chains hydrodynamic volume rather than molecular weight which is largely influenced by polymer architecture.[49]

Catalyst structure did not significantly influence the molecular weights as evidenced by slight M_w variation across the catalyst species (Table 5.4). This manifestation can suggest similar steric crowding around the metal centre. Higher molecular weight polymers were obtained from polymerization of L-LA compared to ε-CL and *rac*-LA. For example, complex **5.3** gave poly(L-LA) or poly(*rac*-LA) with molecular weights of 3284 g mol^{-1} (PDI =1.4) or 3323 (PDI = 1.4) compared to 2898 (PDI = 1.9) for PCL.

Broad molecular weight distributions were observed in bulk polymerization of ε-CL as shown by higher PDI values *ca* 2.0. Viscosity increases as the polymerization progresses, resulting in less heat transfer and less controlled polymerization process resulting in higher PDI values. When polymerization was done in solvents a more controlled polymerization process was evidenced by low PDIs *ca* 1.4, although the values are slightly higher for an ideal "living" ROP behaviour. The addition of alcohol co-initiators further improved polymerization behaviour toward an ideal living process. Notably, benzyl alcohol was more proficient than other co-initiator agents used in this study.

5.7.7 *Kinetics of ROP reactions of ε-CL*

To establish the reliance of reaction rates on monomer concentration, kinetic investigations were carried out at 110 °C with 100:1 monomer-to-catalyst ratio. Complexes **5.1** – **5.8** revealed a linear relationship of ln([M]$_0$/[M]$_t$) *vs* t and the apparent rate constants (k_{app}) of ROP were derived from the slopes of Figure 5.5 and 5.6. The linearity validates that the polymerization reaction is *pseudo* first-order with respect to ε-CL monomer concentration. For *pseudo* first order kinetics, the rate of monomer polymerization can be calculated using equation (**5.3**).

$$-\frac{d[M]}{dt} = k[M] \qquad (5.3)$$

For a specific monomer concentration ([M]), and constant initial initiator concentration ([I]$_0$), $k = k_p[I]^x$ where k_p = rate of chain propagation, and x is the order of reaction
The overall propagation rate (R_p) is expressed a shown in equation (**5.4**).

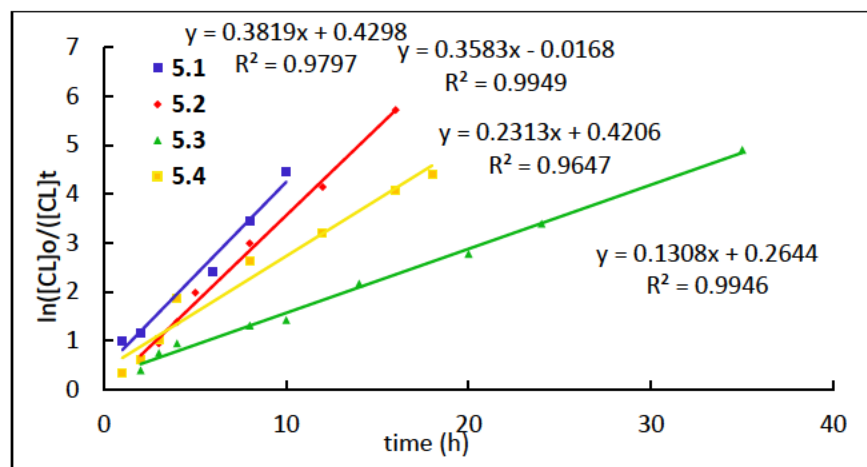$$R_p = \frac{d[M]}{dt} = k_p[M]_0^a[I]_0^x \qquad (5.4)$$

Figure 5.5: Plots of ln([CL]$_0$/[CL]$_t$) *vs t* catalysed by complexes **5.1 – 5.4**. Reaction conditions: [M]$_0$ = 100:1 bulk, T = 110 °C
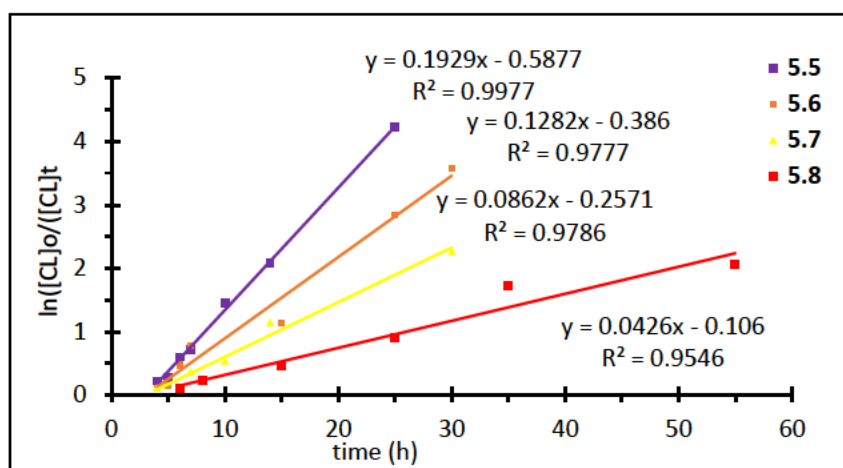

Figure 5.6: Plots of ln([CL]$_0$/[CL]$_t$) *vs t* catalysed by complexes **5.5 – 5.8**. Reaction conditions: [M]$_0$ = 100:1 bulk, T = 110 °C

The catalytic activity was influence by the metal identity with the Mg(II) complexes exhibiting greater activity than Zn(II) complexes. For instance, the most efficient Mg(II) complex **5.5** exhibited (k_{app} = 0.3819 h^{-1}) which is greater than that of complex **5.7** (k_{app} = 0.1929 h^{-1}) the Zn(II) analogue. This trend is attributed to the greater polarizing effect of Mg(II) ion as compare to Zn(II) ion, which in-turn enhance monomer coordination for activation. This same trend was reported by Wang *et al.*,[48] Mg(II) complexes achieved complete monomer conversion in 1 min f compared to 240 min for the Zn(II) counterparts.

143

The ligand skeleton can influence the catalytic performance and stability of the metal complexes.[27] There was a marked improvement in activity when the 5-membered heterocycle rings were introduced. For instance, the apparent rate constants exhibited by complexes **5.3** (k_{app} = 0.3819 h^{-1}) and **5.4** (k_{app} = 0.3583 h^{-1}) bearing thiophene and furyl rings were higher compared to that of complexes **5.2** (k_{app} = 0.2313 h^{-1}) with 4-pyridyl moiety.

5.7.7.1 *Monomer and solvent effects on polymerization*

It is well established that reaction variables and parameters such solvent media and reactant concentration also influence chemical reactions. The polymerization of ε-CL and LAs was carried out by changing the monomer to catalyst ratio between 100:1 and 400:1. The effect of using toluene and THF as solvents was also investigated and the results are presented in Table 5.6.

Table 5.6: Summary of polymerization data for ε -CL catalysed by complexes **5.3** and **5.4**

Entry	Variable	[M:I:ROH]	Time (h)	[b]Conv (%)	[c]M_w (calc)	[d]M_w (NMR)	[f]M_w (GPC)	[g]PDI	k_{app} (h^{-1})
1	**5.3**	100:1:0	8	99	13961.01	3067	2989	2.0	0.382
2	**5.3**	200:1:0	25	99	27920.01	5984	4252	1.9	0.195
3	**5.3**	300:1:0	32	98	41456.01	5234	5102	2.0	0.132
4	**5.3**	400:1:0	50	96	54146.01	6745	5258	2.1	0.067
5	THF	100:1:0	60	90	12692.01	3005	2849	1.4	0.076
6	toluene	100:1:0	40	96	13538.01	4129	3769	1.4	0.112
7	^{i}PrOH	100:1:1	5	99	13961.01	3898	-	-	0.980
8	^{t}BuOH	100:1:1	4	99	13961.01	4865	-	-	0.860
9	BnOH	100:1:1	3	99	13961.01	4982	-	-	1.190
10		100:1:2	1.5	98	13820.01	4221	4098	1.4	1.420
11		100:1:5	1	99	13961.01	3826	-	-	1.550
12		100:1:10	1	99	13961.01	4281	-	-	1.540

[a]Polymerization conditions: 110 °C, Bulk, [M]$_0$:[initiator]$_0$ = 100:1. [b]Determined from NMR. [c]Calculated theoretical Mw. [f,g]Determined by GPC relative to polystyrene standards in THF. [d]Experimental Mw was calculated considering Mark–Houwink's corrections of 0.56.

The polymerization media showed a significant effect on the catalytic activity and the plots of $\ln([M]_0/[M]_t)$ *vs* t are shown in Figure 5.7. The complexes exhibited low activity in solvent as compared to bulk polymerization. For instance, polymerization of ε-CL with complex **5.3** in toluene showed an apparent rate constant of 0.1128 h^{-1} compared to 0.3819 h^{-1} in bulk polymerization. Higher catalytic activities were also observed in toluene than in tetrahydrofuran as shown by a higher rate for **5.4** (k_{app}, 0.1128 h^{-1}) in toluene compared to 0.0762 h^{-1} in THF (Figure 5.7). This decline in activity is possibly attributed to competition between the THF solvent molecules and the monomer for the active site as well as its lower boiling temperature. The rate of polymerization of lactides was slightly higher compared to that of ε-CL. For example, complex **5.3** gave an apparent rate constant (k_{app} = 0.381 h^{-1}) for ε-CL compared to 0.571 h^{-1} in case of L-lactide. This is mainly attributed to the inherent thermodynamic instability of highly strained lactide monomer ring.[50] This trend is consistent with some ROP systems reported in literature.[51,52] Increasing the monomer to catalyst ratio resulted in reduces rates, for instance, complex **5.3** gave a rate of 0.382 min^{-1} for 100 compared to 0.067 min^{-1} for 400 monomer equivalence (Table 5.6). This manifestation can be explained the reduction of catalytic species as the monomer concentration increases.
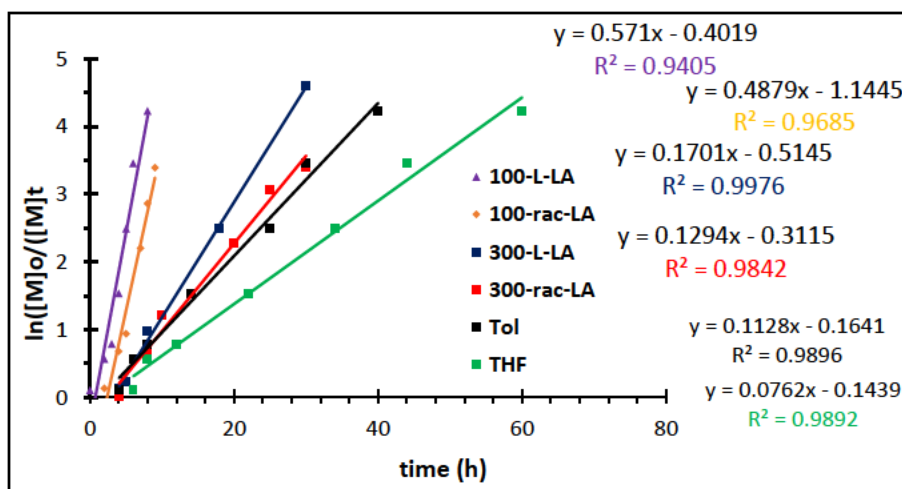

Figure 5.7: Plots of $\ln([M]_0/[M]_t)$ *vs* t for L-LA, *rac*-LA and ε-CL. Reaction conditions: $[M]_0[I]_0$ = 100:1. Toluene and THF, T = 110 °C

145

5.7.7.2 Effect of co-initiator and monomer-to-catalyst ratio on ROP reaction

The effect of co-initiator presence and monomer-to-catalyst ratio was also investigated, and the results are given in Table 5.6. Monomer to catalyst ratios between 100:1 and 400:1 were used at 110 °C in toluene. As expected catalytic activity increased with an increase in catalyst molar ratio. This is because many catalytic sites are introduced in the system. Benzoyl alcohol proved to be a better co-initiator as compared to isopropanol and *tert*-butanol. It was used to further probe the effect of varying the catalyst-to-co-initiator ratio starting from 1:2 to 1:10 on the ROP kinetics. The ROP rate increased initially but levels off reaching a ceiling at 1:5 catalyst-to-initiator molar ratio. This behaviour indicates that higher alcohol concentrations no longer significantly influence the reaction rate but rather, the excess alcohol now congests the system and it is useless from an activation perspective. This observation supports the monomer activation mechanism as highlighted in literature.[47]

5.7.8 Order of ROP of ε-CL, ʟ-lactide with respect to co-initiator and complex 5.3

Further investigations were carried to elucidate the reaction order of complex **5.3** by running the polymerization reactions at varying catalyst and constant monomer concentrations. Plots of lnk_{app} vs ln[I] allow for the deduction of reaction order from the gradients. From these graphs the extrapolated orders were 1.0 (ε-CL toluene), 0.8 (ʟ-LA, toluene) and 0.98 (ε-CL, BnOH). These reactivity trends are similar to those reported for other ROP systems.[53,54]
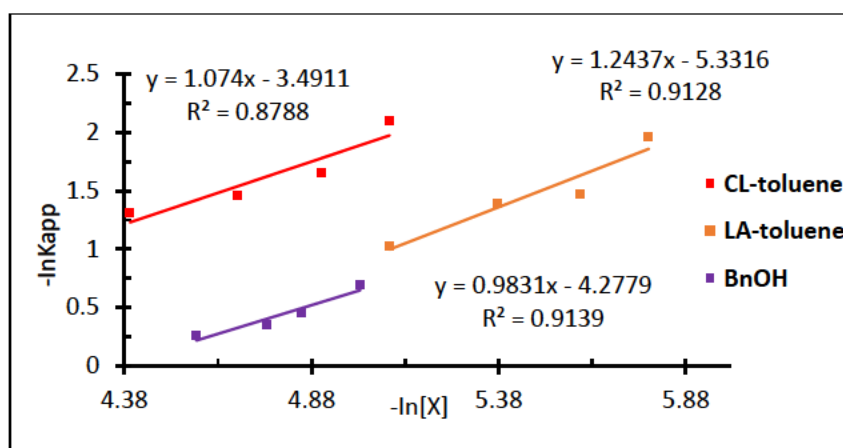

Figure 5.8: Plots of lnk_{app} vs ln[X] for determining the catalyst and co-initiator order of reaction with respect ε-CL and ʟ-LA

Mechanistically non-integer values of reactions order with respect catalyst pose a challenge to fully explain. Nonetheless, fractional orders have been exhibited in many bulk ROP catalytic systems.[55] This is linked with intricate catalytic agglomeration which occur prior to initiation. In the current system under study no conclusive information is available to confirm this phenomenon. To obtain the co-initiator (BnOH) order of reaction a constant monomer-to-catalyst ratio of 100:1 was used while the initial co-initiator ratio was varied from 5 to 20. The logarithmic linear plots of $\ln(k_{app})$ *vs* $\ln[\text{BnOH}]_0$ gave a gradient of 1.0 pointing to a first order reliance in co-initiator. Thus, the overall kinetic equations for the ROP of ε-CL and L-LA are represented by equations (**5.5** - **5.7**).

$$R_p = \frac{d[\varepsilon\text{CL}]}{dt} = k_p[\text{CL}]^1[\textbf{5.3}]^{1.1} \qquad \textbf{5.5}$$

$$R_p = \frac{d[\varepsilon\text{CL}]}{dt} = k_p[\text{LA}]^{\textbf{1}}[\textbf{5.3}]^{\textbf{1.2}} \qquad \textbf{5.6}$$

$$R_p = \frac{d[\varepsilon\text{CL}]}{dt} = k_p[\text{CL}]^1[\text{BnOH}]^{0.5}[\textbf{5.3}]^1 \qquad \textbf{5.7}$$

5.7.9 Catalyst stability and polymerization "living" behaviour

The stability or immortality of complex **5.3** was explored through successive addition of equal amounts of the monomer after the first run without adding another catalyst portion. Monomer conversion of 99% was achieved within 20 h and there was a loss of catalytic activity in the second cycle with a recorded k_{app} value of 0.3177 h^{-1} relative to the first run k_{app} (0.3819 h^{-1}) (Figure 5.9) which translate to 18% loss in activity. This tendency signifies that the complexes maintain its activity although there is loss of catalytic efficiency. It is speculated that the catalyst deactivation is linked to complex decomposition to less reactive species at the high temperatures.

The immortality of the system was also accessed by determining the molecular weights *vs* conversion as the reaction proceeds. Fractions collected at different intervals and after completion of the second cycle were analysed by GPC. The number-average molecular weights (M_n), were also, plotted against conversion and polymer dispersity (PDI) values (Figure 5.10).

The deviation of the plot from linearity points to semi-living behaviour *i.e.* reaction proceeded with reduction in number of growing chains. Although, the change in PDI is minimal, the higher values close to 2.0 also back a semi-living polymerization behaviour.
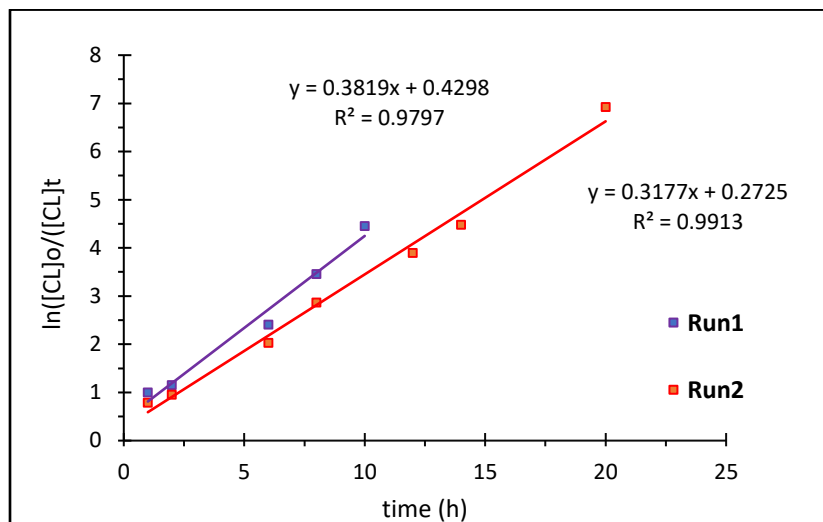

Figure 5.9: Plots of $\ln([CL]_0/[CL]_t)$ *vs* *t* catalysed by complex **5.3** after the first and second run. Reaction conditions: $[M]_0:[I]_0$ 100:1 solvent: toluene; T = 110 °C
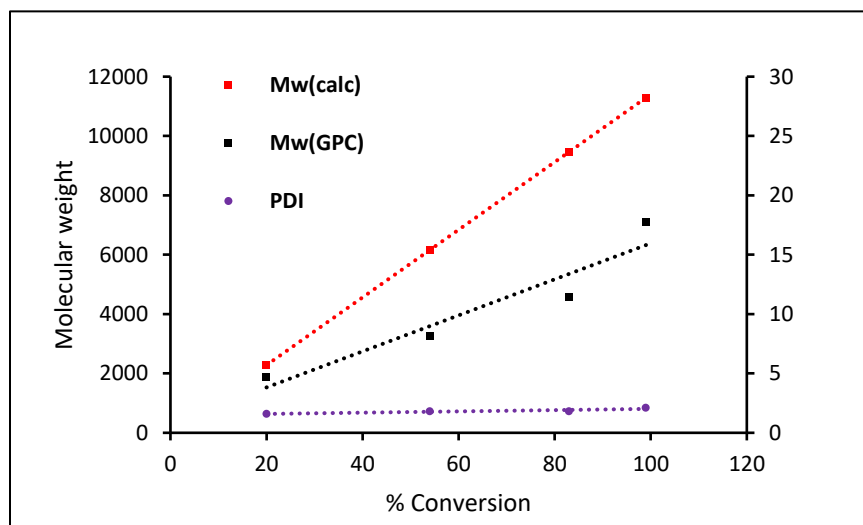

Figure 5.10: Plots of experimental, theoretical molecular weight and PDI against monomer conversion for complex **5.3** at 110 °C

5.7.10 End-group analysis and mechanistic investigations

ROP of cyclic esters is well explained by two reaction mechanisms namely coordination/insertion mechanism (CIM)[56] and activated monomer mechanism (AMM).[57,58] In CIM the initiation step includes monomer coordination to the catalytic site *via* the carbonyl oxygen with subsequent polarization of the M—O$_{(ligand)}$ bond. This is now preceded by ring-opening of the monomer to generate the pre-polymer initiator. Chain growth is achieved by repeated addition of the monomer to furnish the resultant polymer. In the (AMM) which is usually the routine mechanism in the presence of exogenous co-initiators, e.g. amines and alcohols. The cyclic ester is activated after coordinating to the catalytic centre and initiation follows when the co-initiator attacks the monomer. To confirm which mechanisms in operation in absence and in existence of alcohol co-initiator the polymers were analysed by ^{1}H-NMR spectroscopy and ESI-MS.
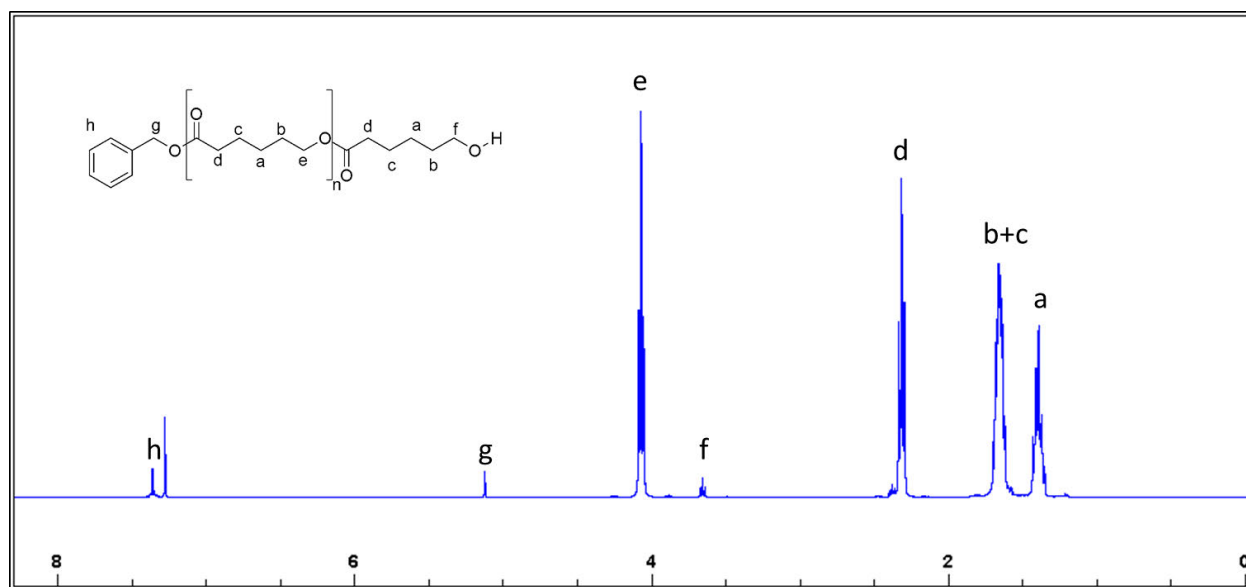
Figure 5.11: The ^{1}H-NMR spectrum of PCL initiated by complex **5.4**/BnOH. Reaction conditions: [CL]$_0$:[BnOH]$_0$ = 100:1, solvent: toluene, T = 110 °C
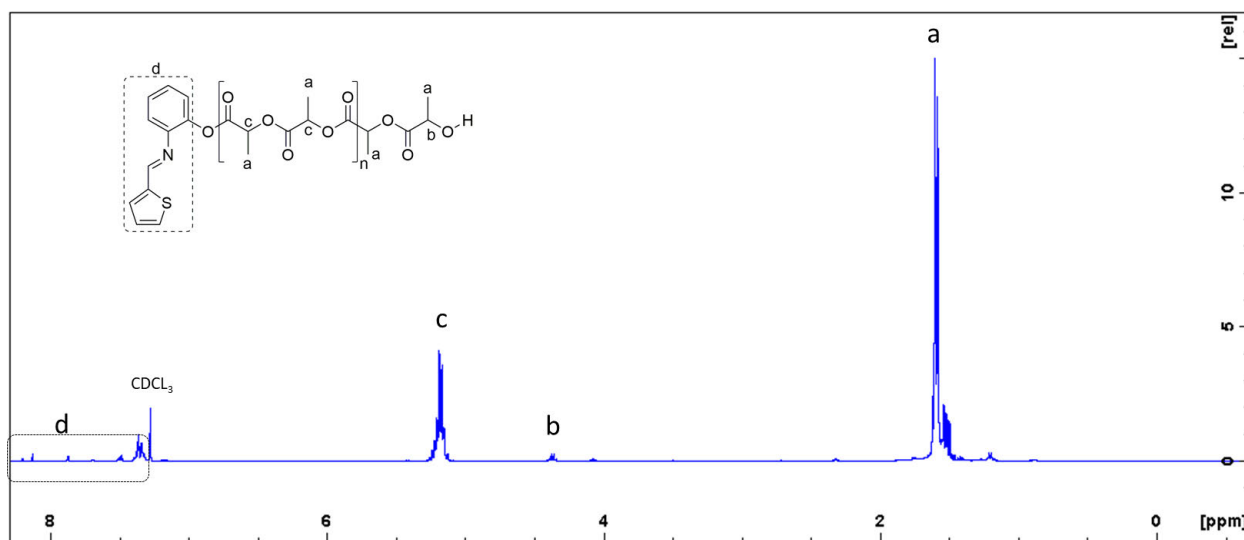
Figure 5.12: The ^{1}H-NMR spectrum of PLA initiated by complex **5.3**. Reaction conditions $[M]_0[I]_0 = 100:1$, solvent: toluene, $T = 110$ °C

The ^{1}H-NMR spectra of PCL and PLA (in the absence of co-initiator are shown in (Figure 4.18 and 5.13). Triplet signals at 3.65 (OCH$_2$) and 4.87 (OCH$_2$) ppm were observed for PCL and PLA respectively due to methylene protons adjacent the hydroxyl end. In addition to polymer signals, peaks assigned to the ligand motif were also observed. This observation shows that the ligand M—O bond was responsible for the initiation. The ligand fragments were also accounted in the ESI-MS spectrum (Figure 4.17), for instance the peak at *m/z* 1140 correspond to a polymer end capped with a -OH and a ligand fragment with degree of polymerization (DP) value of six. This data is in conformity to a CIM in the absence of co-initiator.[60,61] When benzyl alcohol was added a singlet at 5.4 ppm from methylene protons and phenyl aromatic protons showed a benzyl ester terminal end. This evidence backs an AMM mechanism through insertion of benzyloxy into the monomer *O*-acyl bond.[56]
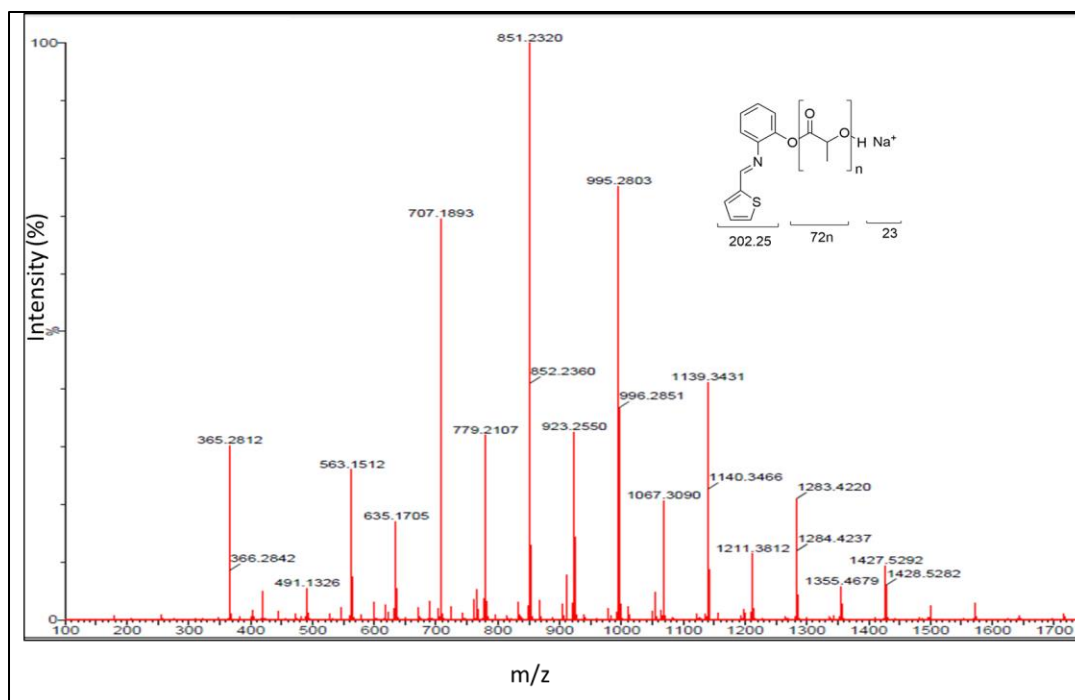
Figure 5.13: ESI-MS spectrum of PLA from complex **5.3**, $[LA]_0:[BnOH]_0 = 100:1$, t =12 h
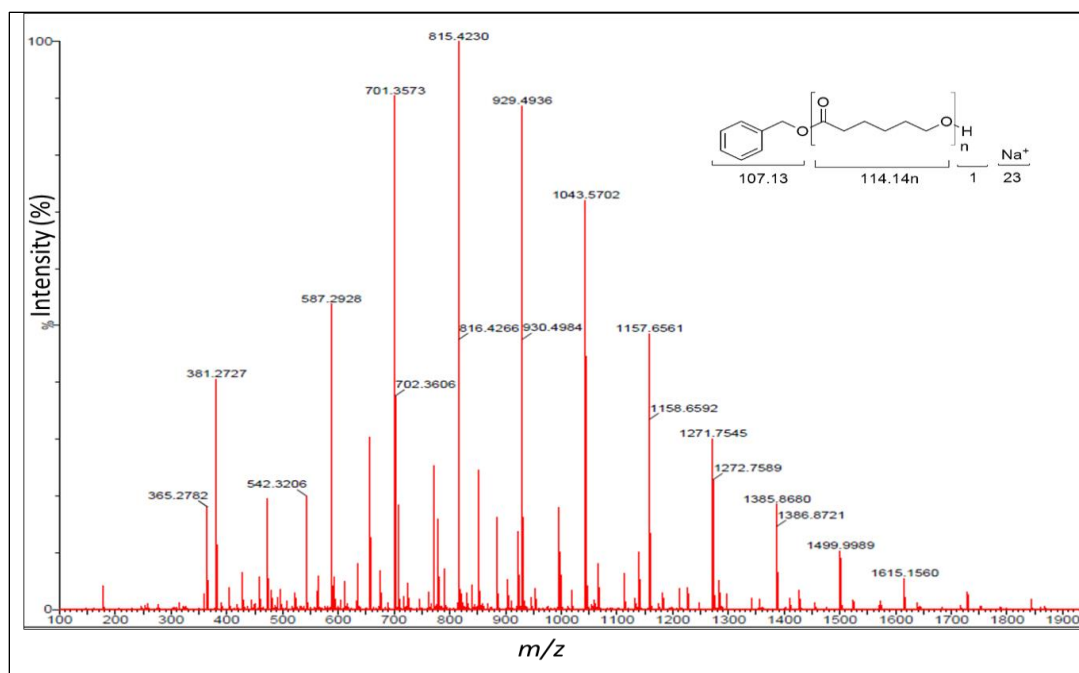
Figure 5.14: ESI-MS spectrum of PCL obtained for complex **5.2**, $[CL]_0:[BnOH]_0 = 100:1$, t = 32 h

5.7.11 Lactides microstructure

Mechanical behaviour of polymers is generally influenced by the stereochemistry on the polymer backbone. Polylactide microstructure stereochemistry (heterotactic, isotactic and syndiotactic) can be controlled by the catalyst used. The overall stereo regulation is anchored on two mechanisms namely chain end control (governed by monomer stereochemistry) and enantiomorphic site control (governed by catalyst chirality).[62-64] The polymer tacticity of the synthesised polymers was unravelled using homonuclear ^{1}H-decoupled and ^{13}C-NMR spectroscopy. The ^{13}C-NMR spectrum of poly(L-LA) ((Figure 5.15) catalysed by complex **5.4** showed a single peak around 69 ppm and some very small peaks around showing that the polymerization proceeded with some degree of epimerization.

Tetrad peaks were allocated based on assignments reported in literature.[65,66] The ^{13}C-NMR methine region of the synthesised -PLLA showed that epimerization had occurred as evidenced by the presence of a satellite peak assigned to *iss*, *iss*, *sii* tacticity tetrads. The *iii* tetrad is intense hence it is the most predominant showing that the polymer chains are isotactic enriched.
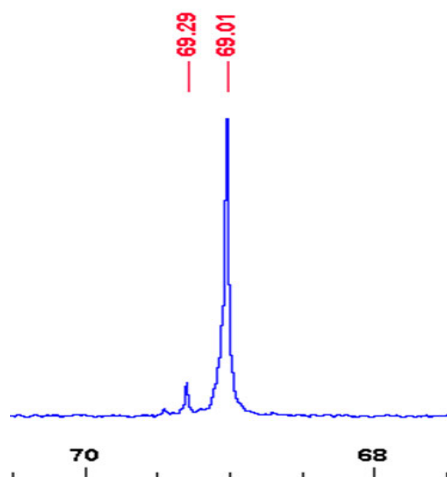
Figure 5.15: ^{13}C-NMR methine region for poly(L-LA) catalysed by complex **5.4**. Reaction conditions $[M]_{0:0} = 100:1$, solvent: toluene, T = 110 °C

For *rac*-PLA the ^{13}C-NMR methine spectrum segment (Figure 3.27a) comprise of two signals which are allocated to the triads *is* and *ii*. The carbonyl ^{13}C-NMR spectrum segment (Figure 3.27b) which has three typical peaks and they are allocated to triads *ii*, (*is,si*) and *ss*.[65] The intermediate peak is spiked a feature noted in other reported work.[65,67]
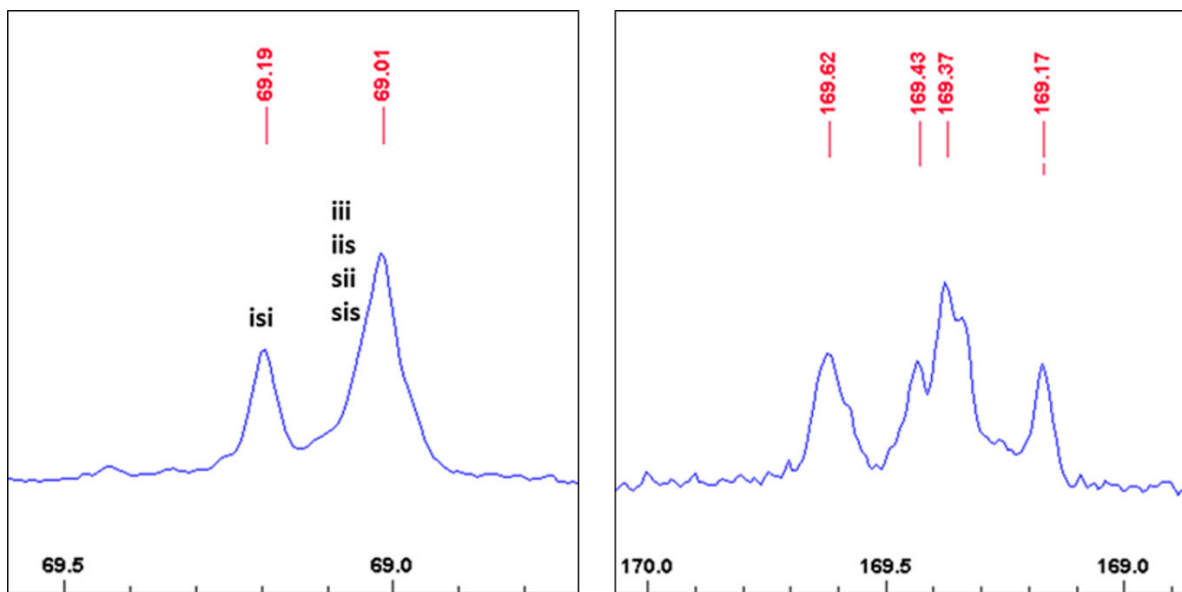

Figure 5.16: (a) ^{13}C-NMR methine region and (b) ^{13}C-NMR carbonyl region spectra of poly(rac-LA). Reaction conditions $[M]_0:[I]_0 = 100:1$, solvent: toluene, T = 110 °C

5.7.12 *Effect of temperature and activation parameters*

The thermodynamics and kinetics of ROP reactions have been exclusively studied using theoretical DFT computations and experimental data.[61,68,69] The apparent activation energy (E_a) and thermodynamic parameters were calculated using the Arrhenius and Eyring equations (**5.10**) and (**5.11**).

$$Ink = InA - \frac{E_a}{RT} \qquad (\mathbf{5.10})$$

$$In\left(\frac{k_{app}}{T}\right) = \frac{\Delta S_p}{R} - \frac{\Delta H_p}{R} \cdot \left(\frac{1}{T}\right) + In\left(\frac{k_b}{h}\right) \qquad (\mathbf{5.11})$$

where E_a is apparent activation energy, A is pre-exponential factor, R is general gas constant k_B and h are the Boltzmann and Planck constants, respectively, ΔS_p and ΔH_p are the activation of entropy and enthalpy of polymerization, respectively.
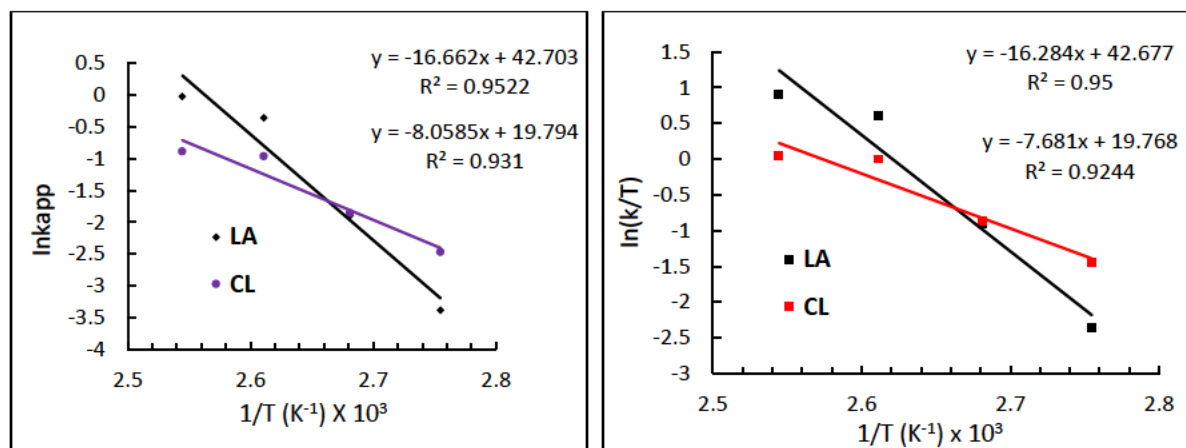
Figure 5.17: (a) Arrhenius plot of lnk_{app} vs T^{-1} for the bulk polymerization of ε-CL initiated by complex 3, M/I = 200 and (b) Eyring plot of temperature dependence of the rate constant

For complex **5.3**, the overall activation energy (E_a) values for the monomers were inferred from the slopes of the Arrhenius plots of lnk_{app} vs T^{-1} (Figure 5.17a) and were found to be 13 and 67 kJ mol^{-1} for L-LA and ε-CL respectively. The E_a values for the all monomer slightly deviate from ΔH_p values. The enthalpy ΔH_p were found to be 23.5 and 63.9 kJ mol^{-1} for L-LA and ε-CL, respectively. These values are in tandem with work other reported systems.[27,70] The entropy ΔS_p energies were tabulated to be -157 and -33 JK^{-1} mol^{-1} for ε-CL and L-LA monomers, respectively.

5.8 Conclusion

Mg(II) and Zn(II) complexes (**5.1 – 5.8**) supported by amino phenolate ligands were successfully synthesised and characterised. Their catalytic activity in the ROP of ε-CL, L-lactide and *rac*-lactide was investigated probing the influence catalyst structural differences, co-initiators and solvents. All complexes proved to be effective catalyst in ROP of the cyclic ester monomer. Higher polymerization rates were obtained with Mg(II) complexes (**5.1 - 5.4**) which were able to transform 100 monomer equivalents within 20 h. Solution polymerization resulted in retarded polymerization rates than solvent free polymerization for ε-CL. Contrasting the different solvents used, polymerization in toluene was much faster than in THF which compete with monomer for activation sites. The polymerizations managed to produce polymers with molecular weights which are less than the calculated values. Relatively low molecular weight ($M_{w(NMR)}$) polymers which range between 6034 to 9673 g mol^{-1} were obtained. Moderate molecular weights increase from

1234 to 4567 g mol^{-1} was observed with an increase in catalyst concentration with polydispersity (PDIs) *ca.* 2.0. These higher PDI values exhibited arguments a semi "living" polymerization process. Addition of alcohol co-initiators resulted in controlled polymerization with the PDI values reducing to 1.4.

With the activity exhibited by the complexes reported in this chapter, chiral ligands were designed to improve stereoselectivity and polymer microstructure tacticity. The investigations and outcomes are discussed in **Chapter 6**.

References

1. R. T. Mathers and M. A. R. Meier, *Green polymerization methods: Renewable starting materials, catalysis and waste reduction*, Wiley-VCH Verlag, Weinheim, Germany, 2011.

2. A. Salerno, M. Fernández-Gutiérrez, J. San Román del Barrio and C. Domingo, *J. Supercrit. Fluids*, **2015**, 97, 238.

3. M. S. Lopes, A. L. Jardini and R. M. Filho, *Procedia Engineering*, **2012**, 42, 1402.

4. C.-W. Lou, C.-H. Yao, Y.-S. Chen, T.-C. Hsieh, J.-H. Lin and W.-H. Hsing, *Text. Res. J.*, **2008**, 78, 958.

5. G. Molea, F. Schonauer, G. Bifulco and D. D'Angelo, *Br. J Plast. Surg.*, **2000**, 53, 137.

6. W. Chen, L. A. Shah, L. Yuan, M. Siddiq, J. Hu and D. Yang, *RSC Advances*, **2015**, 5, 7559.

7. A. Duro-Castano, J. Movellan and M. J. Vicent, *J. Biomater. Sci.*, **2015**, 3, 1321.

8. Z. Ge and S. Liu, *Chem. Soc. Rev.*, **2013**, 42, 7289.

9. Y. F. Al-Khafaji, M. R. J. Elsegood, J. W. A. Frese and C. Redshaw, *RSC Advances*, **2017**, 7, 4510.

10. I. D'Auria, C. Tedesco, M. Mazzeo and C. Pellecchia, *Dalton Trans.*, **2017**, 46, 12217.

11. H.-C. Hsiao, A. Datta, Y.-F. Chen, W. Chang, T.-Y. Lee, C.-H. Lin and J.-H. Huang, *J. Organomet. Chem.*, **2016**, 804, 35.

12. R. Petrus and P. Sobota, *Dalton Trans.*, **2013**, 42, 13838.

13. C. C. Roberts, B. R. Barnett, D. B. Green and J. M. Fritsch, *Organometallics*, **2012**, 31, 4133.

14. M. J. Walton, S. J. Lancaster, J. A. Wright, M. R. J. Elsegood and C. Redshaw, *Dalton Trans.*, **2014**, 43, 18001.

15. V. Balasanthiran, M. H. Chisholm, K. Choojun, C. B. Durr and P. M. Wambua, *Polyhedron*, **2016**, 103, Part B, 235.

16. K. Devaine-Pressing, J. H. Lehr, M. E. Pratt, L. N. Dawe, A. A. Sarjeant and C. M. Kozak, *Dalton Trans.*, **2015**, 44, 12365.

17. H.-Y. Chen, L. Mialon, K. A. Abboud and S. A. Miller, *Organometallics*, **2012**, 31, 5252.

18. J. M. Colwell, E. Wentrup-Byrne, G. A. George and F. Schué, *Polym. Int.*, **2015**, 64, 654.

19. T.-L. Huang and C.-T. Chen, *Dalton Trans.*, **2013**, 42, 9255.

20. Z. Dai, Y. Sun, J. Xiong, X. Pan, N. Tang and J. Wu, *Catal. Sci. Technol.*, **2016**, 6, 515.

21. M. Stolt and A. Södergård, *Macromolecules*, **1999**, 32, 6412.

22. A. B. Biernesser, K. R. Delle Chiaie, J. B. Curley and J. A. Byers, *Angew. Chem. Int. Ed.*, **2016**, 55, 5251.

23. A. B. Biernesser, B. Li and J. A. Byers, *J. Am. Chem. Soc.*, **2013**, 135, 16553.

24. C. M. Manna, A. Kaur, L. M. Yablon, F. Haeffner, B. Li and J. A. Byers, *J. Am. Chem. Soc.*, **2015**, 137, 14232.

25. S. H. Ahn, M. K. Chun, E. Kim, J. H. Jeong, S. Nayab and H. Lee, *Polyhedron*, 127, 51.

26. S. Fortun, P. Daneshmand and F. Schaper, *Angew. Chem. Int. Ed.*, **2015**, 54, 13669.

27. E. D. Akpan, S. O. Ojwach, B. Omondi and V. O. Nyamori, *New J. Chem.*, **2016**, 40, 3499.

28. D. Li, Y. Peng, C. Geng, K. Liu and D. Kong, *Dalton Trans.*, **2013**, 42, 11295.

29. S. Sun, K. Nie, Y. Tan, B. Zhao, Y. Zhang, Q. Shen and Y. Yao, *Dalton Trans.*, **2013**, 42, 2870.

30. P.-H. Liu, F.-J. Chuang, C.-Y. Tu, C.-H. Hu, T.-W. Lin, Y.-T. Wang, C.-H. Lin, A. Datta and J.-H. Huang, *Dalton Trans.*, **2013**, 42, 13754.

31. M.-C. Wu, T.-C. Hu, Y.-C. Lo, T.-Y. Lee, C.-H. Lin, W.-Y. Lu, C.-C. Lin, A. Datta and J.-H. Huang, *J. Organomet. Chem.*, **2015**, 791, 141.

32. D. Appavoo, B. Omondi, I. A. Guzei, J. L. van Wyk, O. Zinyemba and J. Darkwa, *Polyhedron*, **2014**, 69, 55.

33. W. A. Munzeiwa, V. O. Nyamori and B. Omondi, *Appl. Organomet. Chem.*, e4247.

34. P. M. Schäfer, M. Fuchs, A. Ohligschläger, R. Rittinghaus, P. McKeown, E. Akin, M. Schmidt, A. Hoffmann, M. A. Liauw, M. D. Jones and S. Herres-Pawlis, *ChemSusChem*, **2017**, 10, 3547.

35. Bruker, ed., *APEXII*, APEXII Bruker AXS Inc, Madison, Wisconsin, USA, 2009.

36. Bruker, *SAINT*, SAINT Bruker AXS Inc, Madison, Wisconsin, USA, 2009.

37. Bruker, *SADABS*, Bruker SADABS Bruker AXS Inc, Madison,Wisconsin, USA, 2009.

38. G. Sheldrick, *Acta Crystallogr Sect. A: Found. Crystallogr.*, **2008**, 64, 112.

39. B. Dolomanov O. V, L. J. Gildea,R. J, HowardJ. A. K. Puschmann, H, *Appl. Crystallogr*, **2009**, 42, 339.

40. Y.-W. Dong, R.-Q. Fan, W. Chen, H.-J. Zhang, Y. Song, X. Du, P. Wang, L.-G. Wei and Y.-L. Yang, *RSC Advances*, **2016**, 6, 110422.

41. D. M. Epstein, S. Choudhary, M. R. Churchill, K. M. Keil, A. V. Eliseev and J. R. Morrow, *Inorg. Chem.*, **2001**, 40, 1591.

42. N. Zhang, Y.-H. Fan, C.-F. Bi, X. Zhang, P.-F. Zhang, Z.-Y. Zhang and X. Li, *J Inorg. Organomet. Polym. Mater.*, **2013**, 23, 1492.

43. N. Zhang, Y.-H. Fan, C.-F. Bi, J. Zuo, P.-F. Zhang, Z.-Y. Zhang and Z. Zhu, *J. Coord. Chem.*, **2013**, 66, 1933.

44. H.-C. Tseng, M. Y. Chiang, W.-Y. Lu, Y.-J. Chen, C.-J. Lian, Y.-H. Chen, H.-Y. Tsai, Y.-C. Lai and H.-Y. Chen, *Dalton Trans.*, **2015**, 44, 11763.

45. N. Buis, S. A. French, G. D. Ruggiero, B. Stengel, A. A. D. Tulloch and I. H. Williams, *J. Chem. Theory Comput.*, **2007**, 3, 146.

46. R. F. Storey and J. W. Sherman, *Macromolecules*, **2002**, 35, 1504.

47. Y. Huang, W. Wang, C.-C. Lin, M. P. Blake, L. Clark, A. D. Schwarz and P. Mountford, *Dalton Trans.*, **2013**, 42, 9313.

48. Y. Wang, W. Zhao, D. Liu, S. Li, X. Liu, D. Cui and X. Chen, *Organometallics*, **2012**, 31, 4182.

49. S. T. Balke and H. N. Cheng, in *Modern Methods of Polymer Characterization* ed. H. G. M. Barth, J. W, Wiley-Interscience, New York, 1991, ch. 10-300.

50. A. Duda, A. Kowalski, S. Penczek, H. Uyama and S. Kobayashi, *Macromolecules*, **2002**, 35, 4266.

51. Y. F. Al-Khafaji, T. J. Prior, L. Horsburgh, M. R. J. Elsegood and C. Redshaw, *Chemistry Select*, **2017**, 2, 759.

52. W.-L. Kong, Z.-Y. Chai and Z.-X. Wang, *Dalton Trans.*, **2014**, 43, 14470.

53. L. E. Breyfogle, C. K. Williams, J. V. G. Young, M. A. Hillmyer and W. B. Tolman, *Dalton Trans.*, **2006**, 928.

54. Y. Shen, Z. Shen, Y. Zhang and K. Yao, *Macromolecules*, **1996**, 29, 8289.

55. E. D. Akpan, S. O. Ojwach, B. Omondi and V. O. Nyamori, *Polyhedron*, **2016**, 110, 63.

56. N. Ajellal, J.-F. Carpentier, C. Guillaume, S. M. Guillaume, M. Helou, V. Poirier, Y. Sarazin and A. Trifonov, *Dalton Trans.*, **2010**, 39, 8363.

57. H. R. Kricheldorf, I. Kreiser-Saunders and C. Boettcher, *Polymer*, **1995**, 36, 1253.

58. H. R. Kricheldorf, I. Kreiser-Saunders and A. Stricker, *Macromolecules*, **2000**, 33, 702.

59. A. Tardy, J. Nicolas, D. Gigmes, C. Lefay and Y. Guillaneuf, *Chem. Rev.*, **2017**, 117, 1319.

60. J. Liu, J. Ling, X. Li and Z. Shen, *J. Mol. Catal. A: Chem.*, **2009**, 300, 59.

61. E. E. Marlier, J. A. Macaranas, D. J. Marell, C. R. Dunbar, M. A. Johnson, Y. DePorre, M. O. Miranda, B. D. Neisen, C. J. Cramer, M. A. Hillmyer and W. B. Tolman, *ACS Catalysis*, **2016**, 6, 1215.

62. A. P. Dove, V. C. Gibson, E. L. Marshall, H. S. Rzepa, A. J. P. White and D. J. Williams, *J. Am. Chem. Soc.*, **2006**, 128, 9834.

63. M. H. Chisholm, J. C. Huffman and K. Phomphrai, *J. Chem. Soc., Dalton Trans.*, **2001**, 222.

64. N. Nomura, R. Ishii, M. Akakura and K. Aoi, *J. Am. Chem. Soc.*, **2002**, 124, 5938.

65. M. H. Chisholm, S. S. Iyer, D. G. McCollum, M. Pagel and U. Werner-Zwanziger, *Macromolecules*, **1999**, 32, 963.

66. K. A. M. Thakur, R. T. Kean, E. S. Hall, J. J. Kolstad, T. A. Lindgren, M. A. Doscotch, J. I. Siepmann and E. J. Munson, *Macromolecules*, **1997**, 30, 2422.

67. F. Chabot, M. Vert, S. Chapelle and P. Granger, *Polymer*, **1983**, 24, 53.

68. A. Kronast, M. Reiter, P. T. Altenbuchner, C. Jandl, A. Pöthig and B. Rieger, *Organometallics*, **2016**, 35, 681.

69. I. D. Rosal, R. Poteau and L. Maron, *Dalton Trans.*, **2011**, 40, 11228.

70. J.-M. Raquez, P. Degée, R. Narayan and P. Dubois, *Macromolecules*, **2001**, 34, 8419.

Chapter 6

Stereoselective homo- and co-polymerization of lactides and ε-caprolactone catalysed by chiral Zn(II) pyridyl complexes

This chapter builds on previous work, which showed that ligand motifs could influence the catalytic activity and polymer properties. We have introduced chirality into the ligand system with an intention of studying the possible influence in the stereoselectivity of lactide and cross-polymerization of ε-CL and LAs.

Abstract

A series of Zn(II) chlorido complexes (**6.3'** – **6.5'**) supported by *N,N'*-bidentate-*N*-(pyridin-2-ylethyl)amine ligands have been synthesised. Zn(II) alkyl and alkoxy complexes **6.1'-Me** – **6.5'-Me** and (**6.1'-OBn** – **6.2'-OBn**) were synthesised *in-situ* by reacting the chloride Zn(II) derivatives (**6.3'** – **6.5'**) with methyl lithium with subsequent addition of benzyl alcohol. Both species showed excellent catalytic activity with alkoxyl species dominating in ring-opening polymerization (ROP) of cyclic esters. The ROP reactions exhibited *pseudo* first-order kinetics with respect to monomer concentration. Polymer molecular weights increased as ligand steric hindrance decreased and they lie between 3096 and 8837 g mol^{-1}, a relatively high molecular weight distribution with PDI values *ca.* 2 was observed. Poly(*rac*-lactide) polymers are predominantly heterotactic while poly(L-lactides) are largely isotactic. All polymerization reactions proceed through coordination insertion mechanism followed by hydrolysis of the metal. The stereogenic centres of the ligand skeleton influenced control of polymer stereochemistry. Random copolymerization of ε-caprolactone (ε-CL) and lactides (LA) resulted in block gradient copolymers. The sequential addition of lactides after ε-CL gave diblock PCL-b-PLA and reversing monomer addition did not form any copolymer.

Keywords: ε-caprolactone, lactide, *N*-(pyridin-2-ylethyl)amine, zinc(II), ROP

6.1 Introduction

Polyesters, particularly polycaprolactone (PCL) and polylactide (PLA), are gaining prominence as substitutes for petroleum-derived polymers. They have been modified to suit specific applications such as packaging[1], drug delivery[2] and manufacture of medical devices.[3] Ring-opening polymerization (ROP) of specific cyclic esters with metal-based initiators/catalyst has proven to be an effective method for polyester synthesis.[4-7] ROP has a tendency to produce polymers with well-defined microstructures, controlled molecular weights and molecular weight distributions.

Selective polymerization of chiral lactides (LAs) have allowed alteration of the macromolecular tacticity thereby, influencing their physical and chemical properties. Polymerization of pure chiral lactides (e.g. L/D-LA) furnish isotactic polymer polylactide chains (PLLA or PDLA). For *rac*-LA and *meso*-LA, stereo-selective polymerization can be accomplished by two mechanisms namely enantiomorphic-site control mechanism (ESCM),[8] where monomer insertion is predetermined by the absolute stereo-configuration of the catalytic centre or chain-end control mechanism (CEM),[9,10] where monomer selection is communicated from the stereo-centre of the prior monomer inserted in the growing chain. Aluminium complexes have remarkably exhibited supreme stereo-control in *rac*-LA polymerization.[11,12]

Homopolymers of PLA display good mechanical strength but relatively low plasticity.[13] On the other hand, PCLs have good elasticity but poor mechanical strength. The physical and chemical properties of the homopolymers (PCL and PLA) can be enhanced by copolymerization of ε-caprolactone and lactides. Therefore, a hybrid of these two homopolymers could augment the difference. Copolymerization is one of the methods used for preparing copolymers of varying composition with interesting polymer charcteristics.[14-16] The different monomer distribution on the polymer chain can give rise to diblock, gradient and random copolymers. However, purely random copolymers of ε-CL and LAs have been seldom synthesised. This is because the homo-polymerization rate of ε-CL is higher than that of L-LA and D,L-LA, and in cross polymerization the trend is reversed resulting in block (PLA-b-PCL) or gradient poly(LA-grad-CL) copolymers.[17-19] Hence, an enormous effort has been put in pursuit for an excellent catalysts for the copolymerization of ε-CL and LAs. Cross polymerization of ε-CL and LAs can result in different copolymers depicted in Scheme 6.1
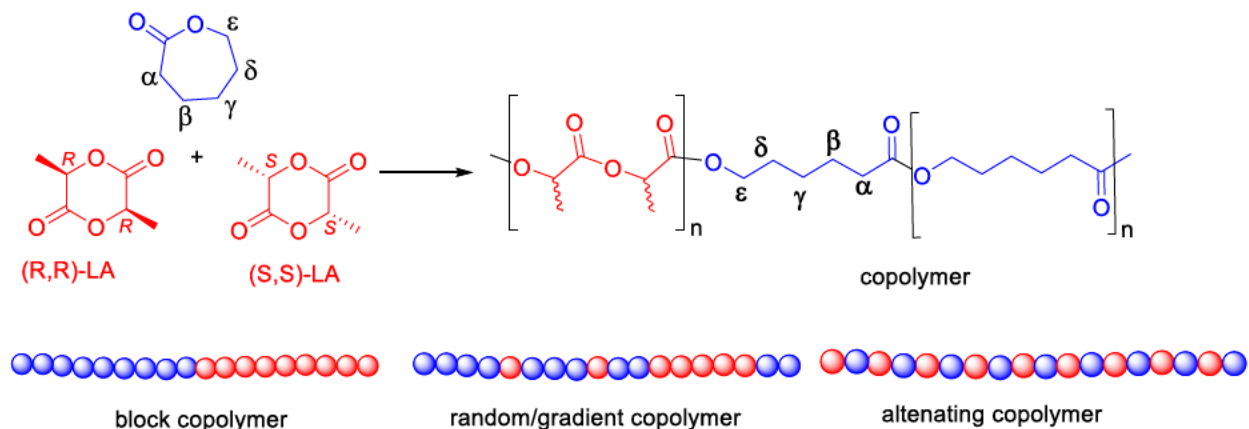
Scheme 6.1: Copolymerization of ε-caprolactone and lactides

Herein, the synthesis of air stable chlorido Zn(II) complexes supported by chiral *N*-(pyridin-2-ylethyl)aniline ligands is presented. The *in-situ* generated dimethyl and alkoxy derivatives were tested for their performance in ROP. Their efficiency in copolymerization of LAs and ε-CL was also undertaken at varying monomer feed ratios. It was envisioned that the chirality will induce stereoselectivity polymerization hence, resulting in polymers with interesting properties.

6.2 Experimental section

6.2.1 Materials

All experiments were carried out under argon, 5.0 technical grade, (Airflex Industrial Gases, South Africa) using Schlenk techniques. All the solvents were obtained from Sigma-Aldrich. Ethanol (98%) and methanol (98%) was distilled and dried from magnesium turnings; dichloromethane (DCM) (99%) dried over P_2O_5. Tetrahydrofuran (THF) 98%, and hexane (98%) were dried from a sodium-benzophenone mixture. Reagents, 2-acetylpyridine (98%), 2,6-diisopropylaniline (98%), 2,6-dimethylaniline (98%), aniline (97%), *p*-chloroaniline (99%), *p*-toludine (99%), ε-caprolactone (ε-CL) (97%), L-lactide (L-LA) (98%) and *rac*-lactide (*rac*-LA) (98%) were also obtained from Sigma-Aldrich.

6.2.2 Instrumentation

Ligands were synthesised using a synthesis reactor-monowave-50 (Anton Paar). ^{1}H- and ^{13}C-NMR spectra were measured at room temperature using a Bruker 400 MHz spectrometer. ^{1}H-NMR data were recorded in DMSO-d_6; chemical shifts were calibrated to the residual solvent signal of DMSO-d_6 (δ 2.5). Similarly, ^{13}C-NMR data were recorded in DMSO-d_6 and referenced to the residual solvent signal at δ 40.00. IR spectra were obtained on a PerkinElmer Universal ATR spectrum 100 FT-IR spectrometer. Mass spectra of compounds were obtained from a Water synapt GR electrospray positive spectrometer.

6.3   General methods

6.3.1   Synthesis of N,N'-bidentate N-(pyridin-2-ylethyl)aniline ligands

An equimolar mixture of 2-acetylpyridine and aniline was subjected to monowave radiation for a period of 10 min to furnish imine ligands **L6.1** – **L6.5**. The resultant oils were transferred to 50 ml round bottled flask together with ethanol (30 ml) and to the mixture then cooled to 0 °C and sodium borohydride (1.5 mmol) was then added while being stirred. Thereafter, the mixture was allowed to warm to room temperature and stirred over 2 h. The reaction was then quenched with water (10 ml) and the mixture extracted with DCM (3 x 25 ml) fractions. The fractions were combined and dried with anhydrous MgSO$_4$ and the solvent removed using a rotary evaporator to furnish the amine derivative ligands as oils: *N*-(1-(pyridin-2-yl)ethyl)aniline (**L6.1'**, 95%), 4-methyl-*N*-(1-(pyridin-2-yl)ethyl)aniline (**L6.2'**, 90%), 2,6-dimethyl-*N*-(1-(pyridin-2-yl)ethyl)aniline (**L6.3'**, 98%), 2,6-diisopropyl-*N*-(1-(pyridin-2-yl)ethyl)aniline, (**L6.4'**, 98%), 4-chloro-*N*-(1-(pyridin-2-yl)ethyl)aniline (**L6.5'**, 85%) (Scheme 6.2). The ligands were pure enough to be used for the next step.
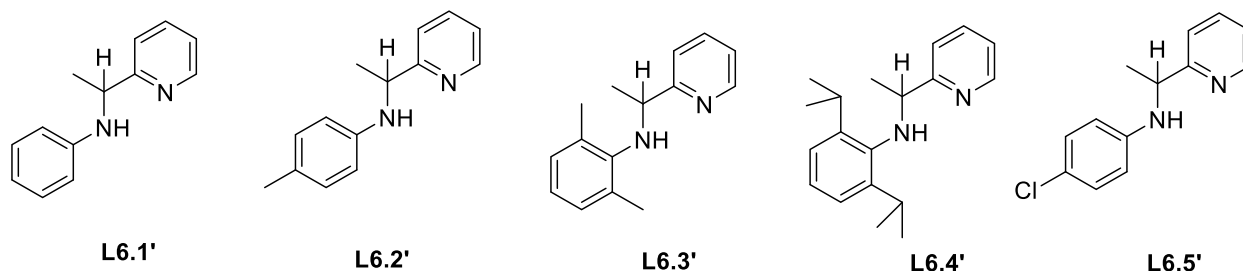
Scheme 6.2: Racemate pyridyl ligands used therein

6.3.2 Synthesis of Zn(II) chlorido complexes

A solution of the respective ligand (1 mmol) either of (**L6.1'** – **L6.5'**) in dry ethanol (10 ml) was added to a solution of $ZnCl_2$ (1 mmol) in dry methanol (10 ml) and stirred for 12 h. The solvent was then removed in *vacuo* to furnish complexes **6.1'** – **6.5'** as solids. In a similar manner complexes **6.3** and **6.4** where synthesised from the imine ligands **L6.3** and **L6.4**, respectively.

6.3.2.1 [Zn(L6.1')Cl₂] (6.1')

Reaction of ligand **L6.1'** (0.5 g, 2.5 mmol) and $ZnCl_2$ (0.30g, 2.5 mmol) gave complex **6.1'** as a pale-yellow powder after workup. Yield 70%. mp 131 °C. ^{1}H-NMR (DMSO-d$_6$, 400 MHz): δ (ppm) 1.37 (s, 3H, N-CCH$_3$), 3.89 (t, $^3J_{H,H}$ = 7.6 Hz, 1H, HC-N), 7.32 (t, $^3J_{H,H}$ = 7.40 Hz, 2H, Ar), 7.42 (t, $^3J_{H,H}$ = 7.5 Hz, 2H, Ar), 7.72 (s, 1H, Ar), 8.11 (t, $^3J_{H,H}$ = 7.64, 2H, Pyr), 8.70 (s, 1H, Pyr), 8.89 (d, $^3J_{H,H}$ = 4.5 Hz 1H, Pyr). ^{13}C-NMR (DMSO-d$_6$, 400 MHz): δ (ppm) 39.4, 121.5, 128.1, 140.4, 147.2, 148.8, 149.2. IR: v (cm^{-1}) 3305(w), 1320(m), 1234(s), 1100(s), 831(w), 453(s). ESI-TOF MS: m/z (%), obtained [M+Na]$^+$ 354.0312, calculated 354. 0398. Anal. calcd for C$_{13}$H$_{14}$Cl$_2$N$_2$Zn: C, 46.67; H, 4.22; N, 8.37. Found: C, 46.48, H, 4.15, N, 8.56.

6.3.2.2 [Zn(L6.2')Cl₂] (6.2')

Reaction of ligand **L6.2'** (0.5 g, 2.4 mmol) and $ZnCl_2$ (0.32g, 2.4 mmol) gave complex **6.2'** as a pale-yellow solid after workup. Yield 68%. mp 143 °C. ^{1}H-NMR (DMSO-d$_6$, 400 MHz): δ (ppm). ^{1}H-NMR (DMSO-d$_6$, 400 MHz): δ (ppm) 1.38 (s, 3H, N-CCH$_3$), 2.12 (s 3H, Ar-CH$_3$), 3.89 (t, 1H, HC-N), 7.02 (t, $^3J_{H,H}$ = 7.36, 1H, Ar), 7.13 (d, $^3J_{H,H}$ = 5.0, 2H, Ar), 7.69 (s, 1H, Pyr), 8.10 (t, $^3J_{H,H}$ = 7.34, 1H, Pyr), 8.23 (s, 1H, Pyr), 8.74 (d, $^3J_{H,H}$ = 4.4, 1H, Pyr). ^{13}C-NMR (DMSO-d$_6$, 400 MHz): δ (ppm) 17.9, 39.4, 124.5, 127.5, 139.4, 148.6, 149.2. IR: v (cm^{-1}) 3298(w), 1268(m),

1229(s), 1104(s), 821(w), 452(s). ESI-TOF MS: m/z (%); obtained [M+Na]$^+$ 384.1100, calculated 384.1112. Anal. calcd for C$_{15}$H$_{18}$Cl$_2$N$_2$Zn: C, 49.69; H, 5.00; N, 7.73. Found: C, 49.48, H, 5.23, N, 7.63.

6.3.2.3   *[Zn(L6.3')Cl$_2$] (6.3')*

Reaction of ligand **L6.3'** (0.5 g, 1.8 mmol) and ZnCl$_2$ (0.24g, 1.8 mmol) gave complex **6.3'** as yellow powder after workup. Yield 76%. mp 142 °C. ^{1}H-NMR (DMSO-d$_6$, 400 MHz): δ (ppm) 1.07 (d, 12H, ^{iPr}CH$_3$), 1.38 (s, 3H, N-CCH$_3$), 2.86 (qn, 2H, CH$_{methine}$), 3.89 (t, 1H, HC-N), 7.13 (t, $^3J_{H,H}$ = 13.4 Hz, 3H, Ar), 8.06 (t, $^3J_{H,H}$ = 7.8, 2H, Pyr), 8.23 (s, 1H, Pyr), 8.74 (d, $^3J_{H,H}$ = 4.5, 1H, Pyr). ^{13}C-NMR (DMSO-d$_6$, 400 MHz): δ (ppm) 22.5, 22.27, 26.6, 27.4, 122.1, 122.9, 124.9, 126.8, 137.1, 138.3. IR: ν (cm^{-1}) 3295(w), 1268(m), 1223(s), 1110(s), 822(w), 455(s). ESI-TOF MS: m/z (%): Obtained [M+Na]$^+$ 440.18, calculated 440.0683. Anal. calcd for C$_{19}$H$_{26}$Cl$_2$N$_2$Zn: C, 54.50; H, 6.26; Cl, N, 6.69. Found: C, 54.68, H, 6.34, N, 6.66.

6.3.2.4   *[Zn(L6.4')Cl$_2$] (6.4')*

Reaction of ligand **L6.4'** (0.5 g, 2.2 mmol) and ZnCl$_2$ (0.30g, 2.2 mmol) gave complex **6.4'** as yellow solid after workup. Yield 67%. mp 128 °C. ^{1}H-NMR (DMSO-d$_6$, 400 MHz): δ (ppm) 1.38 (s, 3H, N-CCH$_3$), 2.29 (s, 3H, Ar-CH$_3$), 3.89 (t, 1H, HC-N), 7.18 (t, $^3J_{H,H}$ = 7.42 Hz, 4H, Ar), 7.82 (s, 1H, Pyr), 8.05 (t, $^3J_{H,H}$ = 5.0 Hz, 1H, Pyr), 8.23 (s ,1H, Pyr), 8.99 (d, $^3J_{H,H}$ = 4.4 Hz, 1H, Pyr). ^{13}C-NMR (DMSO-d$_6$, 400 MHz): δ (ppm) 20.5, 121.3, 126.3, 127.7, 129.26, 140.04, 149.15. IR: ν (cm^{-1}) 3323(w), 1265(m), 1220(s), 1111(s), 820(w), 455(s). ESI-TOF MS: m/z (%); obtained [M+Na]$^+$ 369.2301, calculated 369.2314. Anal. calcd for C$_{14}$H$_{16}$Cl$_2$N$_2$Zn: C, 48.24; H, 4.63; N, 8.04. Found: C, 48.30, H, 4.55, N, 7.90.

6.3.2.5   *[Zn(L6.5')Cl$_2$] (6.5')*

Reaction of ligand **L6.5'** (0.5 g, 2.1 mmol) and ZnCl$_2$ (0.30g, 2.1 mmol) gave complex **6.5'** as a yellow powder after workup. Yield 70%. mp 138 °C. ^{1}H-NMR (DMSO-d$_6$, 400 MHz): δ (ppm) 1.38 (s, 3H, N-CCH$_3$), 3.89 (t, 1H, HC-N), 7.27 (t, $^3J_{H,H}$ = 7.6 Hz, 2H, Ar), 7.35 (t, $^3J_{H,H}$ = 7.4, 2H, Ar), 7.81 (s, 1H, Pyr), 8.02 (t, $^3J_{H,H}$ = 8.0 Hz, 1H, Pyr), 8.17 (s ,1H, Pyr), 8.96 (d, $^3J_{H,H}$ = 5.0 Hz, 1H, Pyr). ^{13}C-NMR (DMSO-d$_6$, 400 MHz): δ (ppm) 115.3, 115.9, 123.4, 127.0, 128.9, 131.8,

137.6, 140.2, 143.5. IR: v (cm^{-1}) 3298(w), 1255(m), 1225(s), 1113(s), 820(w), 453(s). ESI-TOF MS: m/z (%); obtained [M+Na]$^{+}$ 388.9871, calculated 388.9823. Anal. calcd for C$_{13}$H$_{13}$Cl$_{3}$N$_{2}$Zn: C, 42.32; H, 3.55; N, 7.59. Found: C, 42.50, H, 3.57, N, 7.88.

6.4   Polymerization of ε-caprolactone, ʟ-Lactide and *rac*-lactide

All manipulations were performed under an inert atmosphere (argon) using Schlenk techniques. In each reaction, the required amount of ε-CL (bulk) or ʟ/*rac*-LA (in 1 ml toluene) was added to a Schlenk tube and immersed in a preheated oil bath at 110 °C. Polymerization reaction was initiated by adding the required amount of the complex catalyst. Samples for kinetic experiments were withdrawn at regular intervals and quenched quickly by dissolving in pre-cooled CDCl$_3$ in an NMR tube. The quenched samples were then analysed by ^{1}H-NMR spectroscopy to determine the extent of polymerization. For pol(ε-CL), the percentage conversion was obtained by considering signal intensities of ε-CL monomer protons at 4.2 ppm ($I_{4.2}$) and OCH$_2$ protons at 4.0 ppm ($I_{4.0}$) and evaluated using equation (**6.1**).

$$\frac{[Polymer]_t}{[Monomer]_0} \times 100 = \frac{I_{4.0}}{(I_{4.2} + I_{4.0})} \times 100 \qquad (\mathbf{6.1})$$

For poly(LA), the integration values of the methine proton of the monomer and that of the polymer were used to calculate the percentage conversion using the equation (**6.2**).

$$\frac{[Polymer]_t}{[Monomer]_0} \times 100 = \frac{I_{CH\,monomer}}{(I_{CH\,monomer} + I_{CH\,polymer})} \times 100 \qquad (\mathbf{6.2})$$

The observed rate constants were extracted from the slope of the line of best fit, i.e from the ploted graph of ln([M]$_0$/[M]$_t$) *vs t*, where the subscripts denote initial ($_0$) and time (t) concentrations, respectively.

6.5 Copolymerization of ε-caprolactone, ʟ-lactide and *rac*-lactide

In random copolymerization, a mixture of *rac*-LA and ε-CL with LA:CL molar ratios of 2:8, 4:6, 5:5, 6:4 and 8:2 in 5.0 mL of toluene were added into Schleck tubes. The mixtures were equilibrated at 50 °C in an oil bath. The desired amount of catalyst was added with stirring for 10 min. The copolymers were isolated by precipitation and centrifugation in cold ethanol and dried under vacuum at room temperature for 24 h. The method of characterization of copolymers is similar to that described for homopolymers.

6.6 Polymer characterization by size exclusion chromatography (SEC)

Molecular weights and polydispersity indices were determined by size exclusion chromatography (SEC) at Stellenbosch University. The samples were dissolved in tetrahydrofuran (THF) stabilized with butylated hydroxytoluene (BHT) giving a sample with a concentration of 2 mg ml^{-1}. Sample solutions were filtered *via* a syringe through 0.45 mm nylon filters before being subjected to analysis. The SEC instrument consists of a Waters 1515 isocratic HPLC pump, a Waters 717plus auto-sampler, a Waters 600E Paper system controller (run by Breeze Version 3.30 SPA) and a Waters in-line Degasser AF. A Waters 2414 differential refractometer was used at 30 °C in series along with a Waters 2487 dual wavelength absorbance UV/Vis detector operating at variable wavelengths. THF (HPLC grade stabilized with 0.125% BHT) was used as the eluent at flow rates of 1 ml min^{-1}. The temperature of the column oven was kept at 30 °C and the injection volume was 100 ml. Two PLgel (Polymer Laboratories) 5 mm Mixed-C (300 x 7.5 mm) columns and a pre-column (PLgel 5 mm Guard, 50 x 7.5 mm) were used. Calibration was done using narrow poly-styrene standards ranging from 580 to 2 x 10^6 g mol^{-1}. All molecular weights were reported as polystyrene equivalents.

6.7 Single-crystal X-ray diffraction

Crystal evaluation and data collection was done on a Bruker Smart APEXII diffractometer with Mo Kα radiation (I = 0.71073 Å) equipped with an Oxford Cryostream low temperature apparatus operating at 100 K for all samples. Reflections were collected at different starting angles and the *APEX*II program suite was used to index the reflections.[20] Data reduction was performed using the *SAINT*[21] software and the scaling and absorption corrections were applied using the *SADABS*[22]

multi-scan technique. The structures were solved by the direct methods using the *SHELXS* program and refined using *SHELXL* program.[23] Graphics of the crystal structures were drawn using OLEX^2 software.[24] Non-hydrogen atoms were first refined isotropically and then anisotropically with the full-matrix least squares method based on F^2 using *SHELXL.*[23] The crystallographic data and structure refinement parameters for the complexes **6.3** and **6.4** are given in Table 6.1.

Table 6.1: The summary of X-ray crystal data collection and structure refinement parameters for complexes **6.3** and **6.4**

Parameter	**6.3**	**6.4**
Empirical formula	$C_{15}H_{16}Cl_2N_2Zn$	$C_{19}H_{24}Cl_2N_2Zn$
Formula weight	360.57	416.67
T(K)	100(2)	100(2)
λ(Å)	0.71073	0.71073
Crystal system	Monoclinic	Triclinic
Space group	$P2_1/n$	$P\bar{1}$
a (Å)	9.0406(2)	8.2991(2)
b (Å)	11.5935(3)	9.9301(2)
c (Å)	14.9783(4)	12.4125(3)
a, β, γ (°)	90, 91.5480(10), 90	81.2750(10), 85.409(2),74.258(3)
V (Å^3)	1569.34(7)	972.35(4)
Z	4	2
ρ_{calc} (mg/m^3)	1.526	1.423
μ (mm-1)	1.896	1.540
F(000)	736	432
Crystal size (mm)	0.320 x 0.240 x 0.130	0.210 x 0.120 x 0.080
θ range for data collection (°)	2.222 to 27.556	1.661 to 27.587
Index ranges	$-11 \leq h \leq 11$	$-10 \leq h \leq 10$
	$-15 \leq k \leq 9$	$-12 \leq k \leq 12$
	$-19 \leq l \leq 19$	$-16 \leq l \leq 16$
Reflections collected	12007	14316
Independent reflections	3619 [R(int) = 0.0260]	4449 [R(int) = 0.0176]

Completeness to theta = 25.24° (%)	100.0	99.5
Data/restraints/parameters	3619/0/184	4449/0/222
Goodness-of-fit (GOF) on $F2$	1.031	1.051
Final R indices [$I > 2\sigma(I)$]	$R_1 = 0.0242$, $wR_2 = 0.0554$	$R_1 = 0.0206$, $wR_2 = 0.0515$
R indices (all data)	$R_1 = 0.0312$, $wR_2 = 0.0581$	$R_1 = 0.0229$, $wR_2 = 0.0524$
Largest diff. peak and hole (e Å^{-3})	0.331 and -0.281	0.371 and -0.198

6.8   Results and discussion

6.8.1   Synthesis of amine ligands and their corresponding Zn(II) complexes

The *N,N'*-bidentate amine ligands **L6.1'** – **L6.5'** were obtained from the reduction of the corresponding imine analogues, **L6.1** – **L6.5**.   The imine derivatives were synthesised by condensation of 2-acetypyridine and the respective amines *via* monowave assisted radiation affording the products within 10 min and in excellent yields.

L6.1: R$_1$ = R$_2$ = H
L6.2: R$_1$ = H, R$_2$ = CH$_3$
L6.3: R$_1$ = 2,6-Me, R$_2$= H
L6.4: R$_1$ = 2,6-^{i}Pr R$_2$ = H
L6.5: R$_1$ = H, R$_2$ = Cl

L6.1′: R$_1$ = R$_2$ = H
L6.2′: R$_1$ = H, R$_2$ = CH$_3$
L6.3′: R$_1$ = 2,6-Me, R$_2$= H
L6.4′: R$_1$ = 2,6-^{i}Pr R$_2$ = H
L6.5′: R$_1$ = H, R$_2$ = Cl
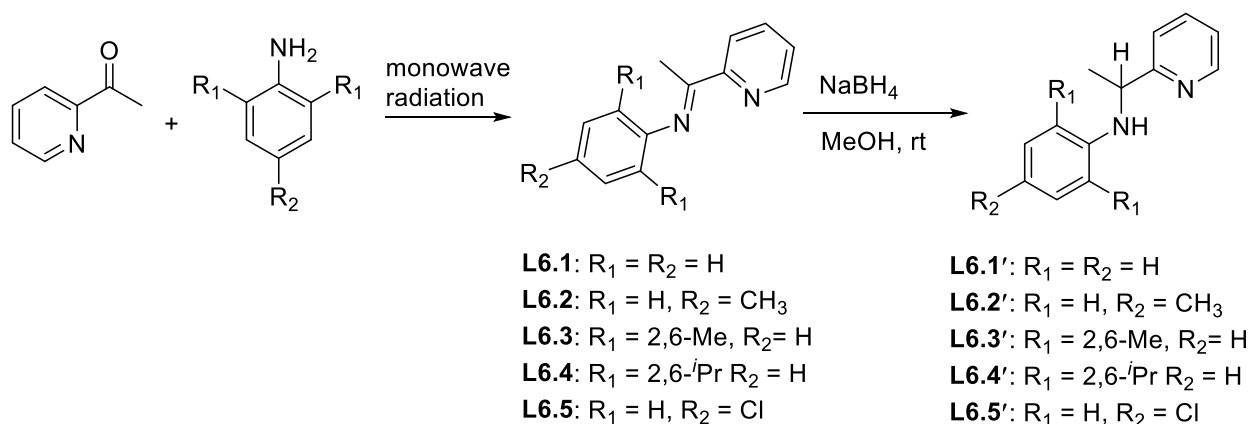
Scheme 6.3: Synthesis of *N,N'*-bidentate *N*-(pyridin-2-ylethyl)aniline ligands

The disappearance of the C=N frequency, around 1633 cm^{-1}, and the emergence of the N—H and C—N peaks at *ca* 3300 and 1258 cm^{-1}, respectively, signified the formation of the amine ligands. Representative ^{1}H-NMR spectra comparing **L6.1** with **L6.1'** are shown in Figure 6.1. Two new resonance peaks at 4.3 and 4.7 ppm due to H$_b$ and H$_a$ confirmed the formation of **L6.1** through the reduction of **L6.1'**.
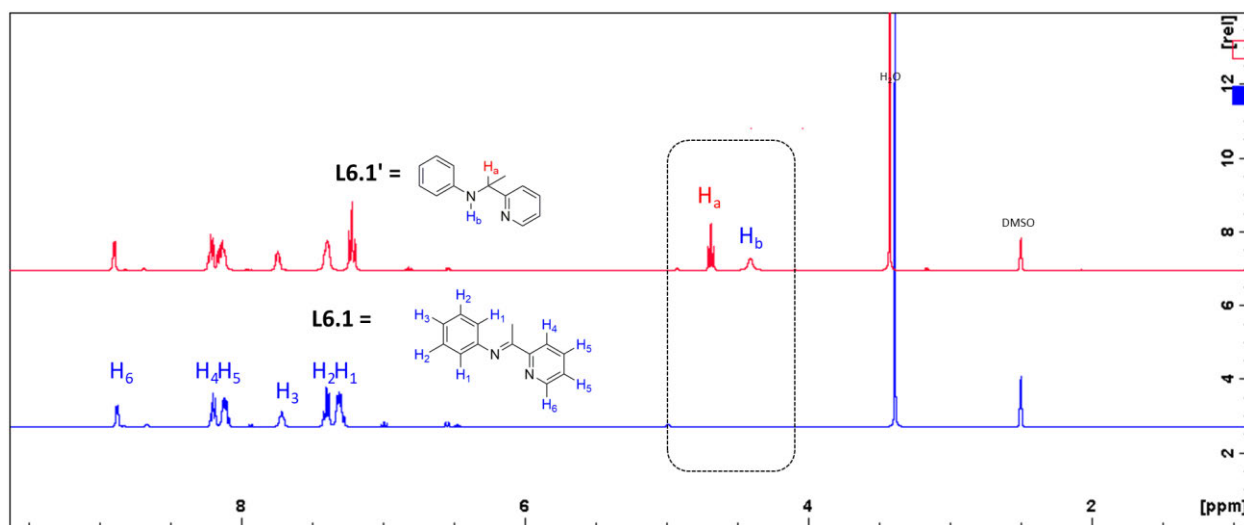
Figure 6.1: ^{1}H-NMR spectra of **L6.1** and **L6.1'** at room temperature in DMSO-d$_6$ (400 MHz)

Reaction of **L6.1'** – **L6.5'** with ZnCl$_2$ in methanol furnished mononuclear zinc complexes, Zn(**L6.1'**)Cl$_2$ (**6.1'**), Zn(**L6.2'**)Cl$_2$ (**6.2'**), Zn(**L6.3'**)Cl$_2$ (**6.3'**), Zn(**L6.4'**)Cl$_2$ (**6.4'**) and Zn(**L6.5'**)Cl$_2$ (**6.5'**) as yellow solids in moderate yields between 55 – 65 % (Scheme 6.4). Complexes **6.3** and **6.4** were also synthesised from the imine ligands **L6.3** and **L6.4**, respectively, and were later used for comparative purposes in catalysis because their crystal structures were fully established (*vide infra*).
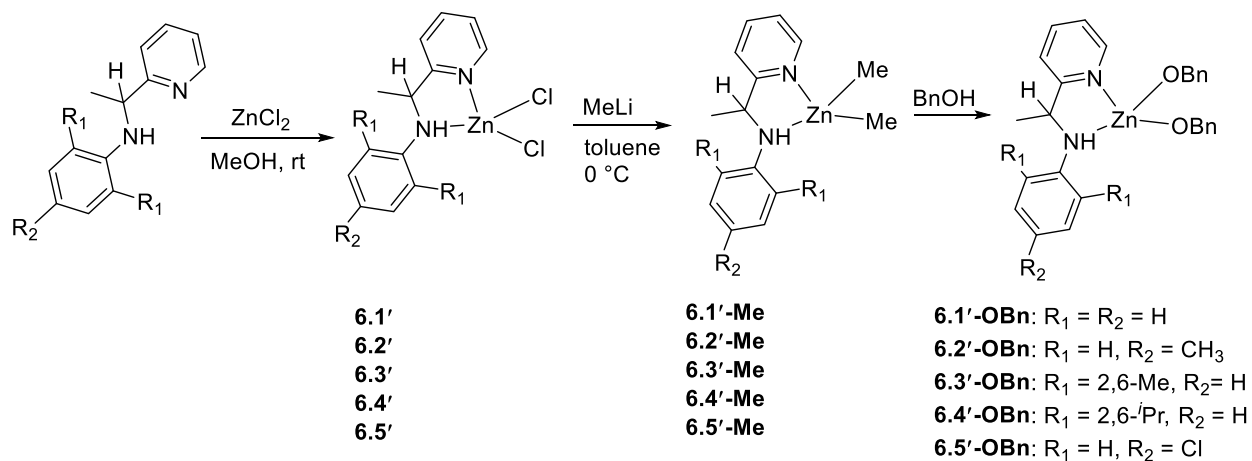
Scheme 6.4: Synthesis of chlorido Zn(II) amine complexes and *in-situ* generated alkyl and alkoxy derivatives

The proposed metal to ligand stoichiometry ratio (1:1) of the chlorido complexes of the form [M(**Ln'**)Cl$_2$] was confirmed by elemental analysis data. The stoichiometry was further corroborated by mass spectrometry. For example, complex **6.1'** showed a base peak at *m/z* 354.6712 which corresponds to a complex-sodium adduct [Zn(**L6.1'**)Cl$_2$+Na]$^+$ (Figure 6.2). Similar results were also obtained for other complexes **6**.**2'** – **6.5'** (see appendix D).
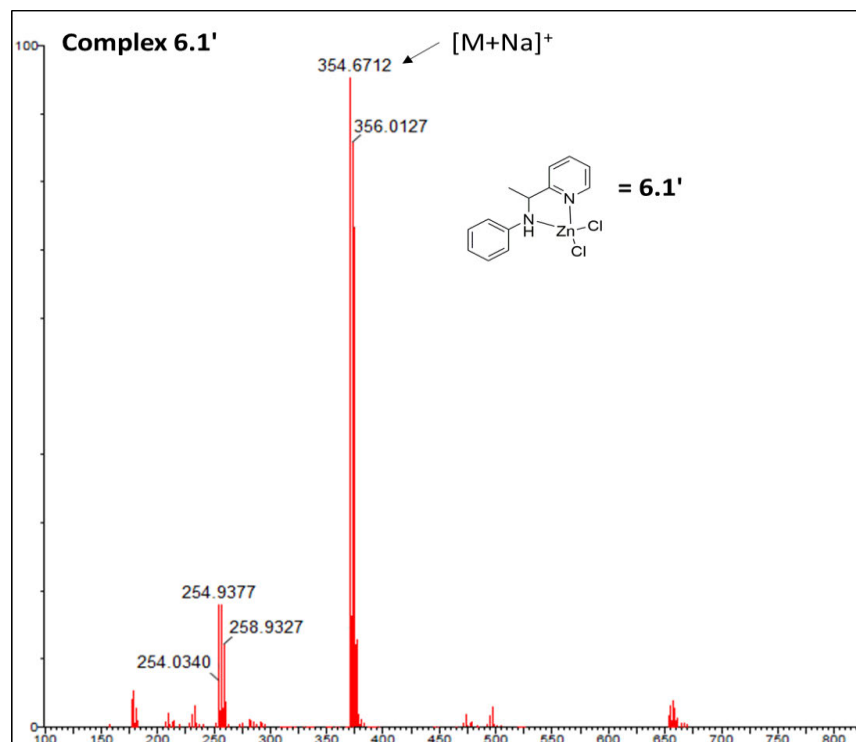
Figure 6.2: ESI-MS spectrum for complex **6.1'**

The catalytic active species **6.1'-OBn** – **6.5'-OBn** were generated *in situ* first by reacting the Zn(II) chlorido derivatives with methyllithium with subsequent addition of benzyl alcohol. The formation of the alkoxy species was confirmed by mass spectrometry. For instance, complex **6.1'-OBn** showed ion peaks at *m/z* 502.1 and 975.0 which correspond to the mononuclear complex-sodium adduct [**Zn**(**L6.1'-OBn**)+Na]$^+$ and the bridged bimetallic derivative, [**Zn**(**L6.1'-OBn**)]$_2$Na$^+$, respectively, (Figure 6.3). Attempts to isolate and analyse the methyl derivatives **6.1'-Me** – **6.5'-Me** were futile as they were unstable in air.
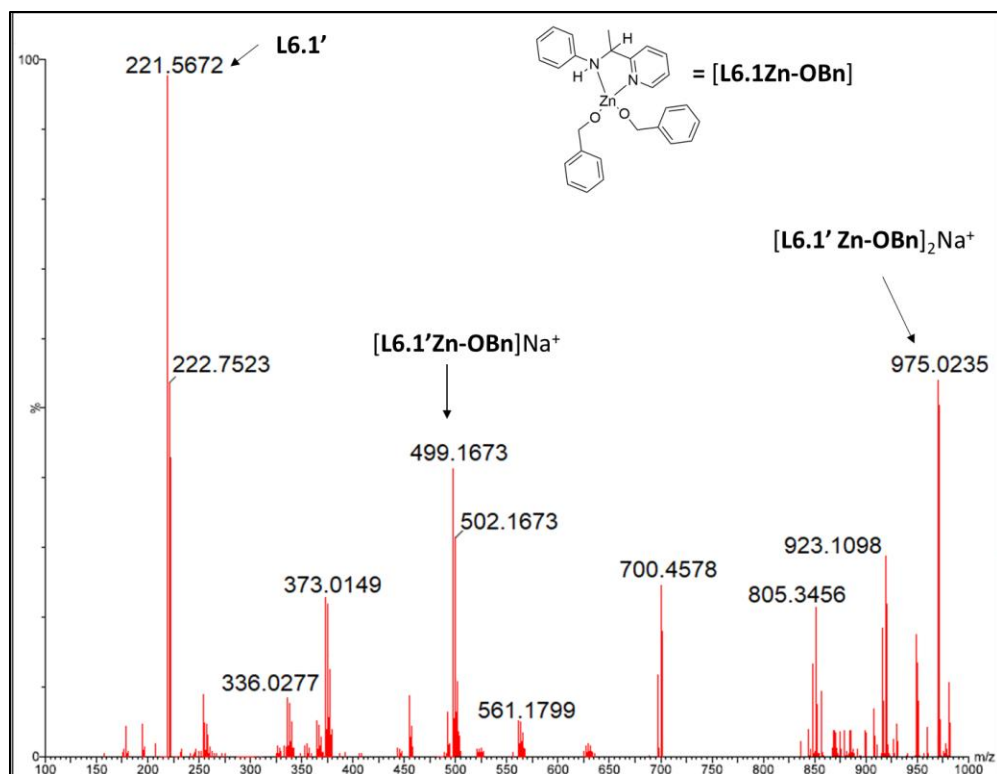
Figure 6.3: ESI-MS spectrum for complex **6.1'-OBn**

6.8.2   IR and NMR spectroscopy analysis of complexes

The complexes were further characterised by NMR and FT-IR spectroscopies. The infrared spectra of the Zn(II) complexes were comparable to those of corresponding ligands with minor shifts. Typical N-H stretching frequency of ligands in the IR spectra were detected in range 3333 - 3398 cm^{-1}, which are shifted to 3262 - 3299 cm^{-1} in complexes **6.1'** – **6.5'**. A new stretching frequency between 543 and 554 cm^{-1} assigned to Zn—N bond was also observed for the synthesised complexes.

The ^{1}H- and ^{13}C-NMR spectra were recorded in DMSO-d$_6$ at room temperature. Representative ^{1}H- and ^{13}C-NMR spectra for complex **6.3'** are given in Figure 6.4 and 6.5, respectively. Coordination of the metal centre did not induce a significant proton shift in the complexes with respect to free ligands. However, a notable shift was observed for the pyridine α-protons resonances in the complexes which were moved downfield due dishielding by the coordinated Zn(II) metal centre.

The resonance of the amine proton is broadened because it interacts with the metal. The ^{13}C-NMR spectrum (Figure 6.5) reviewed that the methine carbon signal was shifted to higher frequency in the complex due to increased ring strain induced upon coordinating to the zinc metal. The ^{1}H- and ^{13}C-NMR spectra for complexes **5.2** – **5.5** are given in appendix D.
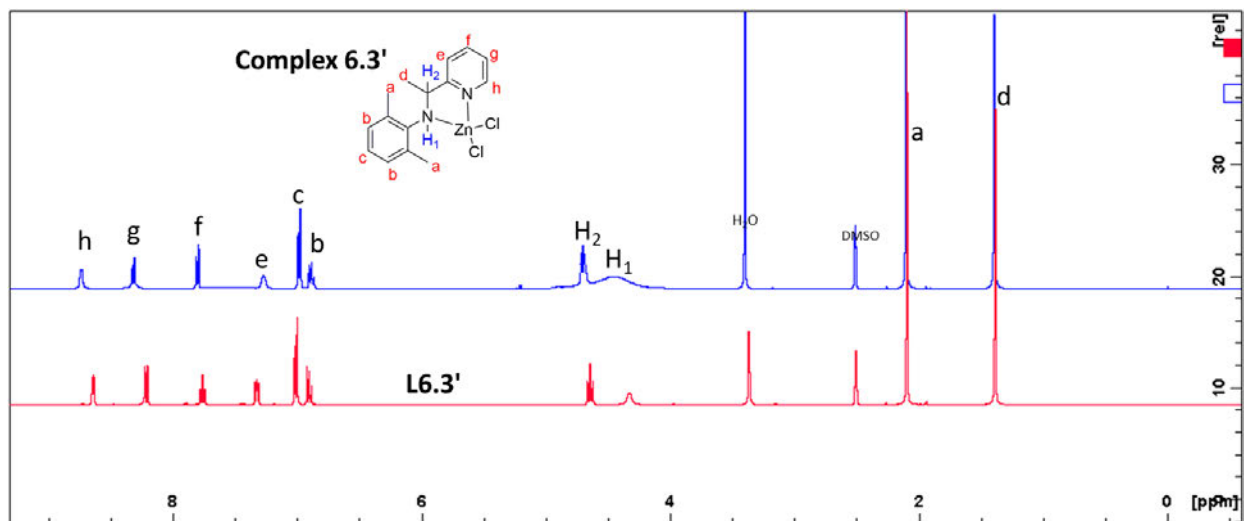
Figure 6.4: H^{1}-NMR spectra of **L6.3'** and complex **6.3'** at room temperature in DMSO-d$_6$ (400 MHz)
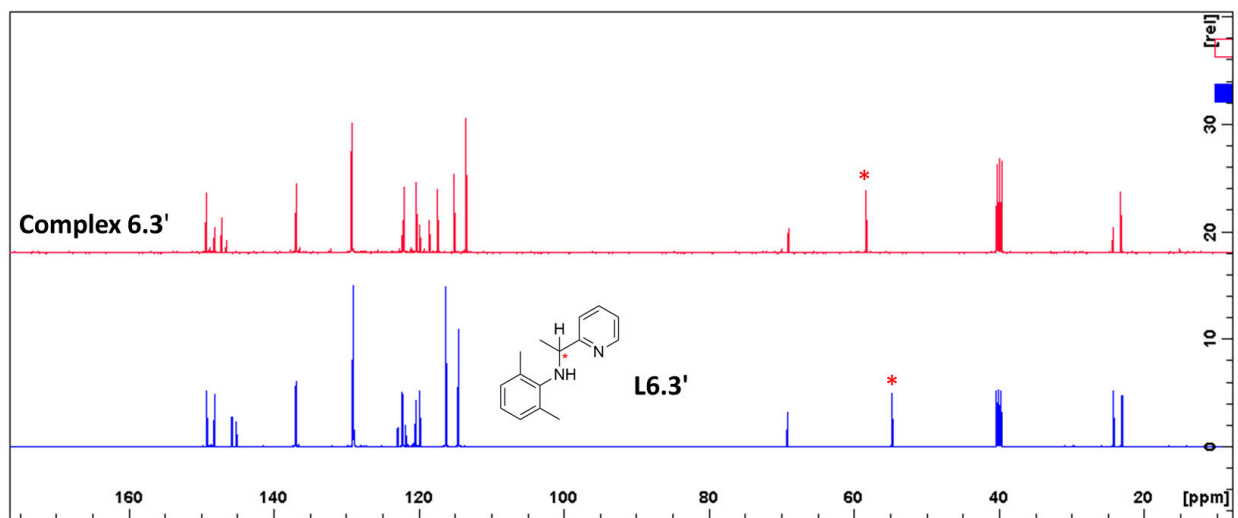
Figure 6.5: ^{13}C-NMR spectrum of complex **6.3'** at room temperature in DMSO-d$_6$ (400 MHz)

The formation of the alkoxy species was confirmed by variable temperature (VT) ^{1}H-NMR analysis of the isolated *in-situ* generated complex **6.4'-OBn**. The spectra were run between -40 to 40 °C with an increment of 10 °C. In addition to ligands signals, methylene and aromatic extra peaks at 4.85 and 7.50 ppm due the benzoyl groups were observed (Figure 6.6a). Signals due to the free ligand were not observed ruling out ligand displacement from the metal sphere. A closer look at expanded spectra region between 4.6 to 4.9 ppm showed that the methylene proton signal remains a singlet as the system is cooled and only shifted toward low frequency (Figure 6.6b). This behaviour points to the formation of mono-nuclear species in solution rather than binuclear species. The formation of binuclear species would imply that one of the benzyl alkoxyl group would bridge the two metals causing the signal to appear as a doublet.
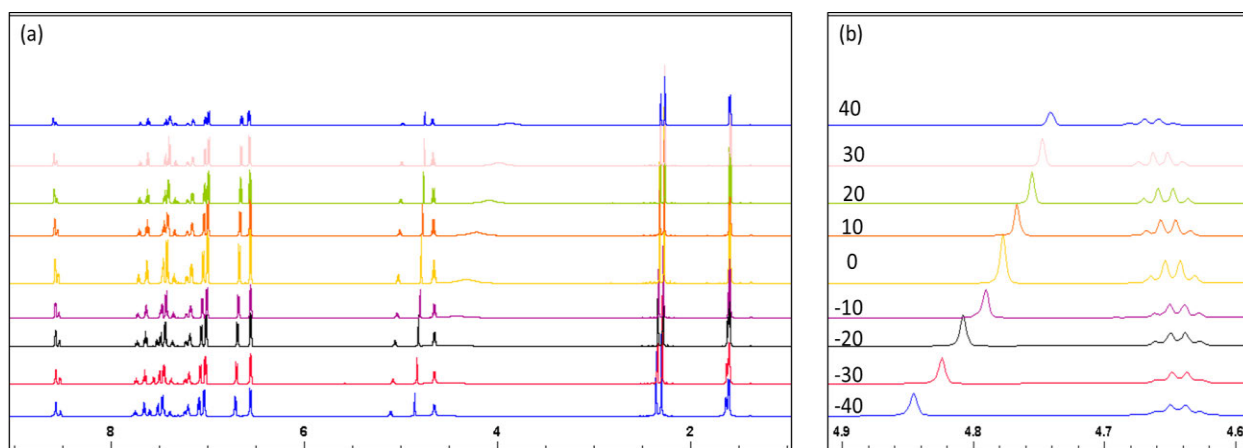
Figure 6.6: (a) VT H^1-NMR spectrum of complex **6.4'-OBn** and (b) expanded region in CDCl$_3$ (400 Hz)

6.8.3   Molecular structures of complexes

Crystal structures of complexes **6.3** and **6.4**, the imine analogues of **6.3'** and **6.4'** were obtained by slow evaporation of acetonitrile complex solutions. The molecular structures are shown in Figure 6.7. Complex **6.3** is known[25] and will not be discussed. The asymmetric unit of complex **6.4** is comprised of one complex molecule. The Zn(II) metal centre has a tetrahedral geometry formed by ligand nitrogens and two auxiliary chloro atoms. The ZnN$_2$C$_2$ chelate ring plane is almost perpendicular to the metal chloro plane. The N—Zn—N and Cl—Zn—Cl cone angles are 79.18(4)° and 115.464(14)°, respectively. The N—Zn—Cl bond angles lie between 110.40 (3)°

and 119.01 (3)°. The average bond distance of Zn—N$_{py}$ (2.0610 (11) Å) is comparable to that of Zn—N$_{imine}$ (2.0801(11) Å) and the Zn—Cl bond (2.1830 (4) Å). Similar bond distances have been observed in related Zn(II) complexes.[25]

In the crystal structure the molecules extent into a chain *via* head-to-head H···Cl interactions in the range 2.523 to 2.764 Å between adjacent molecules. The interactions are less than the sum of the hydrogen and chloro van der Waals radii. The C—H···Cl angle of 152 (2)° deviates from linearity pointing to weak interactions.
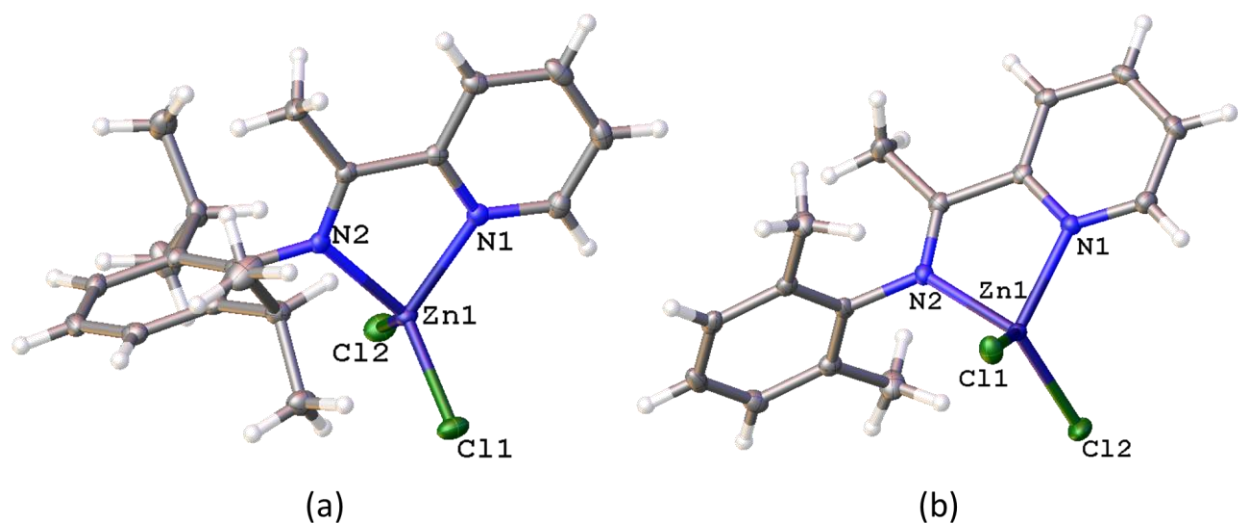
Figure 6.7: X-ray crystal structures (a) complex **6.3** with thermal ellipsoids drawn at 50% probability level and (b) complex **6.4** with thermal ellipsoids drawn at 50% probability level. Hydrogen atoms have been omitted for clarity

6.8.4 *Polymerization of ε-caprolactone and L/rac-lactide*

Initial studies were done by studying the catalytic activity of the *in-situ* generated Zn(II) alkyl complexes in ROP of ε-CL. Reaction of complexes **6.1'** – **6.5'** with two molar equivalence of methyl lithium (MeLi) in tetrahydrofuran or toluene resulted in alkyl Zn(II) complexes of **6.1'-Me** – **6.5'-Me**. These complexes were used without isolation for ROP of ε-CL and they showed high catalytic activity achieving complete monomer conversion within 4 min at room temperature.

The reaction rates were reduced at lower temperatures because of increased energy barrier. Reduced reaction rates due to lower temperatures in expected and has been observed in similar zinc complexes as well as other systems reported in literature.[26,27] On testing the imine derivatives **6.3-Me** and **6.4-Me**, no significant differences was observed on reactivity and as such no further studies using the two were done regarding ROP of ε-CL. The polymerization data for **6.1'-Me** – **6.5'-Me** is presented in Table 6.2.

Table 6.2: Summary of polymerization data of ε-CL catalysed by complexes **6.1'-Me – 6.5'-Me**

Entry	Complex	Solvent	Temp °C	Time (min)	[b]Conv (%)	[c]M_w (NMR)	[d]M_w (calc)	k_{app} (min^{-1})
1	**6.1'-Me**	Toluene	25	>4	97	5918	11166	-
2	**6.2'-Me**	Toluene	25	>4	97	6503	11166	-
3	**6.3'-Me**	Toluene	25	>4	99	3924	11394	-
4	**6.4'-Me**	Toluene	25	>4	99	3621	11394	-
5	**6.5'-Me**	Toluene	25	>4	98	4002	11280	-
6	**6.1'-Me**	THF	25	>4	99	5021	11394	-
7	**6.1'-Me**	Toluene	0	100	99	7456	11394	
8	**6.2'-Me**	Toluene	0	120	98	7556	11280	0.0451
9	**6.1'-Me**	Toluene	0	135	99	5623	11394	0.0301
10	**6.2'-Me**	Toluene	0	150	98	5186	10596	0.0102
11	**6.3'-Me**	Toluene	0	170	97	5034	11166	0.0089
12	**6.4'-Me**	THF	0	280	98	4923	11280	0.0421

[a]Polymerization conditions: $[M]_0:[I]_0 = 100:1$. [b,c]Determined from NMR. [d]Calculated theoretical M_w.

Polymerization studies were further extended by carrying out the polymerization in the presence of two molar equivalents of benzyl alcohol co-initiator. As expected the *in-situ* generated alkoxy complexes exhibited excellent catalytic activity realising 99% monomer conversion in less than 1 min at room temperature. This trend is typical of alkoxy species, which have proven to be relatively more effective ROP initiators.[27-29] In addition, no clear difference in activity with respect to ligand substituents effect was noticed due to fast reactivity rates . The summary of polymerization results complexes **6.1'-OBn – 6.5'-OBn** is listed in Table 6.3.

Table 6.3: Summary of polymerization data of ε-CL catalysed by complexes **6.1'-OBn – 6.5'-OBn**

Entry	Complex	Solvent	Temp °C	Time (min)	[b]Conv (%)	[c]M_w (NMR)	[d]M_w (calc)	k_{app} (min^{-1})
1	**6.1'-OBn**	Toluene	25	>1	99	6984	11394	-
2	**6.2'-OBn**	Toluene	25	>1	97	6124	11166	-
3	**6.3'-OBn**	Toluene	25	>1	99	5173	11394	-
4	**6.4'-OBn**	Toluene	25	>1	98	3893	11280	-
5	**6.5'-OBn**	Toluene	25	>1	98	4645	11280	-
6	**6.1'-OBn**	THF	25	>1	99	4123	11394	
7	**6.1'-OBn**	Toluene	0	70	99	8295	11394	0.0683
8	**6.2'-OBn**	Toluene	0	80	98	7823	11280	0.0613
9	**6.3'-OBn**	Toluene	0	92	99	6246	11394	0.0488
10	**6.4'-OBn**	Toluene	0	100	98	5617	10596	0.0426
11	**6.5'-OBn**	Toluene	0	120	97	4372	11166	0.0234

[a]Polymerization conditions: $[M]_0:[I]_0 = 100:1$. [b,c]Determined from NMR. [d]Calculated theoretical M_w.

Complex **6.3'-OBn** was chosen randomly to investigate the effect of changing the monomer to catalyst mole ratio and temperature (Table 6.4). Although, there was a decline in catalytic activity with a decrease in temperature, the initiators remained active in temperature range of 0 – 25 °C. The activity reduced with a decrease in catalyst concentration. Generally, the reactivity behaviour and trends are in tandem with reported work by Li *et al*[27] and Nayab *et al*.[30,31] Using a similar approach, the authors reported very high catalytic activities using *N,N′* type ligands. Of interest is the higher activity of copper complexes reported by Ahn *et al*[28] which usually display low catalytic activity, achieved complete monomer conversion within seven min.

Table 6.4: Polymerization of ε-CL, ʟ-LA and *rac*-LA by catalysed by complex **6.3'-OBn**

Entry	Variable	[M/I]	Time (h)	[a]Conv (%)	[b]M_w (calc)	[c]M_w (NMR)	[d]M_w (GPC)	[e]PDI	k_{app} (min^{-1})
1	ε-CL	100:1	92	99	11394	6246	3096	1.7	0.0488
2	ε-CL	200:1	150	98	16866	7273	3639	1.7	0.0389
3	ε-CL	300:1	220	99	22680	8013	4189	1.9	0.0232
4	ε-CL	400:1	315	98	33624	1223	8837	1.9	0.0116
5	*rac*-LA	100:1	160	98	14230	7853	5530	1.8	0.0319
6	ʟ-LA	100:1	180	99	14364	8102	4413	1.7	0.0192

[a]Polymerization conditions: Solvent: toluene, 0 °C. [a,c]Determined from NMR. [b]Calculated theoretical Mw. [d,e]Determined by GPC relative to polystyrene standards in THF. [d]Experimental M_w was calculated considering Mark–Houwink's corrections of 0.56.

6.8.5 *Molecular weights and molecular weight distribution of polymers*

The molecular weight and molecular weight distribution of the polymers obtained were determined by GPC and compared with the theoretical values calculated from ^{1}H NMR spectra. Relatively low molecular weight polymers which are comparable for both methyl and alkoxy complexes were produced. For example, complexes **6.2'-Me** and **6.2'-OBn** gave polymers with molecular weights of 6503 and 6984 g mol^{-1}, respectively. The difference can be accounted by the fact that alkoxy complexes control the polymerization process.[32] The calculated molecular weights of the polymers obtained were higher than the experimental values from NMR and GPC analysis. The deviation between calculated and observed molecular weights can be attributed to intermolecular transesterification chain transfer reactions (*vide infra)* which prematurely terminates the reactions without chains reaching maximum length. The difference can also be explained on the fundamental principle of analysis of the two methods. In GPC polymers are analysed after separation based on hydrodynamic volume which depends on polymer architecture thus, it underestimates the actual molecular weights.[33]

A small increase in molecular weights was also observed as the monomer concentration was increased (Table 6.4). Changing the monomer-to-initiator ratio from 100:1 to 400:1, for complex **6.3'-OBn**, the $M_{w(GPC)}$ of poly(ε-CL) improved from 3096 to 8837 g mol^{-1}. This trend is normal as there are less polymer chains propagating per initiating species hence, greater molecular weights are obtained from few growing chains. Ligands substitution effects were not expressed in the molecular weights trends as shown by minor disparity in $M_{w(NMR)}$ among the catalytic species (Table 6.4). The molecular weight distributions (M_n/M_w) are slightly broader *ca.* 2 which suggests a less controlled polymerization process.

6.8.6 *Kinetics of homo- and co-polymerization ROP reactions of ε-CL, ʟ-Lactide and rac-LA*

The kinetics of polymerization was studied by monitoring ^{1}H-NMR spectra of periodically sampled aliquots until conversion was almost complete. The percentage conversions of each monomer were determined by comparing the relative peak intensities of monomer and polymer, respectively. Kinetic studies to determine the reliance of reaction rates of the *in-situ* generated alkoxy catalytic species in ROP reaction was systematically carried out with a monomer-to-catalyst ratio of 100:1 at 0 °C. The apparent rate constant (k_{app}) for each complex was obtained from the slope of ln($[M]_0/[M]_t$) *vs t* plots (Figure 6.8). For both cases *pseudo* first-order kinetic dependency in monomer conversion was observed as shown by the linear plots in Figure 6.8. Thus, the kinetics can be described using equation **6.3**,

$$-\frac{d[M]}{dt} = k[M] \qquad (6.3)$$

where $k = k_p[I]^x$; k_p = rate of chai n propagation and I = initiator/catalyst and x = order of reaction.
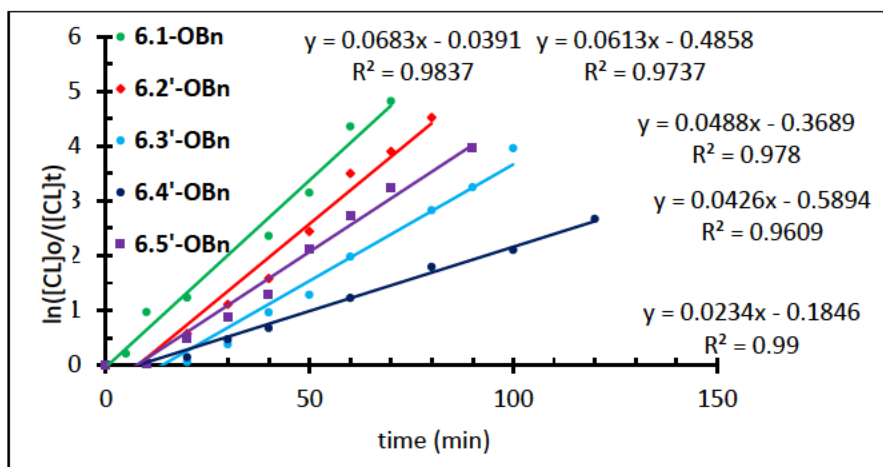
Figure 6.8: Plots of $\ln([CL]_0/[CL]t)$ *vs t* catalysed by complexes **6.1'-OBn – 6.5'-OBn**. Reaction conditions: $[M]_0 = 200:1$. Solvent: toluene, $T = 0\ °C$

Generally, the alkyl species exhibited inferior activity compared to the alkoxy series, for instance complex **6.5'-Me** gave an apparent rate constant of 0.0812 min^{-1} in comparison to **6.5'-OBn** with an apparent rate constant of 0.234 min^{-1}. There are possibly two factors that might cause this observation. Firstly, the alkoxy catalytic species possess less nucleophilic M—C bond in relation to M—O bond, and secondly, the low stability of alkyl species in solution which cause early catalyst death.[34] The rates were dependent on the solvent used where, higher rates were observed in toluene in comparison to THF. The variation in the rates can be alluded to competing tendency of THF with the monomer for the metal centre thereby inhibiting monomer coordination.

The polymerization at low temperature was influenced by ligand substitution. The polymerization data reveal that complex **6.1'-Me** and **6.1'-OBn** without substituents were the most active giving apparent rate constant (k_{app}) values of 0.0331 and 0.0683 min^{-1}, respectively. Steric crowding around the metal centre resulted in reduced rates, for example complexes **6.4'-OBn** with isopropyl substituents gave k_{app} of 0.0488 min^{-1} a drop by factor of 1.3 compared to the most active unsubstituted complex **6.1'-OBn** (k_{app} = 0.068 min^{-1}). A similar observation was also reported by Sun *et al*[18] using Al-bimetallic Schiff base complexes. Generally, bulky substituents are known to inhibit monomer coordination resulting in reduced polymerization rates.[35] The *p*-chloro substituted complex **6.5'-OBn** was the least active achieving apparent rate constant k_{app} value of 0.0426 min^{-1}.

181

The electron withdrawing effect reduces the electron density at the metal centre hence, diminishing the monomer affinity for the catalyst resulting in inferior activity. A similar observation was also reported by Rezayee et al[36], while an opposite trend was also noticed by Cho et al.[37]

The ROP kinetic investigations of L-LA and *rac*-LA were carried out using **6.3'-Me** and **6.3'-OBn**. The linearity of semilogarithmic plots of ln([M]/[M]$_t$) *vs* t (Figure 6.9) revealed that both polymerizations followed *pseudo*-first order reliance on the monomer concentration. For both catalyst the polymerization rates were comparable for both monomers although L-LA conversion was greater than that of *rac*-LA. For example, complex **6.3'-OBn** the reaction rate of L-LA (k_{app} = 0.0319 min^{-1}) was greater than that of *rac*-LA (k_{app} = 0.0192 min^{-1}) although less for ε-CL (k_{app} = 0.0613 min^{-1}) under similar conditions.

The difference rates for *rac*-LA and L-LA were presumed to be due to stereo-selectivity tendency of the zinc catalyst a trend also reported in literature.[38] The higher catalytic activities of the system toward polymerization of ε-CL than *rac*-LA and L-LA makes it a good candidate for LA/CL copolymerization.[39]
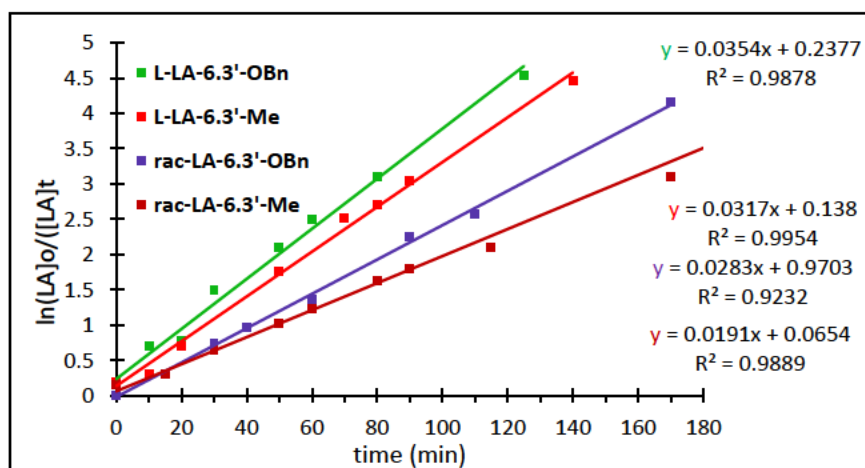
Figure 6.9: Plots of ln([LA]$_0$/[LA]$_t$) *vs* t for lactides homo- and co-polymerization catalysed by complexes **6.3'-Me** and **6.3'-OBn**. Reaction conditions: [M]$_0$:[I]$_0$ = 100. Solvent: toluene, T = 0 °C

To elucidate ROP order with respect to the complex **6.4'-OBn**, 100 equivalent of monomer was used while the catalyst molar ratio was varied from 1 to 5. The logarithmic linear plots of $\ln(k_{app})$ *vs* $\ln[\textbf{6.4'-OBn}]_0$ (Figure 6.10) gave a slope *ca.* 1.0 indicative of first order dependence on catalyst concentration which is consistent with other metal complex catalyst reported in literature.[18,40] The overall rate equation can thus be written as shown in equation (**6.4**).

$$R_p = \frac{d[\text{CL}]}{dt} = k_p[\text{CL}]^1[\textbf{6.4'} - \textbf{OBn}]^1 \qquad (\textbf{6.4})$$
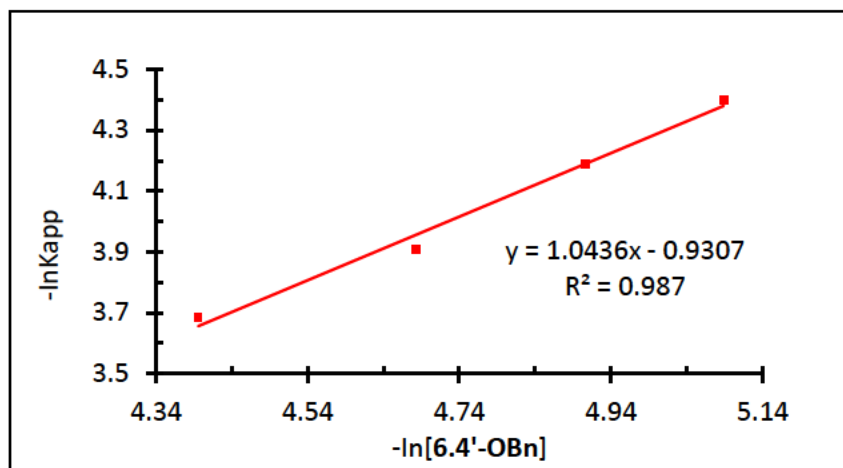
Figure 6.10: Plot of $\ln k_{app}$ vs $\ln[\textbf{6.4'-OBn}]$ for the determination of order of reaction with respect to catalyst

Kinetic experiments were also done to evaluate the copolymerization behaviour of the cyclic ester monomers. The semilogarithmic relationship of $\ln([\text{M}]_0/[\text{M}]_t)$ *vs* t are shown in Figure 6.11. The copolymerization reaction is also defined by *pseudo*-first-order kinetics for both monomers as depicted by the linearity of the plots. However, the polymerization rates were reversed as the presence of LA repressed the incorporation of ε-CL. Two propagation rates were observed for ε-CL (Figure 6.1) with the first section defining low monomer consumption which only increase after the complete conversion of LA in the second stage. After 3 h about 78% LA monomer was converted to polymer with only 23% in case of ε-CL. However, such a manifestation is common in binary CL/LA random copolymerization and has been reported in the literature.[18]
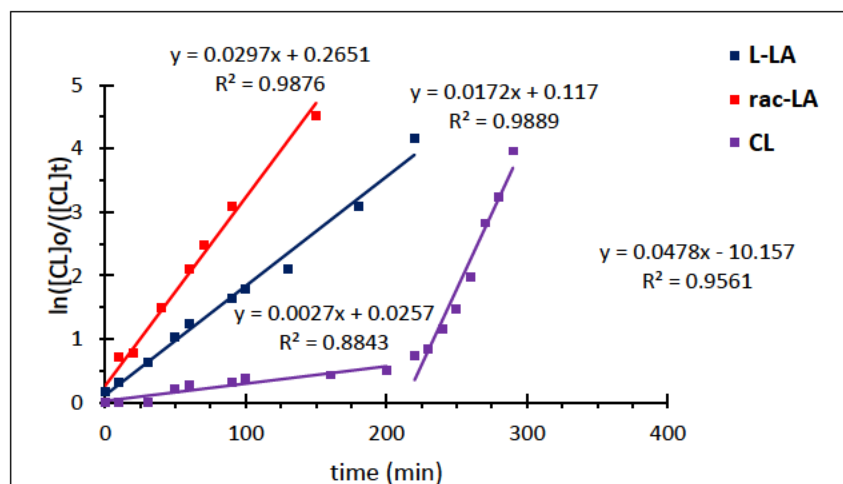
Figure 6.11: Plots of $\ln([M]_0/[M]_t)$ *vs* t for random copolymerization of ε-CL and LAs catalysed by complex **6.3'-OBn**. Reaction conditions: $[M]_0:[I]_0 = 100:1$ Solvent: toluene, T = 0 °C

6.8.7 Copolymerization

6.8.8 Block copolymer synthesis

Complex **6.2'-OBn** was randomly chosen for sequential co-polymerization of ε-CL and L-LA. Firstly, the PCL-b-PLLA block copolymer was synthesized by sequential ROP of ε-CL first followed by addition of L-LA using a catalyst to monomer ratio of 1:100 in toluene at 50 °C. Secondly, the same monomer addition was repeated without a solvent (bulk/melt polymerization) at 100 °C. The copolymerization data is presented in Table 6.5. However, reversing the order of monomer addition did not yield any PLA-b-PCL copolymer. This behaviour has been reported in literature,[14,39,41] and it is attributed to the greater initiation efficiency of the PCL prepolymer probably due to the resting position of the catalyst after consumption of the first monomer.[42] Characterization of the copolymers was done using ^{1}H- and ^{13}C-NMR spectroscopy as shown in Figure 6.12 and 6.13.

184

Table 6.5: Homo and sequential copolymerization of ε-CL, L-LA and *rac*-LA

Entry	Mono/Diblock	$^cM_{w(calc)}$	$^dM_{w(NMR)}$
[a]1	PCL	11394	4198
[a]2	PCL-b-PLA	25264	6967
[b]3	PCL	11394	4098
[b]4	PCL-b-PLA	25264	6222

Polymerization conditions: 50 °C, Solvent: [a]Toluene, [b]Bulk/melt, $[M]_0:[I]_0 = 100:1$. [c]Calculated theoretical M_w. [c]Determined from NMR.

The characteristic homo-polymer methylene proton (HOCH$_2$-O-) signal at *ca* 3.62 is absent in the ^{1}H-NMR spectrum (Figure 6.12), agreeing with the formation of CL-b-LA copolymer. The emergence of two signals at 4.16 and 4.06 ppm corresponds to a CL-LA heterojunction in the copolymer. The carbonyl segment in ^{13}C-NMR spectrum showed two resonance signals at 169.5 and 173.6 ppm due to the PCL and PLA segments in the polymer chains (Figure 6.13).
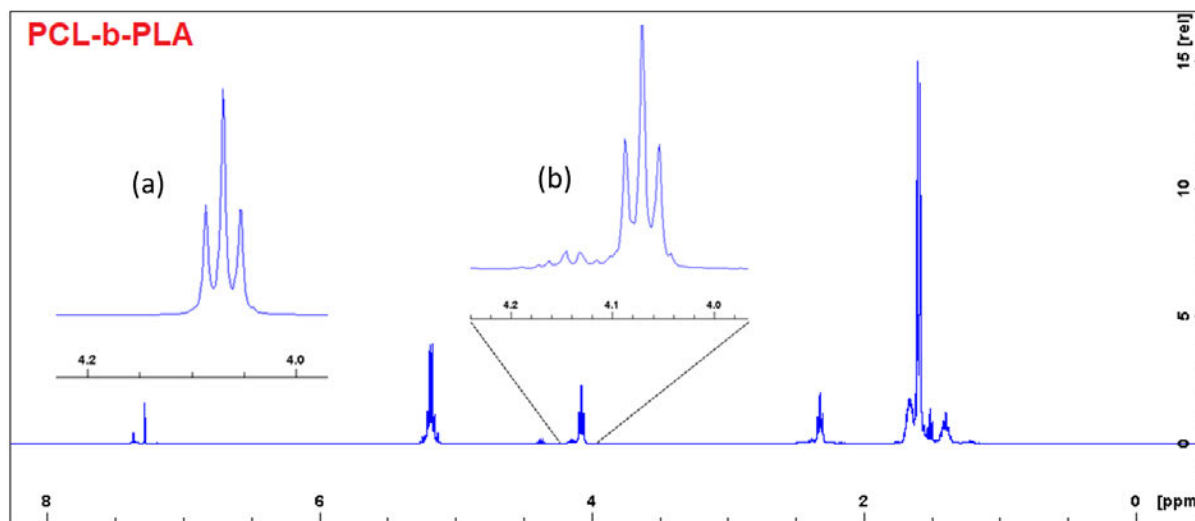
Figure 6.12: The ^{1}H-NMR spectrum of PCL-b-PLA block copolymer catalysed by complex **6.2'-OBn**. Reaction conditions: $[M]_0:[I]_0 = 100:1$ solvent: toluene, T = 50 °C
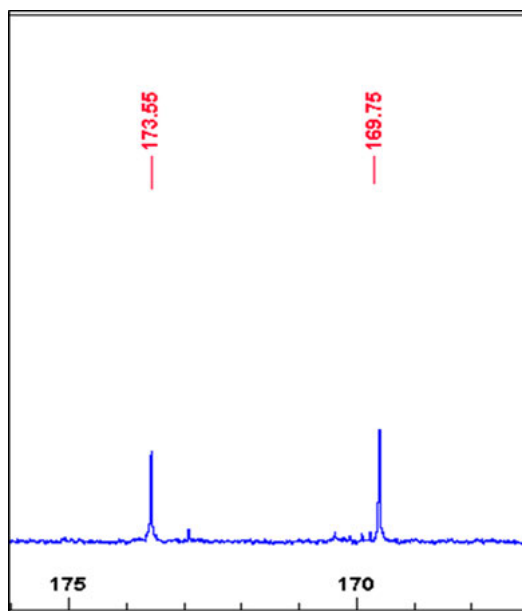
Figure 6.13:   (a) The carbonyl region ^{13}C-NMR spectrum of PCL-b-PLA block copolymer catalysed by complex **6.2'-OBn**. $[M]_0:[I]_0 = 100:1$ solvent: toluene, T = 50 °C

The molecular weights were also determined using ^{1}H-NMR. The $M_{w(NMR)}$ increased from 4198 g mol^{-1} for initial block prepolymer (PCL) to 6967 g mol^{-1} after formation of the second block polymer (PLA) in solution polymerization. The same trend was observed in melt polymerization.

6.8.9   *Random copolymerization*

The random copolymerization capability of complexes **6.1'-OBn** was studied in toluene at 50 °C at varying LA:CL molar ratios. Compiled results for the copolymerization are presented in Table 6.6 and 6.7. The relative final fraction of each monomer in the copolymers were analysed by ^{1}H-NMR spectroscopy in CDCl$_3$ by considering the ratio of the integral intensity values for the methylene signals of the PLC proton in the α- and ε-positions (Figure 6.14).
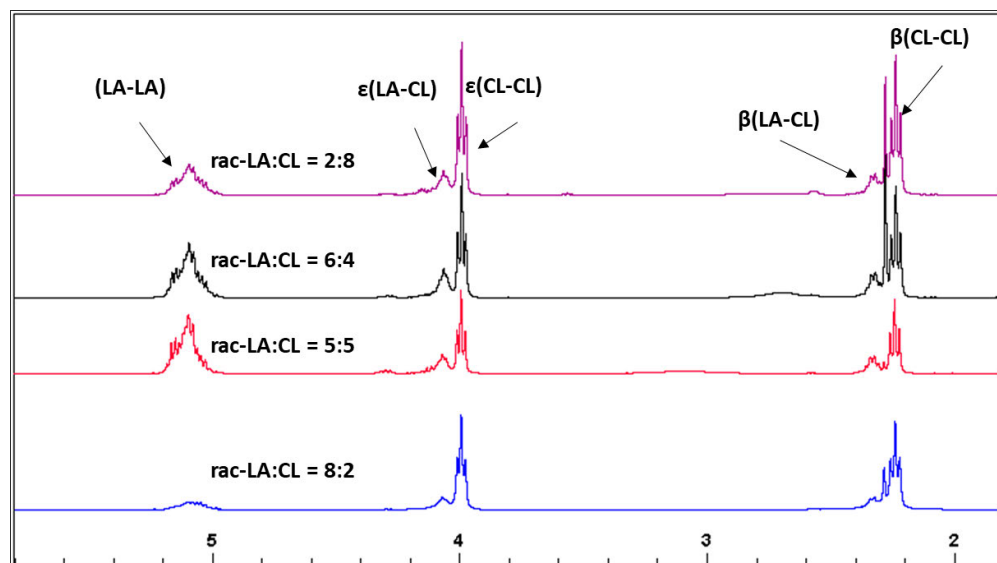
Figure 6.14: The ^{1}H-NMR spectra of PCL-co-PLA copolymer at various mole fractions catalysed by complex **6.1'-OBn**. Reaction conditions: $[M]_0:[I]_0 = 100:1$ solvent: toluene, $T = 50$ °C

The final monomer compositions of the copolymers were consistent with the initial CL:LA feed mole ratios studied. By analysing low monomer conversion samples, it was established that LAs were preferentially inserted at the expense of ε-CL a trend more pronounced at low monomer mole fraction. As the reaction proceeds and the concentration of LAs subsides and the incorporation of ε-CL also increased. As the mole fraction of ε-CL monomers increased in the feed, its insertion was appreciable and comparable to that of LAs. Thus, these phenomena point to formation of gradient co-polyesters with a steady variation in monomer distribution. An LA-enriched chain is initially formed which is preceded by ε-CL enriched chain formation due to the observed difference in rates of monomer polymerization. It can be concluded that not only the monomer incorporation rate determines the type of copolymer, but also the initial monomer mole fraction ratios

Table 6.6: Copolymerization of *rac*-LA and ε-CL at different times

Time(min)	% Linkage ratio			% Con LA	LA %	M_w cal	M_w NMR	M_w GPC	PDI
	LA/LA	CL/CL	LA/CL						
10	84	6	10	60	84	13200	1673	813	1.7
20	70	16	14	85	68	13950	2854	1823	1.6
30	55	32	13	90	56	14100	4015	4128	1.7
40	44	38	18	98	49	14340	7265	6398	1.7

[a]Polymerization conditions: Solvent toluene, 25 °C [M]$_0$:[I]$_0$ = 100:1. Determined from NMR. [b]Calculated theoretical Mw. [d,e]Determined by GPC relative to polystyrene standards in THF. [d]Experimental M_w was calculated considering Mark–Houwink's corrections of 0.56.

Table 6.7: Random copolymerization of *rac*-LA and ε-CL at varying monomer ratios

Feed LA:CL	% Linkage ratio[b]			% Con[c]		LA[d] %	[e] L_{LA}^e/L_{CL}^e	[f] L_{LA}^r/L_{CL}^r	[g]M_w (NMR)
	LA/LA	CL/CL	LA/CL	LA	CL				
10:0	100			99		100			6328
8:2	74	8	18	98	90	88	10.81/1.56	8.23/1.12	5483
6:4	52	28	20	98	95	62	4.34/2.22	3.23/1.33	5613
5:5	43	35	22	97	98	55	2.78/2.40	1.66/1.59	6005
4:6	30	49	21	96	98	43	2.55/3.45	1.42/2.10	4789
2:8	13	77	10	96	97	19	1.29/4.03	1.02/4.15	4925
0:10	0	100		98					7231

[a]Polymerization conditions: 110 °C, Bulk, [M]$_0$:[I]$_0$ = 100:1

[b]CL/LA mole ratio in the copolymer determined by ^{1}H-NMR

[c,g]Determined from NMR

[e,f]Average sequence length of the caproyl and lactyl unit in the copolymer determined by ^{13}C-NMR

6.8.10 Polymer microstructure analysis

A comprehensive characterization of the polymer micro-structures of the homo- and co-polymers was achieved by ^{1}H- and ^{13}C-NMR analysis on diads and triads tacticities as well as the homo- and hetero-diad linkage contents (LA-LA, CL-CL and LA-CL). An increase in LA:CL molar ratio resulted in the increased of LA-LA homo-sequences and LA-CL hetero-sequence while the CL-CL hetero-sequence decreased. This is because the increase in LA in the feed increase its incorporation into the polymer chain at the expense of CL.Analysis by homonuclear decoupled ^{1}H NMR spectrum Figure 13b for poly(rac-LA) prepared at 50°C showed that heterotactic polymer which was verified by pronounced *isi* and *iii* methine resonances peaks. P_r selectivities values increase with bulkiness of the substituents on the ligands and they range from 0.67 to 0.78. The isoselective nature of the racemic catalyst used is rather unexpected since optically active catalysts are required for the synthesis of sterio-block polymers. However, this trend has also been reported is literature using other racemic-catalytic system.[43,44] The authors attributed this unusual behaviour to an enantiomorphic-site control mechanism in conjunction with polymer exchange processes.
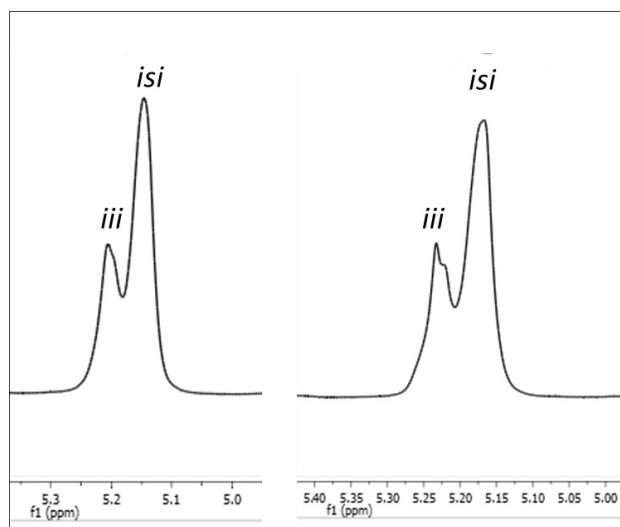
Figure 6.15: Homonuclear decoupled ^{1}H NMR spectrum of the methine part of poly(*rac*-LA). Reaction conditions: $[M]_0:[I]_0 = 100:1$ solvent: toluene, T = 50 °C

^{13}C-NMR spectroscopy is an established technique in terms of polymer microstructure analysis because it is sensitive to monomer environments.[45] The polymeric chain microstructures were also analysed by considering triads patterns in the carbonyl segment on ^{13}C-NMR spectra from 169 to 174 ppm of the copolymers (Figure 6.16). Eight triad resonances, which are consistent with binary random copolymerization phenomena, were observed and assigned based on literature data.[46,47] In some instances, a signal around 171 ppm attributed to LACLLA triad was present and it results from chain reshuffling due to transesterification.[16,46] The degree of transesterification can influence consumption of ε-CL monomer which will subsequently impact the monomer sequence distribution.
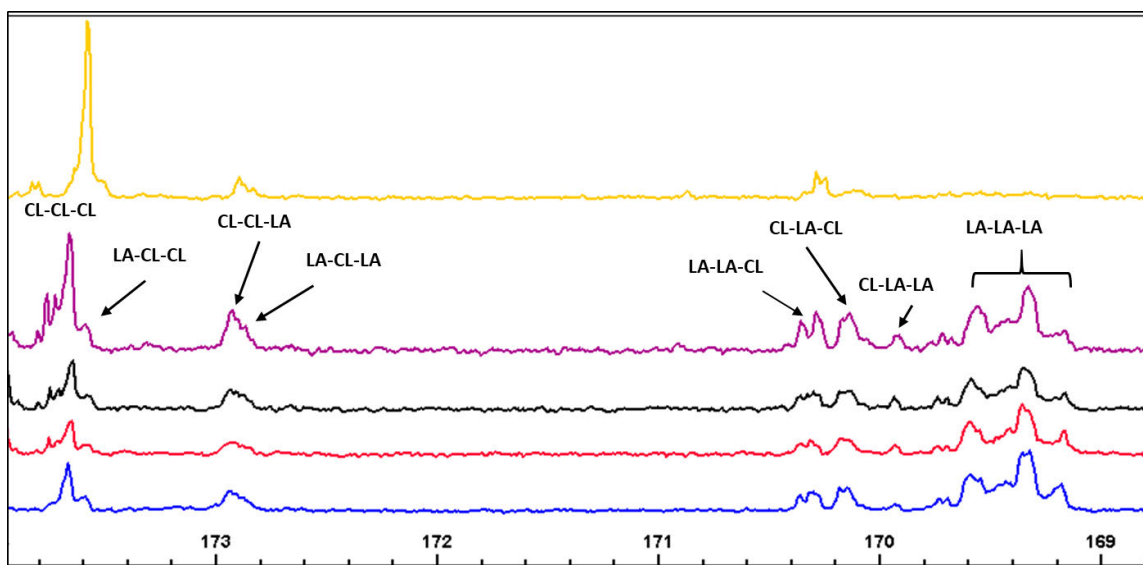
Figure 6.16: ^{13}C-NMR spectra carbonyl region of poly(*rac*-LA). Reaction conditions $[M]_0:[I]_0 = 100:1$, solvent: toluene, T = 50 °C

The average block length (L_{LA}^e and L_{CL}^e) were calculated from triad intensity of the triads from the ^{13}C-NMR according to equations **6.5** and **6.6**,[48,49]

$$L_{LA}^e = \frac{1}{2}\frac{I_{LLLLLL} + I_{LLLLC} + I_{CLLL} + I_{CLLC} + I_{CLC}}{I_{CLC} + 1/2(I_{CLLC} + 1/2(I_{LLLLC} + I_{CLLLL}))} \qquad (6.5)$$

$$L_{CL}^e = \frac{I_{LLCLL} + I_{CCLL} + I_{LLCC} + +I_{CCC}}{(I_{LLCLL} + 1/2(I_{CCLL} + I_{LLCC}))} \qquad (6.6)$$

where I = integral of the signals attributed to triad sequence and the subscript L and C stands for the lactidyl unit and caproyl unit. The random distribution of monomers (Bernouillian statistics), may be calculated from equations **6.7** and **6.8**[39] below,

$$L_{LA}^{r} = \frac{1}{2}\left(1 + \frac{1}{k}\right) \qquad (\mathbf{6.7})$$

$$L_{CL}^{e} = (1 + k) \qquad (\mathbf{6.8})$$

where k = [C]/[L], [L] and [C] stand for the concentration of lactyl and caproyl units in the copolymer chain, respectively. The computed data presented in Table 6.7 show that the L_{CL} and L_{LA} values increased with monomer mole ratio in the initial monomer reaction feed. The average length L_{LA} ranges from 1.02 to 10.6 while, L_{CL} range from 1.12 to 4.15. These values are higher than the expected calculated values a factor, which resonates with gradient copolymer microstructure. The deviation between the theoretical and experimental values are attributed to three factors. Firstly, assuming a constant rate rather than a dropping rate of monomer incorporation. Secondly, experimental errors in rate constant ratio determination and finally, non-homogeneity mixing and characteristic variance in cross-reactivity fractions.[50] All the factors are considered as contributors to molecular weights variation in our system.

6.8.11 Reaction mechanism

To get an understanding of the polymerization mechanism the polymers were analysed by ^{1}H-NMR and ESI-MS spectroscopy (Figure 6.17 – 6.20). PCL and PLA ^{1}H-NMR spectra (Figure 6.17 and 6.18) displayed a triplet proton resonance peaks at 3.66 and 4.88 ppm, which are, attributed to main-chain methylene protons and those adjoining the hydroxyl end, respectively. A singlet at 5.2 ppm due to benzoyl methylene protons points to polymers with a benzyl ester terminus. This backs a CIM mechanism *via* insertion of metal-oxygen bond into the O-acyl bond of the monomer.
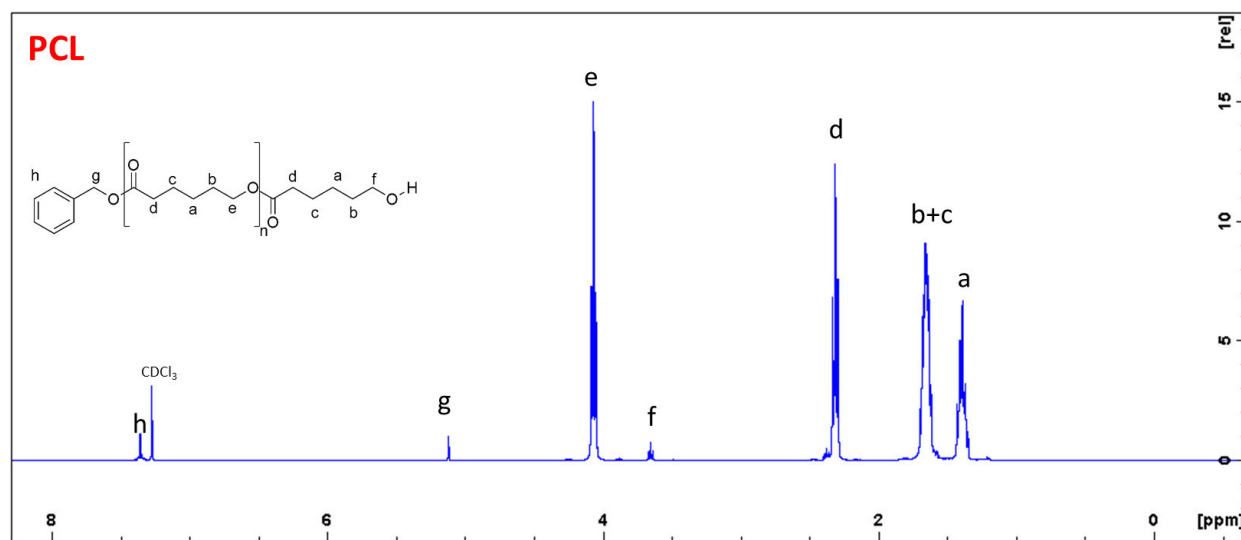
Figure 6.17: The ^{1}H-NMR spectrum of PCL initiated by complex **6.5'-OBn**. Reaction conditions: $[CL]_0:[6.5'-OBn]_0 = 100:1$, solvent: toluene, T = 25 °C
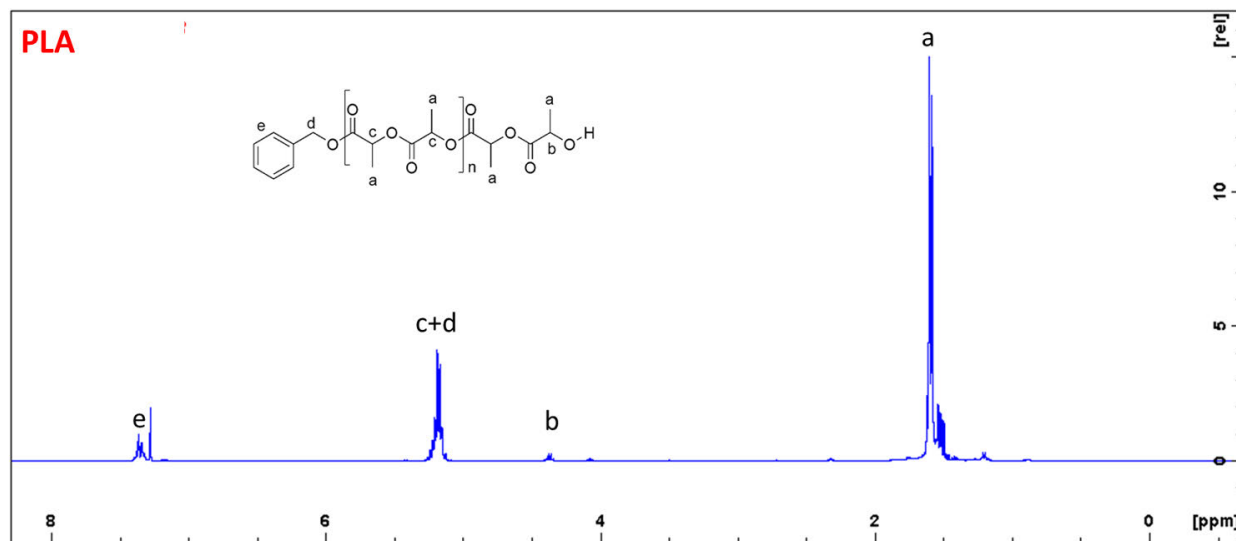
Figure 6.18: The ^{1}H-NMR spectrum of PLA initiated by complex **6.5'-OBn**. Reaction conditions: $[CL]_0:[I]_0 = 100:1$, solvent: toluene, T = 25 °C

The ESI-MS spectra for PCL and PLA recovered after polymerization with complex **6.5'-OBn** are shown in Figure 6.19 and 6.20. Mono-sodiated distribution of peaks corresponding to the respective repeating units were observed. Consecutive peaks are separated by a mass difference ($\Delta m/z$) of 114.1 (caprolactyl unit) and 72 (lactyl unit) for PCL and PLA, respectively.

Substantial transesterification occurred during the polymerization of lactides as shown by Δm value of 72 and appearance of satellite peaks corresponding to cyclic macromolecules. In addition, the molecular weights correspond to polymers capped with benzyl ester and hydroxy end groups. For example, peaks at m/z 1785.71 (Figure 6.19, degree of polymerization (DP) = 15) and 1025.15, Figure 6.20, (DP) = 12) are from a polymers having $C_6H_5CH_2O$- and -OH end groups for PCL and PLA, respectively, which confirm a coordination insertion mechanism similar to documentations in literature[51-54] and is illustrated in Figure 6.21.
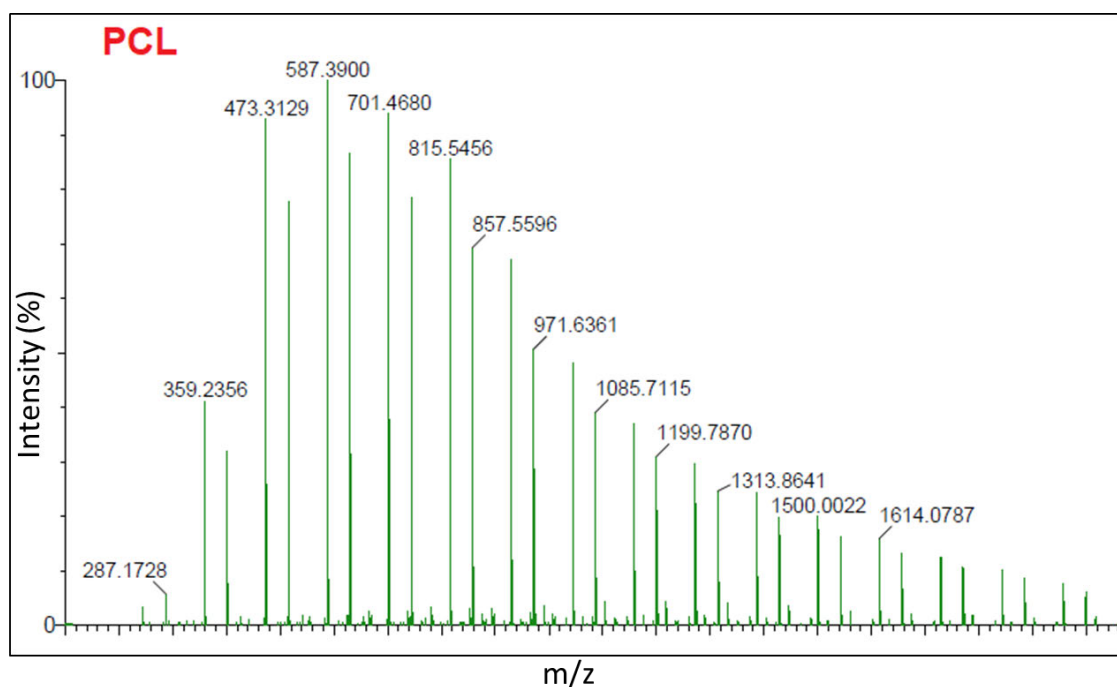
Figure 6.19: ESI-MS spectrum of PCL obtained from complex **6.3'-OBn**, $[CL]_0:[I]_0 = 100:1$, t = 150 min
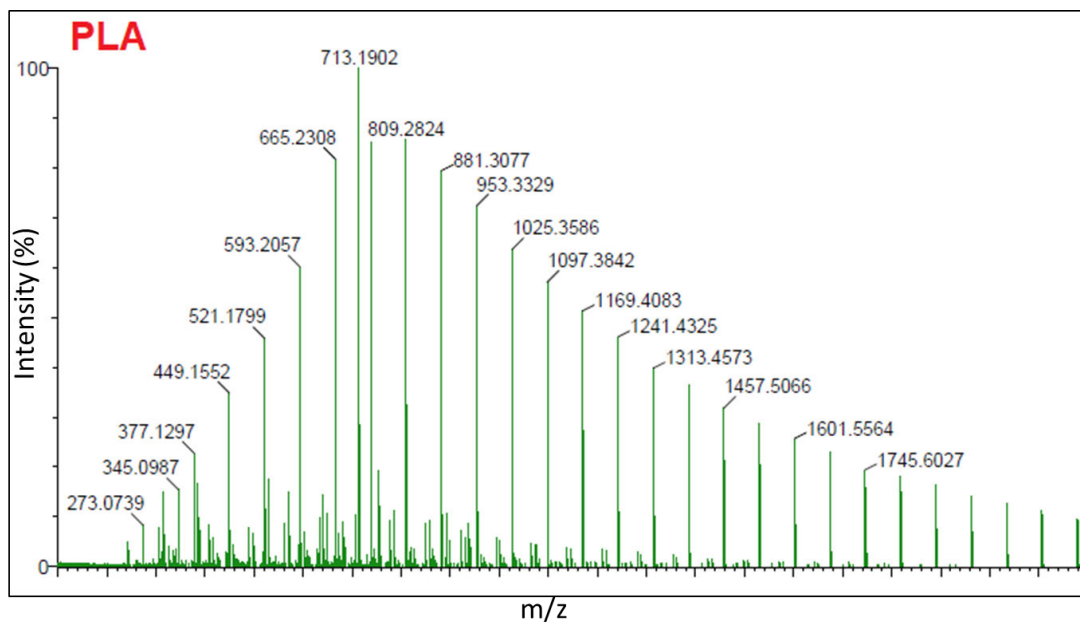
Figure 6.20: ESI-MS spectrum of PLA obtained from complex **6.3'-OBn**, $[CL]_0:[I]_0 = 100:1$, t 200 min
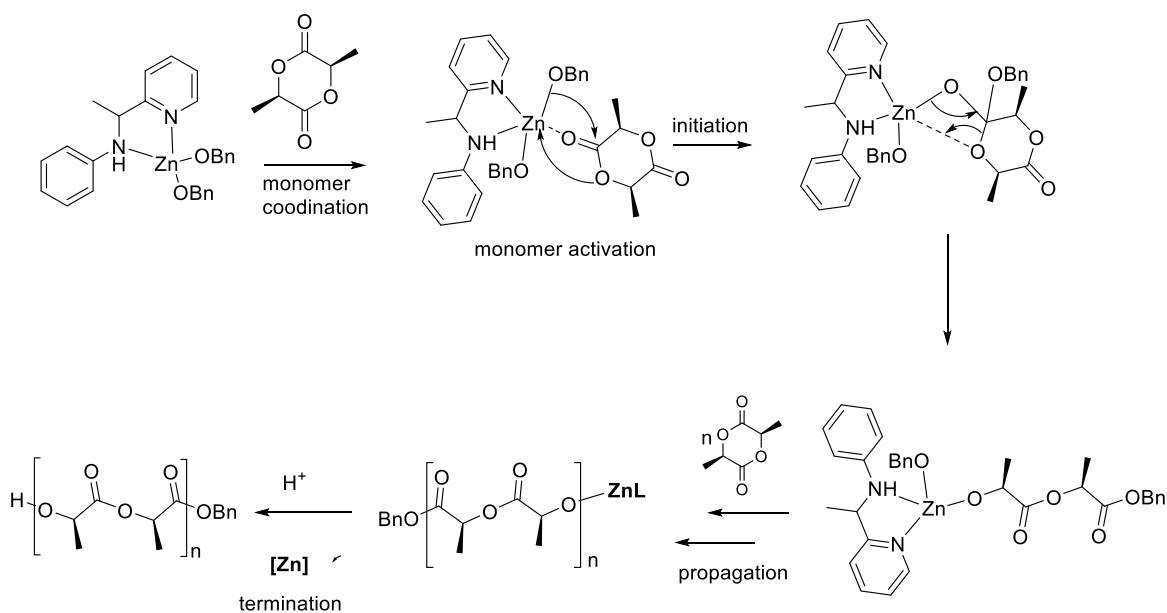
Figure 6.21: Proposed monomer activation mechanism for the polymerization of lactides

6.9   Conclusion

A series of Zn(II) chlorido complexes (**6.1'** – **6.5'**) supported by *N,N'*-bidentate-*N*-(pyridin-2-ylethyl)amine ligands. Zn(II) alkyl and alkoxy complexes **6.1'-Me** – **6.5'-Me** and **6.1'-OBn** – **6.5'-OBn** were synthesised *in-situ* by reacting the chlorido derivatives with methyl lithium with subsequent addition of benzyl alcohol. Both species showed excellent catalytic activity with alkoxyl species dominating in ROP of cyclic esters. The ROP reactions exhibited *pseudo* first-order kinetics with respect to monomer concentration. Polymer molecular weights were seen to increase and lie between 3096 to 8837 g mol^{-1} and they exhibited relatively high molecular weight distributions with PDI values *ca.* 2. Poly(*rac*-LA) polymers are predominantly atactic while poly(L-LAs) are largely isotactic. All polymerization reactions proceed through coordination insertion mechanism followed by hydrolysis of the metal. The stereogenic centres of the ligand skeleton influenced control of polymer stereochemistry. Random copolymerization of ε-CL and LAs resulted in block gradient copolymers. Atactic polymers with stereosequence characterised with *iis* and *iii* signals with almost similar intensity in the decoupled ^{1}H NMR spectra. The relatively high Pr selectivity values around 80 suggest high isotacticity of PLAs polymers. The sequential addition of LA after ε-CL gave diblock PCL-b-PLA and reversing monomer addition did not form any copolymer.

References

1. S. Hong, K.-D. Min, B.-U. Nam and O. O. Park, Green Chem., 2016, 18, 5142.

2. B. Surnar, K. Sharma and M. Jayakannan, Nanoscale, 2015, 7, 17964.

3. R. Samuel, E. Girard, G. Chagnon, S. Dejean, D. Favier, J. Coudane and B. Nottelet, RSC Advances, 2015, 5, 84125.

4. E. D. Akpan, S. O. Ojwach, B. Omondi and V. O. Nyamori, Polyhedron, 2016, 110, 63.

5. Y. F. Al-Khafaji, M. R. J. Elsegood, J. W. A. Frese and C. Redshaw, RSC Advances, 2017, 7, 4510.

6. L. Chen, W. Li, D. Yuan, Y. Zhang, Q. Shen and Y. Yao, Inorg. Chem., 2015, 54, 4699.

7. C. Fliedel, V. Rosa, F. M. Alves, A. M. Martins, T. Aviles and S. Dagorne, Dalton Trans., 2015, 44, 12376.

8. M. H. Chisholm and E. E. Delbridge, Chem. Commun., 2001, 1308.

9. A. P. Dove, V. C. Gibson, E. L. Marshall, H. S. Rzepa, A. J. P. White and D. J. Williams, J. Am. Chem. Soc., 2006, 128, 9834.

10. N. Nomura, R. Ishii, M. Akakura and K. Aoi, J. Am. Chem. Soc., 2002, 124, 5938.

11. H. Du, X. Pang, H. Yu, X. Zhuang, X. Chen, D. Cui, X. Wang and X. Jing, Macromolecules, 2007, 40, 1904.

12. H. Du, A. H. Velders, P. J. Dijkstra, Z. Zhong, X. Chen and J. Feijen, Macromolecules, 2009, 42, 1058.

13. R. E. Drumright, P. R. Gruber and D. E. Henton, Adv. Mater., 2000, 12, 1841.

14. D. J. Gilmour, R. L. Webster, M. R. Perry and L. L. Schafer, Dalton Trans., 2015, 44, 12411.

15. R. Lapenta, M. Mazzeo and F. Grisi, RSC Advances, 2015, 5, 87635.

16. G. Li, M. Lamberti, D. Pappalardo and C. Pellecchia, Macromolecules, 2012, 45, 8614.

17. R. L. Webster, RSC Advances, 2014, 4, 5254.

18. Z. Sun, R. Duan, J. Yang, H. Zhang, S. Li, X. Pang, W. Chen and X. Chen, RSC Advances, 2016, 6, 17531.

19. L. Lin, Y. Xu, S. Wang, M. Xiao and Y. Meng, Eur. Polym. J., 2016, 74, 109.

20. Bruker, ed., APEXII, APEXII Bruker AXS Inc, Madison, Wisconsin, USA, 2009.

21. Bruker, SAINT, SAINT Bruker AXS Inc, Madison, Wisconsin, USA, 2009.

22. Bruker, SADABS, Bruker SADABS Bruker AXS Inc, Madison,Wisconsin, USA, 2009.

23. G. Sheldrick, Acta Crystallogr Sect. A: Found. Crystallogr., 2008, 64, 112.

24. B. Dolomanov O. V, L. J. Gildea,R. J, HowardJ. A. K. Puschmann, H, Appl. Crystallogr, 2009, 42, 339.

25. Y.-W. Dong, R.-Q. Fan, W. Chen, H.-J. Zhang, Y. Song, X. Du, P. Wang, L.-G. Wei and Y.-L. Yang, RSC Advances, 2016, 6, 110422.

26. C. Alonso-Moreno, A. Garcés, L. F. Sánchez-Barba, M. Fajardo, J. Fernández-Baeza, A. Otero, A. Lara-Sánchez, A. Antiñolo, L. Broomfield, M. I. López-Solera and A. M. Rodríguez, Organometallics, 2008, 27, 1310.

27. J. Li, Y. Deng, S. Jie and B.-G. Li, J. Organomet. Chem., 2015, 797, 76.

28. S. H. Ahn, M. K. Chun, E. Kim, J. H. Jeong, S. Nayab and H. Lee, Polyhedron, 127, 51.

29. X.-X. Zheng, C. Zhang and Z.-X. Wang, J. Organomet. Chem., 2015, 783, 105.

30. S. Nayab, H. Lee and J. H. Jeong, Polyhedron, 2011, 30, 405.

31. S. Nayab, H. Lee and J. H. Jeong, Polyhedron, 2012, 31, 682.

32. F. Qian, K. Liu and H. Ma, Dalton Trans., 2010, 39, 8071.

33. S. T. Balke and H. N. Cheng, in Modern Methods of Polymer Characterization ed. H. G. M. Barth, J. W, Wiley-Interscience, New York, 1991, ch. 10-300.

34. R. Steudel and Y. Steudel, J. Phys. Chem. A., 2006, 110, 8912.

35. P. Hormnirun, E. L. Marshall, V. C. Gibson, R. I. Pugh and A. J. P. White, Proc. Natl. Acad. Sci., 2006, 103, 15343.

36. N. M. Rezayee, K. A. Gerling, A. L. Rheingold and J. M. Fritsch, Dalton Trans., 2013, 42, 5573.

37. J. Cho, S. Nayab and J. H. Jeong, Polyhedron, 2016, 113, 81.

38. J. Yang, Z. Sun, R. Duan, L. Li, X. Pang and X. Chen, Sci. China. Chem., 2016, 59, 1384.

39. C. Kan and H. Ma, RSC Advances, 2016, 6, 47402.

40. S. Ghosh, A. Spannenberg and E. Mejía, Helv. Chim. Acta, 2017, 100, e1700176.

41. F. Della Monica, E. Luciano, A. Buonerba, A. Grassi, S. Milione and C. Capacchione, RSC Advances, 2014, 4, 51262.

42. M. Keram and H. Ma, Appl. Organomet. Chem., 2017, 31, e3893.

43. T. M. Ovitt and G. W. Coates, J. Am. Chem. Soc., 2002, 124, 1316.

44. H. Wang, Y. Yang and H. Ma, Macromolecules, 2014, 47, 7750.

45. J. E. Kasperczyk, Polymer 1999, 40 5455.

46. M. Honrado, A. Otero, J. Fernández-Baeza, L. F. Sánchez-Barba, A. Garcés, A. Lara-Sánchez and A. M. Rodríguez, Organometallics, 2016, 35, 189.

47. N. Nomura, A. Akita, R. Ishii and M. Mizuno, J. Am. Chem. Soc., 2010, 132, 1750.

48. J. Kasperczyk and M. Bero, Makromol. Chem., 1991, 192, 1777.

49. J. Kasperczyk and M. Bero, Makromol. Chem., 1993, 194, 913.

50. H. Qian, A. R. Wohl, J. T. Crow, C. W. Macosko and T. R. Hoye, Macromolecules, 2011, 44, 7132.

51. Y. Huang, W. Wang, C.-C. Lin, M. P. Blake, L. Clark, A. D. Schwarz and P. Mountford, Dalton Trans., 2013, 42, 9313.

52. N. Ajellal, J.-F. Carpentier, C. Guillaume, S. M. Guillaume, M. Helou, V. Poirier, Y. Sarazin and A. Trifonov, Dalton Trans., 2010, 39, 8363.

53. D. Li, Y. Peng, C. Geng, K. Liu and D. Kong, Dalton Trans., 2013, 42, 11295.

54. T.-L. Yu, C.-C. Wu, C.-C. Chen, B.-H. Huang, J. Wu and C.-C. Lin, Polymer, 2005, 46, 5909.

Chapter 7   General conclusions and future prospects

The goal of this PhD thesis was to design ROP catalytic systems based on less toxic and cheap metals supported by *N,N′* and *N,O* ligand. This was targeted at improving and controlling the polymerization reactions, in terms of selectivity, activity and sustainability. This was done by modifying the ligand motifs by fine-tuning the steric and electronic environment and utilizing benign metals complexes like magnesium, copper and zinc.

7.1   Research summary

Initial studies investigated the synthesis and characterization of eight zinc and copper complexes of the type [M(**Ln**)$_2$(OAc)$_4$] (M = Zn(II) or Cu(II) supported by unsymmetrical formamidine (**Ln**) (n = 3.1 – 3.4) and their application in the ROP of *rac*-LA and ε-CL is discussed. The coordination in the complexes was established to be paddle wheel consisting of acetate bridging auxiliary ligands. Generally, the complexes exhibited moderate activity after a sluggish initiation period with the Zn(II) complexes being more active than the Cu(II) complexes. The slow initiation is alluded to the strong chelation of bridging acetate initiators and the activity difference between the two metals being attributed to the Lewis acidity of the two metals. The polymers obtained showed experimental molecular weight values, which were slightly less than expected values. Higher molecular weight distribution values were obtained which characterize a *pseudo* living polymerization catalytic system.

The research was extended by investigation the effect of modifying the formamidine ligands in from the previous chapter. The ligands were converted to *N*-hydroxy-formamidine type ligands. A series of eight bis-chelated Zn(II) and Cu(II) complexes of the form [M(**Ln**)$_2$] (**Ln** = **L4.1** – **L4.4**) were investigated in ROP of ʟ-LA and ε-CL. Generation of alkoxide species by addition of a co-initiator resulted in fast polymerization reactions and controlled molecular weight of polymers shown by low polydispersity indices. This was a significant improvement from the catalytic system reported in prior chapter and the catalytic activity followed a similar trend. The activities and polymer characteristics were influenced by ligand symmetry as well as steric and electronic properties.

The thesis also investigated the use of Schiff type ligands to study the effect of changing the spacer between hetero donor atoms. The sterically strained geometry in ligand systems reported in in earlier systems crowded the metal centre. We projected that an increase in spacer length place the atoms away from the metal centre thereby exposing it for fast approach of the monomer hence increasing catalytic activity. Phenolate-ligated Mg(II) and Zn(II) based catalysts of type [M(**Ln**)$_2$] (**Ln** = **L5.1** – **L5.4**) were synthesised and their application in ROP of ε-CL and *rac*-LA is presented. As predicted high activity in polymerization was witnessed as compared to catalytic systems reported initially studied. Moderate experimental molecular weight polymers with broad molecular weight distributions were obtained. Addition of alcohols resulted in a semi "living" polymerization process as witnessed by reduction in PDI values. The polymerization of *rac*-LA did not show appreciable stereoselectivity giving atactic polymers characterised by *ii*, (*is*, *si*) and *ss* tacticity triads.

Finally, a series of five Zn(II) methyl and alkoxide derivatives were synthesised *in-situ* by reacting from dichloro derivatives with methyl lithium with subsequent addition of benzyl alcohol. Both species showed excellent catalytic activity with alkoxyl species dominating in ROP of cyclic esters. The ROP reactions exhibited *pseudo* first-order kinetics with respect to monomer. Polymer molecular weights were seen to increase and exhibited relatively high molecular weight distributions. Poly(*rac*-LA) polymers were predominantly atactic while poly(ʟ-LAs) were largely isotactic. All polymerization reactions proceed through coordination insertion mechanism followed by hydrolysis of the metal. The stereogenic centres of the ligand resulted in stereo-control polymerization of *rac*-LA resulting in heterotactic polymers. Random copolymerization of ε-CL and LAs resulted in block gradient copolymers. The sequential addition of LA after ε-CL gave diblock PCL-b-PLA and reversing monomer addition did not yield any copolymer.

7.2   General conclusions

- ROP active catalysts from less toxic and cheap metals have been designed which is a significant contribution to knowledge in the field of catalysis.
- Coordination flexibility of the ligand designed and the repercussions in ROP process were demonstrated.

- The kinetic data reviewed that the ROP reactions were *pseudo*-first order with respect to cyclic ester monomers.
- Coordination insertion mechanism (CIM) and activated monomer mechanisms (AMM) were typical operational mechanisms as elucidated from NMR and ESI-MS data.
- The catalytic activity follows the order Mg(II) > Zn(II) > Cu(II) as shown by the apparent rate constants (k_{app}).
- All catalytic systems furnished relatively low molecular weight polymers which are good candidates for drug delivery systems.

7.3   Future work

A substantial amount of reported ROP systems has focused on metal complexes supported by *N* and/*O* hetero-donor atoms. The catalytic system reported in chapter 4 showed some catalytic activity. However, the catalytic activities of the complexes were relatively low with respect to some reported related systems. Thus, it would be beneficial to study the inclusion of other hetero-donor atoms such as *P* and *S*. These have been seldom studied, hence it would be interesting to study their influence in ROP reactions. The ligands in chapter three can be modified as depicted in Figure 7.1a and b. Incorporation alkoxide auxiliary ligands would be beneficial in improving activity as they are reported to be good ROP initiators.

The position of nitrogen in the pyridyl ligands can be changed to 3 and 4. This can introduce a possibility to have either homo or heterometallic systems (Figure 7.2). The synergistic effects between the metals if they are in close proximity can enhance catalytic activity.
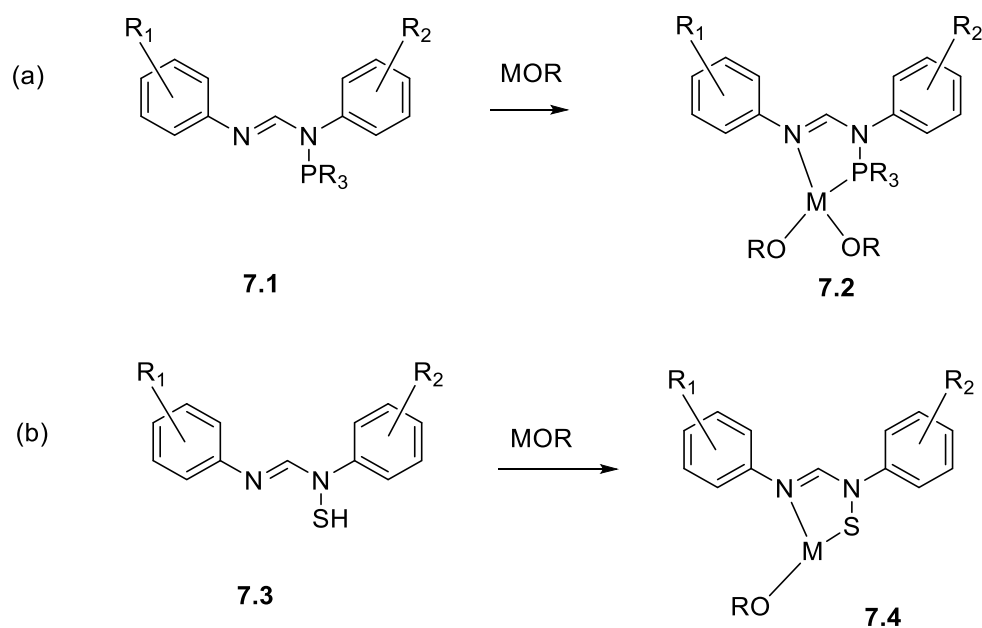
Figure 7.1: Possible modification of *N,N'*-formamidine ligands

X = Nucleophile
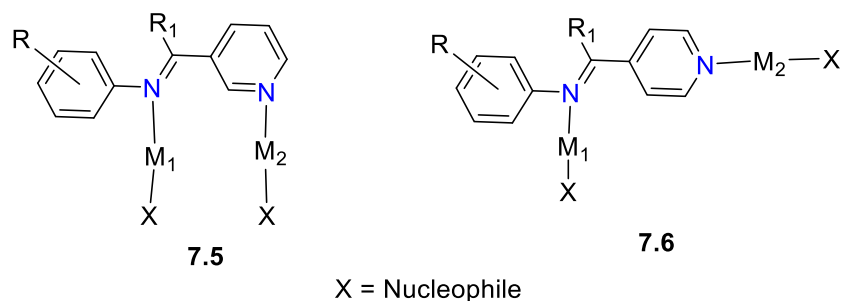
Figure 7.2: Bimetallic N-pyridyl complexes

As earlier established, appreciable explanation on polymerization paths and profiles sometimes cannot be straightforwardly proved experimentally. DFT studies can reveal more insight into operational mechanisms and understanding of steric and electronic effects on the activation profile barriers. DFT computational calculations of the complexes can give information about electron density distributions, energy gaps, HOMO and LUMO energy levels. This could help in explaining and accounting for observed reactivity trends of different catalyst.

Appendix A-Chapter 3

Zn(II) and Cu(II) unsymmetrical formamidine complexes effective initiators for the ring-opening polymerization of cyclic esters
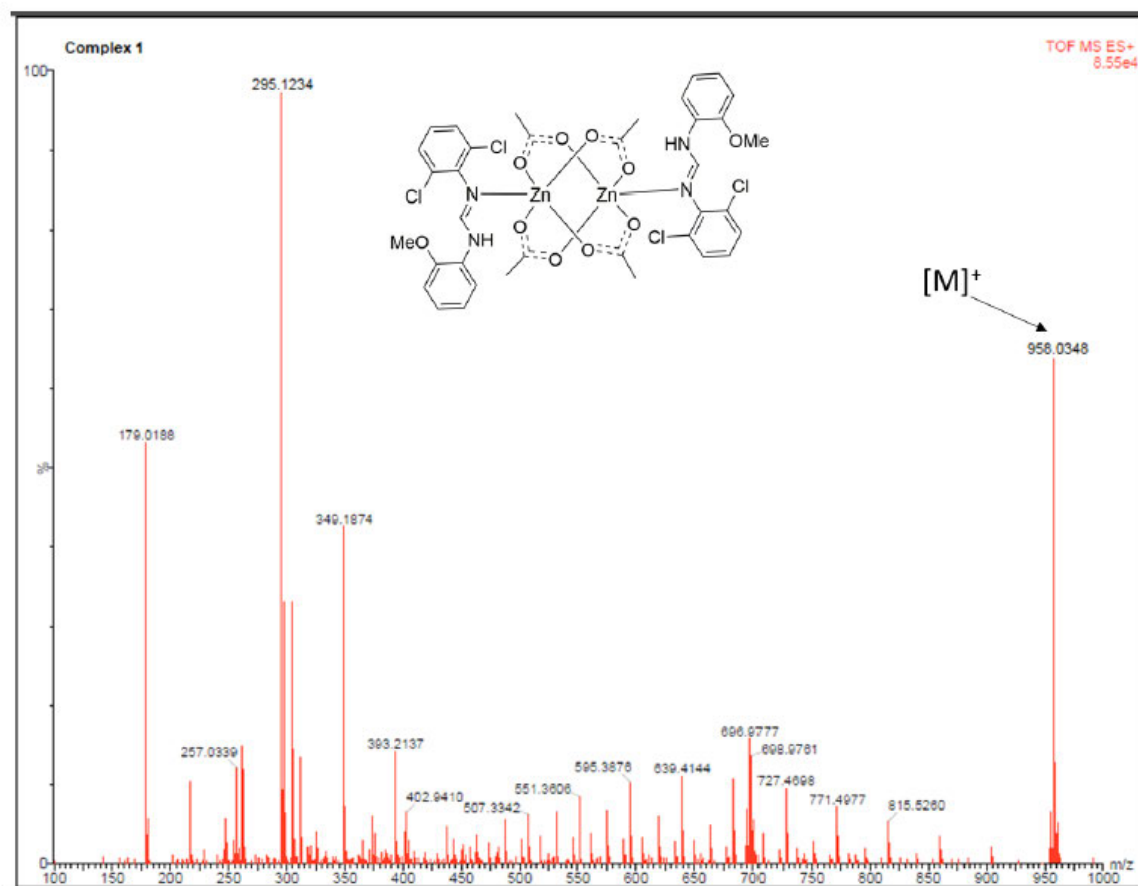
Figure. 1. ESI-MS spectrum for complex **3.1**
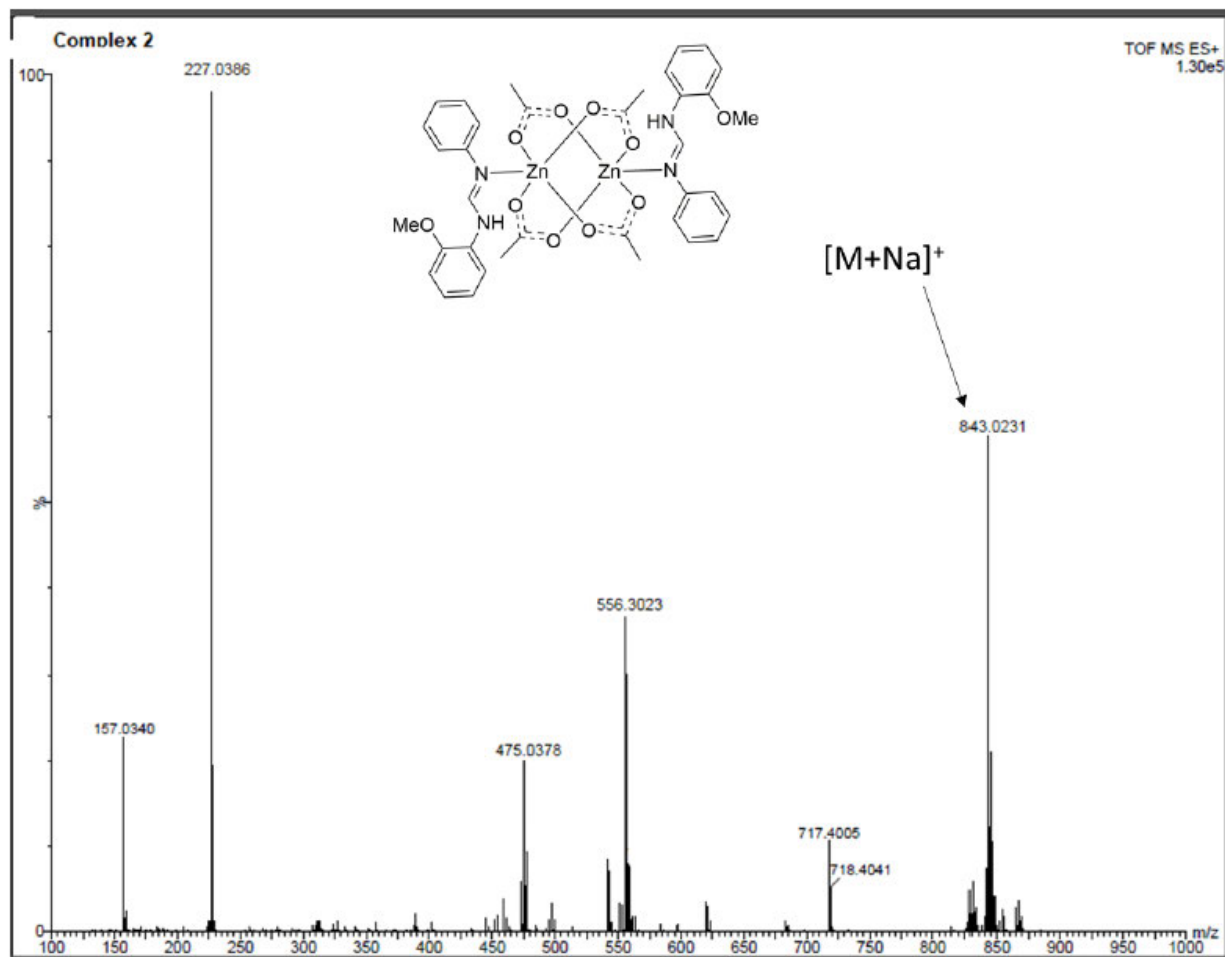
Figure.2. ESI-MS spectrum for complex **3.2**
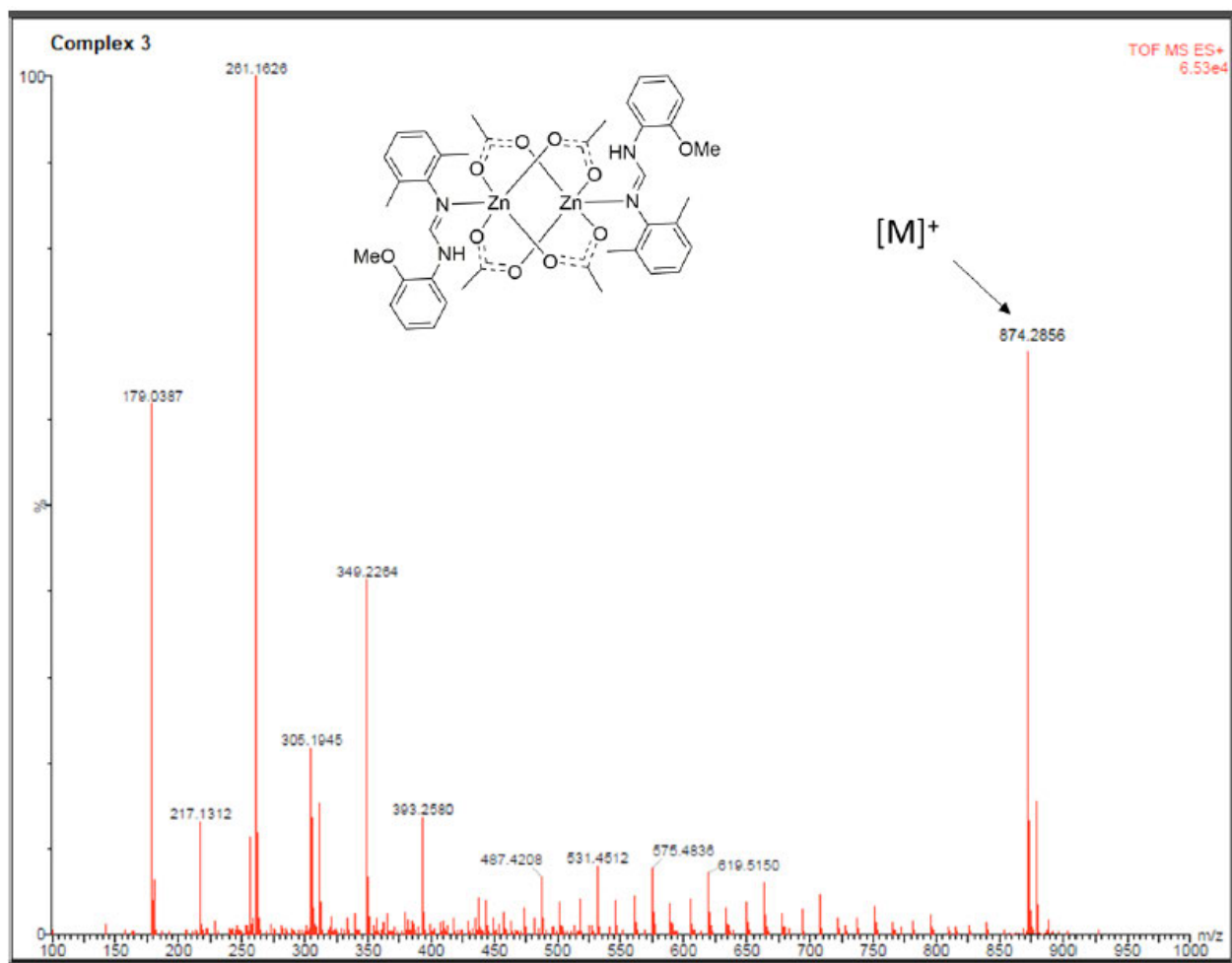
Figure. 3. ESI-MS spectrum for complex **3.3**
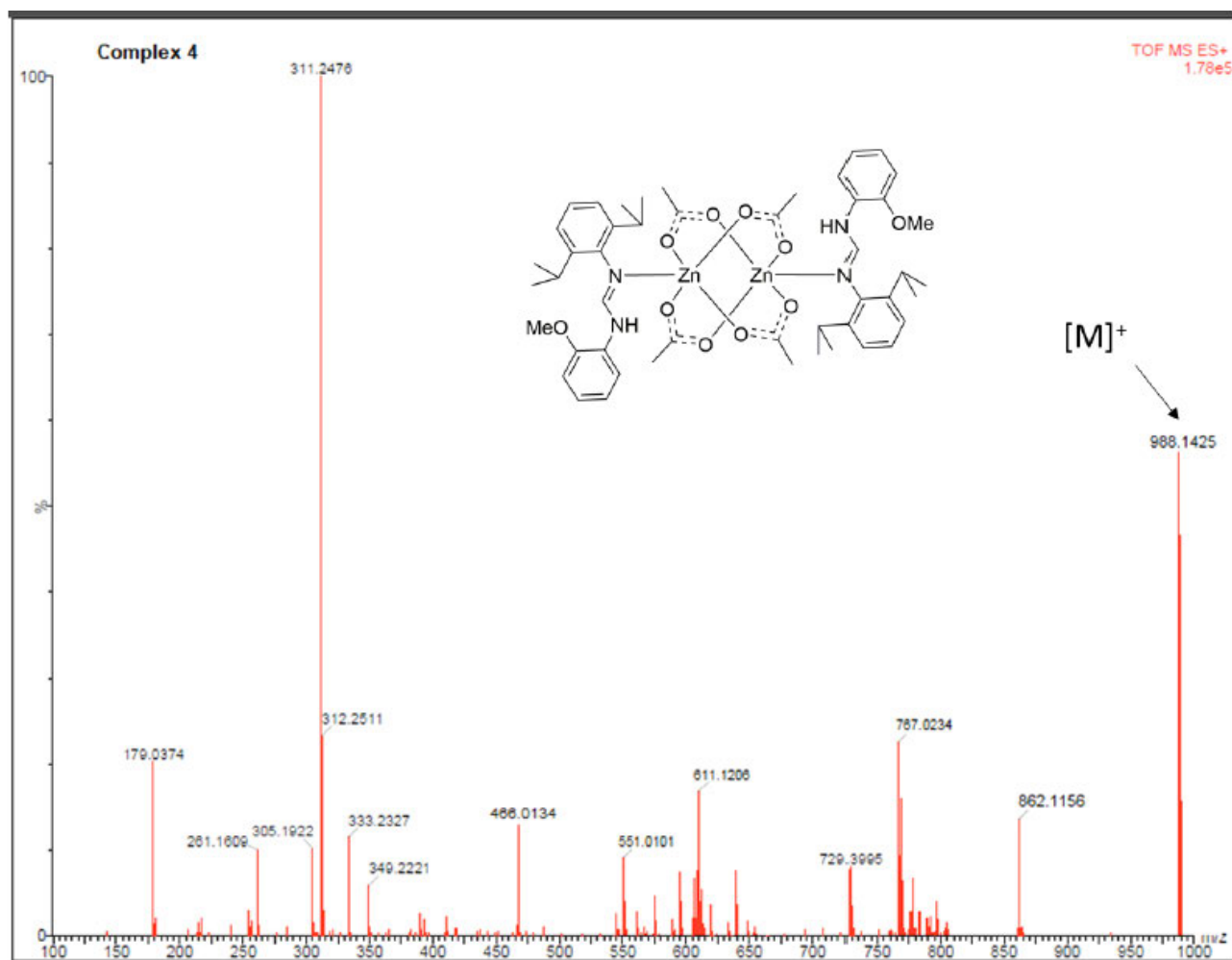
Figure. 4. ESI-MS spectrum for complex **3.4**
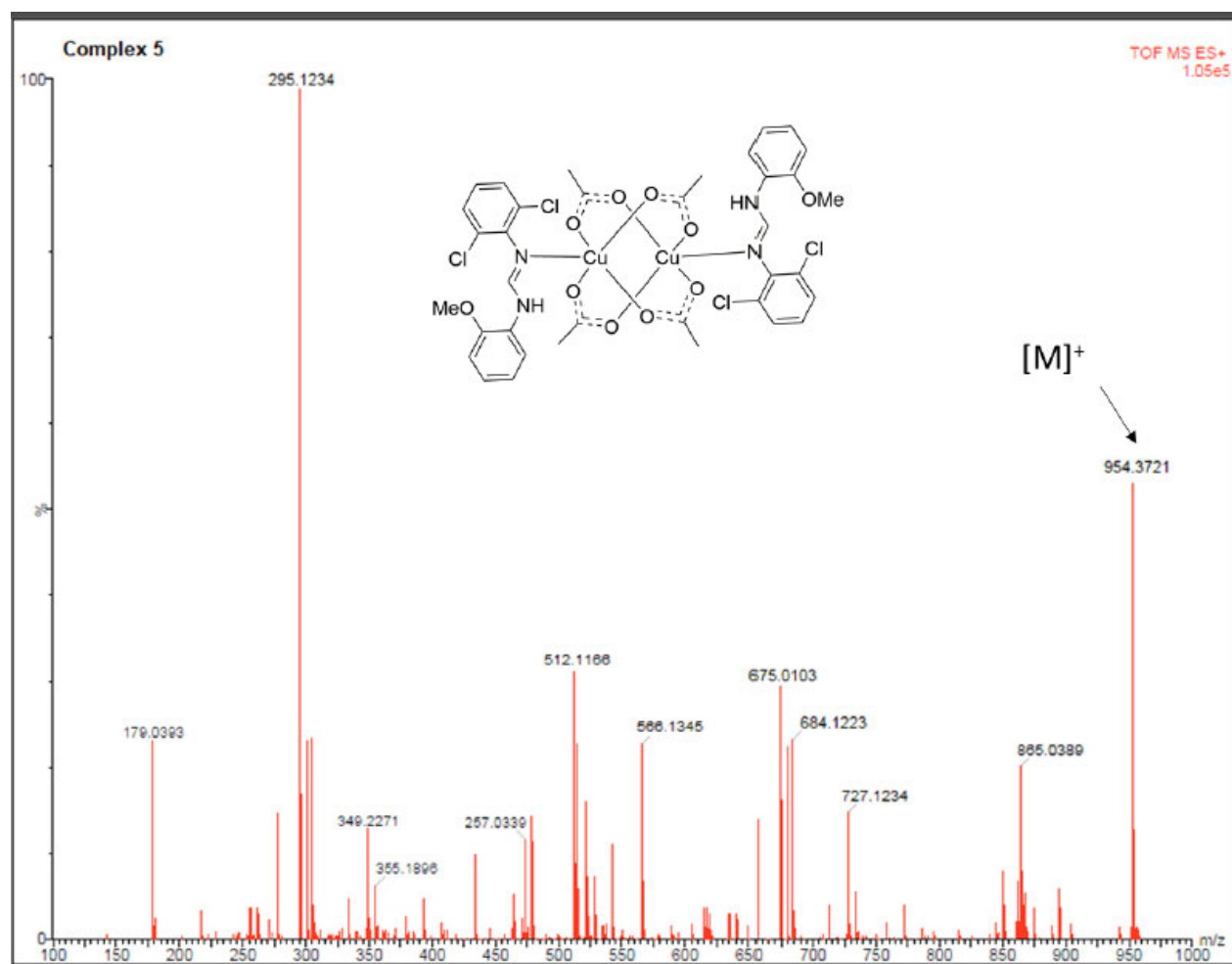
Figure. 5. ESI-MS spectrum for complex **3.5**
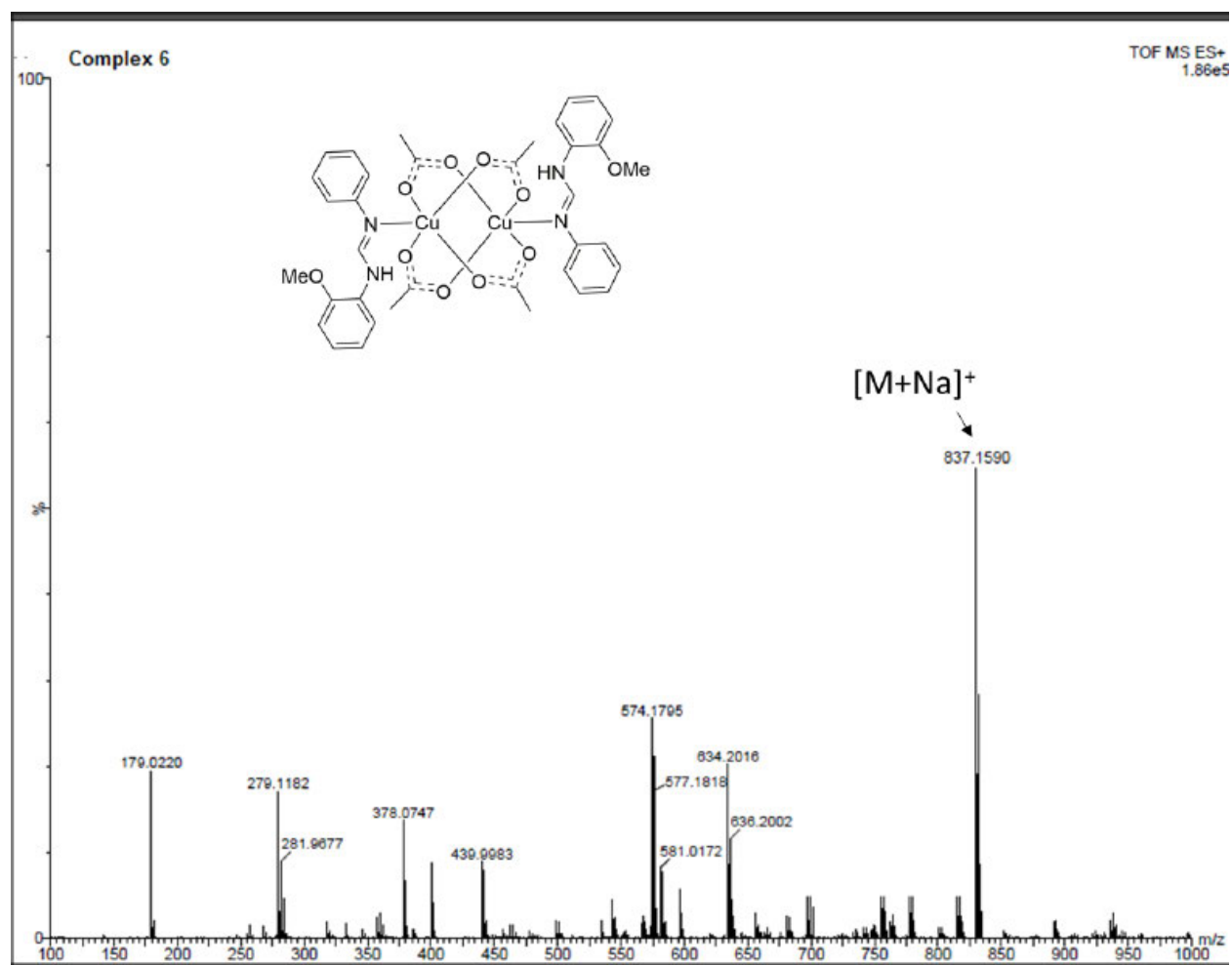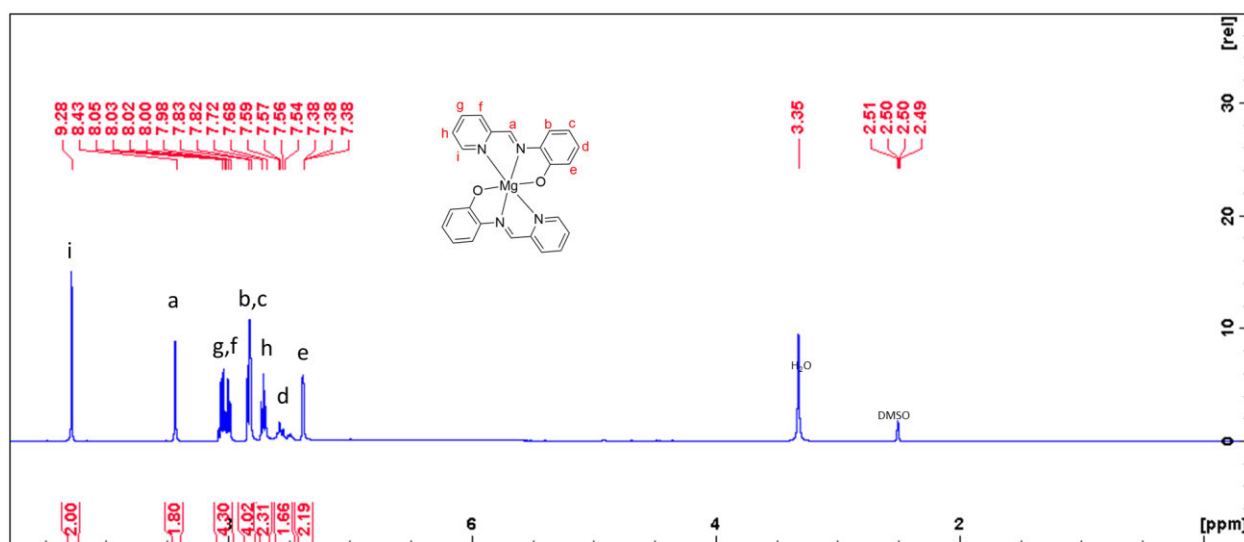
Figure. 6. ESI-MS spectrum for complex **3.6**
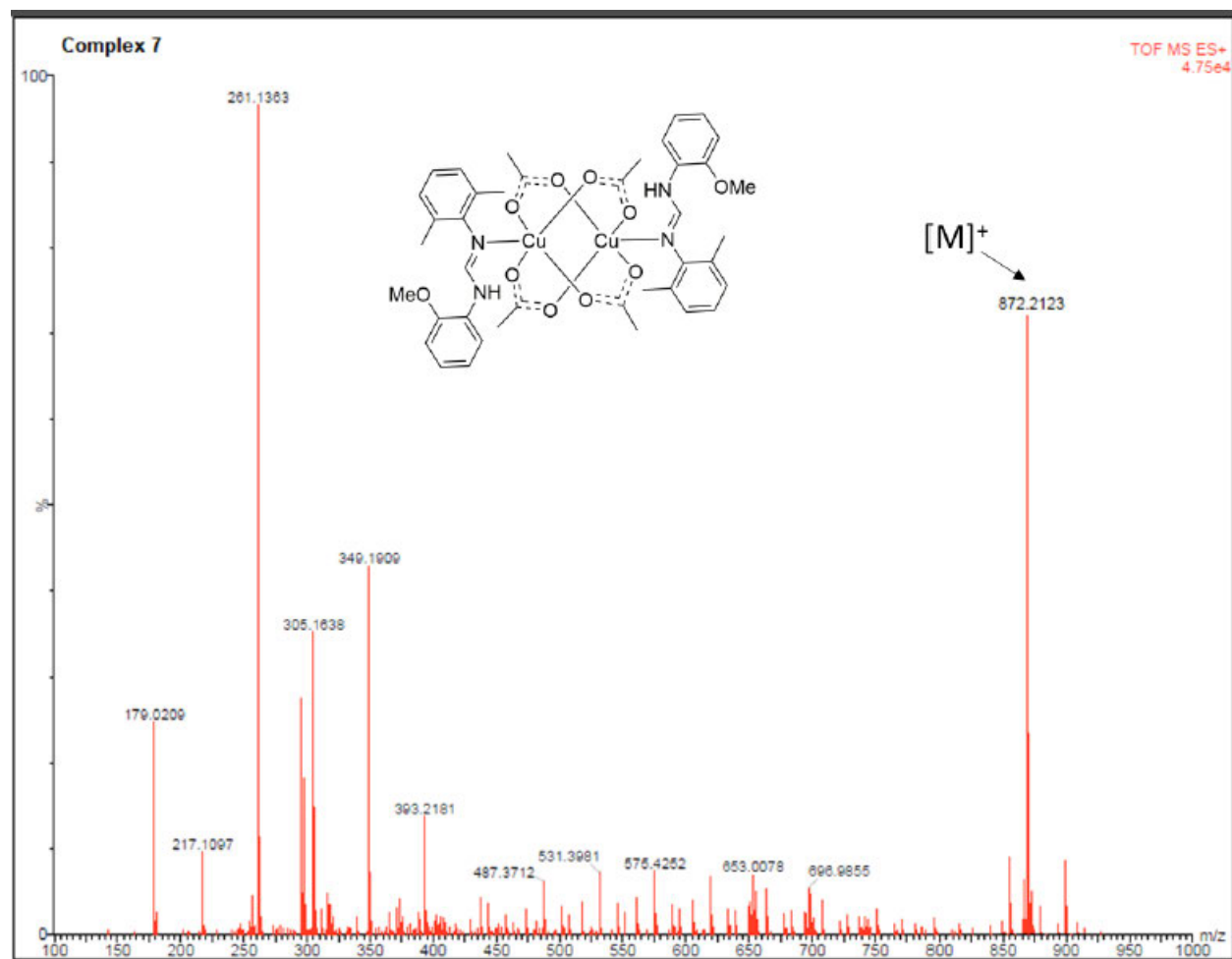
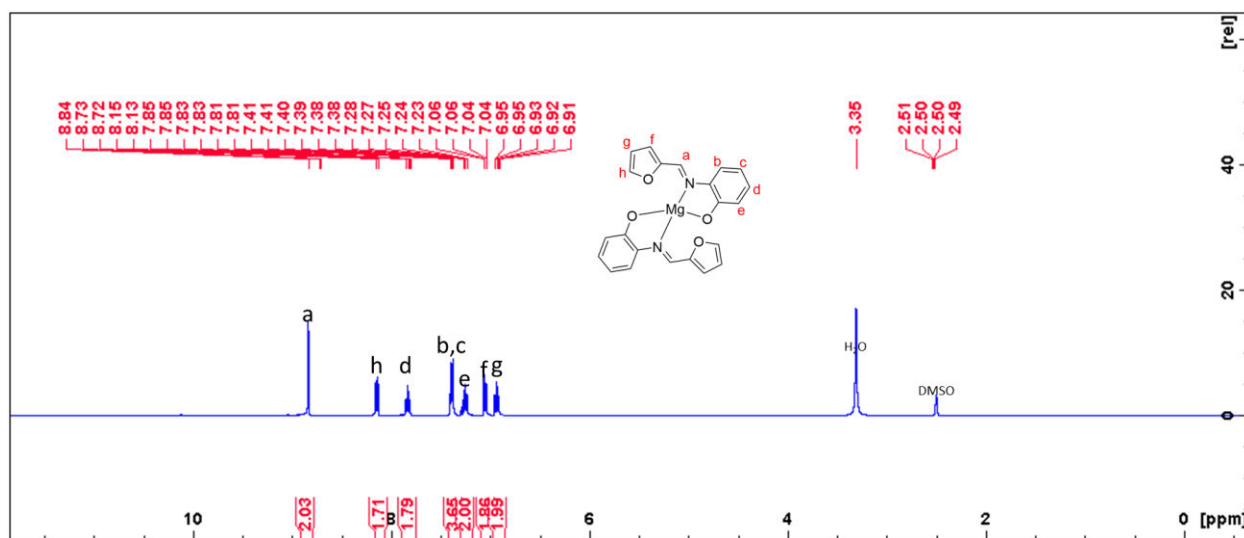Figure. S7. ESI-MS spectrum for complex **3.7**
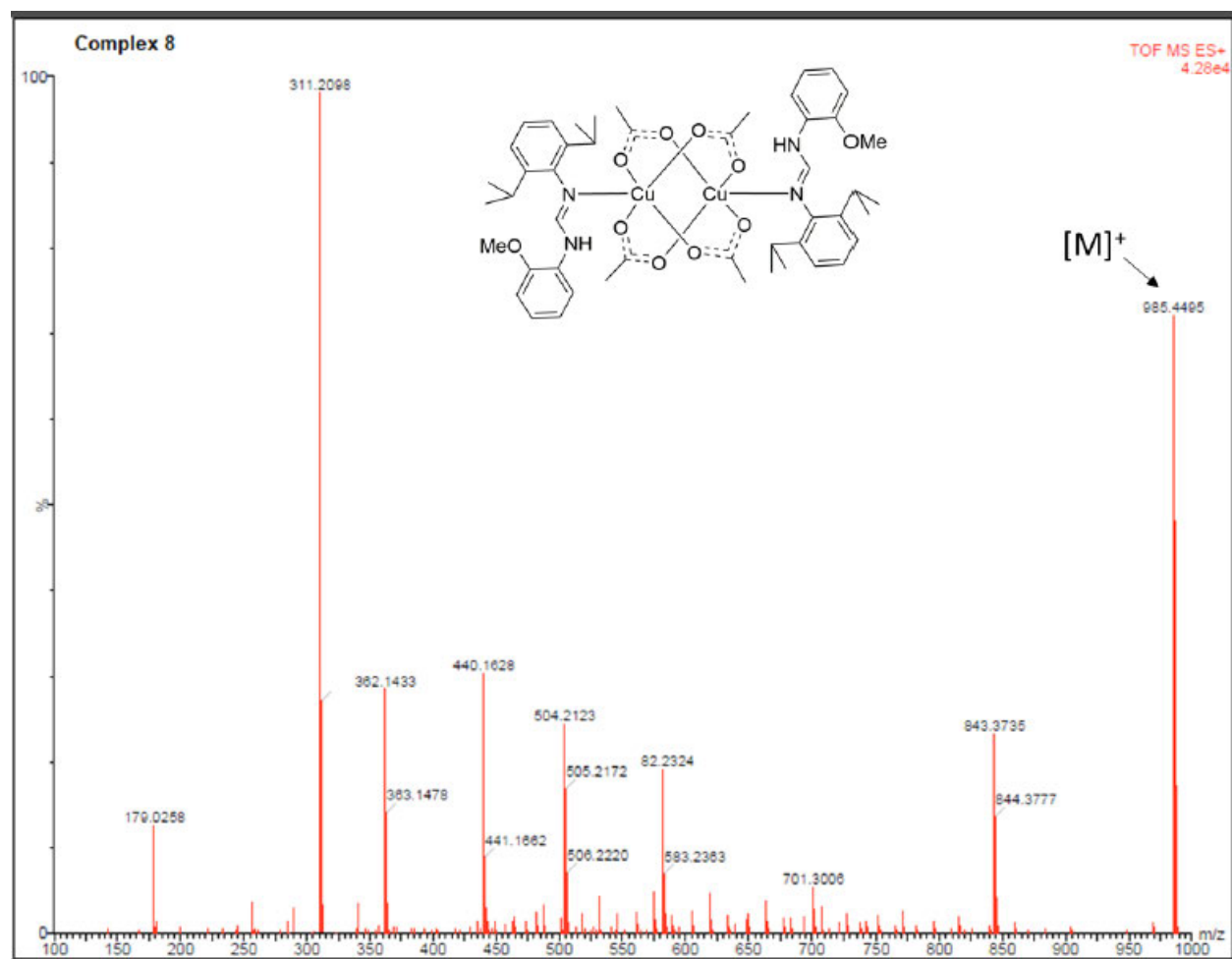
Figure. S8. ESI-MS spectrum for complex **3.8**
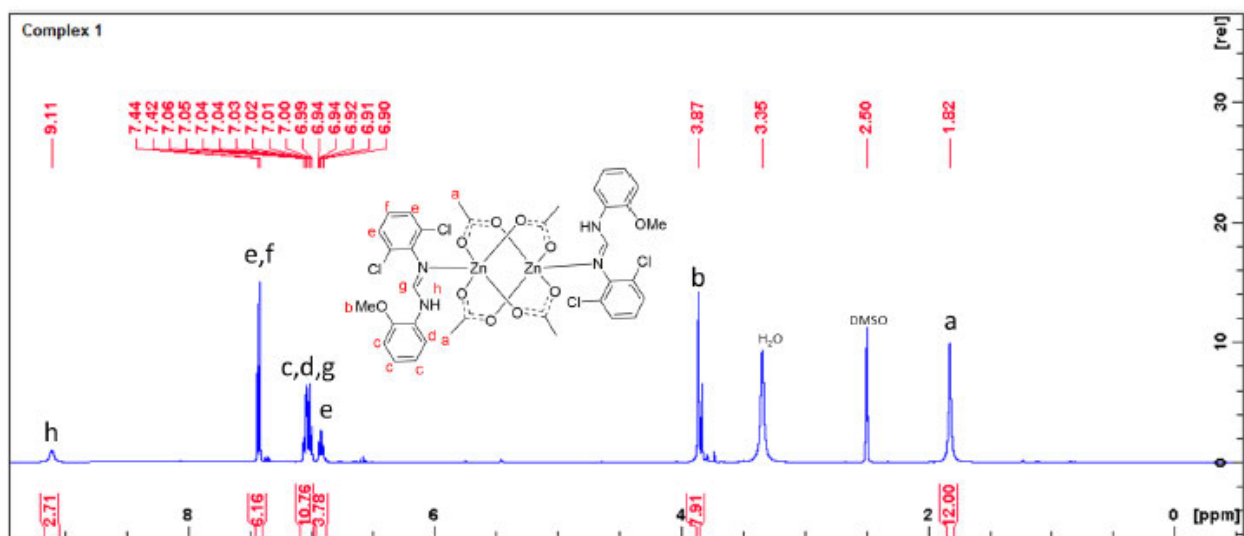
Figure. S9a H^1 NMR spectrum of complex **3.1** at room temperature in DMSO (400 MHz)
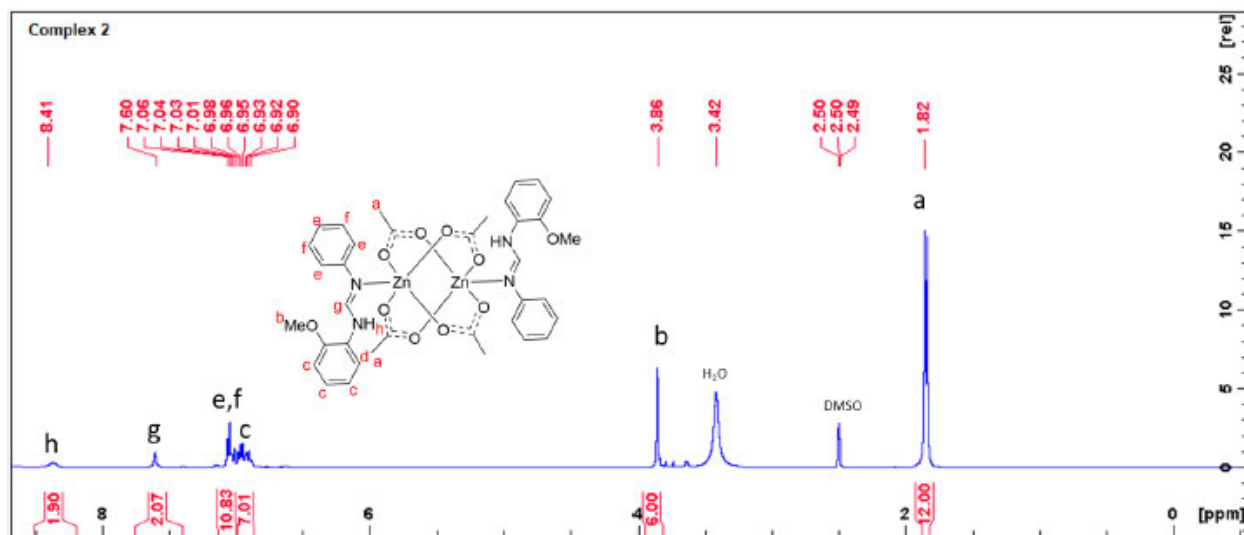
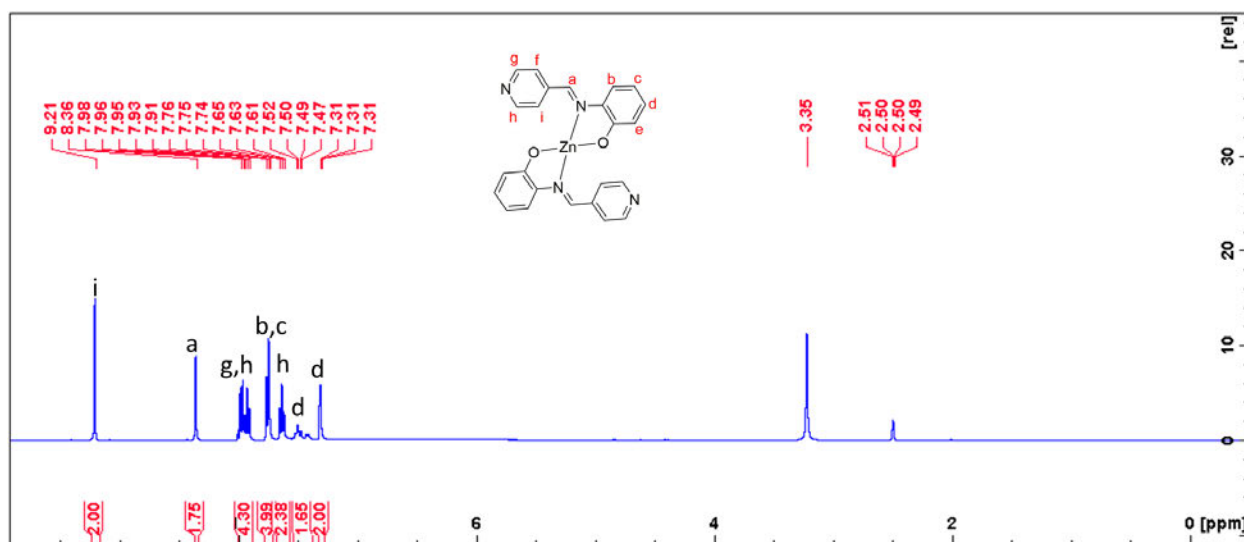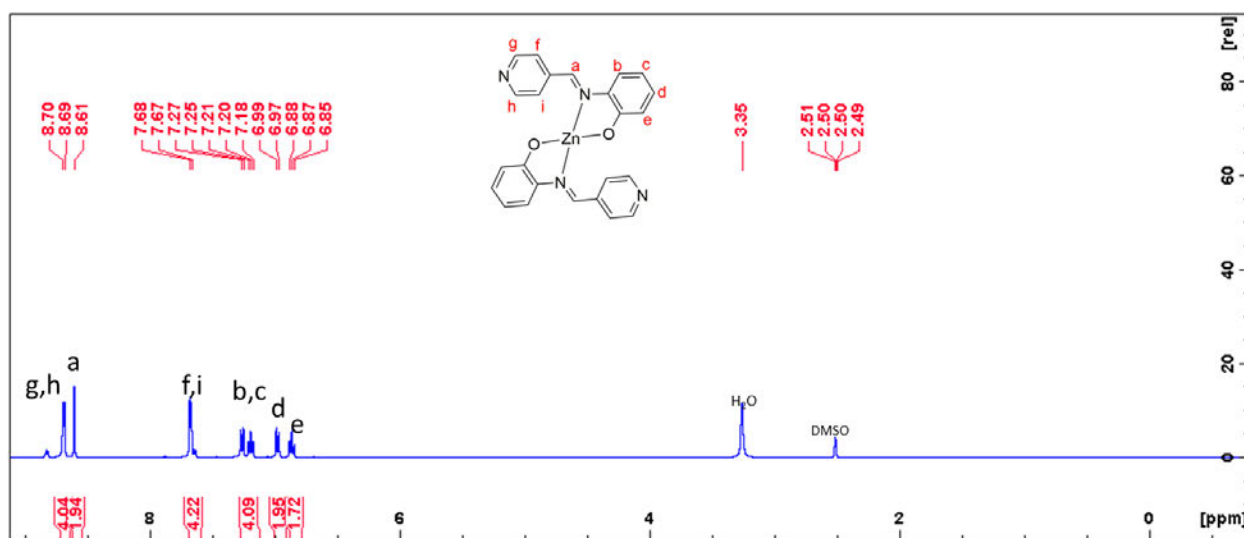Figure. S9b H^1 NMR spectrum of complex **3.2** at room temperature in DMSO (400 MHz)
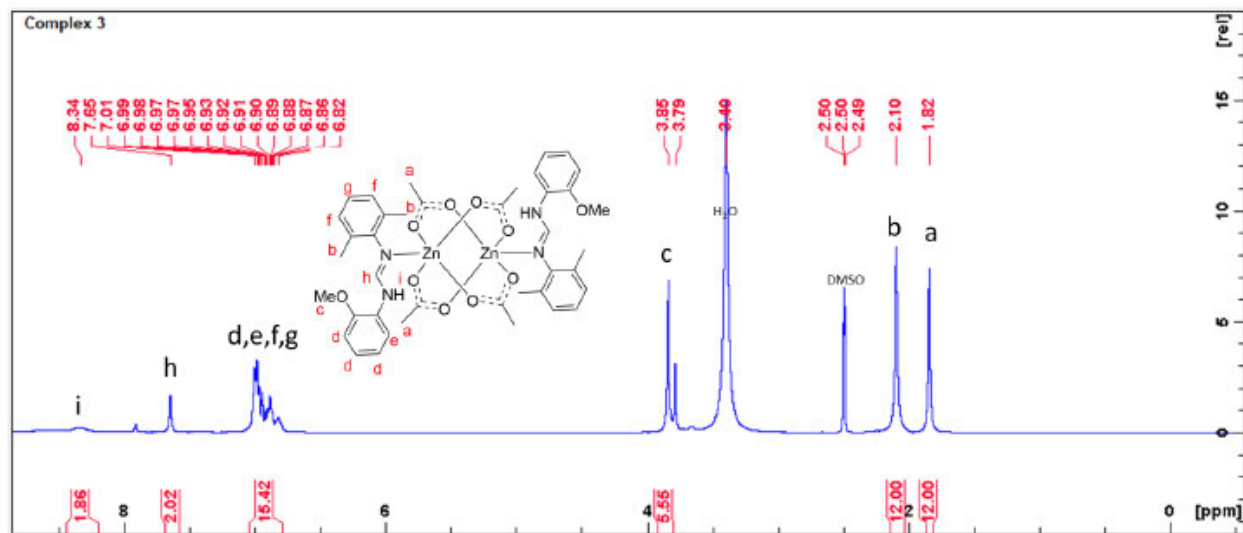
Figure. S9c H^1 NMR spectrum of complex **3.3** at room temperature in DMSO (400 MHz)
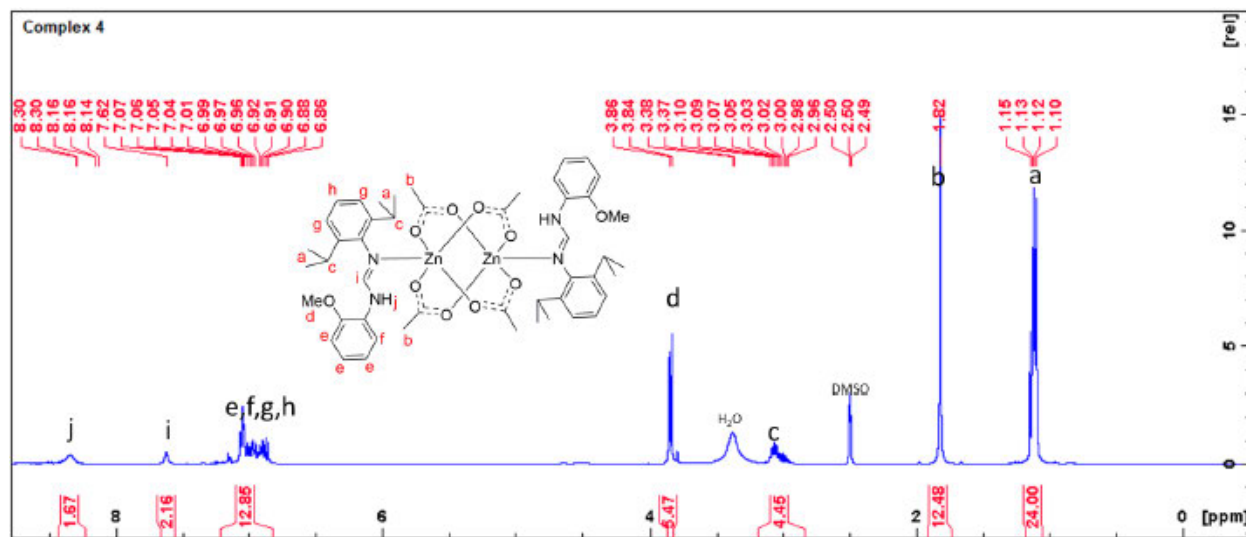
Figure. S9b H^1 NMR spectrum of complex **3.4** at room temperature in DMSO (400 MHz)
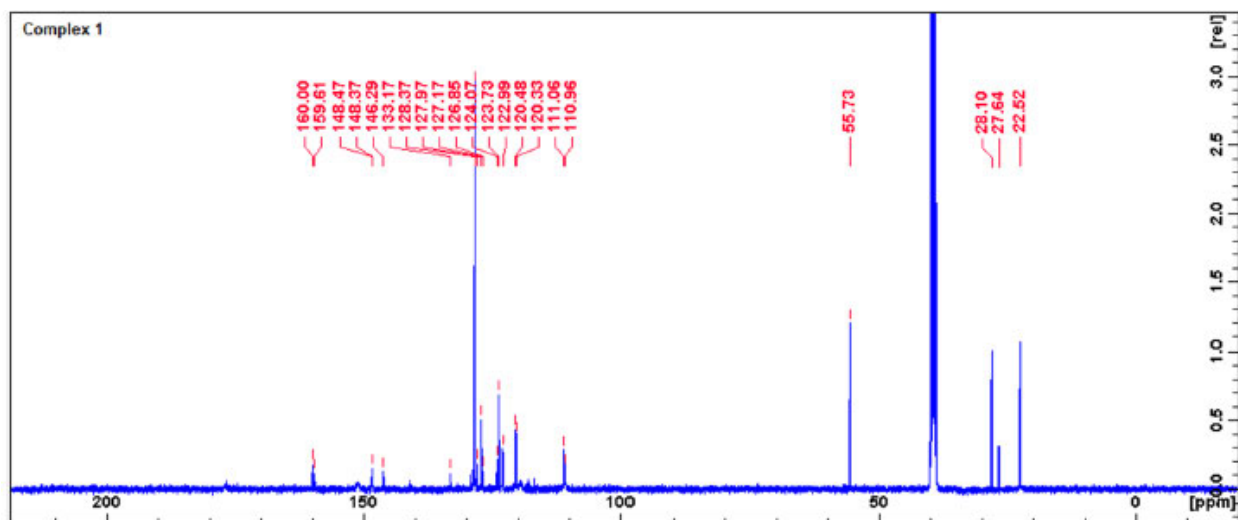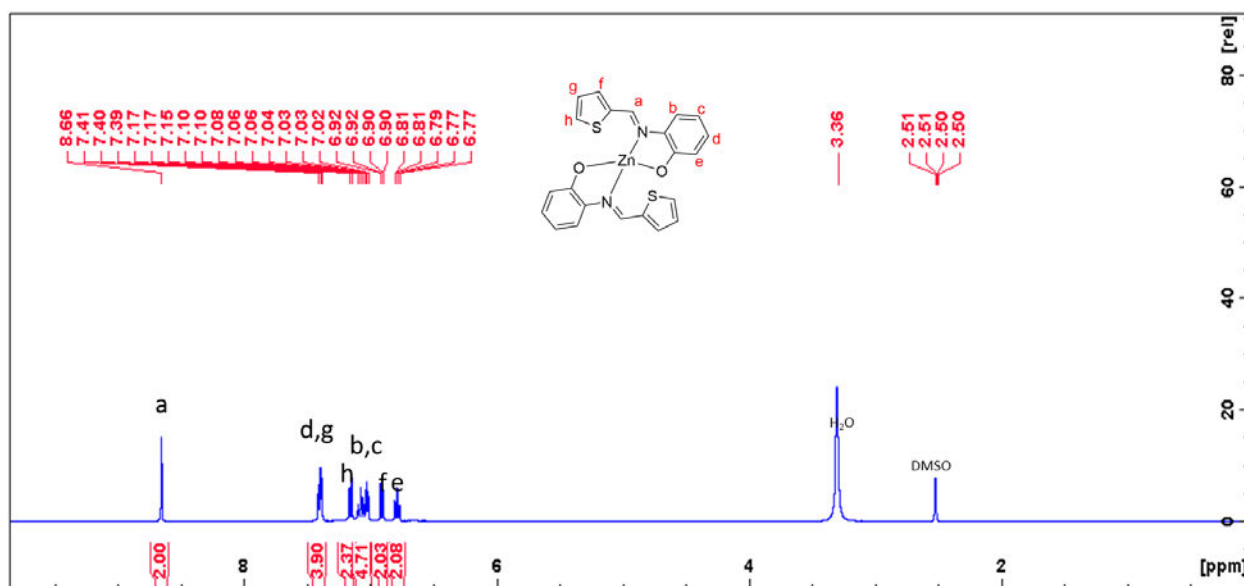
Figure. S9e ^{13}C NMR spectrum of complex **3.1** at room temperature in DMSO (400 MHz)
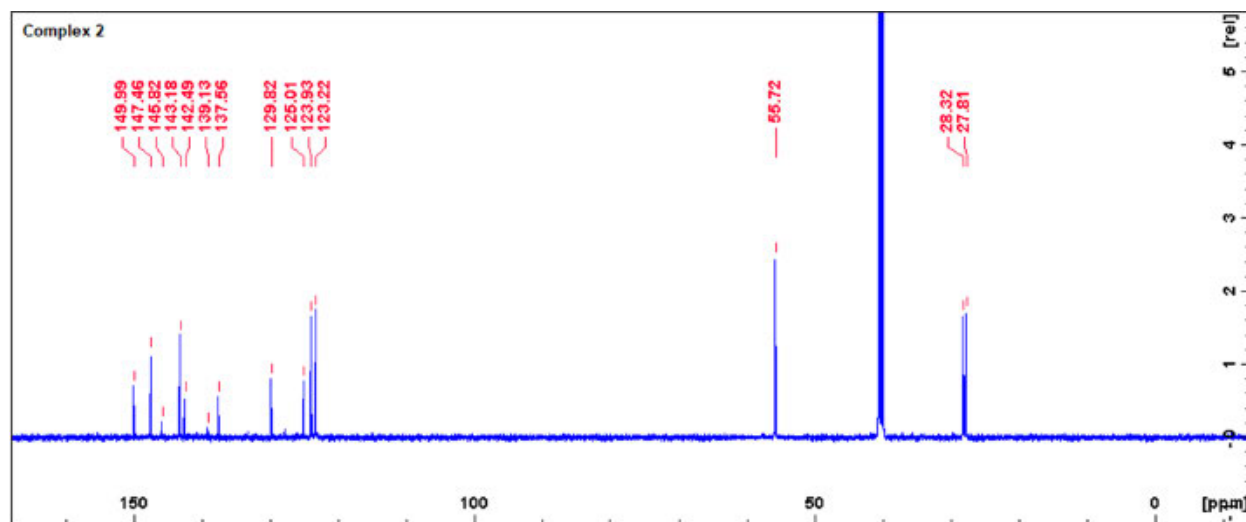
Figure. S9f ^{13}C NMR spectrum of complex **3.2** at room temperature in DMSO (400 MHz)
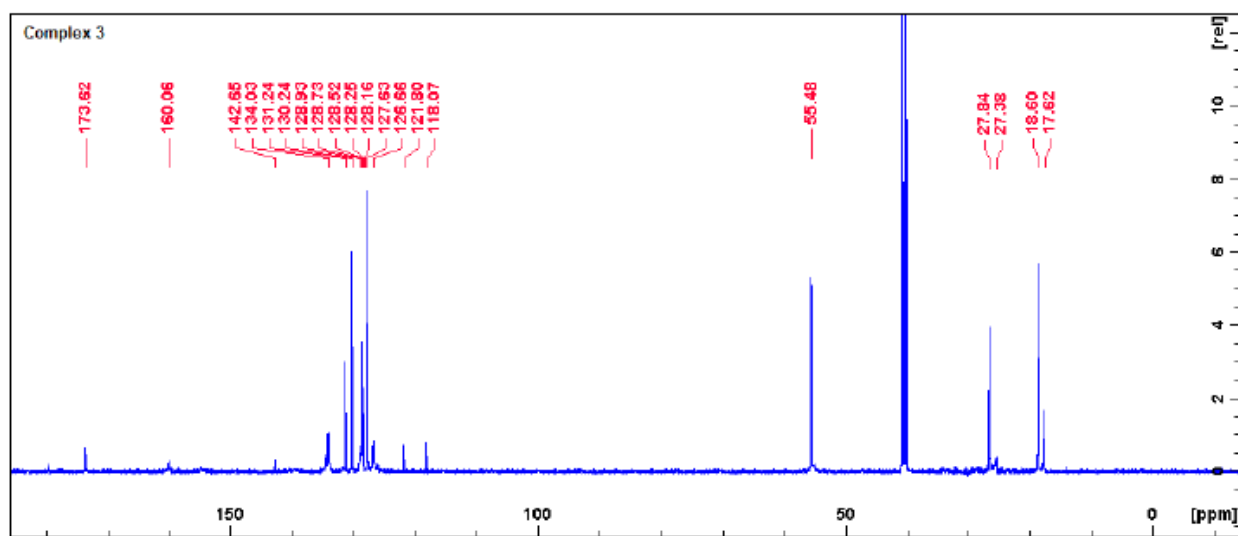
Figure. S9 ^{13}C NMR spectrum of complex **3.3** at room temperature in DMSO (400 MHz)
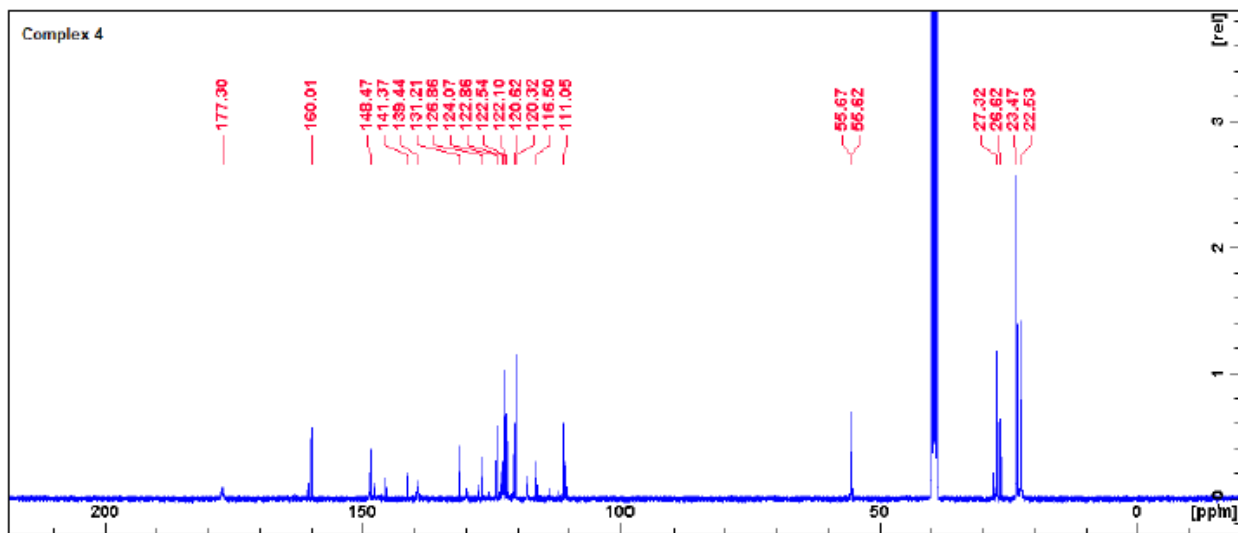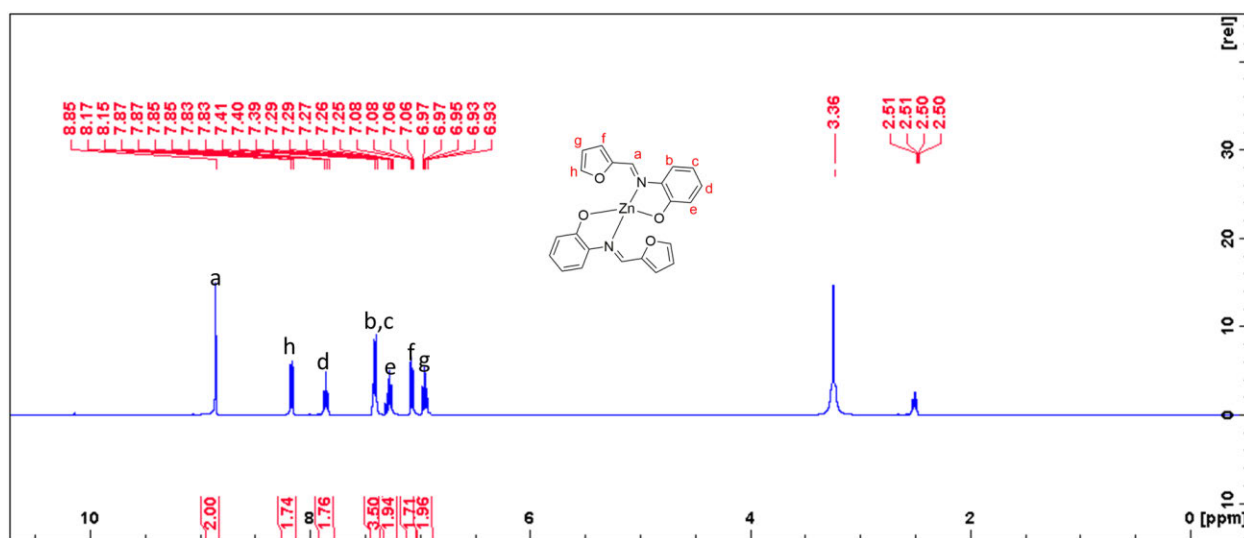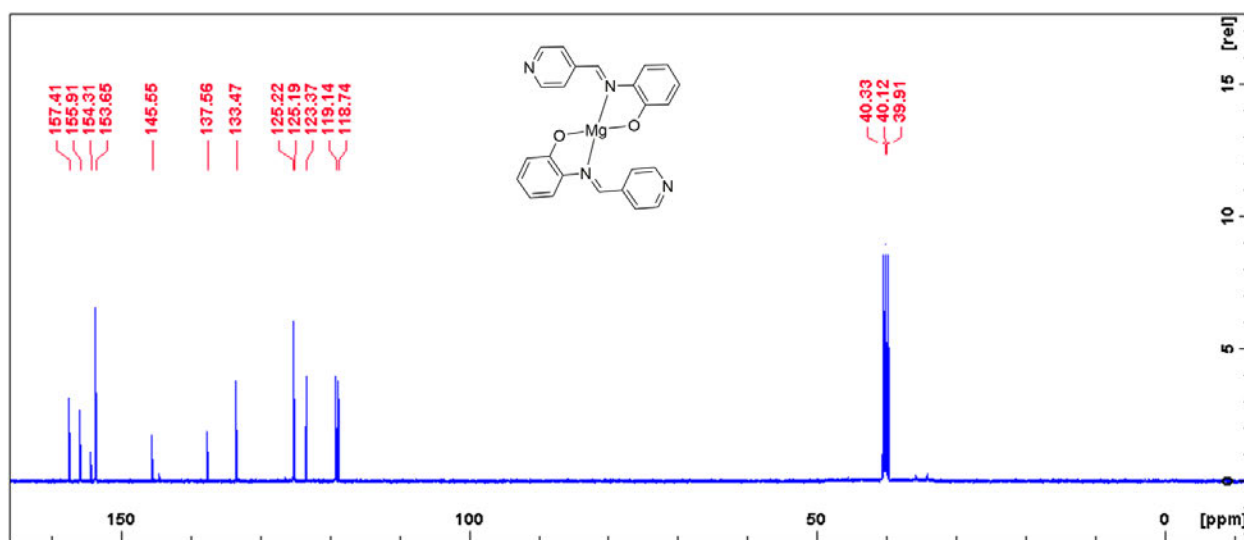

Figure. S9h ^{13}C NMR spectrum of complex **3.4** at room temperature in DMSO (400 MHz)
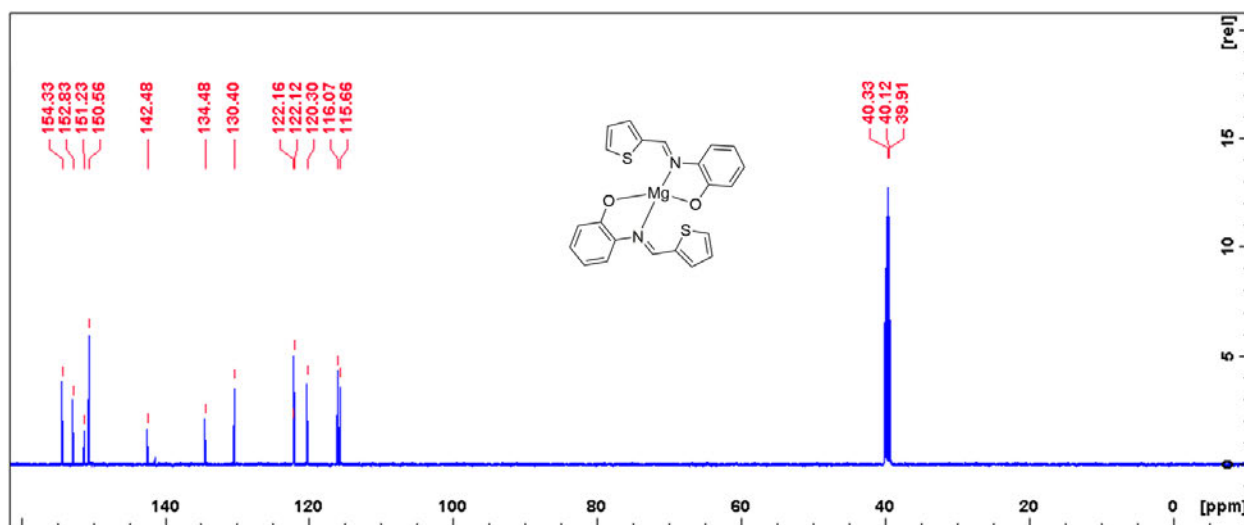
Kinetics and synthesis of low molecular weight polyesters using Zn(II) and Cu(II) *N*-hydroxy *N,N'*-diarylformamidine complexes
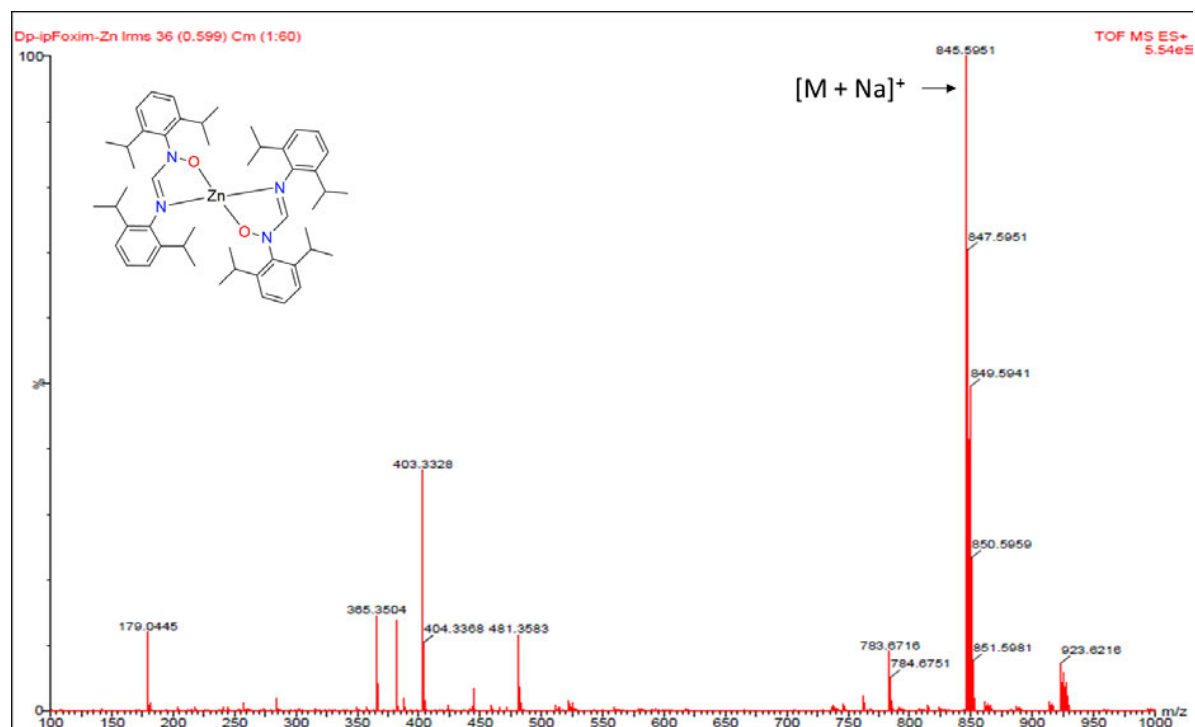
Fig. S1a. ESI-MS spectrum for complex **4.1**
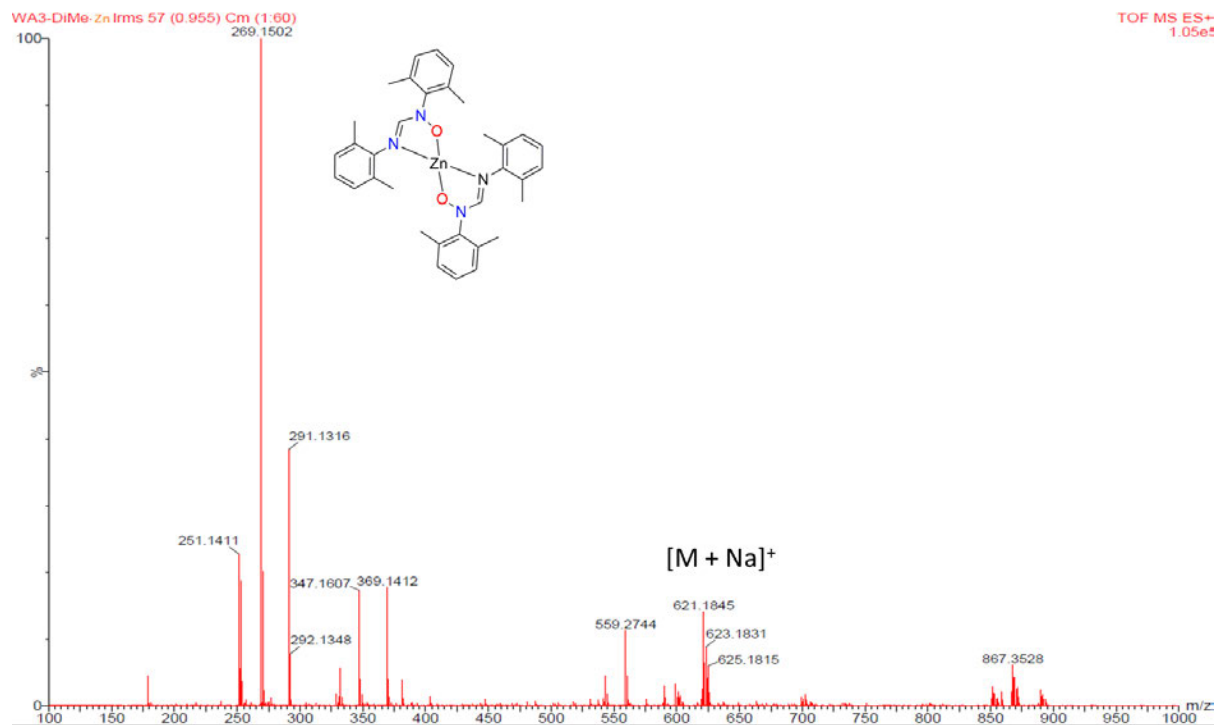
Fig. S1b. ESI-MS spectrum for complex **4.2**
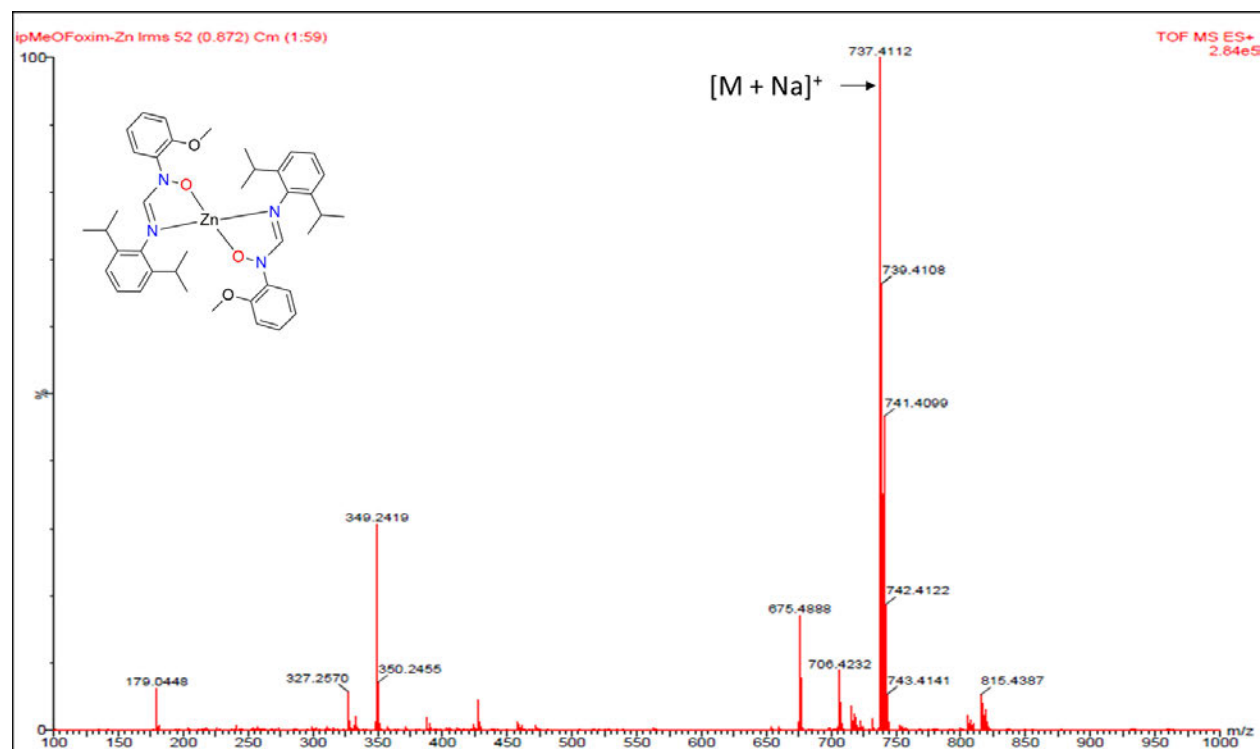
Fig. S1c. ESI-MS spectrum for complex **4.3**
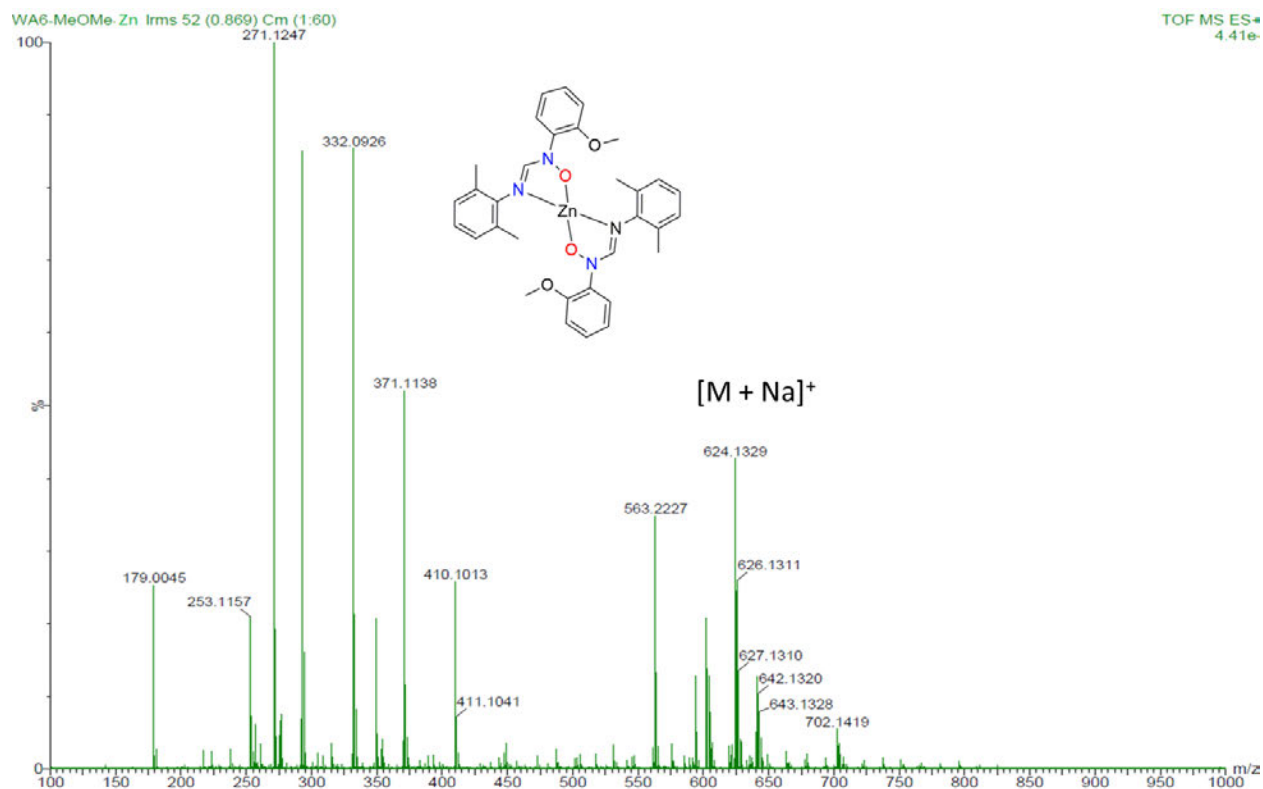
Fig. S1d. ESI-MS spectrum for complex **4.4**
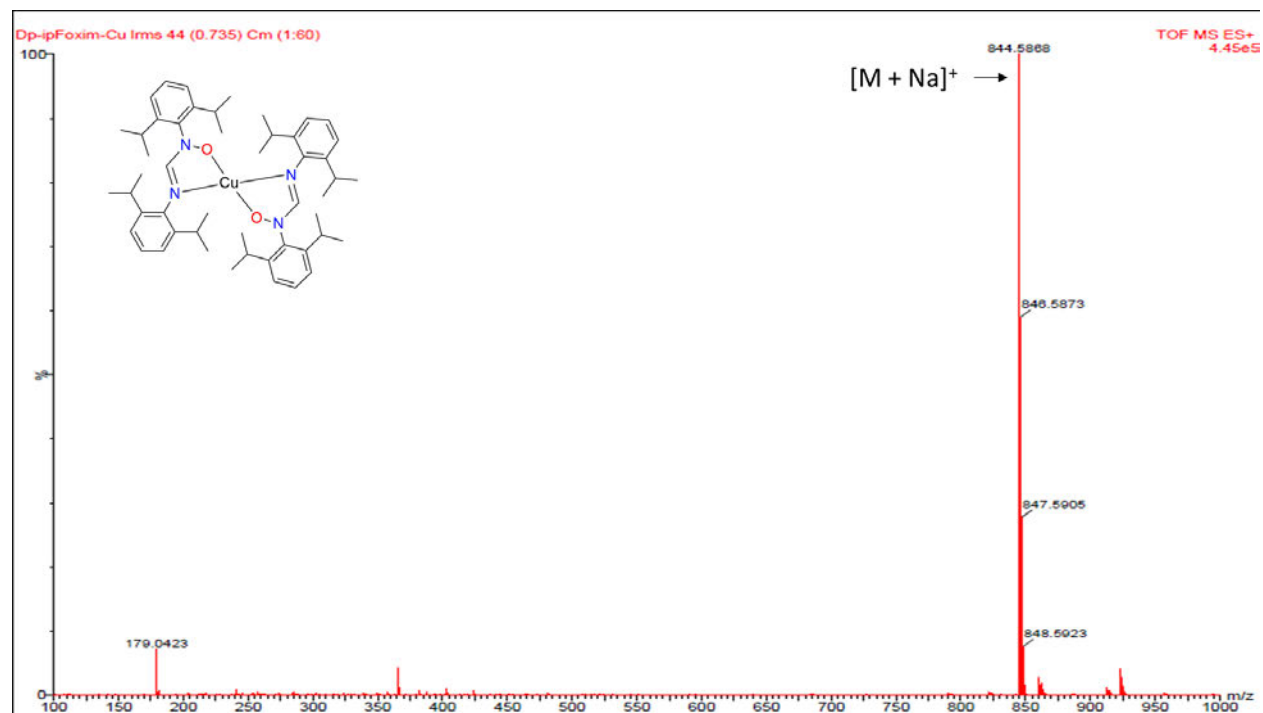
Fig. S1e. ESI-MS spectrum for complex **4.5**
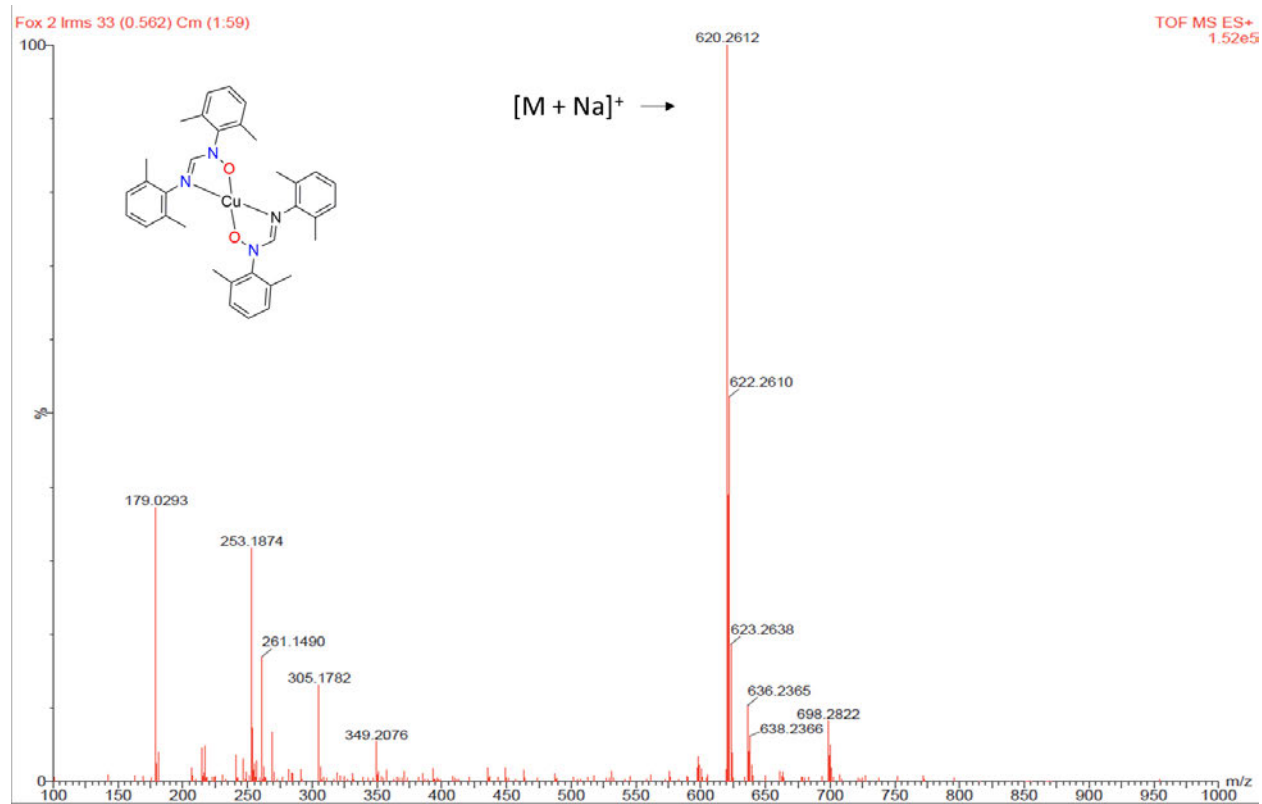
Fig. S1f. ESI-MS spectrum for complex **4.6**
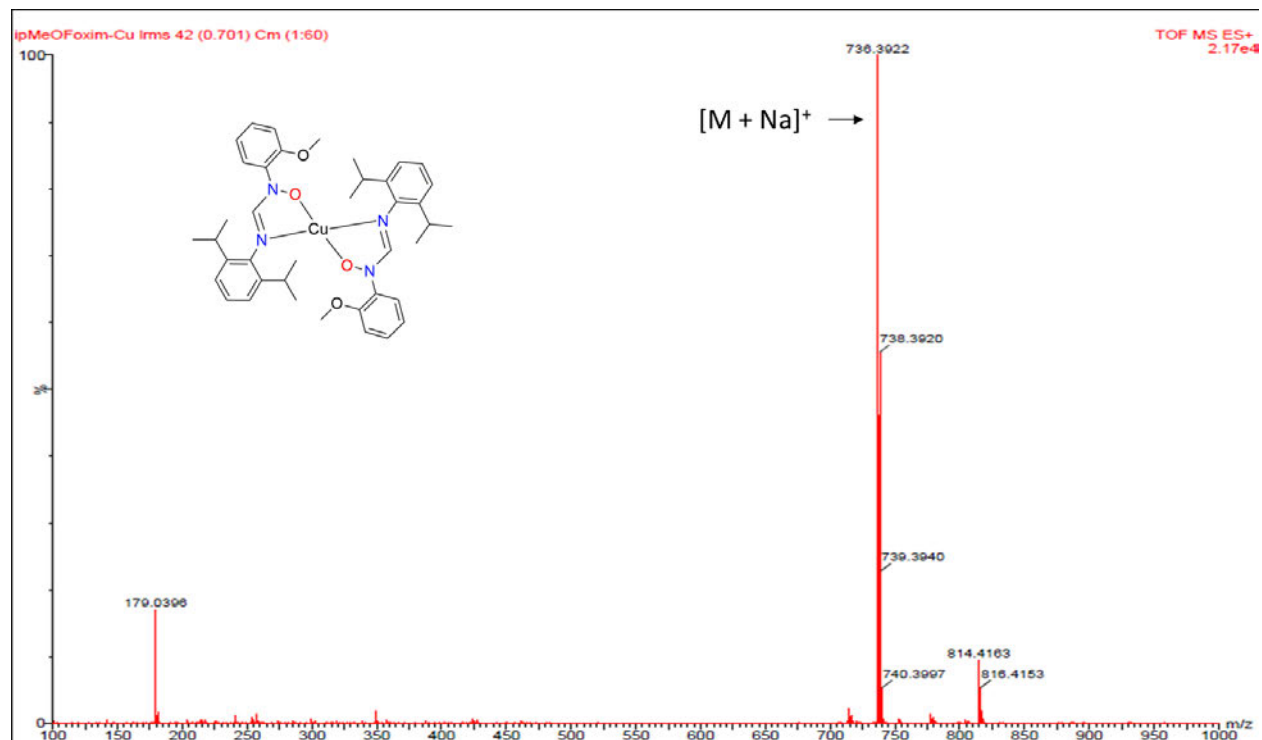
Fig. S1g. ESI-MS spectrum for complex **4.7**
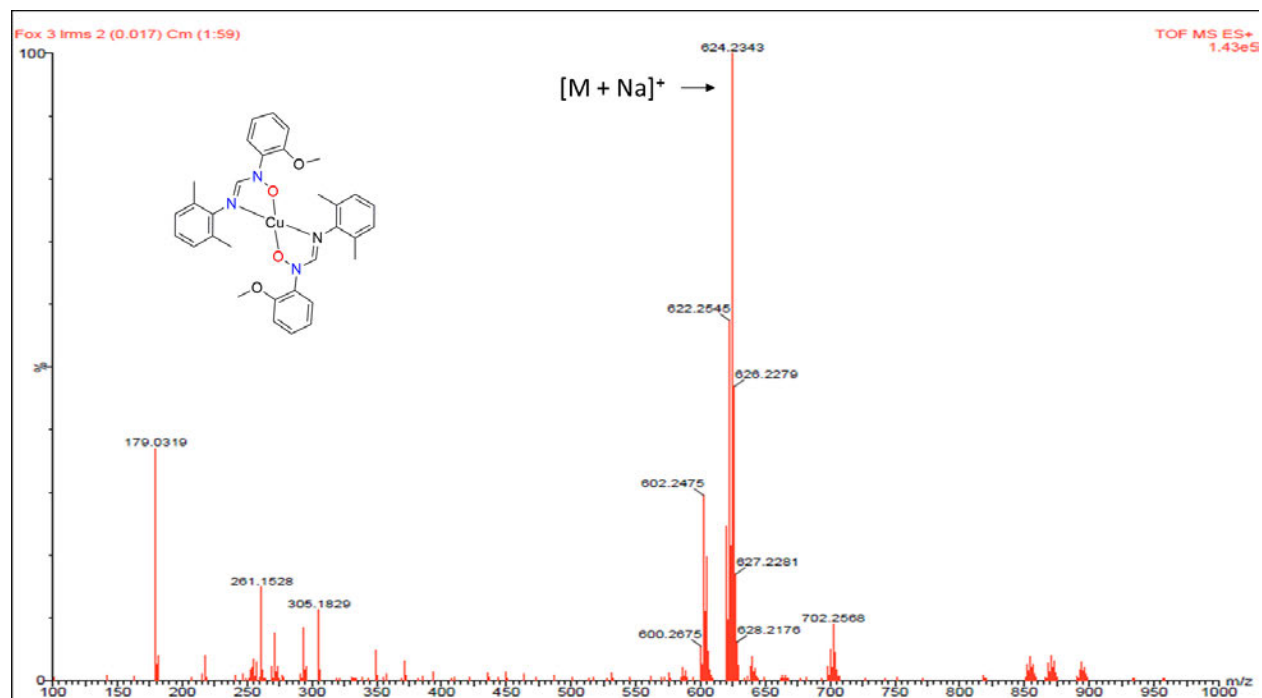
Fig. S1h. ESI-MS spectrum for complex **4.8**
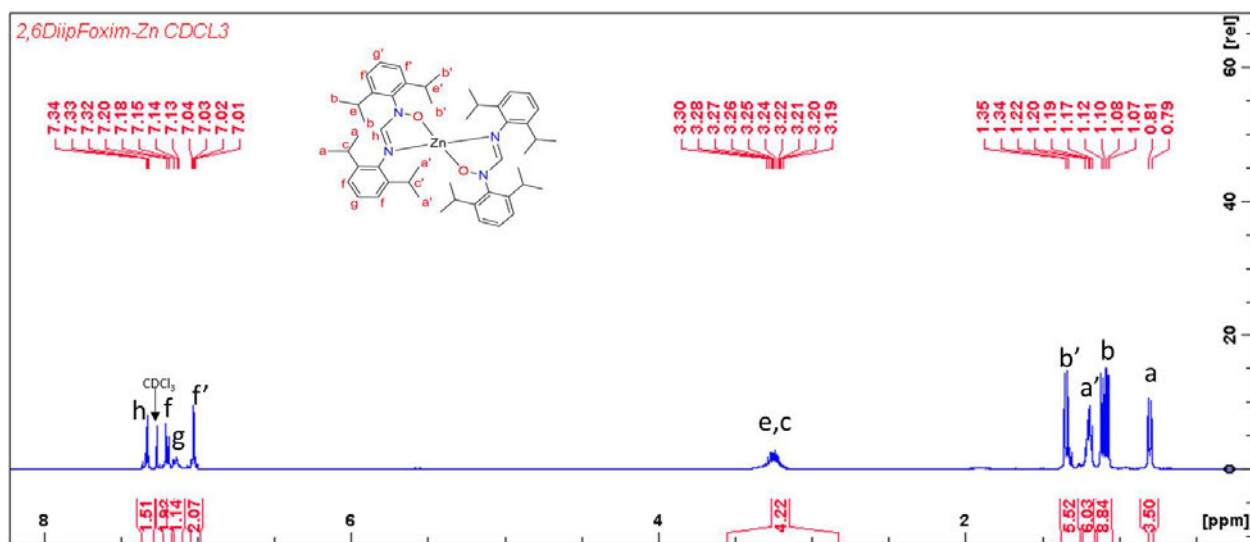
Fig. S2a. H^1 NMR spectrum of complex **4.1** at room temperature in CDCl$_3$ (400 MHz)
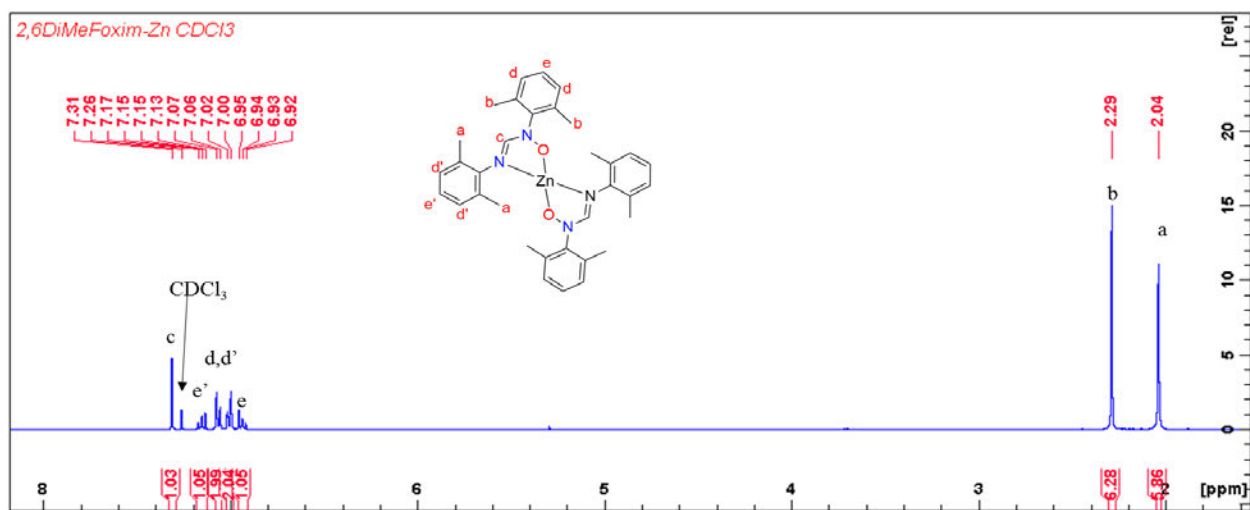
Fig. S2b. H^1 NMR spectrum of complex **4.2** at room temperature in CDCl$_3$ (400 MHz)
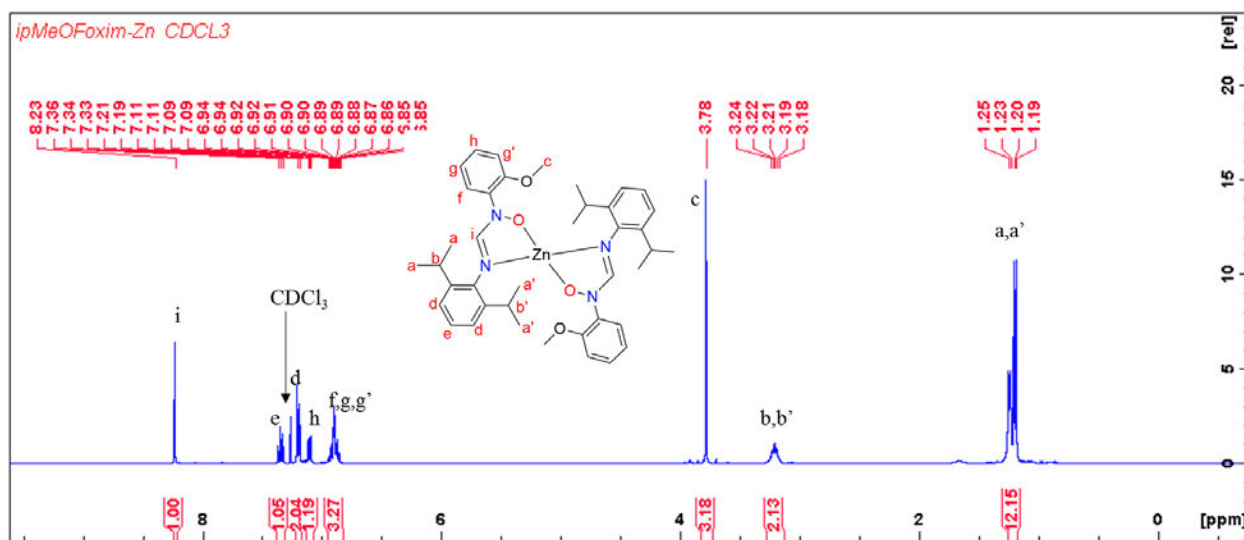
Fig. S2c. H[1] NMR spectrum of complex **4.3** at room temperature in CDCl₃ (400 MHz)
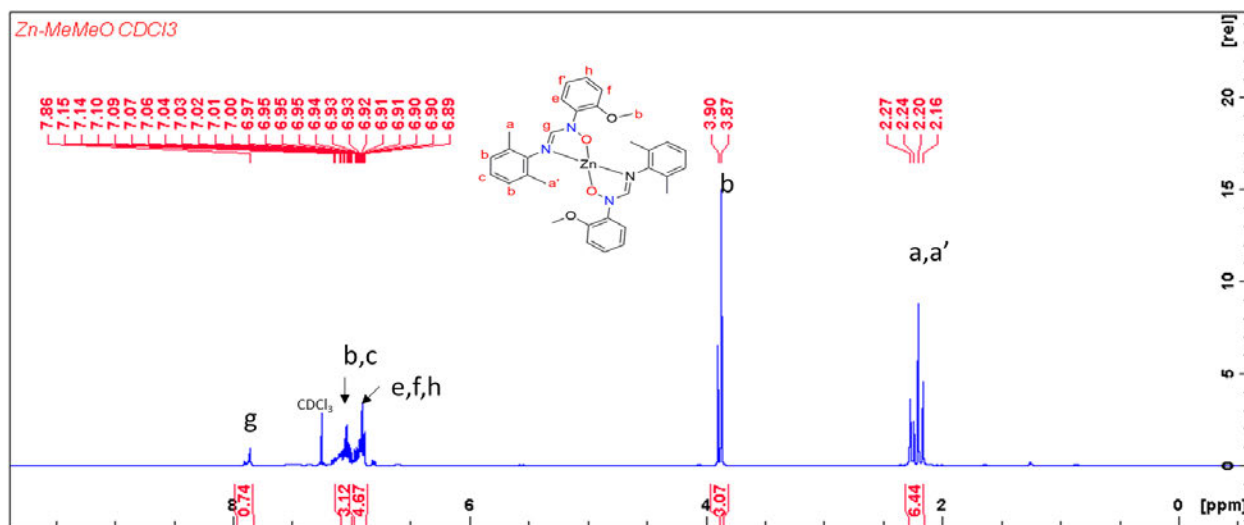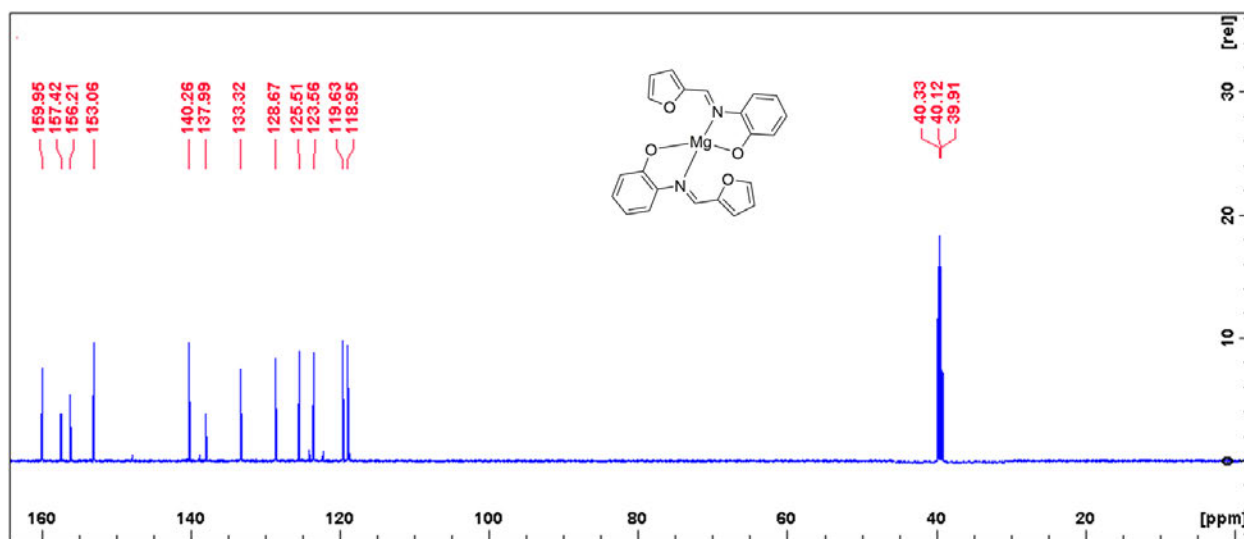

Fig. S2b. H[1] NMR spectrum of complex **4.4** at room temperature in CDCl₃ (400 MHz)
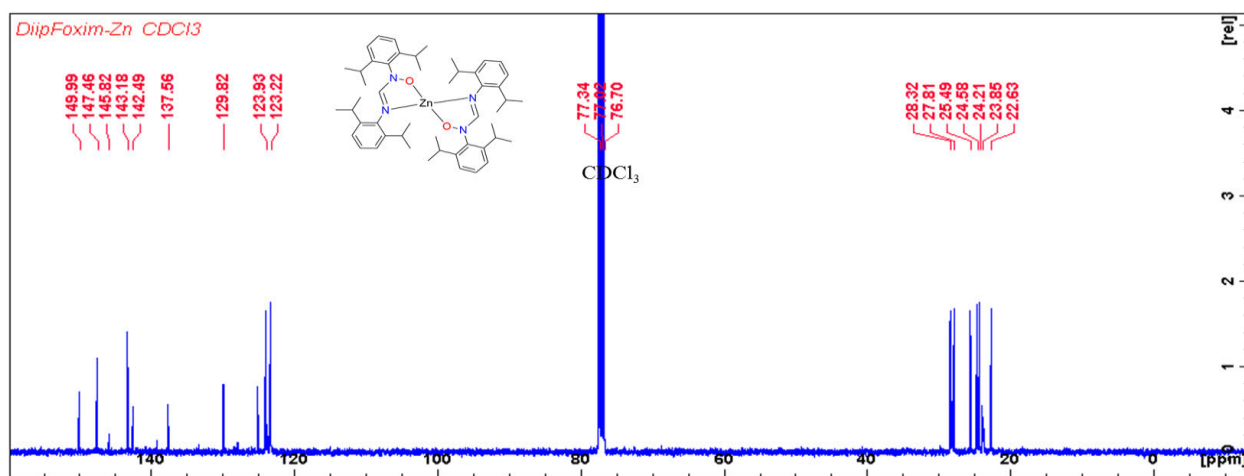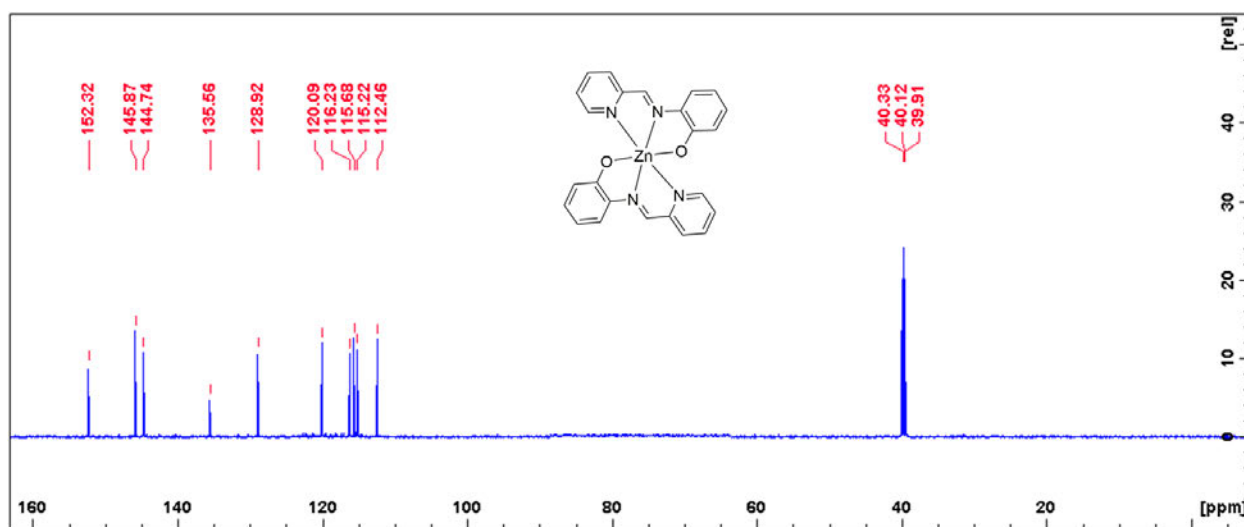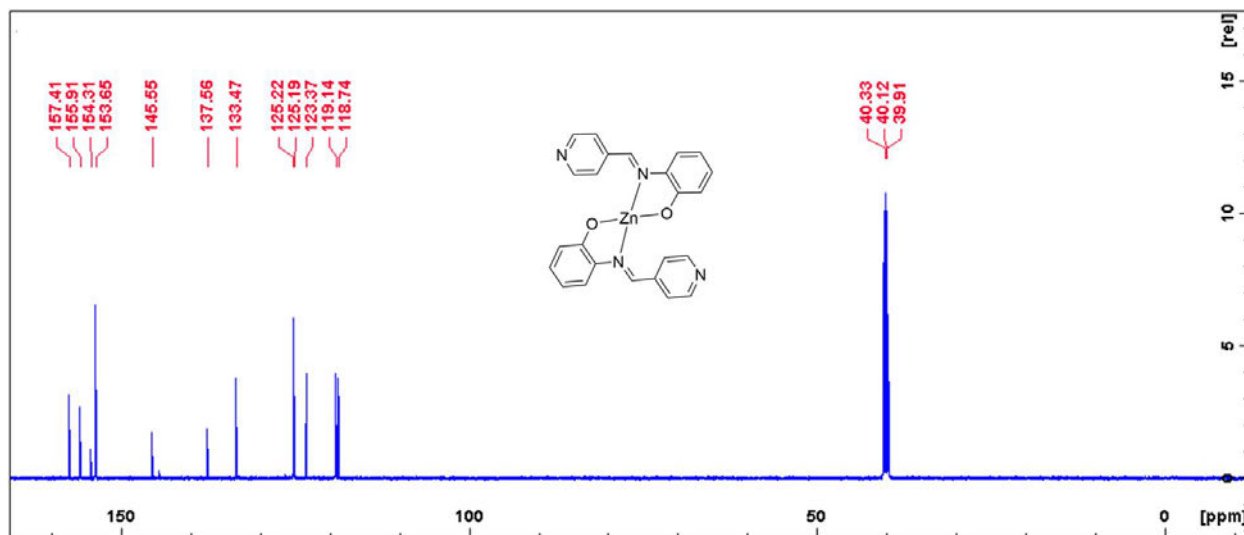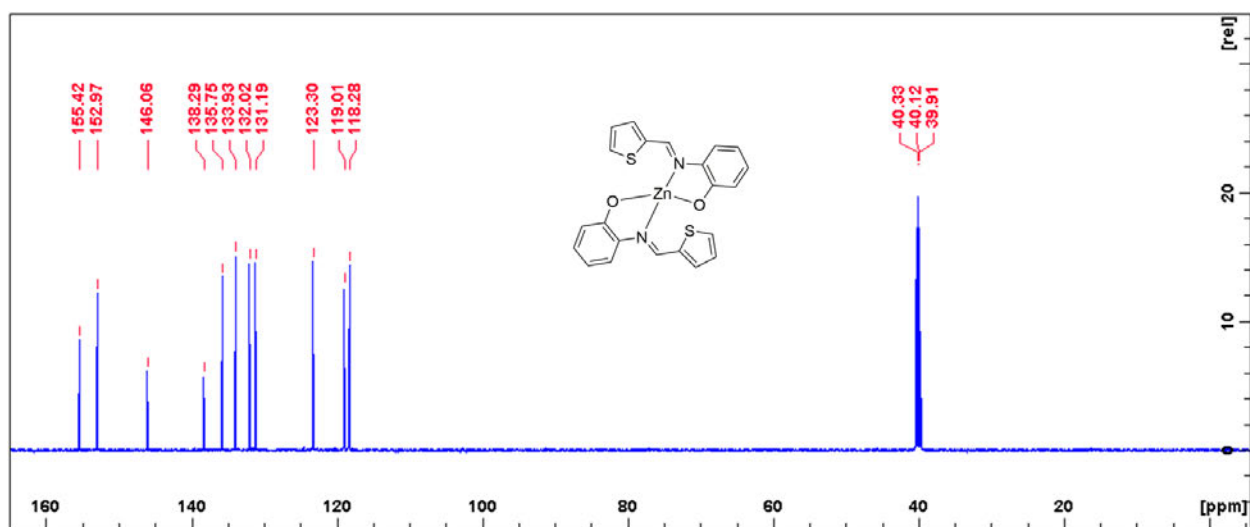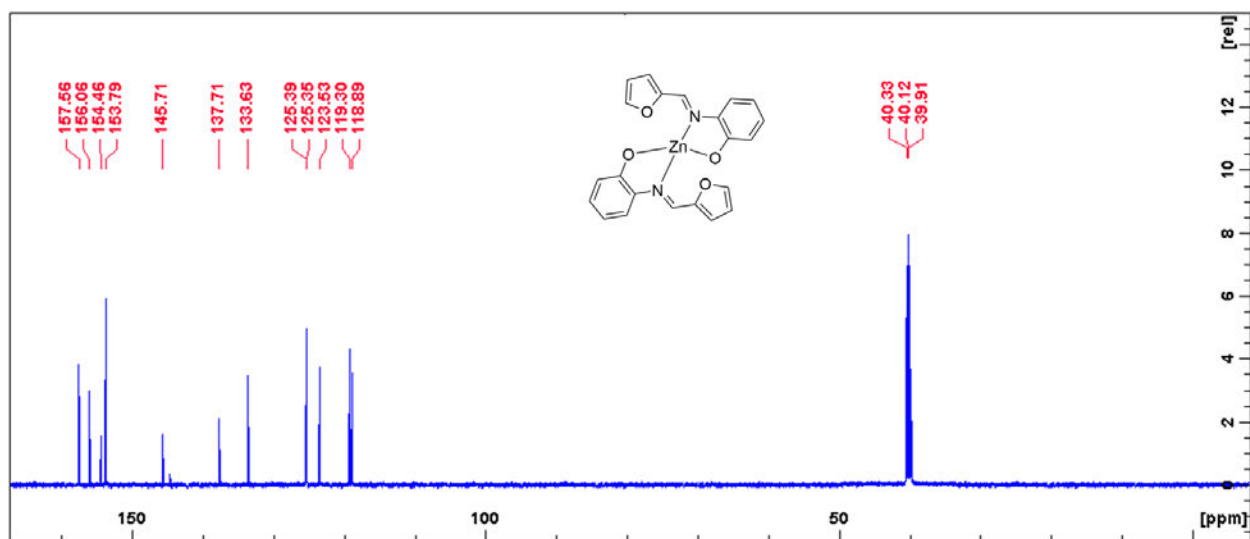
Fig. S2e. ^{13}C NMR spectrum of complex **4.1** at room temperature in CDCl$_3$ (400 MHz)
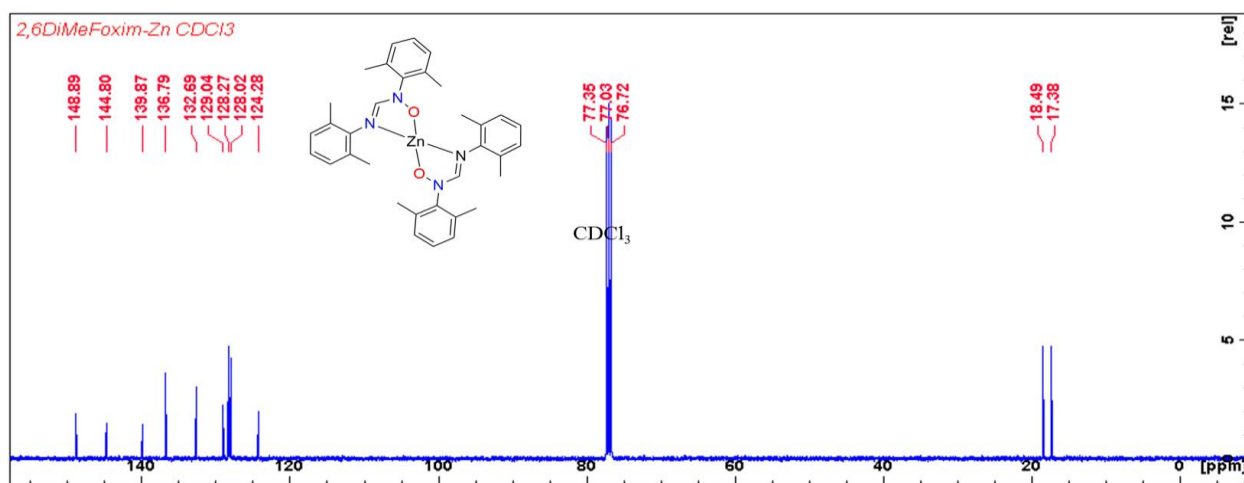
Fig. S2f. ^{13}C NMR spectrum of complex **4.2** at room temperature in CDCl$_3$ (400 MHz)
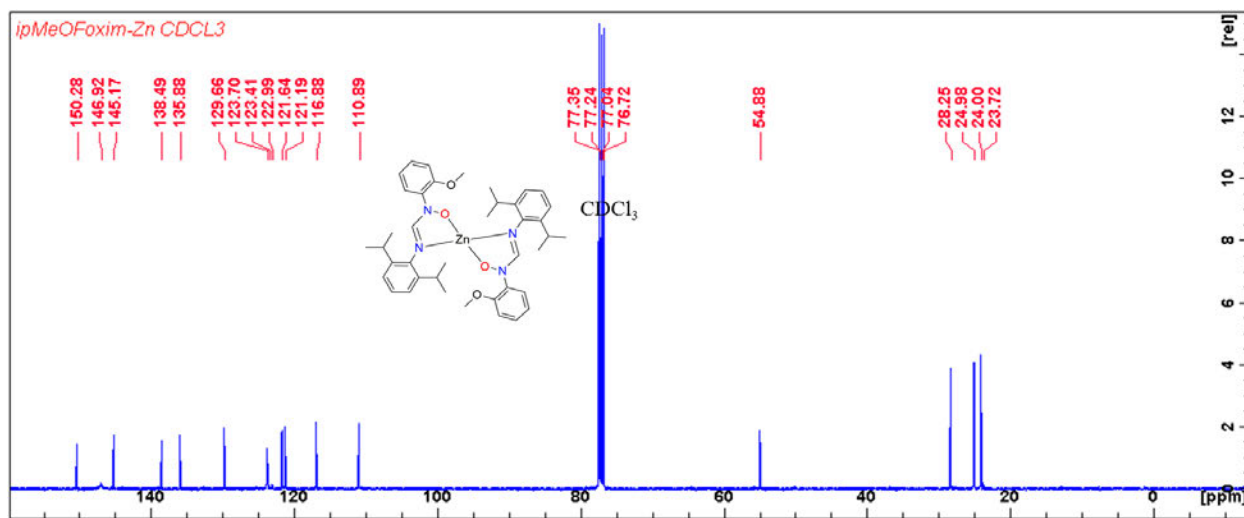
Fig. S2g. ^{13}C NMR spectrum of complex **4.3** at room temperature in CDCl$_3$ (400 MHz)
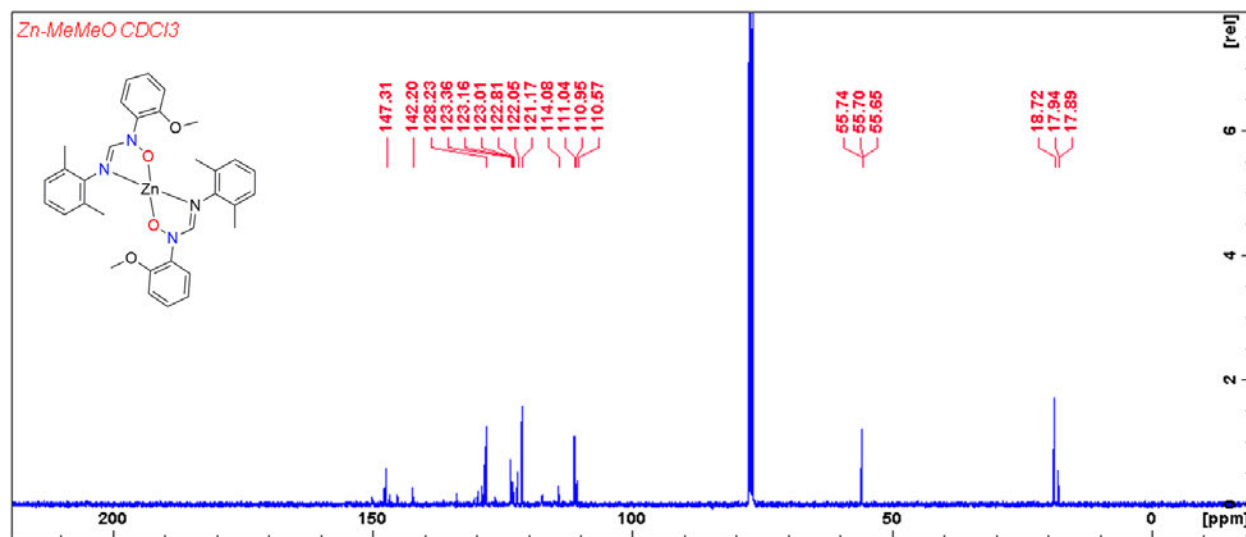
Fig. S2h. ^{13}C NMR spectrum of complex **4.4** at room temperature in CDCl$_3$ (400 MHz)

***N,O*-Amino-phenolate Mg(II) and Zn(II) Schiff base complexes: Synthesis and application in ring-opening polymerization of ε-caprolactone and lactides**
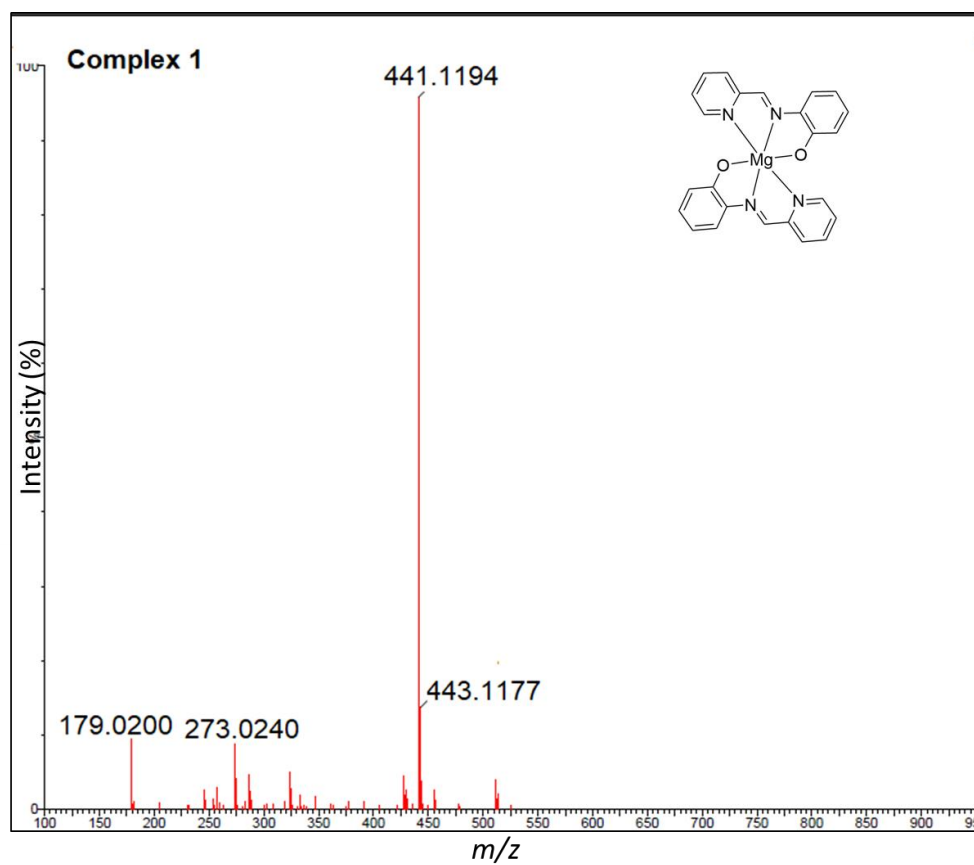
Figure. S1. ESI-MS spectrum for complex **5.1**
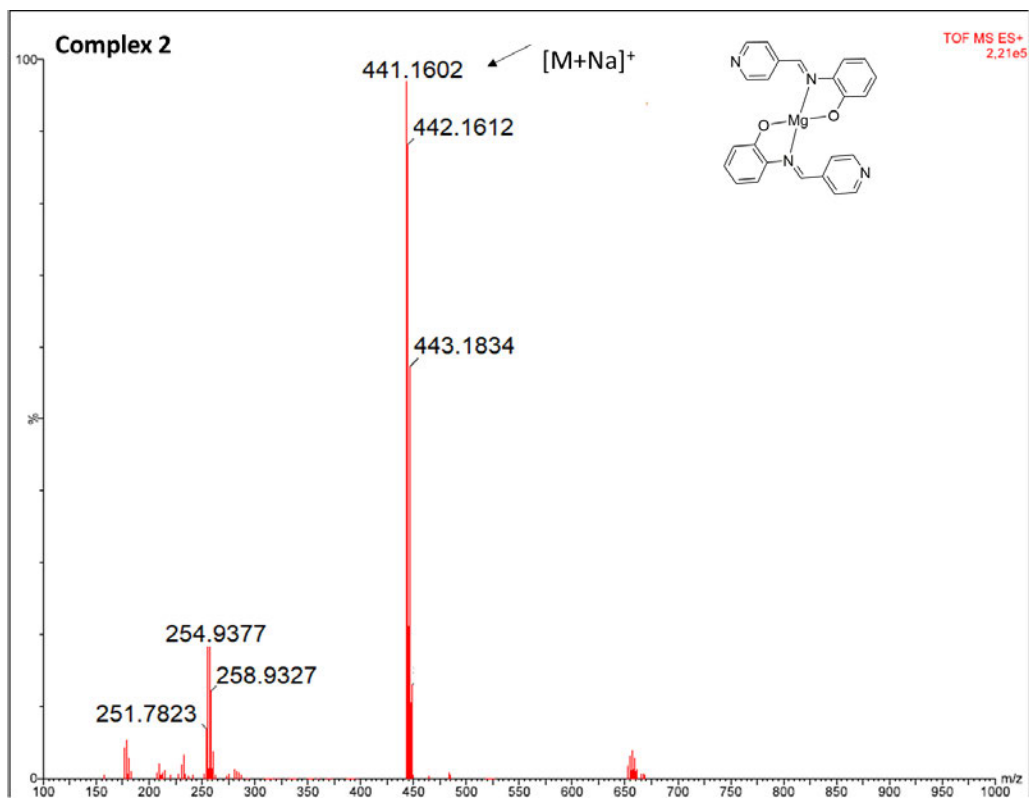
Figure.S2. ESI-MS spectrum for complex **5.2**
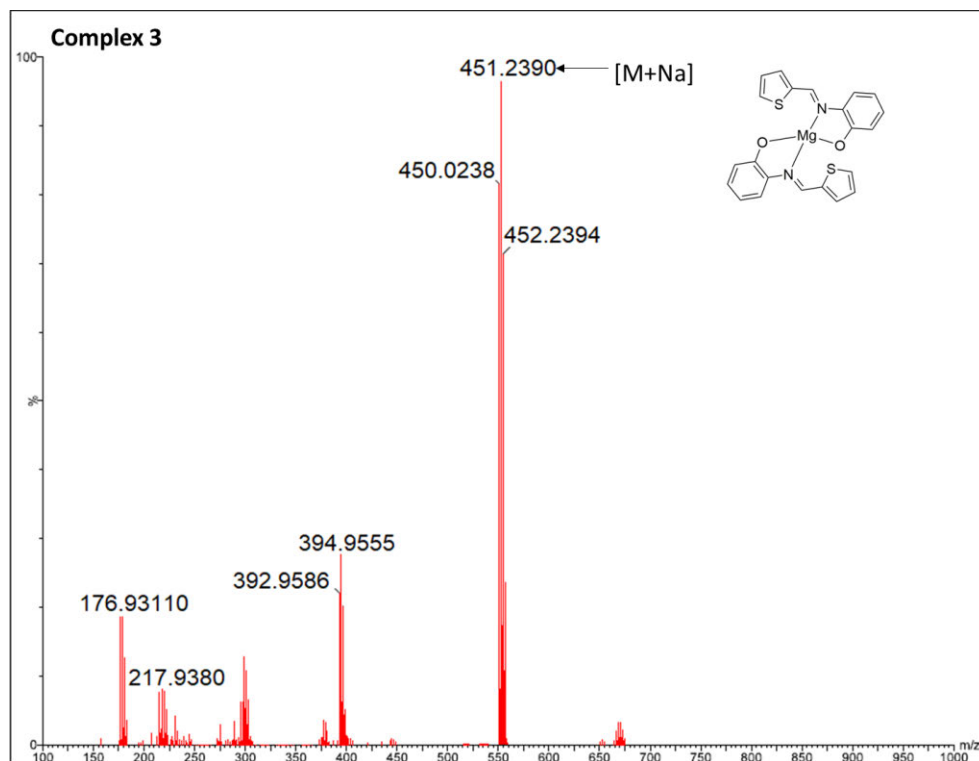
Figure. S3. ESI-MS spectrum for complex **5.3**
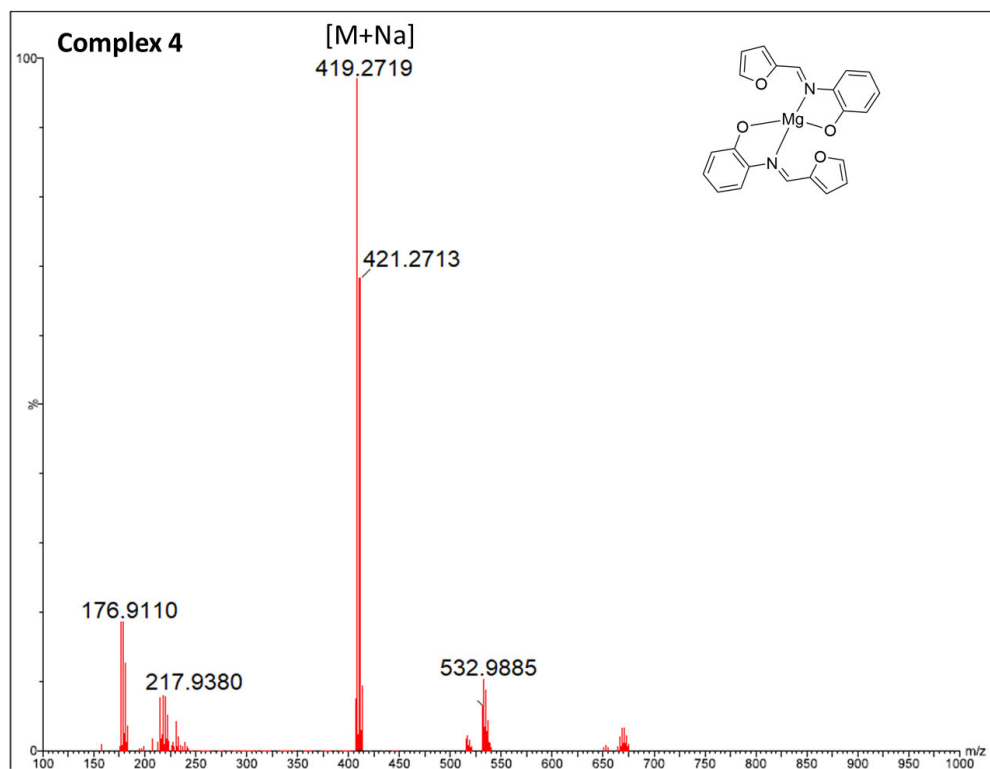
Figure. S4. ESI-MS spectrum for complex **5.4**
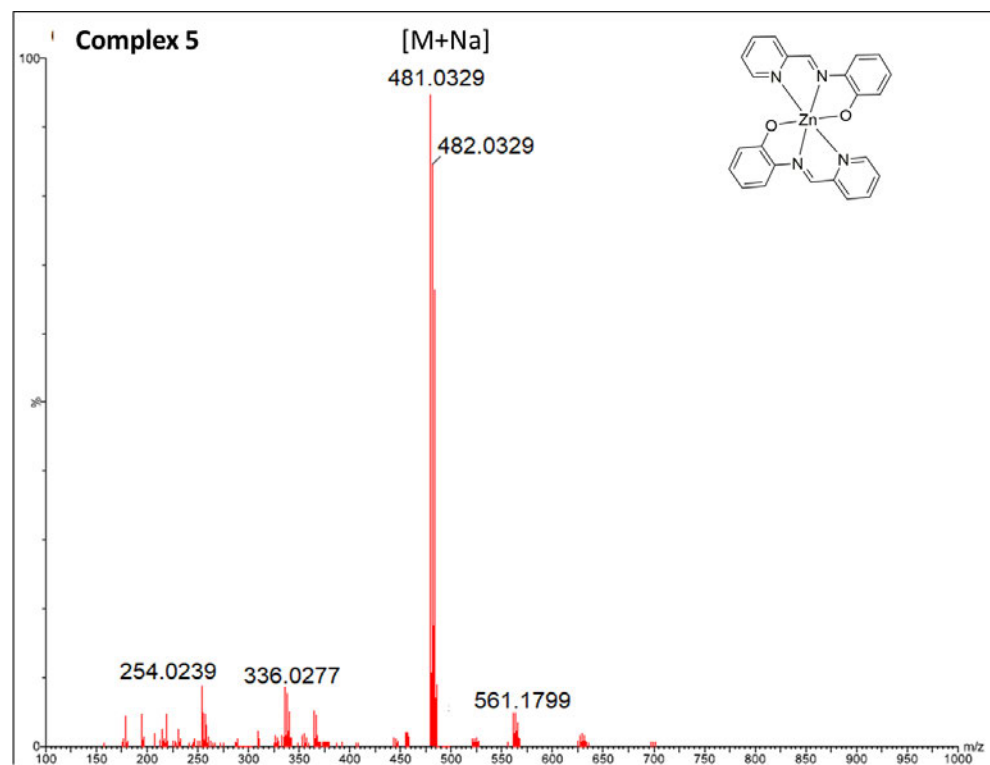
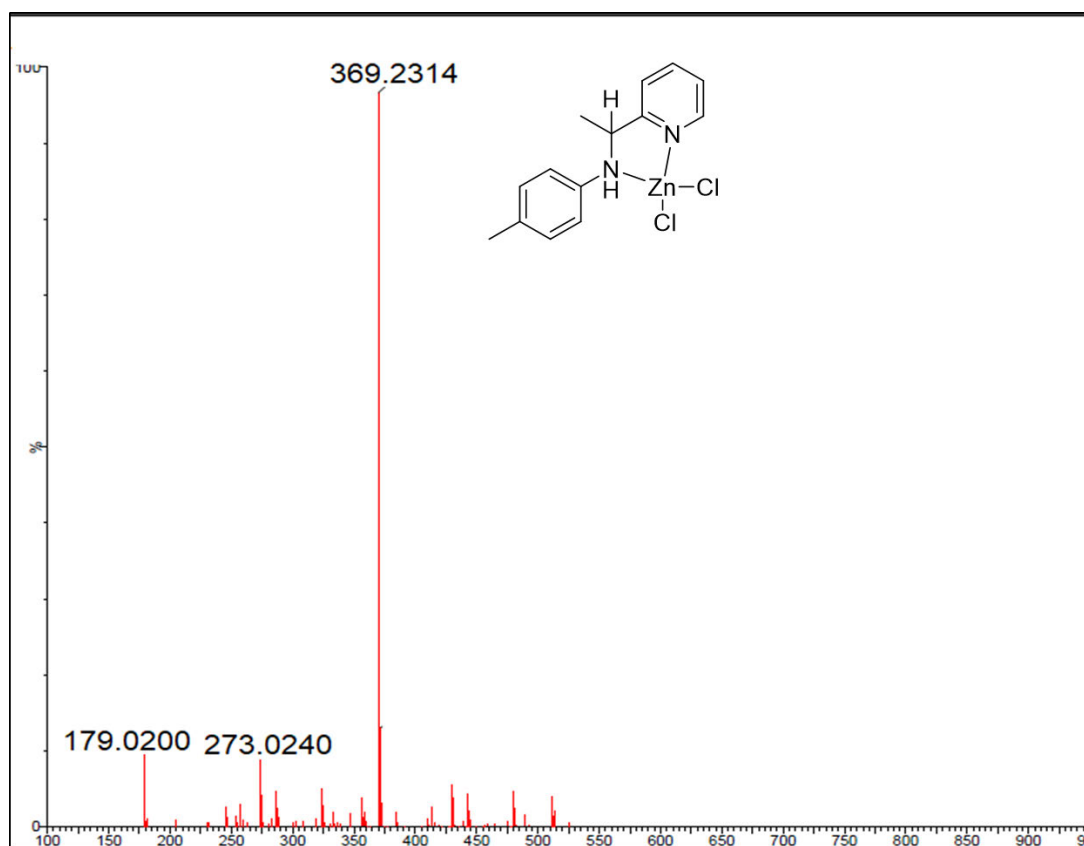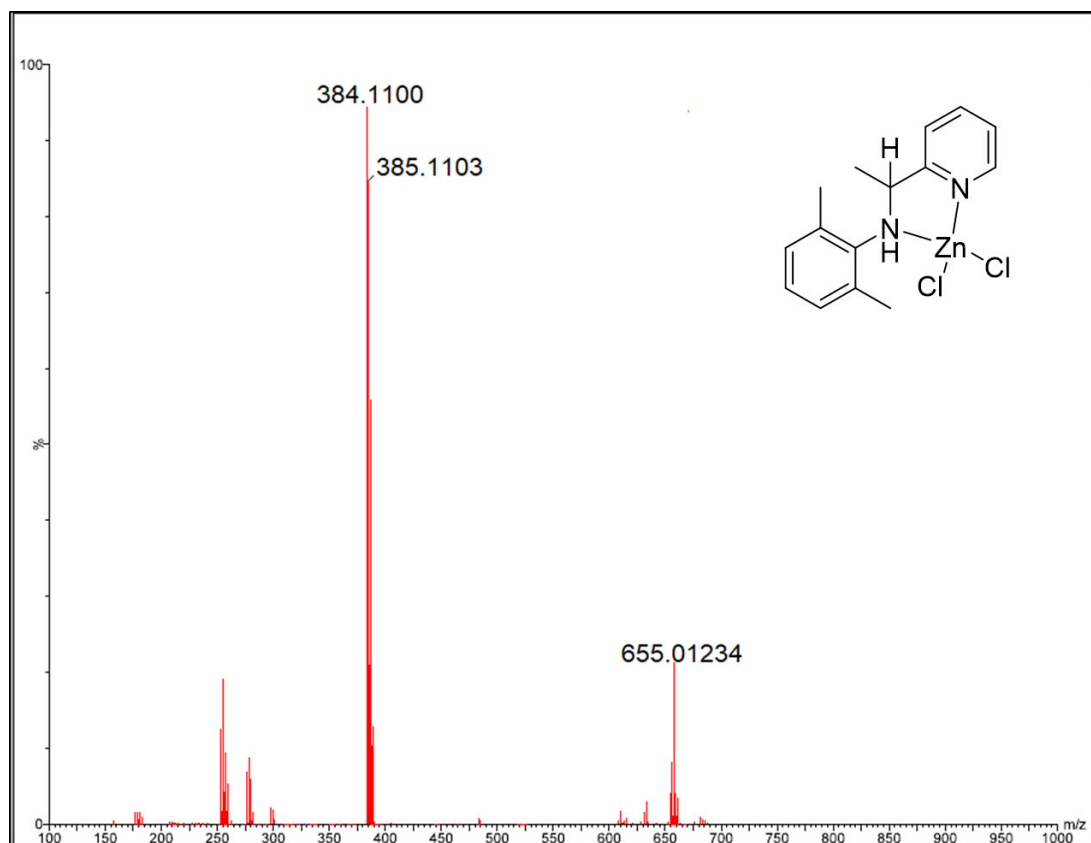Figure. S5. ESI-MS spectrum for complex **5.5**
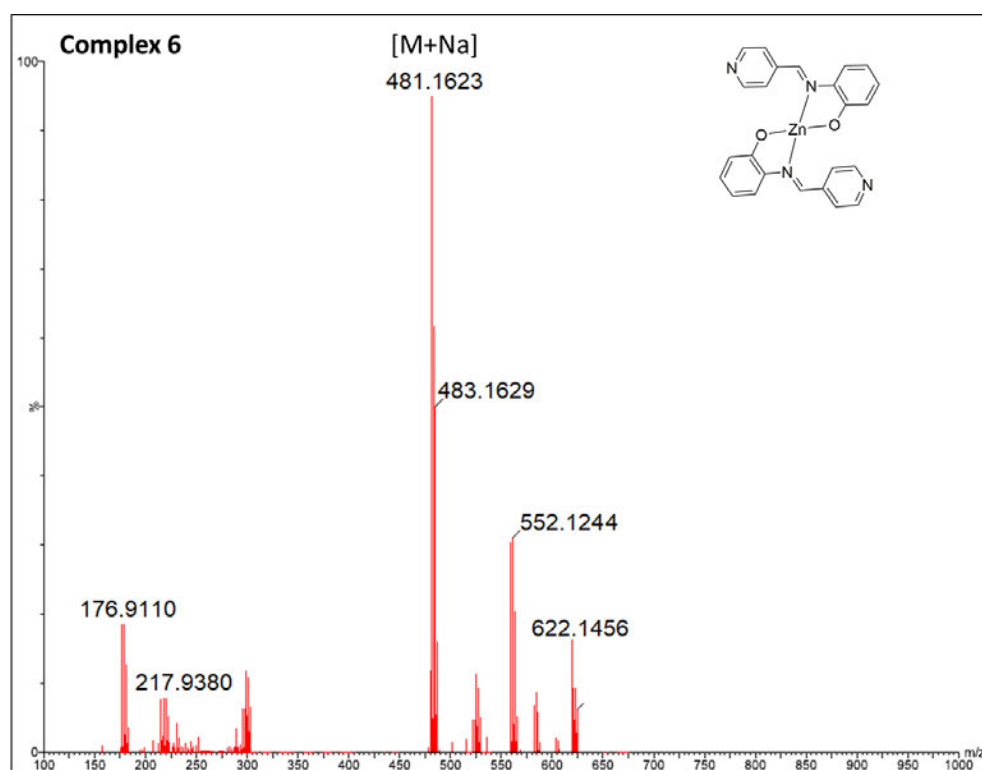
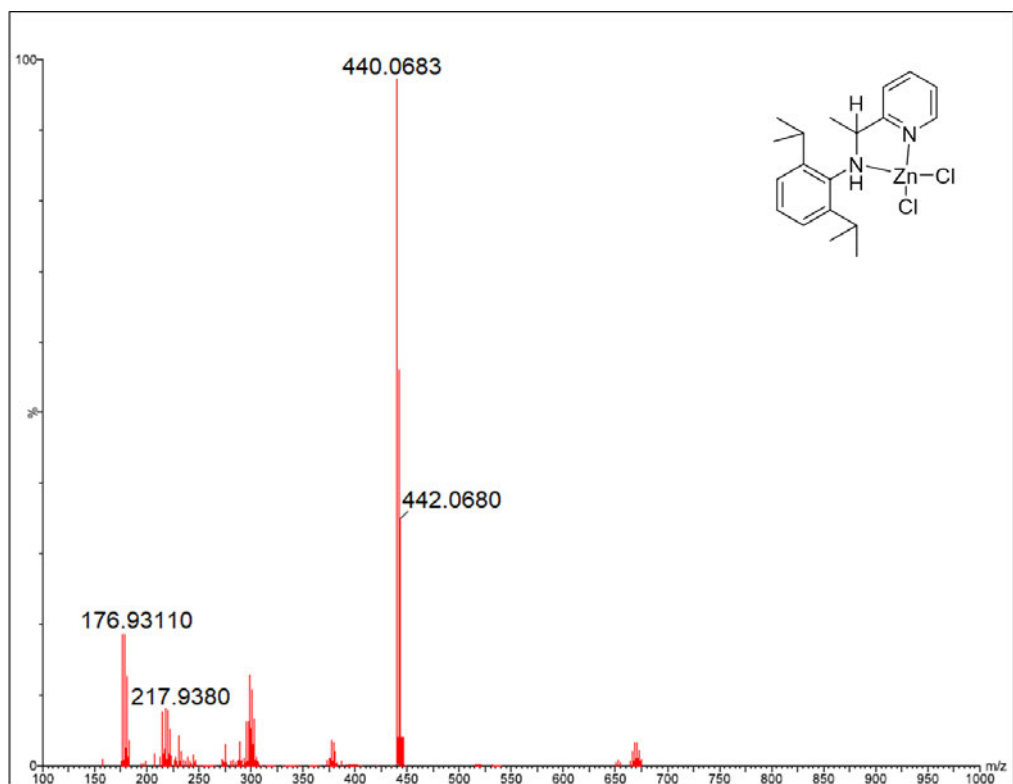Figure. S6. ESI-MS spectrum for complex **5.6**
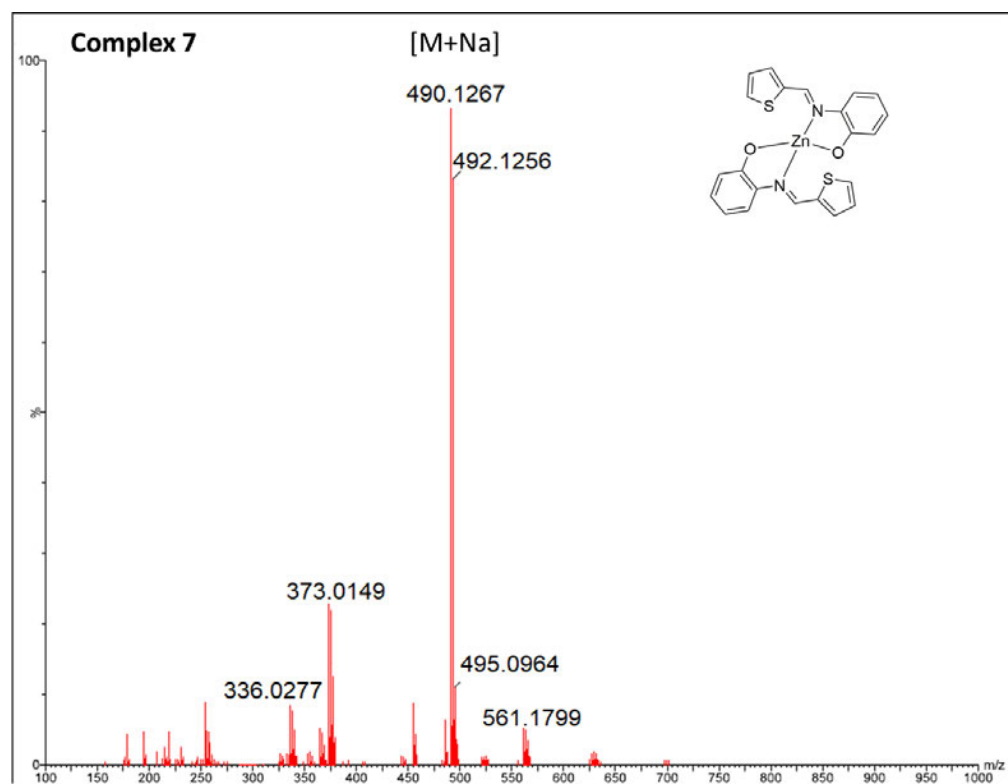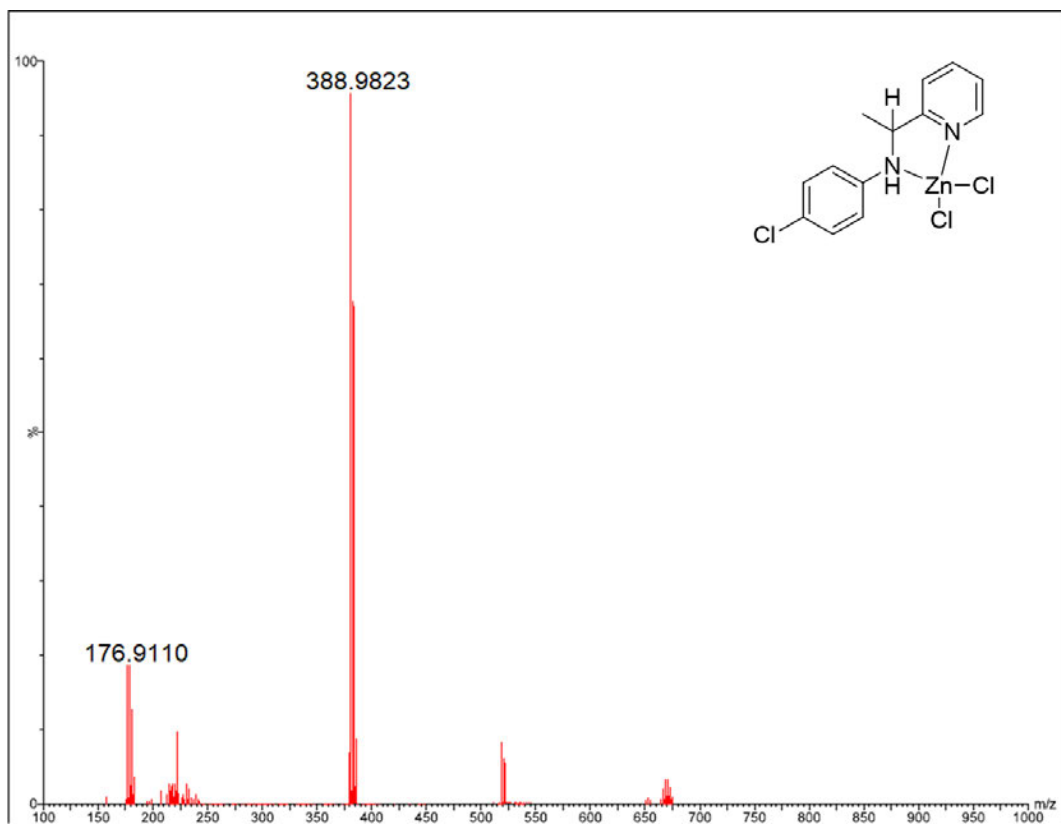
Figure. S7. ESI-MS spectrum for complex **5.7**
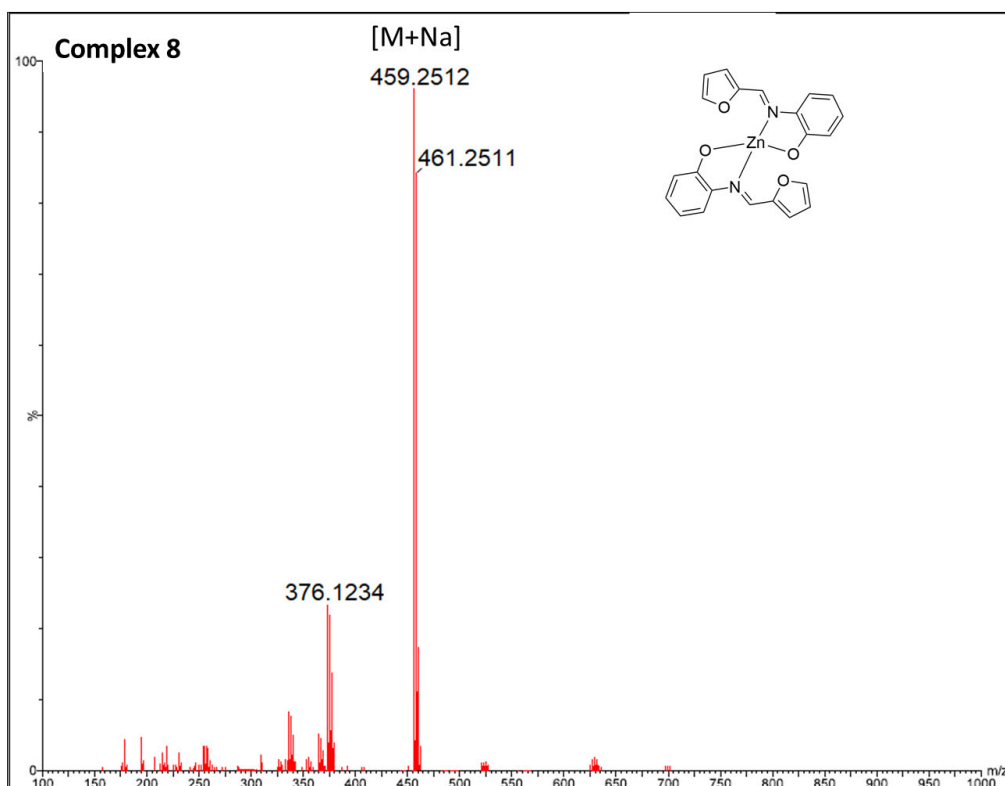
Figure. S8. ESI-MS spectrum for complex **5.8**

Figure. S9a H^1-NMR spectrum of complex **5.1** at room temperature in DMSO (400 MHz)

Figure. S9b H[1]-NMR spectrum of complex **5.2** at room temperature in DMSO (400 MHz)

Figure. S9c H[1]-NMR spectrum of complex **5.3** at room temperature in DMSO (400 MHz)

Figure. S9b H^1-NMR spectrum of complex **5.4** at room temperature in DMSO (400 MHz)

Figure. S10b H^1-NMR spectrum of complex **5.5** at room temperature in DMSO (400 MHz)

231

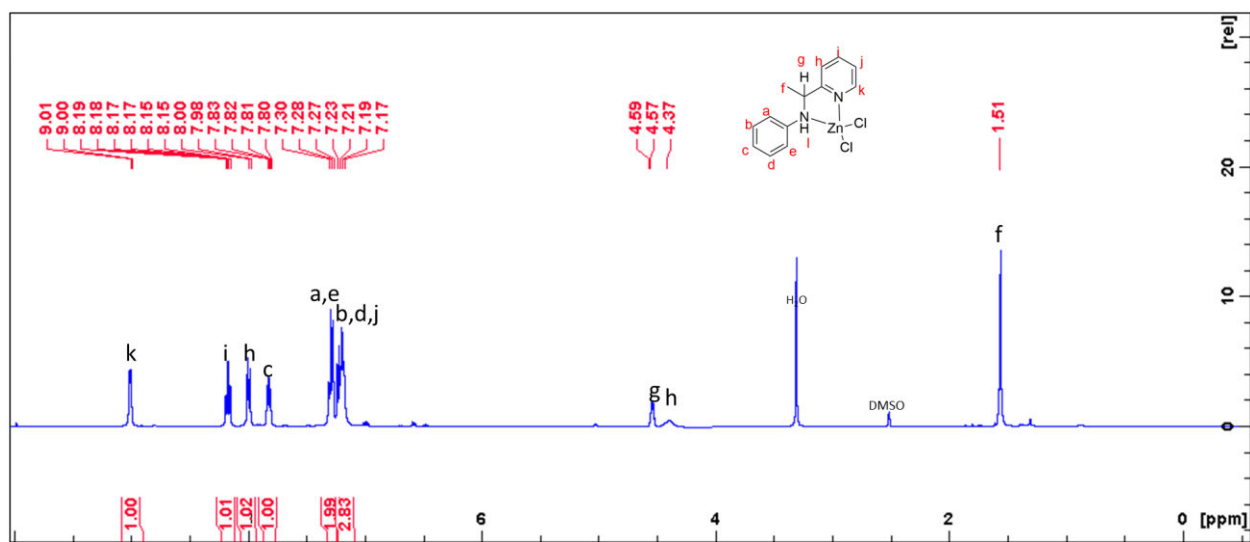Figure. S11b H^1-NMR spectrum of complex **5.6** at room temperature in DMSO (400 MHz)

Figure. S12b H^1-NMR spectrum of complex **5.7** at room temperature in DMSO (400 MHz)

232

Figure. S13b H^1-NMR spectrum of complex **5.8** at room temperature in DMSO (400 MHz)

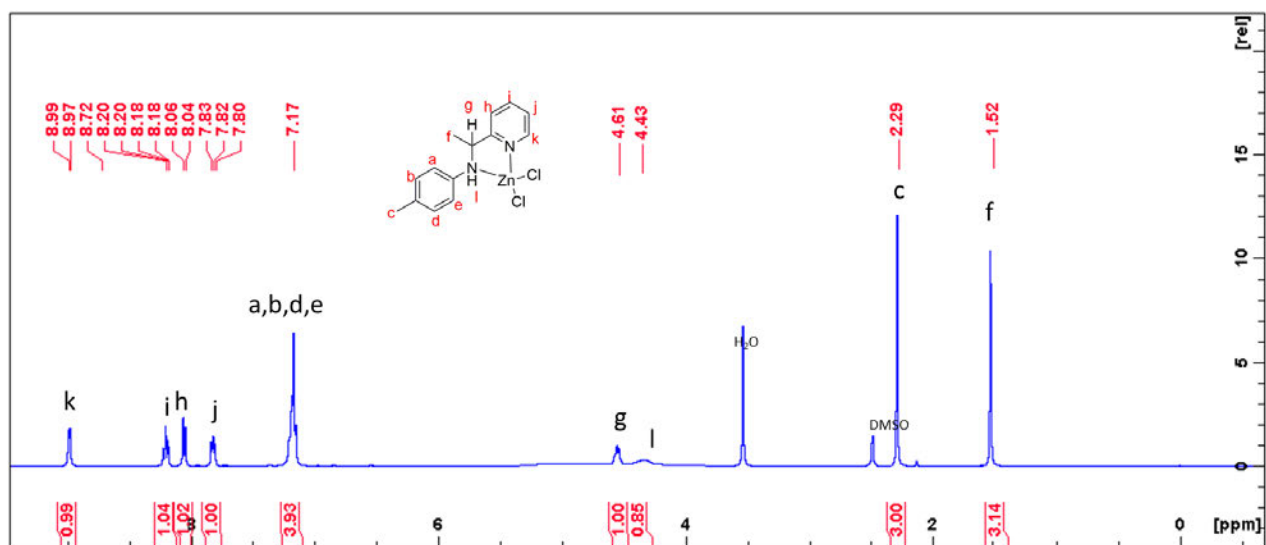Figure. S9f ^{13}C-NMR spectrum of complex **5.2** at room temperature in DMSO (400 MHz)

Figure. S9 ^{13}C-NMR spectrum of complex **5.3** at room temperature in DMSO (400 MHz)

Figure. S9h ^{13}C-NMR spectrum of complex **5.4** at room temperature in DMSO (400 MHz)
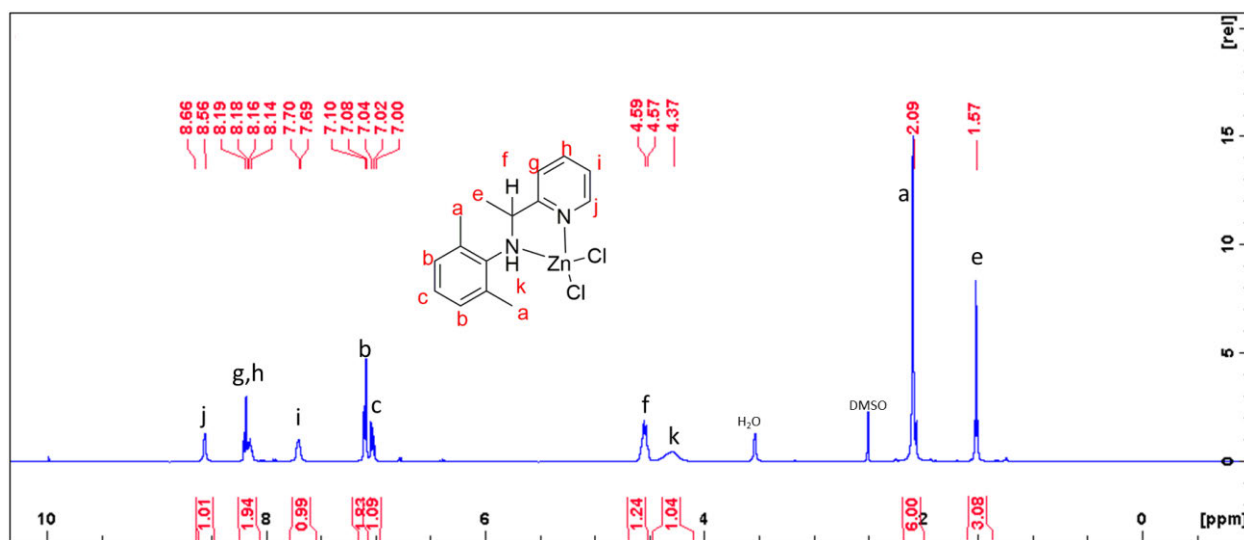
Figure. S9h ^{13}C-NMR spectrum of complex **5.5** at room temperature in DMSO (400 MHz)

Figure. S9h ^{13}C-NMR spectrum of complex **5.6** at room temperature in DMSO (400 MHz)

Figure. S9h ^{13}C-NMR spectrum of complex **5.7** at room temperature in DMSO (400 MHz)
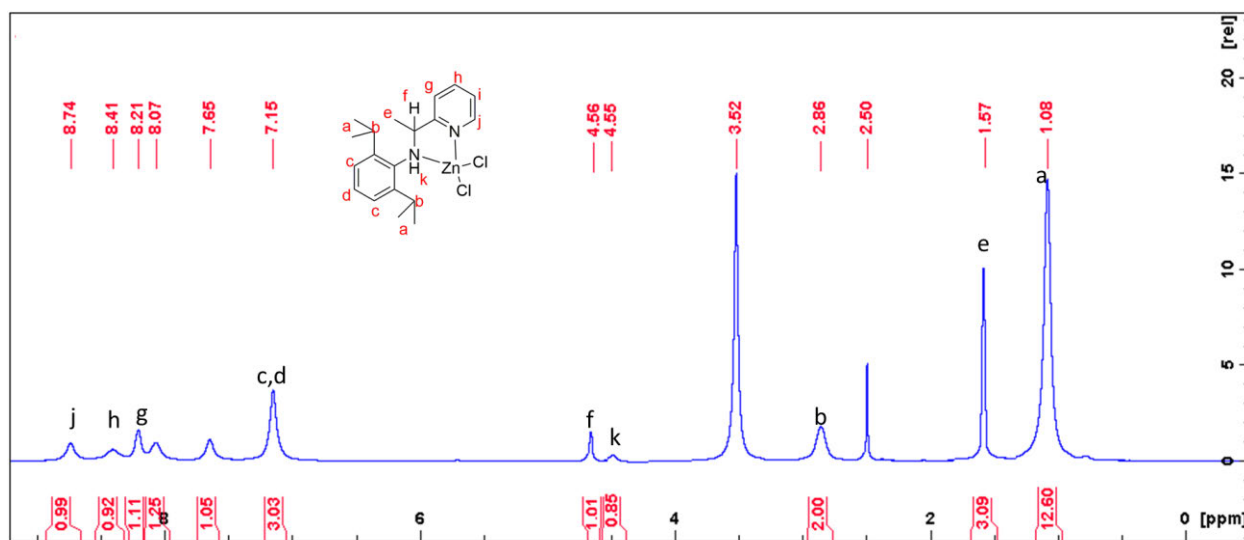

Figure. S9h ^{13}C-NMR spectrum of complex **5.8** at room temperature in DMSO (400 MHz)

Stereoselective homo- and co-polymerization of lactides and ε-caprolactone catalysed by chiral Zn(II) pyridyl complexes

Figure.S2. ESI-MS spectrum for complex **2**

Figure. S3. ESI-MS spectrum for complex **3**

Figure. S4. ESI-MS spectrum for complex **4**

Figure. S5. ESI-MS spectrum for complex **5**

Figure. S9a H^1-NMR spectrum of complex **1** at room temperature in DMSO (400 MHz)

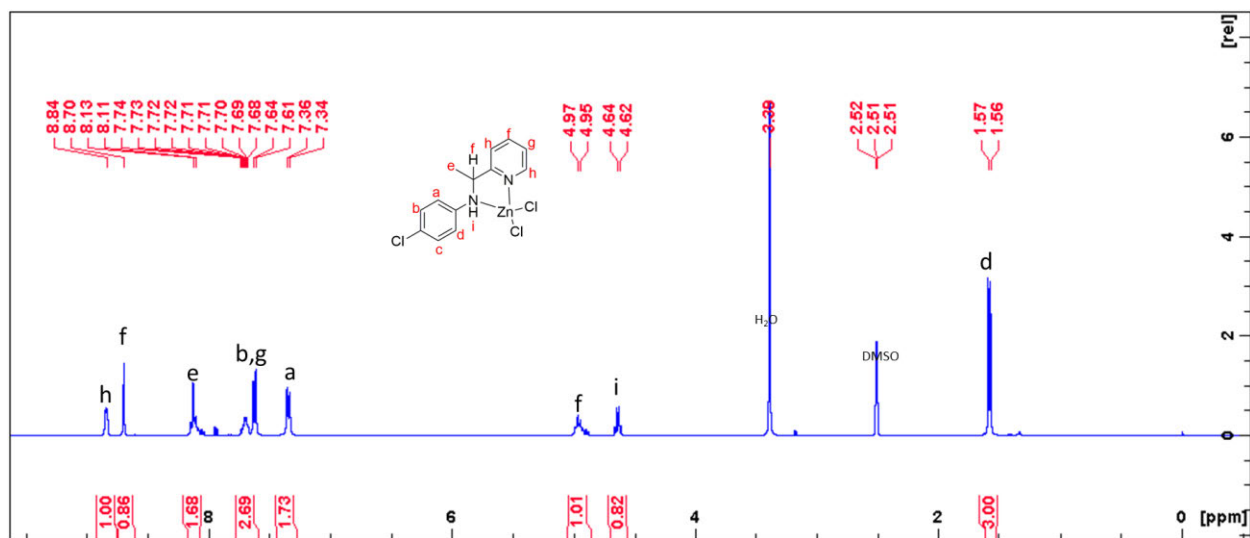Figure. S9b H^1-NMR spectrum of complex **2** at room temperature in DMSO (400 MHz)
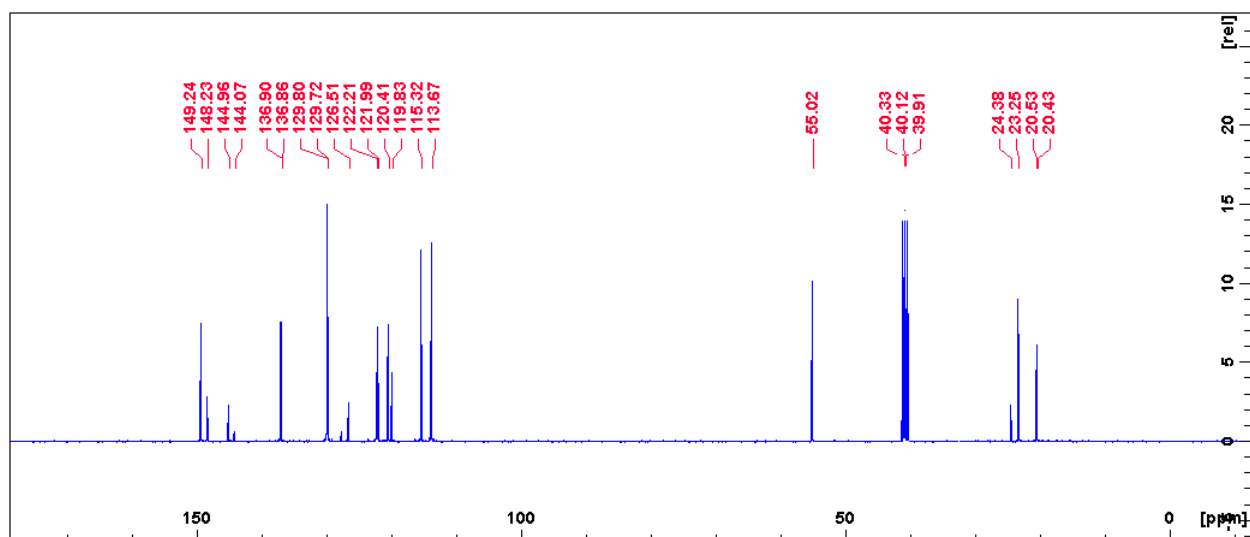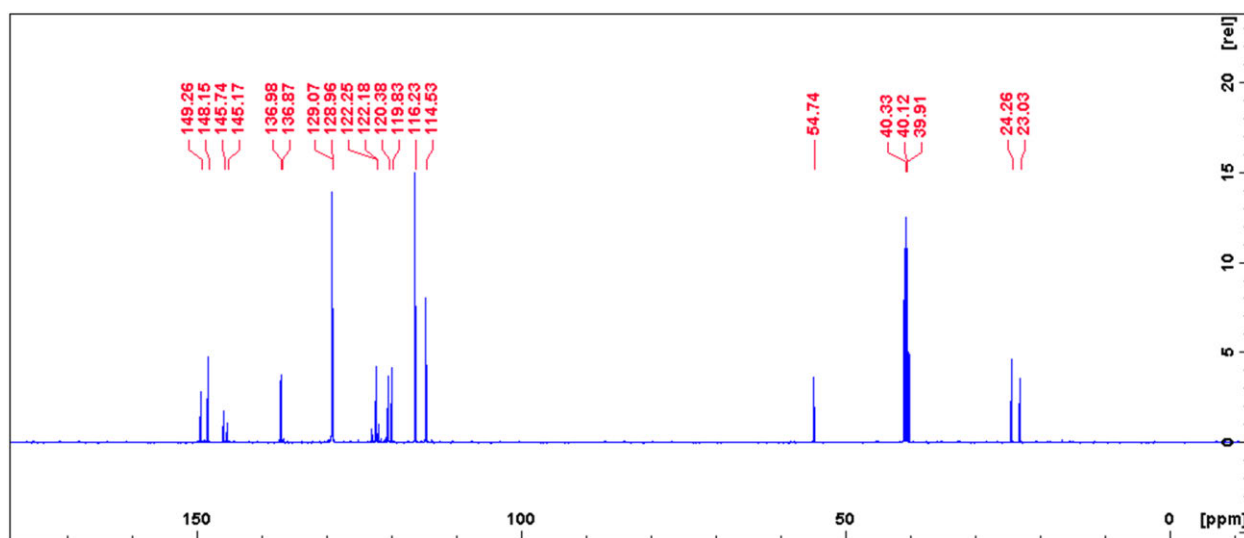
Figure. S9c H^1-NMR spectrum of complex **3** at room temperature in DMSO (400 MHz)

Figure. S9b H^1-NMR spectrum of complex **4** at room temperature in DMSO (400 MHz)

Figure. S10b H^1-NMR spectrum of complex **5** at room temperature in DMSO (400 MHz)

Figure. S9f ^{13}C-NMR spectrum of complex **2** at room temperature in DMSO (400 MHz)

Figure. S9 ^{13}C-NMR spectrum of complex **3** at room temperature in DMSO (400 MHz)
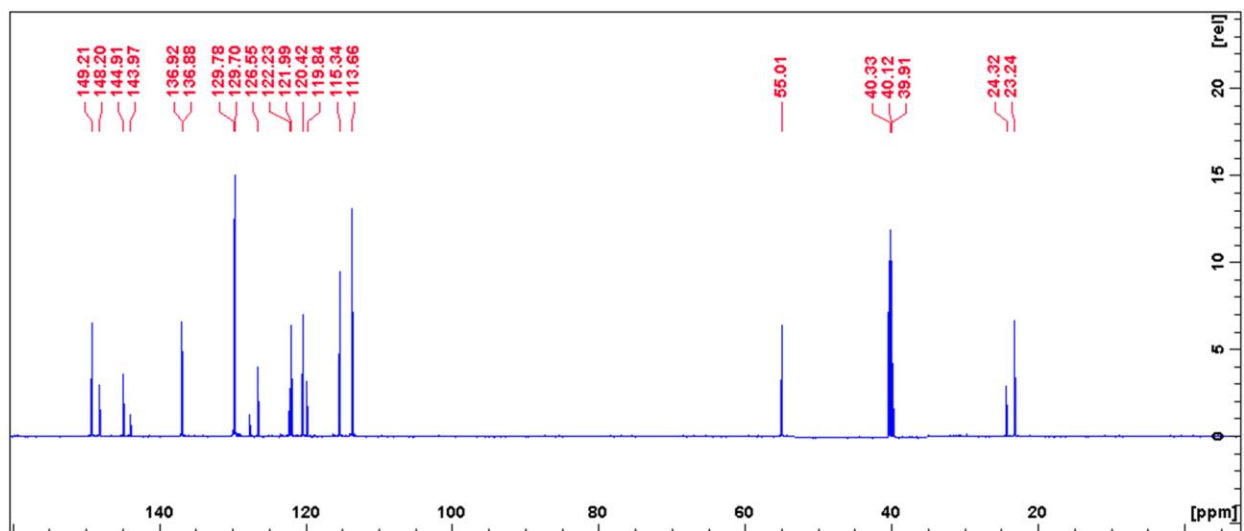

Figure. S9h ^{13}C-NMR spectrum of complex **4** at room temperature in DMSO (400 MHz)
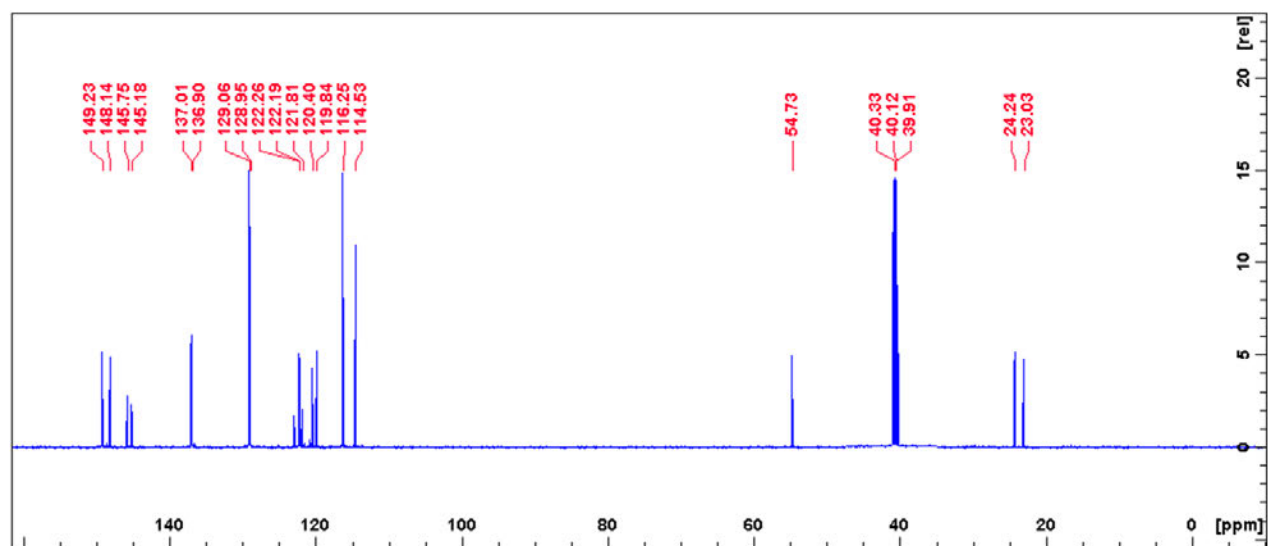
Figure. S9h ^{13}C-NMR spectrum of complex **5** at room temperature in DMSO (400 MHz)